EFFICIENT VALORIZATION OF CO2 INTO FORMATE THROUGH NANOCATALYSIS

María Dolores Fernández Martínez

UNIVERSITAT ROVIRA i VIRGILI

Efficient valorization of CO_2 into formate through nanocatalysis

MARÍA DOLORES FERNÁNDEZ MARTÍNEZ

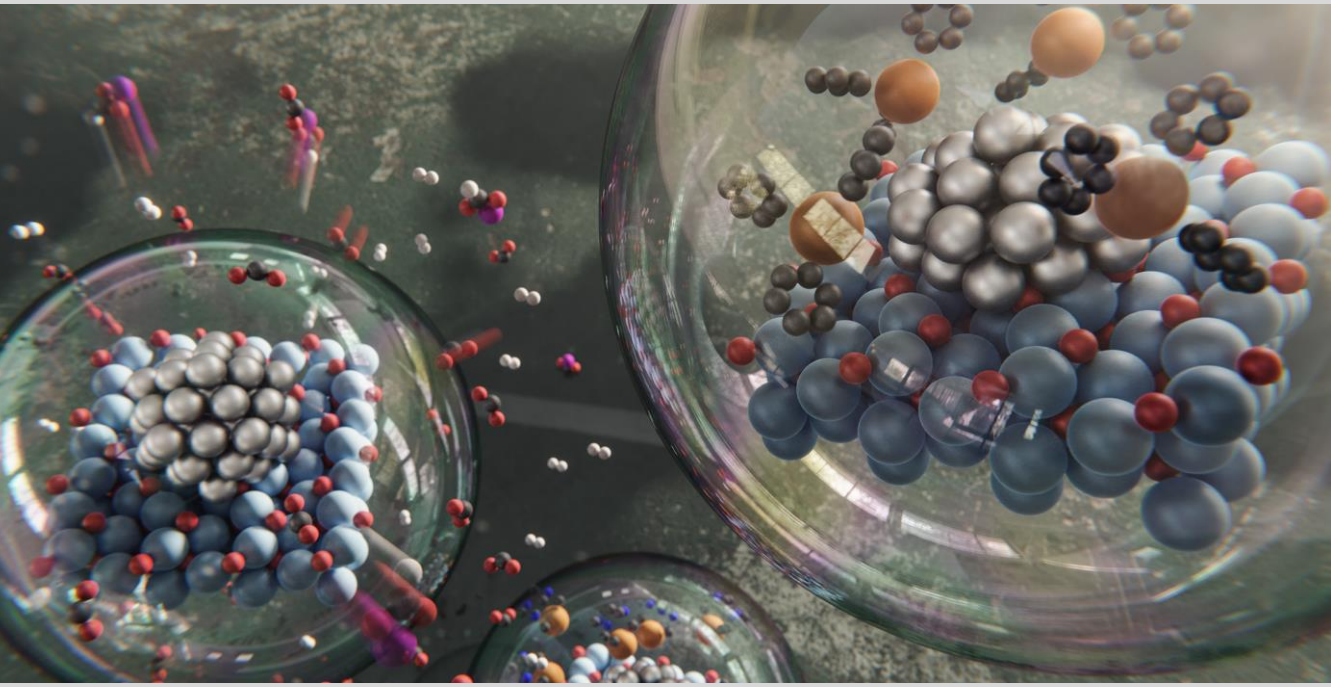

DOCTORAL THESIS
2023

UNIVERSITAT ROVIRA I VIRGILI
EFFICIENT VALORIZATION OF CO2 INTO FORMATE THROUGH NANOCATALYSIS
María Dolores Fernández Martínez

UNIVERSITAT ROVIRA I VIRGILI
EFFICIENT VALORIZATION OF CO2 INTO FORMATE THROUGH NANOCATALYSIS
María Dolores Fernández Martínez

UNIVERSITAT ROVIRA I VIRGILI
EFFICIENT VALORIZATION OF CO2 INTO FORMATE THROUGH NANOCATALYSIS
María Dolores Fernández Martínez

María Dolores Fernández Martínez

Efficient valorization of CO_2 into formate through nanocatalysis

DOCTORAL THESIS

Supervised by

Prof. Dr. Cyril Godard

Departament de Química Física I Inorgánica

UNIVERSITAT ROVIRA i VIRGILI

Tarragona 2023

UNIVERSITAT ROVIRA I VIRGILI
EFFICIENT VALORIZATION OF CO2 INTO FORMATE THROUGH NANOCATALYSIS
María Dolores Fernández Martínez

DEPARTAMENT DE QUÍMICA
FÍSICA i INORGÀNICA
Universitat Rovira i Virgili

C/ Marcel·lí Domingo 1,
Campus Sescelades,
Edifici N4, 2nd floor
43007 Tarragona
Tel. +34 977 55 81 37

Prof. Dr. Cyril Godard from the Department of Physical and Inorganic Chemistry at Universitat Rovira I Virgili.

I STATE that the present study, entitled “Efficient valorization of CO_2 into formate through nanocatalysis”, presented by María Dolores Fernández Martínez to receive the degree of Doctor, and that is suitable for the International Mention, was carried out under my supervision.

Tarragona, June 5th 2023

Doctoral Thesis Supervisor

Prof. Cyril Godard

The present Doctoral Thesis has been developed with a FPI scholarship (BES-2017-081305).

It has been possible thanks to the financial support from the following research projects:

-Ministerio de Ciencia e Innovación (MICINN) and Agencia Estatal de Investigación (AEI), PID2019-104427RB-I00.

-Ministerio de Ciencia e Innovación (MICINN), Agencia Estatal de Investigación (AEI) y Fondo Europeo de Desarrollo Regional (FEDER), CTQ2016-75016-R.

-AGAUR (Agencia de Gestión de Ayudas Universitarias y de Investigación) from Generalitat de Catalunya, 2017 SGR 1472 and 2021 SGR 00163.

Acknowledgments

Parece mentira que el tiempo pase tan rápido. Recuerdo perfectamente el momento de llegar a Tarragona y la ilusión de empezar un proyecto que abarcaría varios años de mi vida, así como gran parte de mi tiempo y dedicación. Ha sido una gran experiencia, tanto a nivel personal como profesional, y quiero agradecer a todas las personas que lo han hecho posible y han contribuido a ella.

Como no puede ser de otra manera, quiero empezar dando las gracias a mi supervisor, Cyril Godard. Muchas gracias por darme la oportunidad de formar parte de tu grupo y, desde el principio, por toda tu paciencia y apoyo. Una Tesis es un largo camino y tener como referente a una persona que siempre brinda comprensión es de un valor incalculable. Y, por supuesto, quiero agradecer el trabajo codo con codo, sobre todo en estos últimos meses. También quiero dar las gracias a Carmen Claver, en parte artífice de mi presencia en el grupo. Gracias por tus ideas, tus contribuciones y por tu positivismo, Carmen.

Quiero agradecer a Josep Manel Ricart y Jordi Carbó la posibilidad de hacer cálculos y por ayudarme con todos los problemas que han ido surgiendo por el camino.

I just want to thanks Dr. Ralf Jackstell and Prof. Matthias Beller for give me the opportunity of learn and work on its group on Rostock during three months during my PhD visiting stay this last year.

Aunque no formen parte de esta etapa, no quiero olvidar a otras personas que me acogieron en sus grupos y me transmitieron su curiosidad y su pasión por la Química durante y después de mis estudios, ya que también han contribuido a que quisiese seguir dedicándome a la investigación. Estas personas son Antonio Márquez Cruz y Jesús Campos.

Quiero seguir dando las gracias a las personas con las que posiblemente he compartido más tiempo durante estos años, mis compañeros de laboratorio. Somos un grupo muy variado, casi tanto como alergias, intolerancias o preferencias alimenticias hay dentro de él. Jèssica, gracias por tus palabras amables y por tu disposición siempre que he necesitado ayuda. A parte de laboratorio y grupo, también hemos compartido muchos momentos fuera del labo como los congresos en Tolouse y en Lisboa, en los cuales te he podido

conocer más. Joris, compañero además de cumpleaños, me alegro de tu vuelta a Tarragona. Muchas gracias por tu alegría y por tu música. Mucho ánimo con la recta final! Jie, thank you so much for your kindness. You are always positive and it is really nice to see your big smile and your energetic greeting everyday! Of course, I don't want to forget all your details and your delicious Chinese hot pot! Siham, me alegro de que te hayas adentrado en el mundo de las nanos. Espero que te transmitan tanta curiosidad y aprendizaje como a mí. Akshit, thank you for forming part of the group during this time! Nassima, nuestra reciente Doctora. Muchas gracias por tu amabilidad y te deseo lo mejor en tu nueva etapa! Oriol y Pol, con vosotros he compartido todos estos años desde mi llegada a la URV. Oriol, has sido muy buen compañero de labo, siempre dispuesto a ayudar en lo que se te necesite. También quiero remarcar la alegría que aportas al lab 216. Gracias por cantar de manera tan apasionada como normalmente lo haces (falsetes y agudos incluidos). En mis últimos días en el labo, a pesar del estrés y las preocupaciones, cantar LODVG entre otros me ha servido de mucho! Gracias por aportar siempre un ambiente relajado y por tu humor con juegos de palabras. Pol, compañero de mesa, de escritura y de penas. Gracias por compartir la manía de que todo esté alineado (llamémosle perfeccionismo) y de las imitaciones. También por tus comentarios que han hecho que muera de risa en muchas ocasiones y de tu infinidad de referencias a los Simpsons. Aunque he de decir que los pingüinos me gustaban más antes de ver tu presentación. Por esto último no te doy las gracias! Sara, tú eres otra de las personas con las que he compartido más tiempo en el labo. Muchas gracias por la alegría, la disposición y las ganas siempre de hacer planes. Sobre todo, gracias por la pegatina de The Office, a veces cuando la miro, parece como si me viese en el espejo. Daniel, gracias por ser otra persona amante de los burros y de las plantas. Al fin alguien les da su lugar. Eres una persona noble y siempre intentas ayudar. Muchas gracias por tu infinidad de historias durante los viajes al último congreso en Barcelona y por tu humor. A veces sin pretenderlo, eres muy divertido. Espero que no se te olvide qué es la RAE. También quiero agradecerles a Mireia y a Paula, todos los momentos compartidos estos años en el labo y fuera de él. Gracias a Angie y Anna, las chicas de heterogénea. Porque son personas que hacen agradable la vida

de los demás y se preocupan por ellos. Angie, gracias por tu idea de plan de vida, lo pondré en práctica. Y Anna, gracias por tu alegría y fortaleza a pesar de todo!! También gracias a Leví (qué pasó!) por saber escuchar, por tener siempre unas palabras de ánimo y por enseñarme expresiones latinas.
En el ámbito de los cálculos, quiero dar las gracias a Toni y Evgenii por su ayuda y, sobre todo, su paciencia siempre que he recurrido a ellos.
También quiero dar las gracias a María, Adrián, Javi, Adrià, Ricardo, Joan, Jana, Valero, Yeamin, Vladimir, Dolores, Aroldo y Aria.
De la otra parte del grupo que se encuentran en Eurecat, quiero dar las gracias a Roger, Emma, David, Aitor, Isa, Miriam y Montse. Muchas gracias siempre por vuestra ayuda desde que llegué al grupo. También quiero dar las gracias a Laia, por los momentos compartidos durante estos años. Gracias siempre por tu positivismo y tus ganas!
Y de la parte InnCAT gracia a Anna, Óscar y Montse. Muchas gracias Montse por resolverme las dudas en lo referente a la Tesis cada vez que he necesitado ayuda.
I also want to thanks all my partners from LIKAT in Rostock. Thanks to ‘’Los Muchachos‘’: Hilario, Coni, Jan, Anna, Hendrik, Niara, José Cobra, Sasha, Gustavo and the rest. It was just three months, but I have enjoyed a lot in your company. Never forget dancing La Macarena and Rodeos, the Quiz night, piñatas, Glühwein at Christmas Market and learning how to open a bottle with a spoon. I want to special mention to Gordon, Pierre and Yao. Thanks for all your help since the beginning!!
Gracias a Marina y a Nere, ellas son las personas que me enseñaron a trabajar en el laboratorio, en el lab 202 concretamente. Siempre recordaré la mudanza, el cajón de anti-depresivos, los días amenizados al son del Kanka, pasión en Cartuja y tantos otros buenos momentos, de risas y de agobios. Guardo todos estos recuerdos con muchísimo cariño. Muchos abrazos van para Londres y Toulouse. Quiero dar las gracias también a Patri, por su alegría, su salero, sus consejos (como el Yoga) y sus contribuciones al cajón que siempre eran bienvenidos en el 202. Pero más aún le quiero agradecer acercarme al mundo de las nanos y por enseñarme que (por mi parte, viniendo de una química en la que los colores son muy importantes), ver el

color negro tras una síntesis era síntoma de buenas noticias. También quiero recordar a otros compañeros como Juan y Sonia, Javi y Elena.

Quiero agradecer a nuestros técnicos Raquel y Josep por su disposición en todo momento. Raquel, muchísimas gracias. Desde que llegué me recibiste con tu característica amabilidad. Muchas gracias por escucharme tantas veces y por poner calma y solución a tantos problemas siempre con tan buena actitud. Te deseo siempre lo mejor.

Muchas gracias al personal del Servei en las diversas técnicas que me ha requerido mi Química. Gracias a Francesc, Sònia, Debora, Cristina, Nuria y Mercè. En especial a Ramón de RMN y a Rita, Mariana y Sergi de Microscopía por ayudarme con muestras complicadas e intentar lo máximo de su parte!

También quiero agradecer a María José Durán y a las personas de administración que me han ayudado con todos los trámites que me han sido necesarios.

A Laura, Lucía y Victoria y a Eli y Mathias. Muchas gracias por vuestra confianza, conversaciones profundas, inventos absurdos y tantísimos buenos momentos.

Por último, quiero agradecer a mi pareja y familia. Jordi, muchas gracias por ser mi compañero en todos los sentidos. Gracias por escucharme siempre y ser un apoyo imprescindible para mí en los buenos y en los malos momentos. Has sido un gran descubrimiento durante mi Doctorado y disfruto muchísimo compartiendo nuestro día a día en tantos aspectos entre los que se encuentra la Química. Gracias por aguantar mis quejas y mis estados de ánimo muchas veces, por conocerme tan bien y, por supuesto, gracias por tu amor y tu paciencia (y por tus paellas). También te quiero agradecer que me hayas incluido en tu familia a la cual le doy las gracias por el cariño y el apoyo durante esta etapa. En especial a tus padres, Mabel y Sisco y, como no, a la iaia Cati, por ser resistencia Madridista junto a mí en campo contrario.

A mis padres y a mi hermano también quiero agradecerles su apoyo incondicional. A veces la distancia no lo ha puesto fácil, pero gracias por comprenderlo siempre y animarme a seguir hacia adelante. Papá, mamá, gracias por darme todo cuanto ha estado en vuestra mano para que hoy sea la persona que soy y por tener las palabras adecuadas para mí en cada

momento. Gracias por los valores y por todo el amor que me habéis dado y me seguís dando día a día. Gracias por enseñarme que en la vida siempre hay que esforzarse y que hay que tomar las cosas con deportividad. Porque como siempre me dices tú, papá, no por mucho trigo es mal año, pero también hay que saber parar. Y a ti hermano, muchas gracias por tu ejemplo como hermano mayor todos estos años, por tus consejos (entre los que se encuentran animarme a estudiar Química), por las risas, la confianza y, como no, por las peleíllas. Por supuesto, muchas gracias también por la portada! Dales un achuchón a Flecha y Uma de mi parte!

Gracias a todas y cada una de las personas que aparecen en estos agradecimientos, y a las que por despiste mío puedan no aparecer, por aportar vuestro granito de arena para que este trabajo saliese adelante y por ayudarme cada uno a vuestra manera en el proceso.

¡¡¡Moltes gràcies a tots!!!

UNIVERSITAT ROVIRA I VIRGILI
EFFICIENT VALORIZATION OF CO2 INTO FORMATE THROUGH NANOCATALYSIS
María Dolores Fernández Martínez

Table of Contents

UNIVERSITAT ROVIRA I VIRGILI
EFFICIENT VALORIZATION OF CO2 INTO FORMATE THROUGH NANOCATALYSIS
María Dolores Fernández Martínez

Abbreviations and acronyms

A	4-AP	4-Aminophenol
	AC	Activated Carbon
	acac	Acetylacetonate
	Acriphos	4,5-Bis(diphenylphosphino)acridine
	APA	3-Aminopropylphosphonic acid
	AP-POP	Amide and Pyridine Porous Organic Polymers
	APTES	(3-Aminopropyl)triethoxysilane
	ASF	Anderson-Schulz-Flory type distribution
B	BCN	Bulk Carbon Nitride
	BE	Binding Energy
	BET	Brunauer-Emmett-Teller
	BF	Bright-Field
	[BMI][OAc]	1-Butyl-3-methylimidazolium acetate
	[BMMI][OAc]	1,2-Dimethyl-3-butylimidazolium acetate
	bpy	Bipyridine
C	CCS	Carbon Capture and Storage
	CCU	Carbon Capture and Utilization
	CN_x	Pyridinic-Nitrogen-Doped Carbon
	CNTs	Carbon Nanotubes
	COD	1,5-Cyclooctadiene
	COFs	Covalent Organic Frameworks
	Cp*	1,2,3,4,5-Pentamethylcyclopentadienyl
	CTF	Covalent Triazine Framework
D	δ	Chemical shift
	d	Doblet
	dba	Dibenzylideneacetone
	DBU	1,8-Diazabicyclo[5.4.0]undec-7-ene
	DFT	Density Functional Theory
	DMC	Dimethyl Carbonate
	DME	Dimethyl Ether
	DMF	Dimethylformamide
	DMSO	Dimethyl Sulfoxide
	dppe	1,2-Bis(diphenylphosphino)ethane

	DRM	Dry Reforming of Methane
E	ECN	Exfoliated Carbon Nitride
	EDS	Energy Dispersive Spectra
	EDX	Energy Dispersive X-ray Analysis
	eq.	Equation
	equiv.	Equivalent
	ESEM	Environmental Scanning Electron Microscopy
	eV	Electronvolt
F	FA	Formic Acid
	FESEM	Field Emission Scanning Electron Microscope
	FPA	Formate-Piperidine-Adduct
	F-T	Fischer-Tropsch
	FT-IR	Fourier-Transform Infrared Spectroscopy
G	g	Gram
	GC-MS	Gas Cromatography-Mass Spectroscopy
	g-C_3N_4	Graphitic Carbon Nitride
H	h	Hour(s)
	H_2SMA	Mercaptosuccinic acid
	HAADF	High-Angle Annular Dark-Field
	HMOSs	Hollow Mesoporous Organosilica Spheres
	^{1}H-NMR	Proton Nuclear Magnetic Resonance
	HR- HAADF STEM	High Resolution-Transmission Electron Microscopy
	HR-TEM	High-Resolution TEM
I	ICP	Inductively Coupled Plasma
	ICP-OES	Inductively Coupled Plasma - Optical Emission Spectrometry
	ICRMs	Interfacially cross-linked reverse micelles
	ILs	Ionic Liquids
	Im^+	Imidazolium
J	J	Coupling Constant

K	K	Kelvin
	KIE	Kinetic Isotope Effect
	kV	Kilovolt
M	m	Multiplet
	M	Molarity
	mA	Milliampere
	MCN	Mesoporous carbon nitride
	$Me_2Im\text{-}CO_2$	1,3-Dimethylimidazolium-2-carboxylate
	MF	Methyl formate
	mg	Milligram
	MHCSs	Mesoporous hollow carbon spheres
	MHz	Megahertz
	min	Minute
	ml	Mililitre
	µmol	Micromole
	MOFs	Metal-Organic Frameworks
	MPa	Megapascal
	mpg-C_3N_4	Mesoporous Graphitic Carbon Nitride
	MSNs	Mesoporous Silica Nanospheres
	MTO	Methanol To Olefin
	MWCNT	Multi-Walled Carbon Nanotubes
N	4-NP	4-Nitrophenol
	N-C	N-doped Carbon
	NEB	Nudged Elastic Band
	NHC	*N*-Heterocyclic Carbene
	nm	Nanometer
	NMR	Nuclear Magnetic Resonance
	N,P-C	N- and P-co-doped Carbon
	NPG	N,P-dual-doped Multilayer Graphene
	NPs	Nanoparticles
	N_s	Number of surface atoms
	N_t	Number of total atoms
P	P	Pressure
	PA	Butylphosphonic acid
	PAs	Organophosphonic acids

	PDA-*r*GO	*p*-Phenilenediamine-functionalized reduce Graphene Oxide
	PDMC	Polyaniline-Derived Mesoporous Carbons
	PEI	Polyethyleneimine
	PILs	Poly(ionic liquid)s
	pm	Picometre
	ppm	Parts per million
	POPs	Porous Polymers
	PTA	1,3,5-Triaza-7-phosphaadamantane
Q	q	Quartet
R	r	Atomic radius
	r-GO	Graphite Oxide Nanosheets
	rpm	Revolutions per minute
	r.t.	Room Temperature
	RWGS	Reverse Water-Gas Shift reaction
S	SAC	Single Atom Catalyst
	SAMs	Self-Assembled Monolayers
	SILP	Supported Ionic Liquid Phase
	SMR	Steam Methane Reforming
	SPS	Solvent Purification System
	STEM	Scanning Transmission Electron Microscopy
T	t	Time
	TEM	Transmission Electron Microscopy
	TEA	Triethylamine
	TESs	Triethoxysilanes
	TGA	Thermo Gravimetric Analysis
	THF	Tetrahydrofuran
	TMB	1,3,5-Trimethyl benzene
	TNTs	Titanate Nanotubes
	TPPMS	3-(Diphenylphosphino) benzenesulfonic acid sodium salt
	TOF	Turnover Frequency
	TON	Turnover Number

	TpPa	1,3,5-Triformyl-phloroglucinol and p-phenylenediamine
	TS	Transition State
V	VHH	Van Hardevel-Hartod method
	v/v	Ratio Volume to Volume
W	wt	% Weight to Weight
X	XPS	X-ray Photoelectron Spectroscopy
	XRD	X-ray Diffraction Analysis
Z	ZIF	Zeolitic Imidazolate Frameworks

UNIVERSITAT ROVIRA I VIRGILI
EFFICIENT VALORIZATION OF CO2 INTO FORMATE THROUGH NANOCATALYSIS
María Dolores Fernández Martínez

Summary

The environmental issues arising from the high concentration of CO_2 in the atmosphere are nowadays regarded as critical and have triggered much interest in research towards the development of non-fossil-based feedstocks. In this context, despite its inertness, CO_2 has become a very attractive C1 source to obtain fuels and chemicals. Among the potential transformations, the hydrogenation of CO_2 into formic acid and derivatives have become a priority in view of the recent progress made in the production of H_2 *via* water splitting. Compared to classical synthetic methods, direct CO_2 hydrogenation for the production of formic acid is important for two important points: the transformation of CO_2 and the use of formic acid and derivatives as hydrogen storage, giving rise to CO_2 mediated hydrogen energy cycle. However, if the reaction is performed in the gas phase, high temperatures are usually required and the most interesting products such as HCOOH and MeOH are thermodynamically disfavored. In aqueous phase, the reaction becomes slightly exothermic due to solvation effects and is even more favorable under alkaline conditions. The hydrogenation of CO_2 under basic conditions or from the hydrogenation of carbonates or bicarbonates has several advantages over the HCO_2H/CO_2 system since it allows the release of H_2 without producing CO.

In the present thesis, the preparation and characterization of a series of Pd-based materials and their application as catalysts in the hydrogenation of CO_2 to formate are described. DFT calculations were also carried out to get insights into the reaction mechanism using some of these catalysts. Moreover, the use of formate as reducing agent for the catalytic reduction of nitroaromatics and the reductive amination of aldehydes was also briefly explored.

In Chapter 1, a general presentation of the CO_2 transformations of interest is presented and the state-of-the-art catalysts for the hydrogenation of CO_2 into formate are described in details. A brief review on the reverse reaction, namely the catalytic dehydrogenation of formic acid and formates, is also presented.

In Chapter 2, the main objectives of this thesis are described.

Chapter 3 focuses on the synthesis of two series of catalysts based on ligand-capped supported Pd nanoparticles using a simple procedure and the testing of the resulting materials in the formate synthesis. Within these series, PPh_3 revealed the most appropriate stabilizing ligand while TiO_2 was the most efficient support for these catalysts. The hydrogenation of CO_2 was carried out under mild reaction conditions (1.8 MPa CO_2,1.8 MPa H_2, 60°C) using water as solvent and in the presence of a base, providing excellent selectivity towards formates with a TON of 1032 (TOF of 69 h^{-1}, [HCOOK]=1.1 mol/l).

Chapter 4 described preliminary results obtained by DFT calculations on some of the systems employed in Chapter 3. A **Pd_{55}** NP model was used for this purpose and the adsorption of different phosphines was looked at. The effect of the ligand structure on the coverage of the Pd surface was also investigated. Moreover, preliminary calculations into the mechanism of hydrogenation on the surface of these catalysts using bicarbonate as substrate were carried out.

In Chapter 5, the preparation of supported Pd-NPs based materials were is described using modifiers of different nature (APTES and PAs) and following two distinct approaches: the so-called reverse deposition approach that requires the modification of the TiO_2 support in the first place prior to Pd NPs deposition while the 2nd approach consisted in the modification of the pre-synthesized **Pd-PPh_3/TiO_2**, by deposition of the modifier over its surface. These catalysts were used in the hydrogenation of CO_2 to formate, and their performance compared with those of the unmodified catalyst **Pd-PPh_3/TiO_2**. The modification of the TiO_2 support by organosilanes provided a beneficial effect in catalysis compared with the catalyst containing unmodified TiO_2 or TiO_2 modified by organophosphonic acids. The concentration was a key parameter during the support modification and lower values provide catalysts with higher activities. When the support was first modified, the presence of a functional group (either NH_2 or imidazolium) in the modifiers improved the activity of the catalysts compared with those containing a simple alkyl chain. The deposition of organosilane and organophosphonic acid modifiers over previously synthesized Pd NPs supported on TiO_2 was not beneficial in most cases to the activity of the catalyst and the deposition of organosilanes

containing an IL substituent had a detrimental effect on the catalytic activity of the resulting materials.
In terms of recyclability, the synthetic procedure used for the modification of the **Pd-Ph$_3$/TiO$_2$** catalyst affected the reusability of these materials in the CO_2 hydrogenation into formate. Indeed, the catalysts formed by modification of the support prior to Pd NP deposition suffered a rapid decrease in activity during their recycling and reuse in spite of the initial beneficial effect. In contrast, some of the materials where the modifiers were deposited over the previously anchored Pd NPs onto TiO_2 showed a much more gradual decrease in activity and reached a TON > 500 after the 3rd recycling.

In Chapter 6, the use of **Pd-PPh$_3$/TiO$_2$** catalyst in the reduction of nitrophenols and nitroarenes in water using potassium formate as reducing agent is described. This catalyst revealed active in the dehydrogenation of formate and in the presence of reducible substrates such as nitroaromatics, the reduction of the nitro group was highly efficient. Using 4-nitrophenol as substrate, an initial TOF (at 15 min of reaction) of 408 h^{-1} was obtained, which is among the best activities reported for this reaction. Preliminary results on the reductive amination using nitrobenzene and butyraldehyde/benzaldehyde in water are also presented. For butyraldehyde, 100% of conversion and 91 % of selectivity to the desired amine were obtained at r.t. in 3 h of reaction, (0.6 mol% Pd, 4 M HCOOK (20 equiv.)). In contrast, when the reaction was carried out using benzaldehyde as substrate, full selectivity to the imine product (mainly using r.t.) or to the amine (0.6 mol% Pd, 8 M HCOOK (40 equiv.) and 50 ºC) were achieved.

UNIVERSITAT ROVIRA I VIRGILI
EFFICIENT VALORIZATION OF CO2 INTO FORMATE THROUGH NANOCATALYSIS
María Dolores Fernández Martínez

CHAPTER 1

Introduction

UNIVERSITAT ROVIRA I VIRGILI
EFFICIENT VALORIZATION OF CO2 INTO FORMATE THROUGH NANOCATALYSIS
María Dolores Fernández Martínez

1.1. Conversion of CO_2 into chemicals

1.1.1. From CO_2 waste to feedstock

Nowadays, carbon dioxide (CO_2) is one of the major greenhouse gases responsible of global warming. Atmospheric levels of CO_2 have reached approximately 423 ppm in 2023 and are expected to keep increasing (Figure 1).[1] Global CO_2 emissions mainly come from anthropogenic activities including fossil fuel combustion and transportation, and industrial processes, which reach 36.8 Gt in 2022.[2] The increase of CO_2 in atmosphere also triggered an increase in temperatures, with catastrophic consequences on Earth.

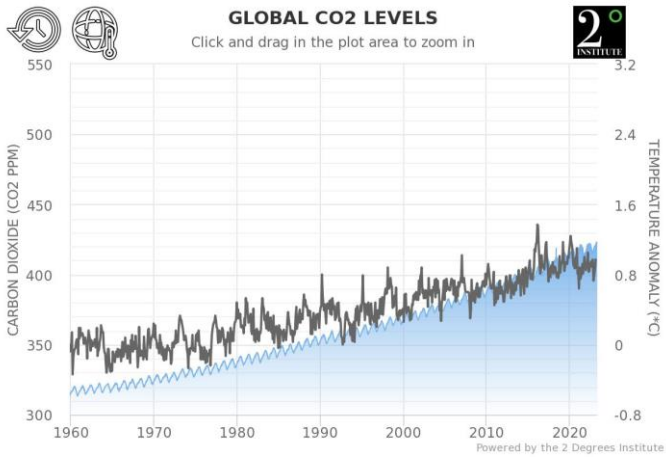

Figure 1. Atmospheric levels of CO_2 and variations in temperature during last years. Graphic from webpage https://www.co2levels.org/#code.

To solve this issue, several climate change mitigation policies were initiated over the last years (Scheme 1).[3,4] One of most attractive is the Carbon Capture and Storage (CCS), which is based on compressing CO_2 and its storage. However, technical and economic limitations remain such as the requirements of underground gas storage capacity and consequently, the alternative Carbon Capture and Utilization (CCU) has gained more attention. The CCU involves the capture of CO_2 released from anthropogenic activities and its conversion into high-added value products. As such, the recycling of CO_2 and its utilization as renewable carbon source has become the focus of research over the last years as a possible way to mitigate climate change.

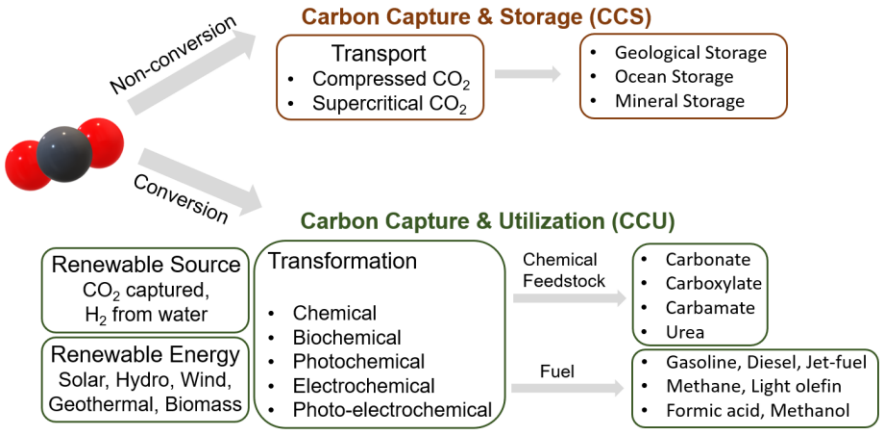

Scheme 1. Carbon Capture and Storage (CCS) and Carbon Capture and Utilization (CCU) climate change mitigation policies.

To reach this objective, CO_2 must first be captured from high concentration sources such as cement plants, thermal power and chemical plants or steel mills (Scheme 2).[3] Indeed, direct air capture (DAC) requires a separation unit to get concentrated CO_2.

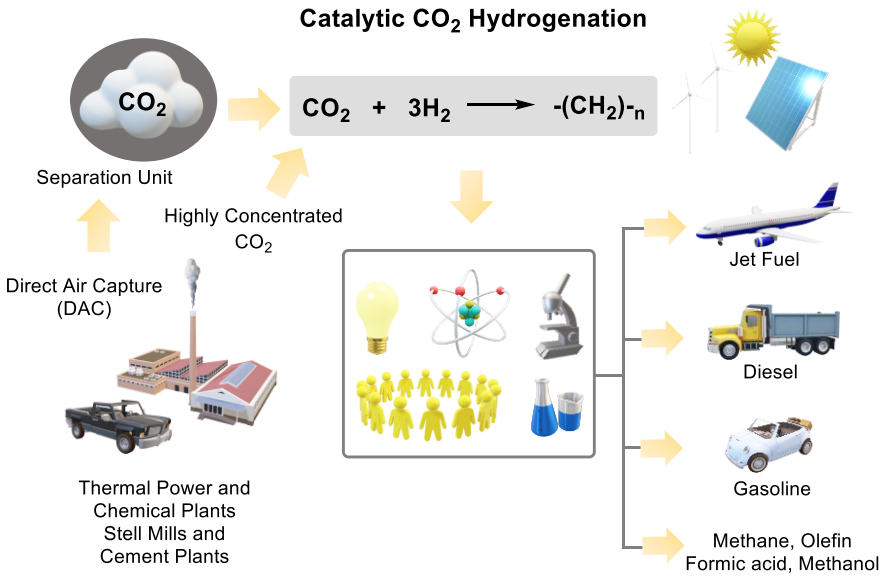

Scheme 2. Recycling of CO_2 as carbon source *via* catalytic hydrogenation to obtain high-added value products.

Once captured, several processes can be used for CO_2 transformations. For instance, its catalytic hydrogenation can provide products such as carbon

monoxide (CO), methane (CH_4), formic acid (HCOOH), methanol (CH_3OH) or hydrocarbons (C_1-C_4 and C_{5+}) that can be used in fuels market as well as in the synthesis of other products.

There are three main pathways for the transformation of CO_2: mineral carbonation into mineral carbonates, chemical conversion and biological conversion.[5] These last pathways can produce high-added value products such as methanol or fuels. For the chemical conversion pathway, thermocatalysis, electrocatalysis and photocatalysis can be employed.[6] In this thesis, we will focus on thermocatalytic transformations of CO_2.

CO_2 is a very stable molecule with an enthalpy of formation (ΔH_f) of -394 kJ·mol^{-1} and for this reason, most reactions involving CO_2 conversion are endothermic. CO_2 can also be transformed directly (without using a catalyst) into products such as urea and salicylic acid, which was obtained from CO_2 in the 19th century.[5]

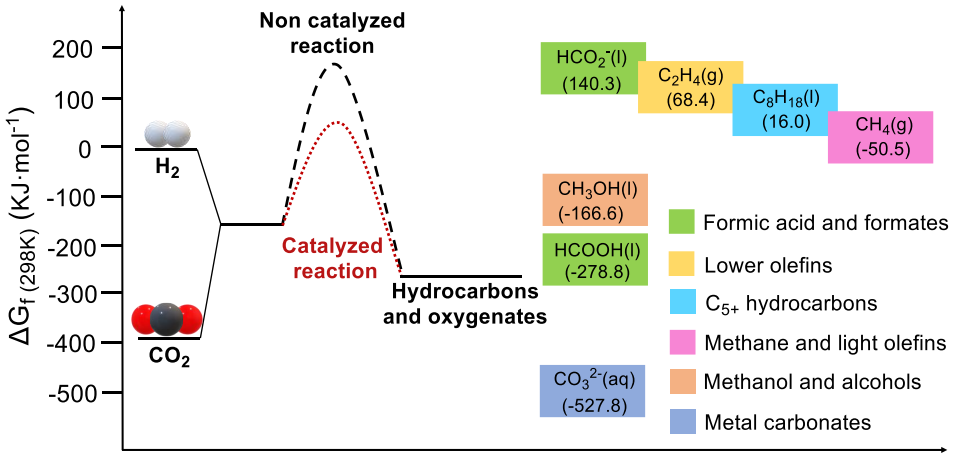

Scheme 3. Gibbs free energies for catalyzed and noncatalyzed CO_2 hydrogenations.

C-oxidation state is one of the key points that can affect reactions of CO_2.[7] It is possible just to incorporate CO_2 into other molecules or use reducing agents to form other products. Using a catalyst, it is possible to decrease the Gibbs free energies of formation (ΔG_f) of different products (Scheme 3) and only inorganic and organic carbonates containing the CO_3^{2-} moiety are more stable than CO_2.[3] The role of the catalyst and additives is usually to activate the CO_2 molecule through the electrophilic character of its C atom.

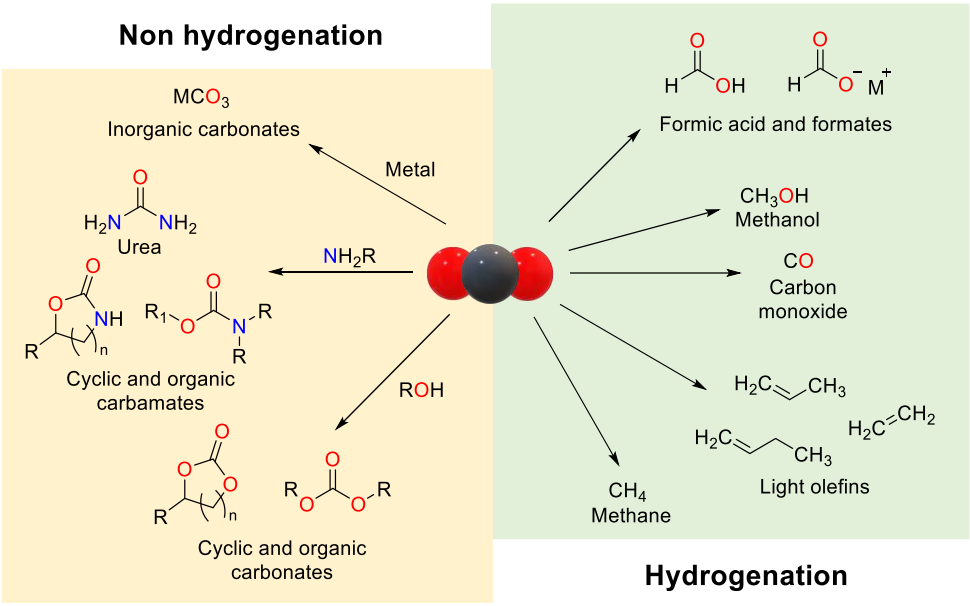

Scheme 4. High-added value products obtained from CO_2.

Two main types of chemical CO_2 transformations can be distinguished to obtain added value products: the processes involving the hydrogenation of CO_2 and those that do not (Scheme 4). Hydrogenation products are going to be the main character of the next section.

For instance, organic carbonates and polycarbonates are important molecules in industry that can be produced from CO_2.[6,8] Alkyl and cyclic carbonates can be obtained directly from the fixation reaction between alcohols or epoxides and CO_2 in the presence of a catalyst. One of the most important carbonates is dimethyl carbonate (DMC), which is mainly used in the production of polycarbonates, but also has applications as solvent in paints and inks and as electrolyte in batteries.[9] As previously mentioned, urea is another product of interest that is obtained by reaction of CO_2 with amines and has applications such as antioxidant in gasoline, pesticides, insecticides and corrosion inhibitors.[7]

Other interesting products that can be obtained from CO_2 are *N*-formamides, carboxylic acids, higher alcohols and other oxygenates.[5,7,8,10,11,12,13,14,15]

For example, *N*-formylation and *N*-alkylation are two processes of importance. They are related as it was suggested that *N*-alkyl formamide might be an intermediate in the synthesis of *N*-methyl amine *via* further

hydrogenation.[16] Formamides are widely used as solvents and medicine components, and are common products in agricultural chemistry.[17]

Moreover, *N*-methylation of amines can produce pharmaceuticals, agrochemicals, dyes, perfumes, among others, and is an important reaction in organic synthesis and chemical industry.[18] Hydrogen[14,19] and hydrosilanes[11,12,13,20] are the most common reductant employed. For *N*-alkylation, homogeneous catalyst based on Ru are the most commonly used,[21] but recently, Pd, Au, Cu, Re and bimetallic heterogeneous[16c,18,22] catalysts were also reported.[23]

The hydrocarboxylation of alkenes and alkynes with CO_2 produce carboxylic acids and constitutes another example of transformation of CO_2 into high-added value products.[24] Carboxylic acids are used in chemical and pharmaceutical industry.[25,26] Most of carboxylic acids are prepared on an industrial scale *via* the aerobic oxidation of hydrocarbons.[27] However, the conditions employed requires the use of expensive reactors. As an alternative, the preparation of carboxylic acids through the formal insertion of CO_2 into a C−H bond is a good option. Ni, Rh and Cu are one of the most employed metals for this reaction.[5,24,28] Due to inert chemical properties of CO_2, the use of additives is indispensable for the reduction. Expensive reductants such as hydrosilanes and organometallic reagents were broadly applied, although hydrogen is also used. To overcome this drawback, it is still necessary to continue investigating in this direction.[28]

In the next section, we will focus on the products derived from the hydrogenation of CO_2.

1.1.2. CO_2 hydrogenation to added-value products

Over the last years, the hydrogenation of CO_2 has become a priority in view of the advances made in H_2 production. Indeed, H_2 was usually obtained by Steam Methane Reforming (SMR), which produces large quantities of CO_2 but the recent progress in the production of H_2 from renewable energies (solar, wind, water electrolysis) offers a great opportunity to transform the CO_2 released from industrial processes into energy carriers in a clean and eco-friendly way.[3,29,30,31]

- **Methanol (MeOH)**

One interesting product that can be produced from CO_2 and H_2 is methanol, which is one of largest scale chemicals produced in the world.[3] It is widely employed as solvent, antifreeze, as raw material to get formaldehyde or other chemicals and so many applications.[29] Conventionally, MeOH was obtained from syngas (since 1965) using the multi-catalyst employed was $Cu/ZnO/Al_2O_3$ under harsh conditions (200-300 ºC and 3.0-5.0 MPa).[32] But, in 1989, Rozovskii et al. discovered that CO_2 could be used in the synthesis of methanol.[33] $Cu/ZnO/Al_2O_3$ also demonstrated to be active for this transformation, which can take place through two reaction pathways: the direct hydrogenation of CO_2 which involves a formate, HCOO* intermediate (eq. 1) or the reverse water-gas shift (RWGS) and CO hydrogenation (eq. 2 and 3) *via* the hydrocarboxyl, COOH* intermediate.

$$CO_2 + 3H_2 \leftrightarrow CH_3OH + H_2O;\ \Delta H^{\circ}_{298\,K} = -49.5\ kJ \cdot mol^{-1} \text{ (eq. 1)}$$

$$CO_2 + H_2 \leftrightarrow CO + H_2O;\ \Delta H^{\circ}_{298\,K} = 41.2\ kJ \cdot mol^{-1} \text{ (eq. 2)}$$

$$CO + 2H_2 \leftrightarrow CH_3OH;\ \Delta H^{\circ}_{298\,K} = -90.5\ kJ \cdot mol^{-1} \text{ (eq. 3)}$$

The mechanism of these reactions was studied using theoretical calculations.[3,29] Thermodynamically, low temperatures and high pressures favor the formation of MeOH due to the exothermic character of this process. As the catalyst for the synthesis of MeOH from syngas is active when CO_2 is use as a C1 source, but also in the RWGS reaction, this results in a lower selectivity to methanol and an increase of the amount of water, which can deactivate the Cu catalyst *via* sintering.[34] Attempts at stabilizing the Cu-based catalysts through the tuning of the metal-support interactions has led to many variations in support and promotor.[35,36,37,38] $ZnO\text{-}ZrO_2$ solid solution catalyst developed by Wan et al. was used on on continuous-flow and reaches 86-91% selectivity to MeOH.[39] Hu et al reported a very active MoS_2 nanosheet catalyst working at lower temperature (180 ºC)[40] and providing a methanol selectivity of 94.3%. Moreover, this catalyst showed high stability, and was active for over 3000 h. The same year, Zeng and coworkers developed a cobalt-based system (Co_4N) for the hydrogenation of CO_2 into MeOH.[41] This catalyst incorporates nitrogen atoms into cobalt nanosheets, which can

adsorb H atoms in the presence of H_2. These species interact with CO_2 to yield HCOO* intermediates. A TOF of 25.6 h^{-1} (3.2 MPa, CO_2/H_2= 1:3, 150°C, 3 h) was reached with high selectivity to MeOH although some formic acid was also obtained.

Cascade systems were also investigated to obtain MeOH. For instance, Chen et al. developed a pair of catalyst (Cu-Cr and Cu/Mo_2C) to produce MeOH through a formate intermediate.[42] A TOF of 4.7 x 10^{-4} s^{-1} was obtained at 135 ºC. Cu/Mo_2C was active in the hydrogenation of CO_2 to methanol and fomic acid and in formate ester hydrogenation. For this process, homogeneous catalysts were also developed over the last years but mainly to obtain mechanistic information.[5]

- **Dimethyl ether (DME)**

Dimethyl ether (DME), which is an excellent diesel fuel substitute, can also be obtained from CO_2. DME is a common byproduct in methanol production formed *via* the dehydration reaction of methanol over solid acid catalysts. This process is mildly exothermic (eq. 4 and eq. 5)[43,44]

$$2CH_3OH \leftrightarrow CH_3OCH_3 + H_2O;\ \Delta H^{\circ}_{298\,K} = -23.4\ kJ \cdot mol^{-1} \text{ (eq. 4)}$$

$$2CO_2 + 6H_2 \leftrightarrow CH_3OCH_3 + 3H_2;\ \Delta H^{\circ}_{298\,K} = -123.0\ kJ \cdot mol^{-1} \text{ (eq. 5)}$$

Then, a dual catalyst is required to first obtain MeOH from CO_2 and later dehydrate MeOH, so direct transformation of CO_2 to DME involves a bifunctional catalyst capable of performing these two reactions simultaneously.[8,29]

For MeOH dehydration, alumina-based materials are the most commonly used. The reactions take place in the range 250-400 ºC and 10-25 bar of pressure. Under these conditions, both reactions are favored and direct synthesis of DME from CO_2 is possible.[8] Under these conditions, methanol conversion ranges from 70% to 85% with high selectivity.[45] Only traces of formaldehyde are observed as a byproduct.

Nevertheless, the physical mixture of γ-Al_2O_3 as solid acid catalyst with $Cu{-}ZnO/Ga_2O_3$ or Cr_2O_3 was reported as catalyst for the direct DME synthesis.[46] The addition of Ga_2O_3 increased the number of active sites

whereas the role of Cr_2O_3 was highly remarkable in increasing intrinsic activity toward DME and methanol synthesis.

H-ZMS-5 is another support present in very active systems for that process.[29,47] H-ZSM-5 zeolite, having both Lewis and stronger Brønsted acid sites than γ-Al_2O_3,[48] showed high activity[49] and excellent water resistance, improving long-term stability during the reaction.[50]

Due to their high catalytic activity and stability, several types of zeolites were evaluated in several types of methanol synthesis catalysts. The combinations of Cu−ZnO−ZrO_2 or Cu−ZnO−Ga_2O_3 as methanol synthesis catalyst and Na-ZSM-5, H-ZSM-5, H-Ga-silicate, or SAPO-34 zeolites were studied extensively.[51] In conjunction with Cu−ZnO−ZrO_2 methanol synthesis catalyst, H-ZSM-5 showed very high DME (60.1%) selectivity at 35% CO_2 conversion.[51b]

- **Carbon monoxide (CO) and methane (CH_4)**

Carbon monoxide (CO) and methane (CH_4) are C1 products that can be obtained from the hydrogenation of CO_2. Syngas can be obtained by dry reforming of methane (DRM) (eq. 6) and RWGS (eq. 7). They are usually two parallel processes, depending on the catalytic materials and reaction conditions. Depending on the process used, different ratios of CO:H_2 are obtained and can be used for the synthesis of different products. For example, the ratio of CO to H_2 1:2 works for methanol synthesis and 1:1 is preferred for hydroformylation.[8] RWGS is sometimes used to readjust the CO:H_2 ratio in the obtained syngas for required applications.

Dry reforming: $\mathrm{CO_2 + CH_4 \leftrightarrow 2CO + 2H_2;\ \Delta H^{\circ}_{298\,K} = 247\ kJ \cdot mol^{-1}}$ (eq. 6)

RWGS: $\mathrm{CO_2 + H_2 \leftrightarrow CO + H_2O;\ \Delta H^{\circ}_{298\,K} = 41\ kJ \cdot mol^{-1}}$ (eq. 7)

RWGS is used in several important industrial processes. This reaction can take place using homogeneous catalysts under mild conditions. However, when heterogeneous catalysts are used, higher temperatures are required (in the range of 200-600 ºC).[8] Non-noble metals are usually employed for this reaction. Cu is one of the most commonly used despite its lower activity than other noble metals, as it presents some advantages such as low-cost, abundance and no poisoning in the presence of CO.[52,53] However, a thermal

stabilizer (such as Fe) is usually required to make copper-based catalysts suitable for high temperature reactions.[8,54]

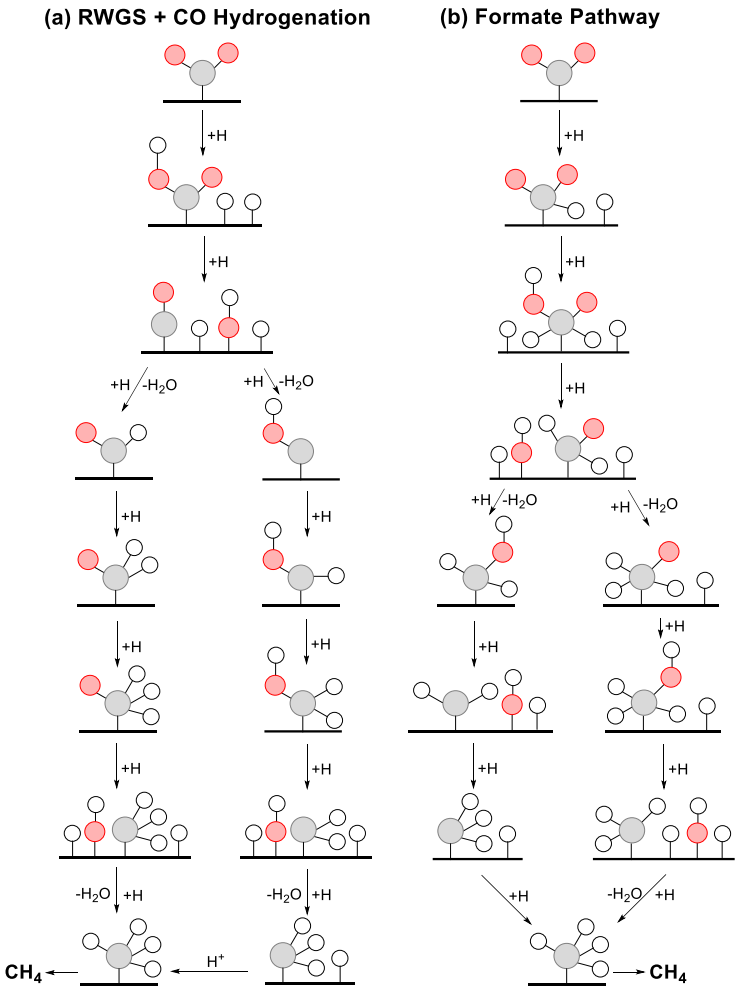

Scheme 5. RWGS pathway (a) and formate pathway (b) for the hydrogeantion of CO_2 to obtain CH_4.

For DRM, Ni is one of the most used metals supported over metal oxides,[8,55,56,57] despite issues of deactivation due to deposition of carbon on the surface of catalysts. By introducing changes in metal-support interactions, the selectivity to CO or CH_4 can be tuned, and the stability of catalysts is improved.[34] For instance, when metal oxides with strong basic centers are used as supports, an increase in stability of the catalysts was observed.[58]

Another possibility to reduce the deactivation by coke deposition is the use of noble metals such as Pd, Pt or Ir.[8,57]

CH_4 is another important molecule that can be obtained from CO_2 and that presents high potential in terms of fuel storage. The methanation reaction was discovered by Sabatier and Senders employing an heterogeneous Ni catalyst and is highly exothermic (eq. 8).[59]

$$CO_2 + 4H_2 \rightarrow CH_4 + 2H_2O;\ \Delta G^{\circ}_{298\,K} = -114\ kJ \cdot mol^{-1} \quad \text{(eq. 8)}$$

For CO_2 methanation, there are two possible pathways: the formate route and the RWGS + CO hydrogenation route (Scheme 5).[3]

Others metals such as Rh, Ru, Pd and Co are used nowadays.[3,34,60] Some auhors reported the dependance of the selectivity on the size of particles. For example, Kwak et al. developed a system based on Ru over Al_2O_3.[61] Depending on the metal loading, cluster size vary and for larger metallic clusters, the selectivity to CH_4 increased (and selectivity for CO is lower). For Ni catalysts over SiO_2, higher metal loading also led to higher selectivity to CH_4.[62] The authors observed that at lower Ni loading, smaller nanoparticles were formed and that less hydrogen was adsorbed resulting in a lower interaction with CO_2.[60f,63] Variations in metal-support interactions and promotors were also studied in this reaction.[3]

- **Light olefins**

The production of light olefins from CO_2 is also an important process. Indeed, these products constitute a very important part of the petrochemical industry production due to their applications in cosmetics, plastics and solvents. The conventional production methods such as steam craking involve high amount of energy waste and production of CO_2. Therefore, a new synthetic routes to obtain light olefins from CO_2 presents high potential. Two processes can be employed for this purpose: MeOH to olefin (MTO) and CO_2-Fisher-Tropsch (CO_2-FT) (Scheme 6).[3,64]

For CO_2-Fisher-Tropsch, Fe-based catalysts are used for both steps (eq. 9 and 10).

$$\text{RWGS: } CO_2 + H_2 \rightarrow CO + H_2O;\ \Delta H^{\circ}_{573\,K} = 38\ kJ \cdot mol^{-1} \quad \text{(eq. 9)}$$

$$\text{FTS: } nCO + (2n+1)H_2 \rightarrow C_nH_{2n+2} + nH_2O;\ \Delta H^{\circ}_{573\,K} = -166\ kJ \cdot mol^{-1} \text{(eq. 10)}$$

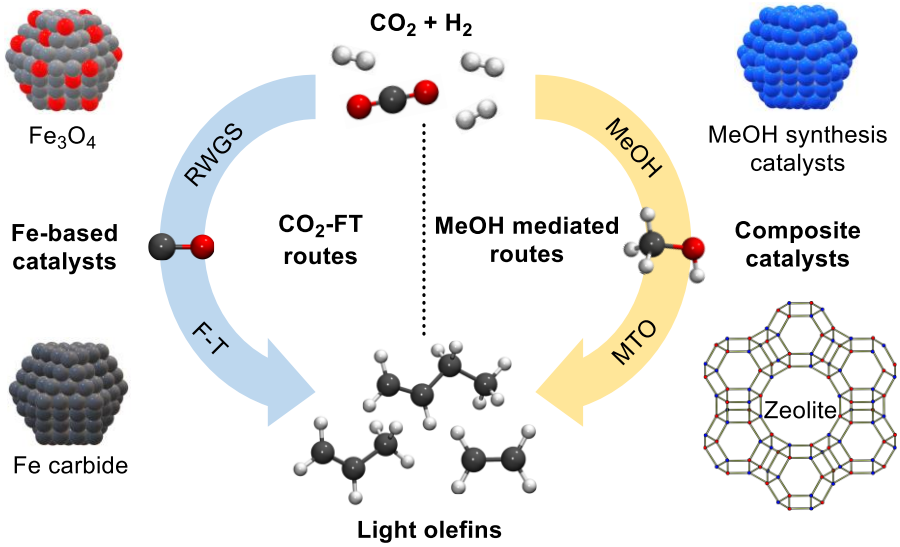

Scheme 6. Catalytic hydrogenation of CO_2 to light olefins following CO_2-FT route (left) and MeOH mediated route (right).

In contrast, the MTO route requires a composite material. The MeOH synthesis from CO_2 is achieved using the type of catalysts previously described, while the second catalyst is usually based on zeolitic materials to provide light olefins from the MeOH previously synthesized. The CO_2-FT process normally takes place at temperatures in the range of 250-300 ºC and the ratio of light olefins (C_2-C_4), medium chain (C_5-C_{10}), heavier hydrocarbons (C_{10}-C_{20}) and waxes (C_{20+}) depends on the catalyst and temperature used.[5,8,54] The formation of fractions with different carbon range are determined by the chain growth mechanism (Anderson-Schulz-Flory (ASF) type distribution).[65] To modulate the selectivity to light olefins using Fe catalysts, some promotors (such as alkali), bimetallic systems (Mn, Cu or Co as second metal) can be used. Variations in the support (carbon based, metal oxides, MOFs) was shown to increase activity and selectivity.[3,8] For CO_2-FT, the selectivity to light olefins is limited by ASF distribution (< 50% of selectivity to light olefins, ≈ 40% CO_2 conversion)[34] while using tandem catalyst, higher selectvities were obtained to light olefins. For example, when bifunctional catalysts using Zn and SAPO zeolites, selectivity to light olefins were increased until ≈ 80% at similar CO_2 conversion.[3,66,67]

To get selective systems for hydrogenation of CO_2 to C_{5+} hydrocarbons (gasolines), hybrid catalysts are commonly employed using Fe and other non-noble metals together with metal oxides or/and zeolites.[3,64,68]

A variety of the main high-added value products can thus be obtained by hydrogenation of CO_2. The work presented in this manuscript deals with another CO_2 hydrogenation process that produces formate.

In next section, we will describe in details the state-of-the-art catalysts for the production of formic acid and formate from CO_2.

1.2. CO_2 transformation into formic acid/formate

Formic acid (FA) and formates constitute another type of high-added value C1 products that can be obtained from the hydrogenation of CO_2.

Formic acid has many applications in industry such as in textiles, paper, pharmaceuticals and is also used as an intermediate in several chemical reactions.[29,69] In recent years, formic acid has gained much interest as a hydrogen storage material.[54] Despite having a low hydrogen content (4.4 wt%, 53 g/l in ambient conditions), it is considered one of the best liquid hydrogen storage and transport options.[47] The current production method consists of two stages, starting with the use of methanol and CO to get methyl formate.[70] Compared to classical synthetic methods, the direct CO_2 hydrogenation present two main advantages: the conversion of the greenhouse CO_2 gas and its utilization in the clean energy cycle of hydrogen, giving rise to CO_2 mediated hydrogen energy cycle (based on storage and release of H_2).[71,72,73]

In this section, thermodynamic aspects and other variables that affect the catalytic hydrogenation of CO_2 into formic acid/formate are introduced, followed by a description of the most efficient catalytic systems in this process.

The hydrogenation of CO_2 to formic acid in the gas phase is not energetically favorable (eq. 11) because it requires a phase change.[8,29,74]

$$H_{2(g)} + CO_{2(g)} \leftrightarrow HCO_2H_{(l)};\ \Delta G = 32.9\ kJ \cdot mol^{-1} \quad \text{(eq. 11)}$$

However, the use of a solvent alters the thermodynamics of the reaction, making it slightly exergonic (eq. 12):

$$H_{2(aq)} + CO_{2(aq)} \leftrightarrow HCO_2H_{(aq)};\ \Delta G < 0\ kJ \cdot mol^{-1}$$ (eq. 12)

The importance of the solvent was investigated (mainly using organometallic complexes as catalytic systems), since it is relevant from the point of view of the solubility of the gases (CO_2 and H_2) and the products. For example, Zhang et al. reported that using a Ru-based system, the reaction is less efficient in non-protic solvents such as THF or toluene than in protic solvents such as alcohols (EtOH and MeOH), or in DMSO.[75] This was attributed to the strong polarity of these solvents, as well as their ability to dissolve large amounts of CO_2. Water is an environmentally benign solvent from the viewpoint of green chemistry[76] and is inexpensive and abundant. It offers certain advantages such as amphoteric behavior in Brønsted sites, high absorption for some gases, and easy separation from apolar compounds. However, it is noteworthy that the solubility of both CO_2 and H_2 revealed much higher in MeOH than in pure water.[77,78,79] In this reaction, both water alone or mixtures of water and another solvent were reported and it was observed that the presence of even small amounts of water in the system can improve the catalytic activity.[80] For instance, Laurenczy and coworkers used DMSO as a solvent and reported the importance of the presence of small amounts of water to reach a TON of 475 with $[RuCl_2(PTA)_4]$ complex (10% H_2O, 100 bar total pressure (CO_2:H_2, 1:1), 50 ºC, 120 h).[81,82] They reported that both solvents were favorable for CO_2 hydrogenation as hydrogen bonds play an important role in stabilizing the formic acid product. Rohmann et al. reported DFT calculations on the nature of this interaction that also revealed the importance of the presence of H_2O.[80]

The use of Ionic Liquids (ILs) as solvent or additive was also reported in the hydrogenation of CO_2 to FA. ILs can indeed interact with both CO_2 (Scheme 7) and the product that is formed although these depend on the nature of their cation and anion. For instance, ILs containing imidazolium as cation (Figure 2) can stabilize formate by formation of an adduct.[83,84,85]

The inclusion of amine group in the alkylic chain of imidazolium can also lead to interactions of the cations with CO_2.[86,87] The effect of different anions was also studied for absorption of CO_2 in these molecules.[88,89,90]

Possible reaction mechanism for the carboxylation of imidazolium acetate by CO_2

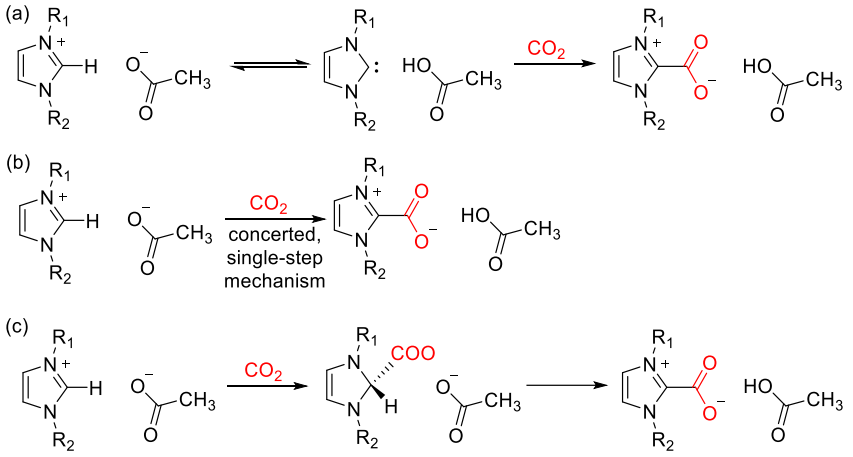

Stabilization of the carboxylation reaction products by an imidazolium-acetate ion pair

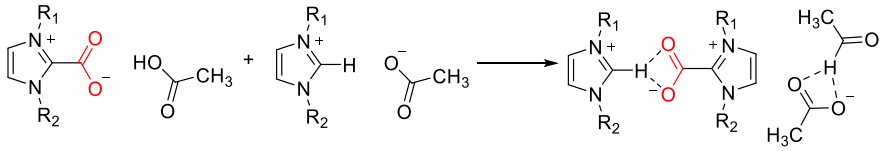

Scheme 7. Possible mechanisms of interactions and stabilization of CO_2 with Imidazolium acetate ILs.

The presence of small amount of water in ILs containing an acetate anion can have an effect on the supramolecular organization of IL, favoring the interaction with CO_2 (Scheme 8) and the stabilization of formic acid.[83,88,91]

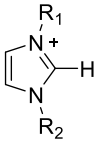

$DMIM^+$: R_1= Me, R_2= Me
$EMIM^+$: R_1= Me, R_2= Et
$PMIM^+$: R_1= Me, R_2= Pr
$BMIM^+$: R_1= Me, R_2=Bu
$EEIM^+$: R_1= Et, R_2= Et

Figure 2. Some of the imidazolium based ILs.

Furthermore, Qadir et al. observed that using a system composed of bimetallic RuFe nanoparticles and ILs with basic and non-basic anions, the selectivity of the hydrogenation of CO_2 could be affected depending on the

properties of the IL used and that different products of interest could be formed.[89]

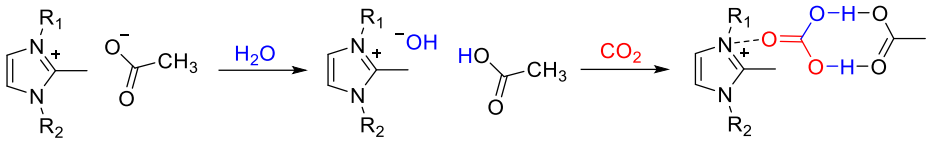

Scheme 8. Possible mechanism of interactions and stabilization of CO_2 with imidazolium acetate ILs in presence of H_2O reported by Dupont and coworkers.[90]

Another factor that energetically favors the reaction is the presence of a base, since under basic conditions, the reaction becomes exothermic (eq. 13).[92,93]

$$H_{2(g)} + CO_{2(g)} + Base_{(aq)} \leftrightarrow HCO^{-}_{2(aq)} + HBase^{+}_{(aq)};\ \Delta G < 0\ kJ \cdot mol^{-1} \quad \text{(eq. 13)}$$

Moreover, the presence of a base also influences the solubility of CO_2, since it is an acidic molecule (a water solution saturated with CO_2 shows a pH of 4 at 20 ºC) that is only slightly soluble in water.[94] The bicarbonates $NaHCO_3$ and $KHCO_3$ are usually used rather than carbonates since in the hydrogenation of carbonates is more complicated than that of bicarbonates because the protonation of carbonate ions was considered to be inferior.[95,96,97] The lower reactivity of the carbonyl group in carbonates compared to CO_2 or bicarbonates makes them proceed in low yields.[98] Formate formation thus depends on the pH of the solution, since increasing the pH, the balance changes from bicarbonate to carbonate, decreasing the yield to formate. Furthermore, the pH of the solution can influence the stability of organometallic hydride species when homogeneous catalysts are used. At pH 6-9, the true substrate of the reaction is not CO_2, but bicarbonate (HCO_3^-) since when CO_2 is dissolved in water, it is in a pH-dependent equilibrium between the HCO_3^- species (pKa_1= 6.35 at 25 ºC) and CO_3^{2-} (pKa_2= 10.33).[94] In contrast, for heterogenous catalysts, the concentration of hydrides mainly depends on the exposed surface of palladium and the degree of oxidation of the nanoparticles.[99] NEt_3 is also commonly used in this reaction.[100] However, the formation of an adduct is one of the main drawbacks and studies were reported a separation of FA from this adduct.[101,102,103]

In the hydrogenation of bicarbonates catalyzed by heterogeneous catalysts, higher efficiency was reported using $KHCO_3$ than $NaHCO_3$. This was

explained by the effect of the cation on the balance between carbonate and bicarbonate and the solubility of bicarbonates ($NaHCO_3$ (0.61 M) <$KHCO_3$ (0.89 M)).[95,96,97]

Another parameter that can influence the reaction is temperature. Conversion of CO_2 to FA is an exothermic reaction, so the rate decreases with increasing temperatures. In terms of selectivity, the reaction between H_2 and CO_2 at high temperatures can lead to the formation of CO and H_2O (RWGS reaction) or the decomposition of FA to CO_2 (CO) and H_2.[104] In addition, at high temperatures, the stability of the formed FA and the low solubility of CO_2 and H_2 can be compromised.[78] Moreover, in somes cases, the decomposition of FA into CO and H_2O can cause the poisoning of the catalyst.[105]

In the hydrogenation of CO_2 under basic conditions or from the direct hydrogenation of carbonates or bicarbonates, the HCO_2^-/HCO_3^- dual system is involved, which presents several advantages in terms of H_2 storage compared to the HCO_2H/CO_2 system[106] considering factors such as the volumetric density of hydrogen.[96]

In next subsections, the most active catalytic systems for the CO_2 hydrogenation to FA and formate are described and classified as a function of their nature (homogeneous, heterogeneized and heterogeneous).

1.2.1. CO_2 hydrogenation to formic acid/formate using homogeneous catalysts

Homogeneous catalysts have been widely studied for the hydrogenation of CO_2 into FA/formate.[8,93,107,108] In this area, the first work was reported by Inoue et al. in 1976.[109] They used a Ru complex bearing PPh_3 phophine ligands. Since then, a number of catalysts based on Ru,[81,103,90,110] Rh,[111] Ir,[112] Pd,[113] Pt,[114] Re,[115] Au[116] were reported.[117] The most relevant homogeneous catalysts reported for this reaction are presented in the next pages.

Some of the most active Ru and Ir systems for the synthesis of free FA from CO_2 are displayed in Figure 3.

In 2012, Leitner and coworkers reported a biphasic system employing ILs to obtain free formic acid.[118] They devised a continuous-flow biphasic system where a $scCO_2$ phase was the extractive mobile phase and an IL phase containing the ([Ru(cod)(methallyl)$_2$]) catalyst and the base (Scheme 9).

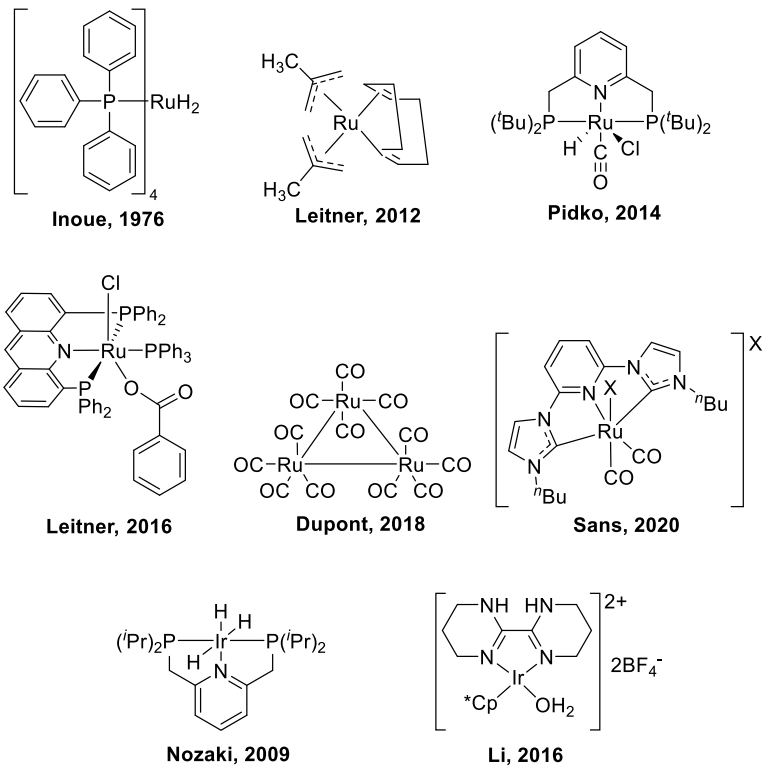

Figure 3. Examples of homogeneous catalysts based on Ru and Ir for the hydrogenation of CO_2 to formic acid/formate.

The ILs contained imidazolium cations with and without amines in the allylic chains and several anions were tested.

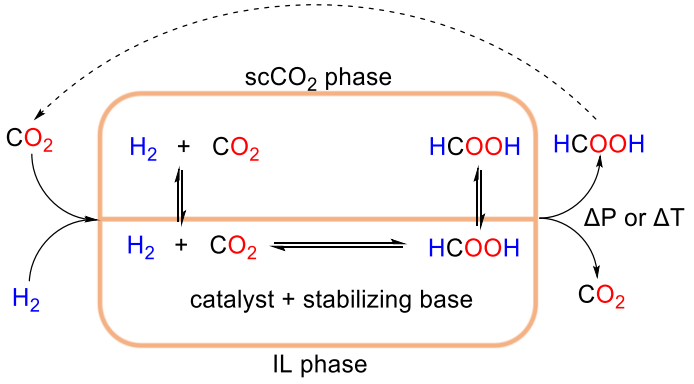

Scheme 9. Continuous-flow system based on two phases: $scCO_2$ and IL for the hydrogenation of CO_2 to formic acid.

Under optimized conditions using an IL containing formate as anion, this system reached a TON of 1968 (50 ºC, 5.0 MPa total pressure, H_2/CO_2= 1:1, 20 h).

In 2016, the same group reported the use of [Ru(Acriphos)(PPh_3)(Cl)($PhCO_2$)] (Acriphos= 4,5-bis(diphenylphosphino) acridine) (Figure 3) as precatalyst for CO_2 hydrogenation under amine base-free conditions.[80] Acriphos is a very robust ligand and confer a very stable pincer-type coordination to metallic center. The authors demonstrated the relevance of the solvent system employed obtaining the best activity when DMSO/H_2O (95:5 v/v) was used. Hydrogen bonds between HCOOH and several solvent molecules act as a driving force for the reaction. High TON of 4200 and TOF of 260 h^{-1} were obtained under optimized conditions (60 ºC, 12.0 MPa total pressure, H_2/CO_2= 2:1, 16 h). Even higher activity was obtained when buffered solutions with acetate were employed, giving a TON of 16000 and TOF of 1000 h^{-1}.

In 2018, another Ru catalyst ($Ru_3(CO)_{12}$) was employed by Dupont and coworkers in the presence of ILs to obtain FA.[90] In this study, imidazolium-based ILs with anions of different nature were employed and 1,2-dimethyl-3-butylimidazolium acetate ([BMMI][OAc]) provided the highest activity with a TON of 17000 (DMSO/H_2O 95:5 v/v, 70 ºC, 3.0 MPa CO_2, 4.0 MPa H_2, 168 h). The ILs played several roles such as the stabilization of the catalyst, the transformation of CO_2 into bicarbonate in solution and buffer the system, shifting the equilibrium toward production of formic acid and stabilizing the pH of the media. To separate FA from IL, the authors tested immobilized ILs onto Merrifield resin. However, the reusability of the catalyst was not efficient due to the leaching of Ru species.

In 2020, Sans and coworkers reported even higher activities using a Ru complex in the presence of [BMMI][OAc].[119] In this work, the authors achieved a robust catalyst that avoids the deactivation that normally pincer-type active ligands suffer during catalysis (Scheme 10). In the presence of [BMMI][OAc], a TON of 162900 was obtained (1,4-dioxane/H_2O 95:5 v/v, 120 ºC, 6.0 MPa total pressure, H_2/CO_2= 1:1, 72 h). When [$Sc(OTf)_3$] was added to the media, a TON of 833800 (1,4-dioxane/H_2O 95:5 v/v, 120 ºC, 6.0 MPa total pressure,

H_2/CO_2= 4.5:1.5, 5 days) was obtained and a TOF of 20600 h^{-1} was reached after 18 h.

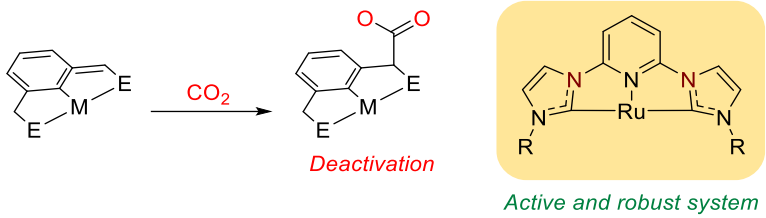

Scheme 10. Robust catalyst with a backbone that avoids deactivation proposed by Sans and coworkers.[119]

Li and coworkers reported a very active Ir catalyst for hydrogenation of CO_2 to FA in aqueous media.[112k] [Cp*Ir(N,N')Cl]Cl (N,N'= 2,2'-bi-1,4,5,6-tetrahydropyrimidine) was employed and a TON over 10000 (40 ºC, 7.6 MPa total pressure, H_2/CO_2= 1:1) with an initial TOF over 13000 h^{-1} (80 ºC, 5.0 MPa total pressure, H_2/CO_2= 1:1). This catalyst was even active when a 2 M solution of $KHCO_3$ was present, giving a TON of 196000 (80 ºC, 5.0 MPa total pressure, H_2/CO_2= 1:1, 24 h).

For the production of formate from CO_2, Nozaki and coworkers developed in 2009 a highly active system based on iridium bearing a pyridine-based PNP-pincer ligand.[112b] Hydrogenation of CO_2 was performed in the presence of a KOH aqueous solution with a small amount of THF, reaching a TON of 3500000 and TOF of 150000 h^{-1} (120 ºC, 6.0 MPa total pressure, H_2/CO_2= 1:1, 48 h).

In 2014, Filonenko et al. also reported a PNP-pincer catalyst for this process.[110j] Interestingly, this system was also active in the dehydrogenation of formate to release H_2. To produce formate, DBU was employed as a base, giving an initial TOF of 1100000 h^{-1} (DMF, 120 ºC, 4.0 MPa total pressure, H_2/CO_2= 3:1, 24 h).

Non-noble and earth-abundant metals (Fe, Co, Ni, Mn) were also explored to obtain formic acid and formate from CO_2.[120] They have several advantages compared with noble metals such as abundance and low cost, which make these first-row transition metals suited to the large-scale production of fuels. Some of the most active examples are described below (Figure 4).

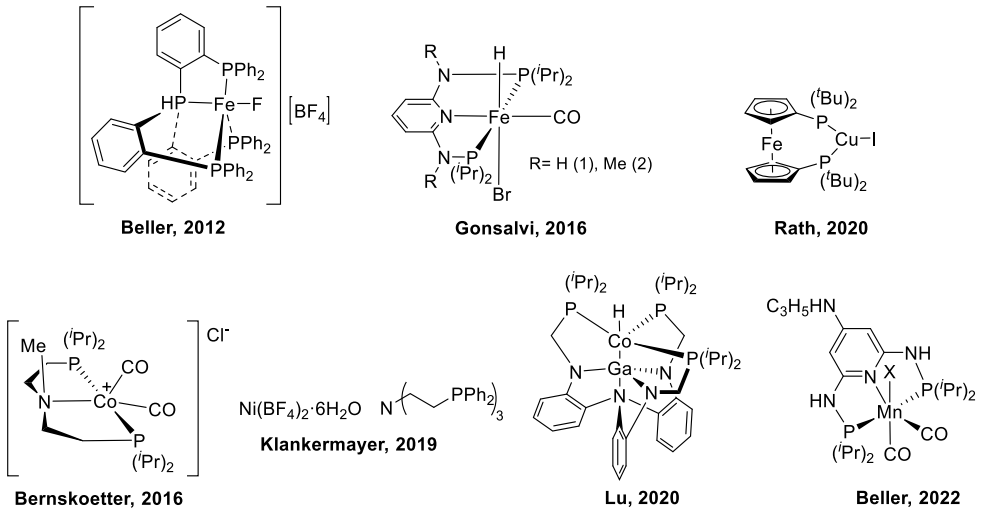

Figure 4. Examples of non-noble metal homogeneous catalysts for hydrogenation of CO_2 to formic acid/formate.

In 2012, Beller and coworkers reported the use of air stable Fe based systems active in this process (Figure 4).[121] The iron(II)-fluoro-tris(2-(diphenylphosphino)phenyl)phosphino]tetrafluoroborate complex was active in the hydrogenation of both CO_2 and bicarbonate. The hydrogenation of CO_2 was investigated in the presence of amines. FA was obtained in the presence of NEt_3 with a TON of 1897 (MeOH, 100 ºC, 6.0 MPa total pressure, H_2/CO_2= 1:1, 20 h). In contrast, when dimethylamine ($HNMe_2$) was used, DMF was obtained as product with a TON of 5104 (MeOH, 100 ºC, CO_2, 20 h). In the absence of CO_2, formate was obtained by direct hydrogenation of $NaHCO_3$ with a TON of 7546 (MeOH, 100 ºC, 6.0 MPa total pressure of H_2, 20 h).

Later, Gonsalvi and coworkers employed Fe(II) hydrido carbonyl complexes coordinated to PNP pincer ligands (Figure 4) to hydrogenate CO_2 and bicarbonate to formate.[122] In the hydrogenation of CO_2, employing system 2 (Figure 4), a TON of 10275 was obtained in the presence of DBU (EtOH, 80 ºC, 0.9 MPa total pressure, H_2/CO_2= 1:1, 21 h). However, for the hydrogenation of $NaHCO_3$ to formate, the catalyst 1 was employed (Figure 4), obtaining a TON of 4560 (H_2O/THF, 4/1, 80 ºC, 0.9 MPa total pressure of H_2, 24 h).

In 2016, Bernskoetter and coworkers synthesized several Co (I) complexes as catalysts for the hydrogenation of CO_2 to formate (Figure 4).[123] The

dicarbonylcobalt complex [(^{iPr}PNP)Co(CO)$_2$]$^+$[Cl$^-$] revealed to be active in the presence of lithium triflate (LiOTf) and DBU, giving a TON of near 30000 (THF, 80 ºC, 7.0 MPa total pressure, H_2/CO_2= 1:1, 48 h).

Klankermayer and coworkers developed a Ni (II)-based catalyst in combination with tailored multidentate ligands.[124] Hydrogenation of CO_2 was carried out in presence of DBU as base and reached a TON of 4650710 (MeCN, 120 ºC, 9.0 MPa total pressure, H_2/CO_2= 6:3, 72 h).

More recently, Lu and coworkers reported the use of a bimetallic Co(I)-Ga system.[125] This low-valent Co center directly bonded to the Ga metalloligand was active in the hydrogenation of CO_2 into formate at room temperature providing a TON of 19200 and an initial TOF of 27000 h^{-1} employing Verkade's base (THF, 20 ºC, 3.4 MPa total pressure, H_2/CO_2= 1:1).

Rath and coworkers reported the utilization of a series of copper(I) complexes bearing the 1,1'-bis(di-tert-butylphosphino) ferrocene ligand to hydrogenate CO_2 to formate in the presence of DBU as a base.[126] [CuI(dtbpf)] revealed particularly active and reached a TON of 106500 (DMF, 80 ºC, 0.2 MPa total pressure, H_2/CO_2= 1:1, 48 h). In this work, DBU did not only act as a base also stabilized the Cu catalyst through coordination under reaction conditions.

Recently, Beller and coworkers reported the use of a Mn complex in the presence of lysine for the hydrogenation of CO_2.[127] Formate was obtained with a TON of 230000 (H_2O:THF 1:1, 115 ºC, 8.0 MPa total pressure, H_2/CO_2= 6:2, 12 h).This catalyst also showed excellent recyclability and could be reused in 10 consecutive cycles with 80% activity remaining, resulting in a remarkable total TON (TTON) of 2050000. The authors attributed the slight decrease in activity to the incomplete catalyst separation between each run rather than catalyst deactivation. It is noteworthy that this system also revealed active in the reverse dehydrogenation reaction with a TON of 29000 (TTON of 600000).

Most of these homogeneous catalysts reached higher activities than heterogeneous systems and provided mechanistic information into the reaction. However, in most cases, no recyclability experiments were reported and the inherent air sensitivity of these catalysts makes them incompatible with the production of formic acid/formate from CO_2 at industrial scale.

1.2.2. CO_2 to formic acid/formate using heterogeneized catalysts

To combine the advantages of homogeneous and heterogeneous catalysts, the anchoring of homogeneous systems onto solid supports to form heterogenized systems is an attractive alternative. Such catalysts were developed for the hydrogenation of CO_2 to formic acid and formate and the most relevant examples are presented in this section.

Monometallic systems based on Ru and Ir are the most employed although Co,[128] Rh[78] and RuMn[129] were also reported. The most common support is silica but in recent years, the interest in carbon-based materials such as covalent organic frameworks (COFs) and porous polymers (POPs) has increased. Indeed, COFs demonstrated to be good materials to capture CO_2 and H_2 gases and the presence of N in their backbones also makes them good support to anchor metallic species.[130,131,132]

Hicks and coworkers reported the anchoring of Ir complexes over modified silica (silica-tethered).[133] They were the first authors to use an organic-inorganic hybrid system based on a bidentate Ir complex with an iminophosphine ligand tethered to mesoporous SBA-15 silica for the hydrogenation of CO_2 to formate (Scheme 11).

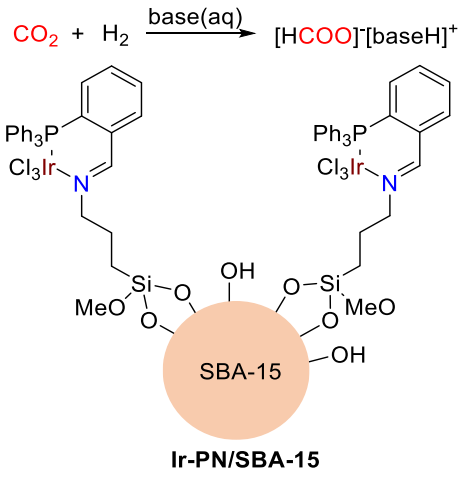

Ir-PN/SBA-15

Scheme 11. SBA-15-tethered Ir catalyst for CO_2 hydrogenation.

For support modification, several organosilanes were employed in which functional groups (amine, iminophosphine and phosphines) were located at the end of the alkyl chain. In terms of activity, when iminophosphine ligand

was employed, a TON of 2800 was reached (60 ºC, 4.0 MPa total pressure, H_2:CO_2= 1:1, 20 h) in the presence of NEt_3. The highest activity was obtained at 120 ºC, 4.0 MPa in 2 h (TOF of 12000 h^{-1}). The bidentate nature of this ligand provided higher stability than monodentate ligands and this catalyst could be reused 10 times by simple filtration. A slight decrease on activity was observed after six cycles due to metal leaching. The same authors developed another system using the same iminophosphine ligand but polyethyleneimine (PEI) was employed instead of silica (Scheme 12).[134]

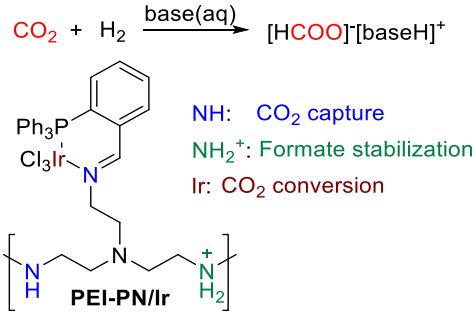

Scheme 12. Multifunctional PEI-tethered Ir catalyst for CO_2 capture and conversion.

This aim of this modification was to obtain direct interaction of CO_2 with the amine group. In this work, the role of H_2O is remarkable since in neat NEt_3, no product is obtained whereas activity was obtained when H_2O was present in 0.4%, and strongly increased with 4% H_2O.

Park et al. also developed an Ir system but using a highly porous 2,2'-bipyridine-based covalent triazine framework (bpy-CTF) as support.[135] In this work, $[IrCp^*Cl_2]_2$ (Cp^*= η^5-pentamethylcyclopentadienyl) was used as metal precursor. The bpy-CTF-[IrCp*Cl]Cl catalyst was described to hydrogenate CO_2 into formate in an aqueous solution containing NEt_3 with high activity (TON of 5000 after 2 h and initial TOF of 5300 h^{-1} after 15 min of reaction) (120 ºC, 8 MPa total pressure H_2:CO_2= 1). However, during recycling experiments, a loss of activity was observed during the 3rd cycle.

Gunasekar et al. reported Ir (III) catalysts supported on heptazine-based Covalent Organic Frameworks (HBFs).[136] $[IrCp^*Cl_2]_2$ was also used as metal precursor in this study and the $[IrCp^*(HBF\text{-}2)Cl_2]$ system revealed highly active with a TON of 6400 and a TOF of 1500 h^{-1} (120 ºC, 8.0 MPa total

pressure, H_2/CO_2= 1) in basic aqueous solution (NEt_3). The loss of activity of this catalyst during recycling experiments was attributed to metal leaching.
Similar results were obtained by Gascon and coworkers using an Ir complex ($[IrCp^*Cl_2]_2$ as metal precursor) anchored onto a Covalent Triazine Framework (CTF) spheres with accessible porosity.[137] In this work, authors employed a solution 0.5 M of $KHCO_3$. With an Ir loading of a 0.2%, a TON of 219 (90 ºC, 2.0 MPa total pressure, H_2/CO_2= 1, 2 h) was reached. Higher activity was measured when $KHCO_3$ was used as base (compared to KOH), which confirmed that the reaction was taking place through the hydrogenation of the bicarbonate. This catalyst was recycled four times with no decreasing on the activity. Interestingly, they also study the activity of this catalyst in the dehydrogenation of formic acid and obtained good activity (TOF of 800 h^{-1} at 80 ºC, 2 wt% Ir loading and 3 M aqueous solution of FA).
Gunasekar et al. obtained a highly active system based on Ir ($[IrCp^*Cl_2]_2$ as metal precursor) and a porous organic framework functionalized with *N*-heterocyclic carbene monomers (Ir-NHC-CTF).[138] This system was highly active with TONs up to 24300 (120 ºC, 8.0 MPa total pressure, H_2/CO_2= 1, 15 h) and TOF of 16000 h^{-1} (120 ºC, 8.0 MPa total pressure, H_2/CO_2= 1, 0.25 h). In terms of recyclability, a decrease of activity was observed due to metal leaching. The same authors developed other Rh (III) and Ir (III) systems based on two- and three-dimensional Bipyridine-based Covalent Triazine Frameworks (bpy-CTF) as supports.[139] For both metals, Cp* based complexes were employed. Ir provided higher activity than Rh with a TON of 5000 (Ir1.4@bpy-CTF400) for Ir and 1410 for Rh (Rh1.7@bpy-CTF400) (1 M NEt_3 aqueous solution, 120 ºC, 8.0 MPa total pressure, H_2/CO_2= 1, 2 h). Deactivation of the catalyst occurred after several cycles. These authors used DFT methods to determine the origin of leaching and concluded that interactions between N from the support with H_2 molecule during heterolysis of this molecule was the main factor that promoted the Ir-N bond dissociation. To overcome this deactivation issue, the same authors used bpy-CTF Ir and Ru catalysts bearing oxyanionic ligands such as acetylacetonate (acac), carboxylate and bicarbonate to block the interaction of H_2 with N from support.[140] These ligands can intercept the proton transfer and facilitates the heterolysis of H_2. A TON of 21180 (3 M NEt_3 aqueous solution, 120 ºC,

8.0 MPa total pressure, H_2/CO_2= 1, 10 h) was reached using the [bpy-CTF-Ru(acac)$_2$]Cl system. This catalyst was tested in recycling experiments using 1 and 3 M NEt_3 aqueous solution and in both cases, no loss of activity was observed after 4 cycles.

The same authors reported the first phenanthroline-based porous organic polymer (phen-POP) for the anchoring of Ir ($IrCl_3$ as metal precursor).[141] A TON value of 14400 was reached (1 M NEt_3, 140 ºC, 8.0 MPa total pressure, H_2/CO_2= 1, 24 h) with an initial TOF of 40000 h^{-1} after 10 minutes of reaction. Furthermore, this system showed good recyclability since no loss of activity was observed after several runs.

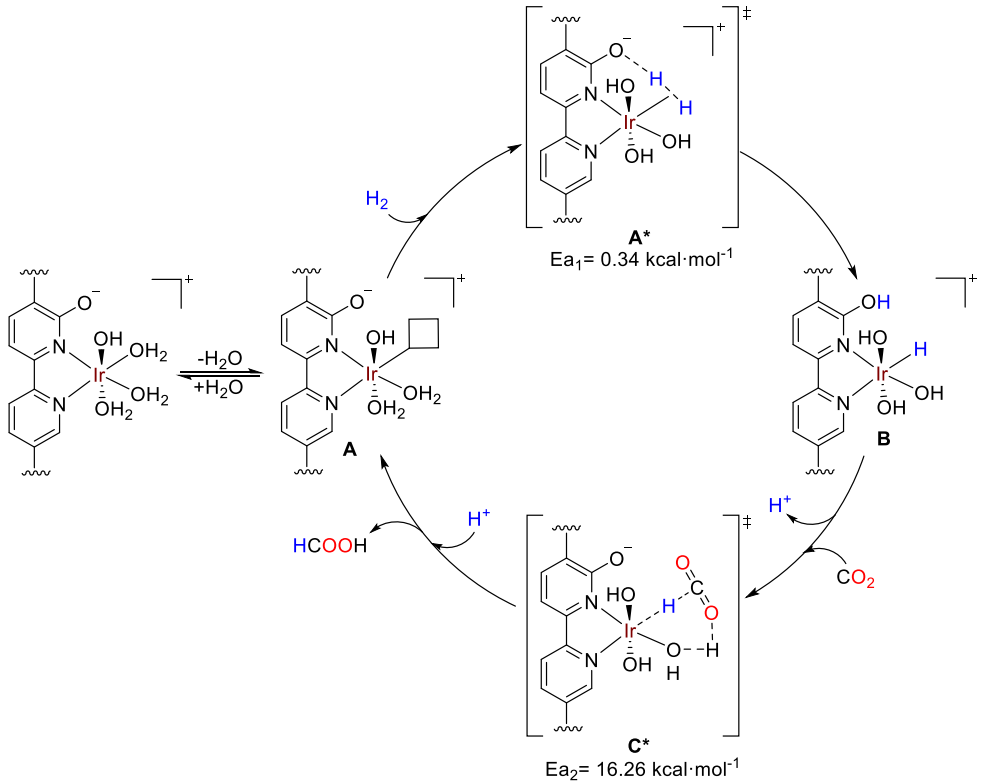

Scheme 13. Proposed mechanism for the hydrogenation of CO_2 by mbpyOH-[IrIII]-UiO catalyst.

Kuwahara et al. reported a poly(ethyleneimine)-tethered Ir-iminophosphine complex (Ir-PN-PEI) immobilized on titanate nanotubes (TNTs) with Na^+, Ir-PN-PEI@TNT(Na^+).[142] They use a 0.1 M aqueous solution of NaOH and obtained a TON of 1012 (140 ºC, 2.0 MPa total pressure, H_2/CO_2= 1, 20 h).

Several catalysts were employed in recyclability, obtaining the best results with Ir-PN-PEI@TNT(Na^+) although loss of was observed after first and attributed to the dissolution of PEI and agglomeration of Ir active sites.

An et al. reported a system based on Ir immobilized on Metal-Organic Frameworks (MOFs).[112e] They obtained a highly active system, mbpyOH-[Ir^{III}]-UiO, (TON of 6149, TOF of 120 h^{-1}) under mild conditions using a condensing chamber of a Soxhlet extract (1 M $NaHCO_3$, 85 ºC, 0.1 MPa total pressure, H_2/CO_2= 1, 15 h). Mechanistic studies by DFT and deuterations were carried out to understand the mechanism of reaction (Scheme 13). The transitions states were calculated for H_2 heterolysis (A*) and proton−hydride transfer (C*). The proton−hydride transfer to be the rate-determining step, which is in accordance of the H/D kinetic isotope effects (KIEs).

Copéret and coworkers immobilized Nozaki Ir-based catalyst over post-functionalized silica beads modified with an organosilane containing a propyl azide group (Scheme 14).[143] This system was highly active and provided a TON of 28000 (1 M 1,8-diazabicyclo[5.4.0]undec-7-ene (DBU) solution in DMF, 150 ºC, 5.0 MPa total pressure, H_2/CO_2= 1, 24 h). In terms of recyclability, this catalyst showed a loss of activity after a recycling experiment (18600) although leaching was discarded.

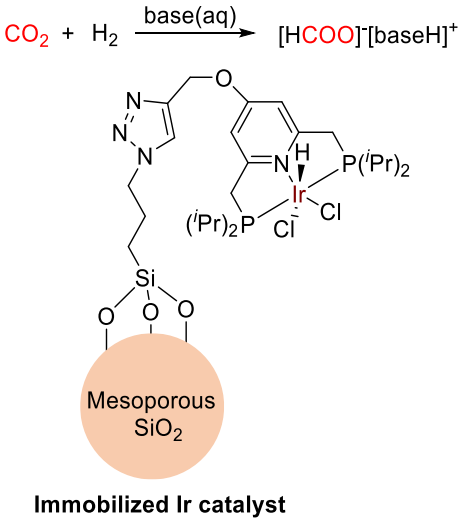

Scheme 14. Ir catalyst for CO_2 hydrogenation.

Urakawa and coworkers developed a system for the hydrogenation of CO_2 to FA and methyl formate in continuous flow at high temperatures (100-180 ºC) and pressure (300 bar).[144] The Ir complex $[IrCp^*Cl_2]_2$ was immobilized in a covalent triazine framework (CTF and depending on the reactant mixture, different products were obtained. When a mixture of CO_2 + H_2 + MeOH (4:4:1 ratio) was reacted at 100 ºC, total selectivity to methyl formate (MF) was observed with a TOF of 0.85 h^{-1}. Increasing temperature, CO was also detected, but TOF for MF increased (3.03 h^{-1}). Using CO_2 + H_2 + H_2O at 100 ºC, a complete shift in selectivity to FA (TOF of 0.23 h^{-1}) was described and when in the presence of a base (CO_2 + H_2 + NEt_3) at 100 ºC, only formate (TOF of 1.61 h^{-1}) was obtained. If the temperature was increased until 180 ºC, CO was also observed. The CO detected could be formed *via* the RWGS reaction or by decomposition of MF or FA. This system was stable under working conditions during several days.

More recently, Oh et al. developed a single atom catalyst based on Ir embedded into a Zeolitic Imidazolate Frameworks (Ir-NHC@ZIF-11).[145] This system provided high TONs comparable to that obtained with an homogeneous Ir-NHC complex (TON 38 196). The TON obtained in this work for the hydrogenation of CO_2 to formate reached 30807 (1 M KOH, 150 ºC, 6.0 MPa total pressure, H_2/CO_2= 1, 24 h).

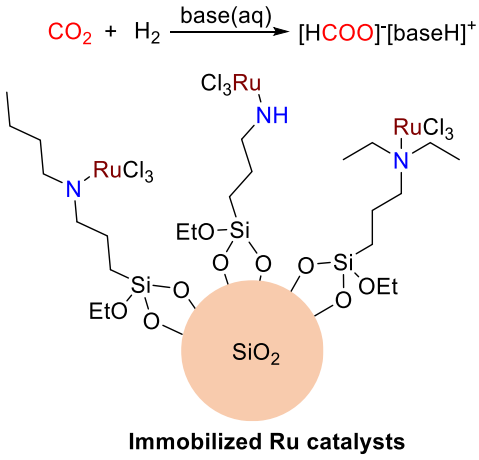

Scheme 15. Ru systems supported over silica modified with different organosilanes containing amine groups for CO_2 hydrogenation.

Ruthenium is another common metal for the hydrogenation of CO_2 to FA/formate and modified silica and carbon-based supports are mainly used. Zheng and coworkers developed a series of Ru systems supported over silica modified with different organosilanes containing amine groups (primary, secondary and tertiary) at the end of the chain (Scheme 15).[75]

PPh_3 was added as an additive to the catalytic system in a ratio 10:1 respect to Ru with the aim of improve activity. NEt_3 was used as base in ethanol. In this study, $scCO_2$ or expanded CO_2 were used to obtain formate with a TOF of 1384 h^{-1} (80 ºC, 16.0 MPa total pressure, H_2= 4.0; $scCO_2$, PPh_3:Ru= 10:1, 1 h). The same authors later reported variations of this system including modification of the support,[146,147,148] and of the ligand[149] employed as additive.

Zhang et al. reported another series of Ru catalysts immobilized over modified silica support.[87] An organosilane with a thioacetamide was employed and PPh_3 was used as additive (Scheme 16).

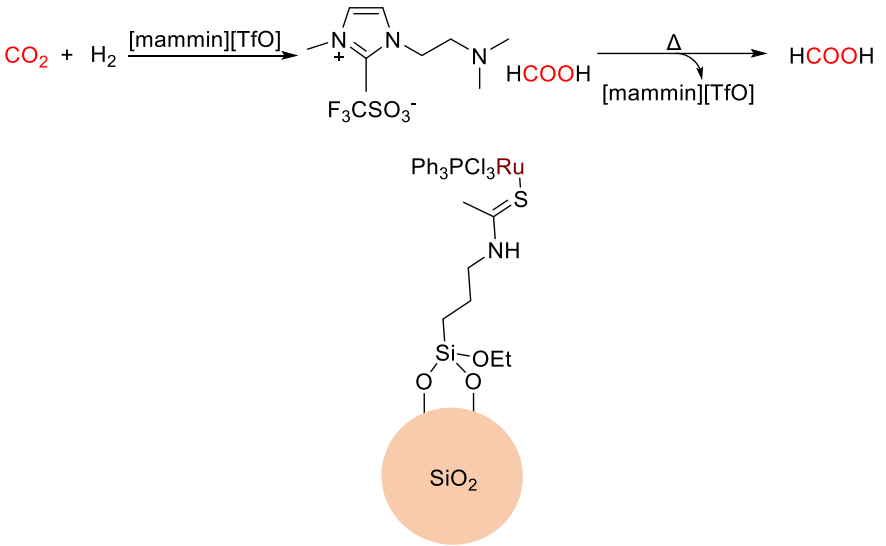

"Si"-$(CH_2)_3$-NH$(CSCH_3)$-$RuCl_3$-PPh_3

Scheme 16. Ru catalyst immobilized over modified silica support for hydrogenation of CO_2.

One of the most relevant part of this work was the use of Ionic Liquids (ILs). They synthetized the new IL 1-(*N*,*N*-dimethylaminoethyl)-2,3-dimethylimidazolium trifluoromethanesulfonate ([mammim][TfO]) bearing a

tertiary amine group which forms a salt with FA and make very easy its recovery from the catalytic mixture (Scheme 17).

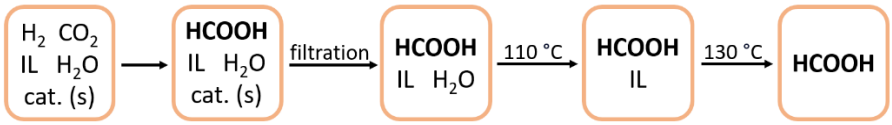

Scheme 17. Recovery of pure FA from reaction media through IL.

A TON of 206 and TOF of 103 h^{-1} were reached (H_2O as solvent, 60 ºC, 18.0 MPa total pressure, H_2/CO_2= 1, 2 h). Catalyst and IL could be recycled four times and no loss of activity was observed.

One year later, the same authors reported a similar system using a diamine functionalized IL, 1,3-di(*N,N*-dimethylaminoethyl)-2-methylimidazoliummethylimidazolium trifluoromethanesulfonate ([DAMI][TfO]) and could obtain two moles of formic acid per mole of IL in each reaction cycle.[86] Using the same separation process, they obtained a TON of 1840 (TOF 920 h^{-1}) that was higher than in their previous work (H_2O as solvent, 80 ºC, 18.0 MPa total pressure, H_2/CO_2= 1, 2 h). Other authors also used ILs with immobilized Ru systems.[150]

Carbon-based support were also employed for the immobilization of Ru in this process. For instance, Yhang et al. employed a Tröger's base-derived microporous organic polymer.[151] Using PPh_3 as additive, this sytem reached a TON of 2254 (NEt_3, 40 ºC, 12.0 MPa total pressure, H_2/CO_2= 1, 24 h). A TON of 2179 was obtained after reusing the catalyst three times, demonstrating the good stability of this catalyst.

In 2019, Gunasekar et al. immobilized Ru catalysts over carbon-based materials.[152] The bipyridinefunctionalized covalent triazine framework was used to produce the [bpy-CTF-$RuCl_3$] catalyst that revealed highly active and provided a TON of 20000 (NEt_3,120 ºC, 8 MPa total pressure H_2:CO_2= 1, 2.5 h and an initial TOF of 38800 after 15 min of reaction. This system was much more active than its Ir analogue.[135] This Ru-based was efficiently recycled (stable TON even after 5 cycles) and was air stable, which allow the scale-up of this system and its use in a pilot-scale production.

MOFs,[153] polymers[154,155] and other supports[156] were also employed for hydrogenation of CO_2 to formate in basic media.

To conclude, heterogeneized catalysts represent a good option in terms of activity and recyclability and could constitute a promising type of catalysts for production of FA/formate from hydrogenation of CO_2 at large-scale in the future.

1.2.3. Hydrogenation of CO_2 to formic acid/formate using heterogeneous catalysts

Heterogeneous catalysts have been widely applied for CO_2/bicarbonates hydrogenation to FA/formates.[64,69,157,158,159]

The first example of heterogeneous system for the hydrogenation of $KHCO_3$ was reported by Bredig and Carter using Pd black in 1914.[160] Later, RANEY® Ni catalyst developed by Farlow et al. was employed for hydrogenate CO_2 to formate using an amine as base.[161]

More recently, the use of nanometric or even sub-nanometric catalysts have caused great improvements in this field.[162,163] Indeed, nanometric catalysts largely improved the atom economy of these processes due to the higher surface area of the catalysts. Moreover, the support is another very important component of the system that can be modulated.[130] These nanometric metal phases tend to agglomerate under catalytic conditions and as such, their stabilization through interactions with the support is needed. Therefore, the fine tuning of the support properties together with the development of appropriate synthetic methodologies for the active metal nanoparticles are required to reach high activity and stability. Nowadays, despite the large number of heterogeneous catalysts that have been developed for the hydrogenation of CO_2 into formic acid/formates, their activities remain far from those displayed by homogeneous species.

Preti et al. prepared gold catalysts for the hydrogenation of CO_2 into FA in the presence of NEt_3 (Scheme 18).[100] Using black gold and commercial Au/TiO_2 (AUROlite), a continuous production process using a solventless system was used during 37 days. They obtained the $[HCOO]^-[NHEt_3]^+$ adduct and isolated FA through an amine-exchange method using the high-boiling point hexylamine. One year later, the same authors employed syngas (mixture of H_2, CO and CO_2) to get formic acid employing these Au-based catalysts.[164]

Filonenko et al. developed an Au/Al_2O_3 system and compared the performance of unsupported and supported Au NPs, revealing the

importance of metal-support interactions (Scheme 18).[165] The TON obtained was up to 215 (EtOH, 4.0 MPa, CO_2:H_2= 1:1, 70 ºC, 20 h), which was higher than that reached with other Au NPs.[166]

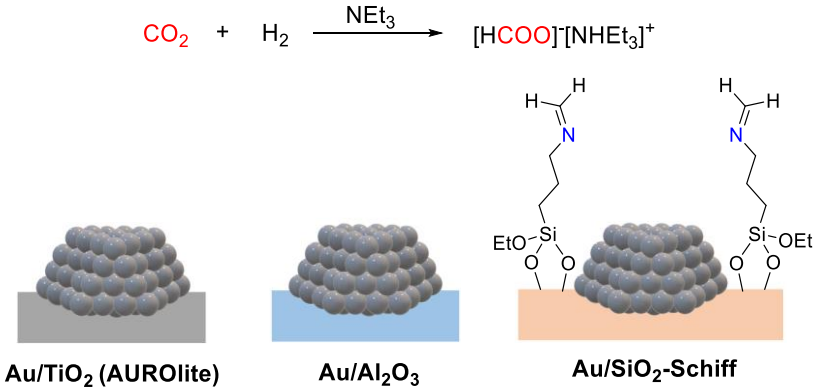

Scheme 18. Gold catalysts reported for the hydrogenation of CO_2.

Liu et al. developed a highly active catalyst based on Au NPs deposited over Schiff-base-modified SiO_2 reaching a TON of 14470 (MeOH/H_2O (4/1), NEt_3, 8.0 MPa, CO_2= 30, H_2= 50, 90 ºC, 12 h) (Scheme 18).[116] These authors carried out DFT calculations and showed that the nitrogen groups on the support can increase the catalyst activity *via* electron donation to Au. CO_2 was captured in solution by the amine (NEt_3) and activated over the surface as a carbamate zwitterion by the Schiff base which was anchored to the support.

Several examples of copper catalysts were also reported to directly obtain FA from CO_2 (Scheme 19). In 2017, Chiang et al. developed a Cu/$CuCr_2O_4$ system for both FA and MeOH synthesis in a fixed-bed reactor.[167] Although deactivation of the catalyst by agglomeration was observed, they obtained a high CO_2 conversion (14.6%) with a selectivity/yield to FA of 87.8/12.8% with a TON of 4.19 and TOF of 0.84 h^{-1}. The other product obtained was MeOH. Later, the same authors reported the Cu/ZnO/Al_2O_3 system and obtained similar results.[168] The conversion of CO_2 was 13.1%, with a HCOOH selectivity of 59.6% and yield of 7.6% (the other product obtained was also MeOH). Reymond et al. also studied a Cu-based catalysts to obtain FA under flow conditions through a two-step process with methyl formate as intermediate.[169] In a first step, Cu/ZnO/Al_2O_3 produces MeOH (260 ºC) and

formate which together using a 1 wt% Ag/Al_2O_3 catalyst produces methyl formate (140 ºC). Then, a resine (Amberlyst 15) was used as a third catalyst to produce both FA, and MeOH.

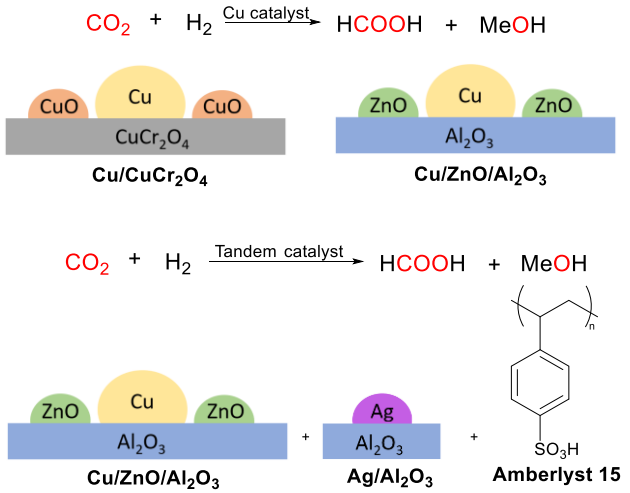

Scheme 19. Reported catalytic systems for the hydrogenation of CO_2.

Ruthenium is one of the most used metals for hydrogenation of CO_2 to formic acid (Figure 5). Hao et al. employed Ru NPs over γ-Al_2O_3 where Ru-OH species was identified as the active species.[170] However, at high Ru loading and pH, RuO_2 is formed, exhibiting low activity in catalysis.

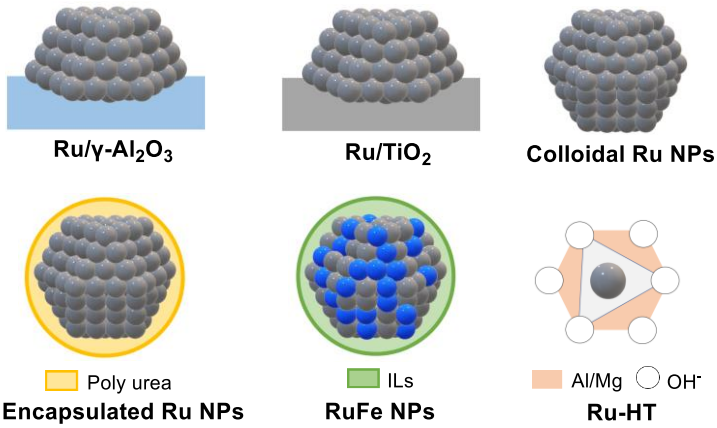

Figure 5. Ruthenium based catalysts for hydrogenation of CO_2.

The authors compared various supports and Al_2O_3 provided the best results with a TON of 91 was obtained (EtOH, 5 MPa H_2, 8.5 MPa CO_2, 80 ºC, 1 h)

when NEt_3 was employed as additive. Increasing the pH to 12 increased the TON (116) of the catalyst. Other systems based on Ru/γ-Al_2O_3 and γ-Al_2O_3 nanorods were reported.[171,172] For instance, Zhang et al. employed a system with PPh_3 as additive to improve the activity due to the donating of electron from phosphine to Ru centers.[173] A PPh_3:Ru ratio of 9:1 was employed reaching a TOF of 751 h^{-1} (NEt_3 in EtOH, 12.0 MPa, CO_2:H_2= 1:1, 80 ºC, 1 h). Other metal oxides as support were also employed. Srivastava and coworkers employed TiO_2 in several studies.[174,175] When 1 wt% Ru was employed, higher dispersion and TON were obtained. The incorporation of ionic liquids with two amine groups per molecule also enhanced activity with a TON reaching at 23360 and TOF of 4670 h^{-1} (H_2O, 4.0 MPa, CO_2:H_2= 1:1, 80 ºC, 5 h).[174] This catalyst was reused in 10 cycles, with only a slight loss of activity due to leaching and agglomeration of Ru species. The same authors varied other parameters such as the structure of TiO_2 and the impregnation method obtaining TONs up to 19050 and TOF of 3811 h^{-1}. In terms of recyclability, the best system was reused for eight cycles and only a slight loss of activity was detected due to the agglomeration of monometallic Ru particles.[175] *In-situ* generated colloidal Ru NPs in these ILs were also tested without support, resulting in highly active systems.[176,177] In contrast, Ru NPs system anchored onto montmorillonite as support in the presence of the same ILs provided lower TON values.[178] Kabra et al. also employed ILs with a system of poly-urea encapsulated Ru catalyst under supercritical conditions.[179] A TOF value of 11900 h^{-1} was reached (14.4 MPa, CO_2:H_2= 1:1, pressure at reaction temperature ($scCO_2$), 70 ºC, 4 h). This system could be recycled twice although a slight decrease in activity was observed.

Dupont and coworkers also employed bimetallic RuFe NPs in ILs for the catalytic hydrogenation of CO_2.[89] Depending on the nature of the anion employed, the selectivity of CO_2 hydrogenation could be shifted. If non basic IL anions were employed, such as in [BMI][NTf_2], the reaction was selective to heavy hydrocarbons (up to C_{21} at 150 ºC). However, if [BMI][OAc] was employed, FA was obtained with a TON of 400 calculated from Ru surface atoms (MeOH/H_2O (5/1), 6.0 MPa, CO_2:H_2= 1:1, 60 ºC, 24 h).

Maru et al. reported a Ru-Hydrotalcite (Ru-HT) catalyst with Ru hydroxide species incorporated into HT framework.[180] TON values up to 11389 were

reached (DMSO/H_2O (78/1), 3.0 MPa, CO_2:H_2= 1:2, 60 ºC, 17 h), which constitute another example of very high active system for this transformation without the use of additive.

Very recently, Leitner and co-worked reported a Ru-based catalyst supported over imidazolium-based SILP for the hydrogenation of CO_2 into formate in the presence of NEt_3,[181] obtaining excellent productivity with TONs up to 16100 at an initial TOF of 1430 h^{-1}.

Apart from these metals, Pd is the most used and numerous studies were reported.

In 2014, Lee et al. employed a mesoporous graphitic carbon nitride (Pd/*mpg*-C_3N_4) as support.[73] Using this catalyst in the CO_2 hydrogenation reaction, a TON of 106 was reached (NEt_3, 150 ºC, 4.0 MPa total pressure, H_2/CO_2= 2:1, 24 h). This system will be further detailed in Section 1.3.1. as this catalyst was the first example of heterogeneous system which was active for both hydrogen storage and release using FA obtained by CO_2.

In 2015, Nguyen et al. used a bimetallic PdNi alloy supported over carbon nanotube-graphene (CNT-GR) for the hydrogenation of CO_2 to FA without additive.[182] A TON of 6.4 was obtained by this catalyst (40 ºC, 5.0 MPa total pressure, H_2/CO_2= 1:1, 15 h).

In 2016, Park et al. developed the first system for the direct hydrogenation of CO_2 to FA under neutral conditions, using Pd NPs anchored onto graphitic carbon nitride (*g*-C_3N_4).[183] The authors observed a dependence between particle size and TOF. With the smallest Pd NPs size, the highest TOF was reached. However, a decrease in activity was observed after six cycles and was attributed to the oxidation of Pd. Pérez-Ramírez and coworkers also employed *g*-C_3N_4 as support for their Pd-based system.[184] Modifications of the support were carried out to maximize edge-defect carrier and introduce amino groups able to activate CO_2 by different post-treatments: thermal exfoliation of bulk carbon nitride (BCN) to obtain exfoliated carbon nitride (ECN), hard templating to form mesoporosity (MCN) and copolymerizing with 2,4,6-triaminopyridine (C-enriched ECN). Under optimized conditions, the TOF obtained was 2.4 h^{-1} for the Pd/ECN-1-h (H_2O, 5.0 MPa, CO_2:H_2= 1:1, 40 ºC, 16 h). This catalyst could be recycled several times without loss of activity using a pre-treatment (heating at 473 K, 1.5 h, under He flow) to clean

the catalyst surface. Another system based on carbon of support was developed by Wu et al. with Pd NPs over carbon (Pd/C).[85] In this work, FA was obtained employing 1-butyl-3-methylimidazolium acetate, [BMI][OAc]) as IL under mild conditions. A TON of 594 was reached under optimal conditions (H_2O, 8.0 MPa, CO_2= 50, H_2= 30, 40 ºC, 24 h). This catalyst was robust and could be reused during five cycles with no loss of activity. NMR studies revealed the presence of an intermediate in which CO_2 is interacting with C2 of the IL imidazolium cation that indicated the activation of CO_2 by [BMI][OAc]. Moreover, they reported the stabilization of the product through H-bonding between FA and OAc from IL (Scheme 20).

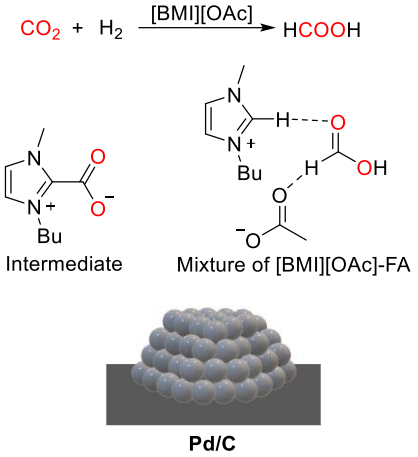

Scheme 20. Intermediate of CO_2 interaction with [BMI][OAc] and stabilization of HCOOH by IL in the hydrogenation of CO_2 with Pd/C catalyst.

Palladium was also used for the CO_2 hydrogenation into formate. In 1988, Wiener et al. employed this Pd over activated carbon to obtain formate from bicarbonates under mild conditions of temperature and pressure.[185] Higher amount of formate was obtained when K^+ was the cation (5.8 M of HCOOK *vs.* 2.5 M of HCOONa). González et al. also employed Pd/C as catalyst and measured an initial rate (mmol $NaHCO_3 \cdot g_{cat}^{-1} \cdot h^{-1}$) of 3.5.[186] This catalyst was stable for three cycles and a small decreasing on the activity was observed during the fourth run.

In 2016, Zhang and coworkers developed a system based on Pd NPs over mesoporous graphitic carbon nitride (*mpg*-C_3N_4) that reached a TON of 6595 (4 M $KHCO_3$, 80 ºC, 60 bar H_2, 1.5 h).[187] This catalytic system was active for

both hydrogenation and dehydrogenation of CO_2 and will be detailed in the last section of this chapter. A year later, Zhao et al. used Pd NPs deposited in the core of interfacially cross-linked reverse micelles (ICRMs) for CO_2 and bicarbonates hydrogenation.[188] Quaternary ammonium-based surfactants can interact with bicarbonates while tertiary amine-based surfactants are most relevant for CO_2 hydrogenation. For bicarbonate hydrogenation (in the absence of gas CO_2), the TON obtained was 580 ($NaHCO_3$ solution in 1,4-dioxane/D_2O (3/2), 4.0 MPa H_2, r.t., 8 h). However, for CO_2 hydrogenation, a lower TON value of 250 was reached (NEt_3, 1,4-dioxane/D_2O (3/2), 8.0 MPa, CO_2:H_2= 1:1, 40 ºC, 20 h). No recycling experiment was reported. Gai and coworkers employed a palladium catalyst over chitin.[104] This support contains both nitrogen and acetamide groups, which serve as chelating sites for metal NPs deposition. A TOF of 257 h^{-1} was obtained after 1 h (Na_2CO_3 aqueous solution, 4.0 MPa, CO_2:H_2= 1:1, 60 ºC). This catalyst could be recycled five times with a slight decrease in activity. Another Pd system using an enriched nitrogen support was reported by Liang and coworkers.[189] This Schiff base modified graphitic carbon nitride provided an active catalytic system for hydrogenation of CO_2 in presence of NEt_3. A TOF of 98.9 h^{-1} was obtained after 2 h (EtOH, 7.0 MPa, CO_2:H_2= 1:1, 110 ºC). Shao et al. synthesized Pd NPs over porous organic polymer containing amide and pyridine functional groups (AP-POP).[190] The pyridine groups served to modulate the electronic properties of Pd. NEt_3 was added as additive and a TON of 1262 was reached (respect to the total Pd) (H_2O, 8.0 MPa, CO_2:H_2= 1:1, 80 ºC, 12 h). This system was also robust and could be used in five cycles with no loss of activity. Examples of Pd catalysts supported over metal oxides were also reported. A series of catalyst based on Pd over three different crystalline zirconia phases (tetragonal (-T), monoclinic (-M) and hybrid tetragonal and monoclinic (-MT)) was developed by Yan and coworkers (Scheme 21).[191] The most active in catalysis was ZrO_2-T with a TOF of 2817 h^{-1} (H_2O, 4.0 MPa, CO_2:H_2= 1:1, 100 ºC). The authors observed the same formate production in absence or presence of CO_2, demonstrating that bicarbonate was the real substrate of this reaction.

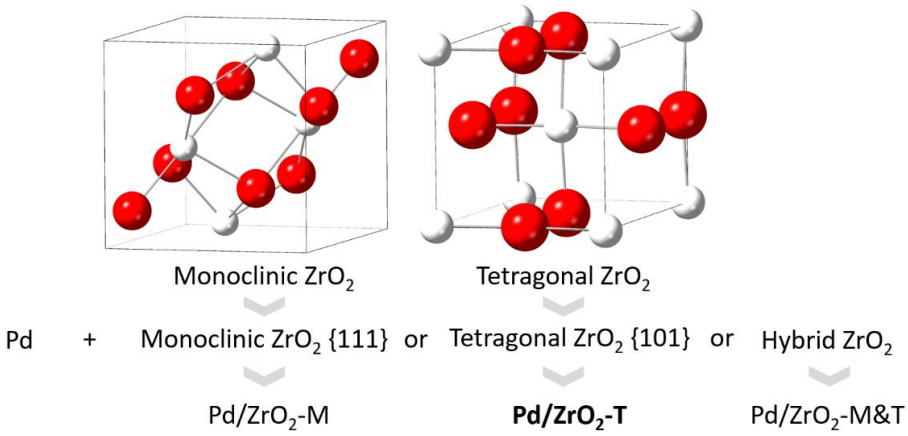

Scheme 21. Crystalline zirconia phases for Pd supported systems in hydrogenation of CO_2.

Zhang et al. employed anatase TiO_2 with different morphologies and exposing different facets and they observed that {1 0 0} was the most active.[192] A TOF of 1369 h^{-1} was obtained employing $NaHCO_3$ as base (H_2O, 2.0 MPa, CO_2:H_2= 1:1, 40 ºC, 1 h). These last studies evidenced the importance of the morphology of the material used as support not only for the stabilization of the nano structured catalyst, but also for their activities and recyclability.

Alloying Pd with other non-noble metals is another method reported to tune the electronic properties of the catalytic system. For instance, Sun et al. developed a bimetallic Pd-CoO NPs (≈ 1.8 nm) encapsulated within mesoporous silica nanospheres (MSNs).[193] They optimized the composition to $Pd_{0.8}Co_{0.2}$@MSN catalyst and obtained a TOF od 1824 h^{-1} (1.5 M $KHCO_3$ in aqueous solution, 2.0 MPa, CO_2:H_2= 1:1, 100 ºC, 1 h). The authors observed that the presence of K^+ ion increased the basicity of the MSNs, making the catalyst more active than with other bicarbonate cations. This encapsulated catalyst was recycled 5 times with no loss of activity.

Yan and coworkers developed a new zeolite-encaged Pd-Mn nanocatalyst for the CO_2 hydrogenation in the presence of NEt_3.[194] This system was also active for the FA dehydrogenation and will be presented in more details in the next section of this chapter.

In the CO_2 hydrogenation to formate, the PdAg bimetallic systems in the presence of a base constitute some of the most common catalysts. Some of

these catalysts were used in both hydrogenation and dehydrogenation reactions and will be described in the last section.[195,196,197]

In 2018, Yamashita and coworkers reported a novel bimetallic PdAg/TiO_2 catalyst.[113] They studied the electronic properties of their catalyst using DFT and through a detailed characterization. They also tested different ways of alloying these metals, concluding that when a core-shell structure Ag covers Pd in Pd@Ag/TiO_2 was the best alternative and a TON of 14839 was reached (1 M $NaHCO_3$ in aqueous solution, 2.0 MPa, CO_2:H_2= 1:1, 100 ºC, 24 h). This value was calculated using the surface of Pd atoms obtained from CO chemisorption. With Ag covering part of the surface of the NP, the surface Pd atoms become more electron rich (more negative Muliken charge) which plays a role in H_2 dissociation. This catalyst also showed good recyclability performance.

Two years later, the same authors proposed different PdAg bimetallic NPs where the PdAg/TiO_2 system was modified with Metal-Organic Framework (ZIF-8).[198] Compared to the unmodified pristine PdAg/TiO_2, PdAg/TiO_2@ZIF-8 was more active with a TON of 913 (1 M $NaHCO_3$ in aqueous solution, 2.0 MPa, CO_2:H_2= 1:1, 100 ºC, 6 h). Depending on the growth time of ZIF-8 over the previously synthesized PdAg/TiO_2 catalyst, differences in catalytic activity were observed. The optimal time was 30 min and at longer times, the activity decreased due to the formation of a layer about 2.2-3.1 nm which slow down the diffusion of reactants. DFT calculations were carried out and showed that the modification of the catalyst affected the electronic properties of the metallic system. Moreover, ZIF-8 also improved the stability of the system, avoiding deactivation of catalyst by agglomeration of the nanoparticles.

Other Pd monometallic[96,106,199,200,201] systems and PdAu[202] and PdAg[72] bimetallic catalysts were employed in the hydrogenation of bicarbonates/carbonates to formate and revealed active in the reverse H_2 release reaction.

The introduction of amine groups on the support was also reported. Yamashita and coworkers employed mesoporous hollow carbon spheres (MHCSs) containing a polymer (polyethylenediamine) to encapsulate PdAg NPs of 2.8 nm diameter.[203] A TON of 2680 was obtained using this system (1 M $NaHCO_3$ on aqueous solution, 2.0 MPa, CO_2:H_2= 1:1, 100 ºC, 24 h).

Variations in Pd/Ag ratio (2:8 reached best activity) and polymer content were also performed. A minimal amount of polymer revealed necessary to improve activity but, when an excess was used, the pores of MHCSs were blocked.

Similar work was reported employing poly(ethyleneimine) and PdAg NPs confined in hollow mesoporous organosilica spheres (HMOSs).[204] High TON (2754) was obtained by this system (0.1 M NaOH on aqueous solution, 2.0 MPa, CO_2:H_2= 1:1, 100 ºC, 22 h). This system was also tested in recycling experiments, observing that after five cycles, activity remained with a total TON of 13700 over 110 h of reaction. Xu et al. reported a system based on PdAg NPs over a Cr^{3+} based MOF functionalized with amine groups (MIL-101-NH_2).[205] The PdAg NPs synthesized were very small, with an average diameter of 1.6 nm and the TON obtained was 1500 (1 M $NaHCO_3$ on aqueous solution, 5.0 MPa, CO_2:H_2= 1:1, 70 ºC, 10 h). The authors proposed that decorated amine groups in MOFs favored the formation of very small PdAg NPs and a strong metal-support interaction which provided electron-rich states of Pd to promote H_2 dissociation in catalysis. This system was tested in recyclability experiments for five cycles and a decrease of 23% of activity was observed. A slight loss of Pd was detected by ICP (from 1.77% in fresh catalyst to 1.59% after catalysis) but the deactivation observed was attributed to agglomeration of nanoparticles.

For the hydrogenation of CO_2 into formate, several examples of non-noble metal-based catalysts were reported. For instance, a cobalt catalyst was developed by Khan and coworkers who employed a nitrogen-rich graphitic carbon support and could hydrogenate CO_2 into formate with a TON of 82265 in the presence of KOH (6.2 MPa, CO_2:H_2= 1:1, 120 ºC, 24 h). [206] Furthermore, this catalyst was recycled four times without loss of activity.

Using copper NPs over TiO_2 (CuO_x-TiO_2), higher temperature was required (200 ºC).[207] When an inorganic base was used, the TON increased up to 6.62 (NaOH, 4.0 MPa, CO_2:H_2= 1:3, 220 ºC, 4 h). Comparing several metal oxides as supports, the catalysts anchored onto TiO_2 provided the highest activity. They tested this catalyst and deactivation was observed due to intermediates deposited over surface of catalyst.

Nickel is another cheap and abundant metal that was employed in CO_2 hydrogenation using KBH_4 as reductant and under atmospheric

pressures.[208,209] Fu et al. developed an air-stable and reusable Ni@Ni(OH)$_2$ nanocatalyst.[210] The synthesis of this foam-like system was performed using the organometallic approach[211] and a TOF of 3.4 h^{-1} was obtained when CO_2 + H_2/NaOH was used (1 M base, 2.0 MPa, CO_2:H_2= 1:1, 100 ºC) while using KOH, an increase in TOF was observed (4.8 h^{-1}). Interestingly, when CO_2 was not present in the catalytic mixture and the hydrogenation was carried out over bicarbonate, lower activities were found. The core-shell structure of this catalyst provided stability to the system, which reamined active after five cycles.

Yan and coworkers reported another series of catalysts based on Ni.[212] Alloys were tested and the NiPd bimetallic system in a composition 7:3 stabilized by PVP revealed the most active for formate production. Compared to the monometallic Ni and Pd systems, the alloying of these metals increased the activity for the hydrogenation of $NaHCO_3$ with a TOF of 1.2 h^{-1} (H_2O, 2.0 MPa H_2, 80 ºC, 2 h). Moreover, when CO_2 was introduced in the system (0.5 MPa CO_2), the TOF increased to 2.8 h^{-1}.

To date, Pd is therefore the most employed metal for the hydrogenation of CO_2 to formic acid and formate using heterogeneous catalysts. However, lower activities were obtained when compared with the performance of homogeneous catalyst.

1.3. Reversible hydrogenation/dehydrogenation systems for the use of CO_2 as storage and release of H_2

Hydrogen (H_2) is considered a clean and sustainable energy source and many efforts are dedicated to improve its generation and its storage.

The chemical storage of H_2 is based on the reversible hydrogenation/dehydrogenation of specific molecules.[213] This constitutes the concept of circular H_2 storage and release and requires the use of a catalyst that is highly active and robust in both processes. Ideally, the same catalyst should perform both transformations.

Some of the molecules that can play a role in the chemical hydrogen storage are represented in Scheme 22.

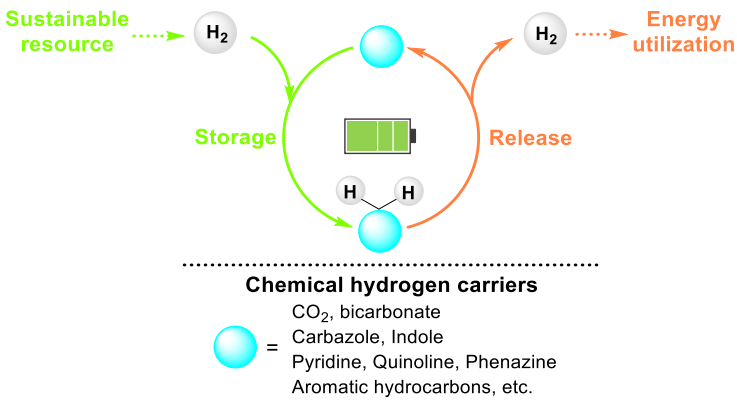

Scheme 22. Schematic representation of circular storage of H_2 using different chemical hydrogen carriers.

In this thesis, we will focus on the use of CO_2 and formate as chemical hydrogen carriers.

The use of FA[107g,214,215,216,217] and formates[218] for the storage and release of H_2 has been studied over the last decades. For both transformations, homogeneous complexes were used. Mainly, Rh, Ru, Ir, Ni, Fe and Mn have been employed.[213] However, the conditions required for these reactions and their application on a large-scale production make heterogeneous catalysts more suitable to industry.

For interconversion of both CO_2 or bicarbonate to FA or formates,[219] Pd is the most commonly employed metal, even if other metals such as Ru were also reported.[220,221,222] This metal is highly active in hydrogenation reactions, and also revealed efficient in dehydrogenation of FA and formates.[223] The drawbacks associated to the use of catalysts based on Pd is the cost of this element and their poisoning in the presence of CO. To avoid the latter issue, alloying with other metals and modification of the support are the most common strategies.[224]

1.3.1. Heterogeneous catalyst-promoted hydrogen storage and release cycles based on the interconversion of CO_2 and formic acid

In this subsection, some of the most active systems for the reversible interconversion of CO_2 and formic acid are presented (Scheme 23).

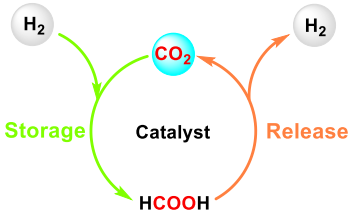

Yoon, 2014
Pd/*mpg*-C_3N_4, H_2O, 0 cycle
FA, 25 ºC, 3 h, TOF: 144 h^{-1} (DH)
CO_2:H_2 (1:2), NEt_3, 150 ºC, 24 h, TON: 106 (H)

Cao, 2016
Pd/$CN_{0.25}$, H_2O, 0 cycle
FA: 25 ºC, 1 h, TOF: 5530 h^{-1} (DH)
CO_2:H_2 (1:1), NEt_3, 100 ºC, TON: 135074 (H)

Mori & Yamashita
2017
Pd/Ag/SBA-15-phenylamine, H_2O, 0 cycle
FA:HCO_2Na= 9:1, 75 ºC, 1 h, TOF: 631 h^{-1} (DH)
CO_2:H_2 (1:1), $NaHCO_3$, 100 ºC, TON: 874 (H)
2018
PdAg/amine-MSC, H_2O, 3 cycles
FA:HCO_2Na= 9:1, 60 ºC, TOF: 5638 h^{-1} (DH)
CO_2:H_2 (1:1), $NaHCO_3$, 100 ºC, TON: 839 (H)

Lin, 2018
Pd/AC, piperidine, 2-propanol, 5 cycles
FA, 100 ºC, 30 min (DH)
CO_2, 30 ºC, 1 h, TOF: 5504 h^{-1} (H)

Yan & Yu, 2020
$PdMn_{0.25}$@S-1 zeolites, H_2O, 0 cycle
FA: 60 ºC, 40 min, TOF: 6860 h^{-1} (DH)
CO_2:H_2 (1:1), NaOH, 80 ºC, TOF: 2151 h^{-1} (H)

Liang & Huang, 2022
Pd-Cu/AC, EtOH, NEt_3, 0 cycle
FA, 80 ºC, 2 h, TOF: 430 h^{-1} (DH)
CO_2:H_2 (1:1), 110 ºC, 2 h, TOF: 100 h^{-1} (H)

Scheme 23. Heterogeneous catalyst for the use of CO_2 as chemical carrier due to it reversible transformation on FA.

Yoon and coworkers studied a Pd monometallic system using mesoporous graphitic carbon nitride (*mpg*-C_3N_4) as support,[73] which was one of the first heterogeneous systems reported for FA hydrogen storage-release. Very small Pd NPs were synthesized (1.7 nm) that were stabilized by the nitrogen atoms located at the support surface. A function of these nitrogen atoms is to initiate the H_2-release by deprotonation of FA. For CO_2 hydrogenation, a TON of 106 was reached (NEt_3, 150 ºC, 4.0 MPa total pressure, H_2/CO_2= 2:1, 24 h). For dehydrogenation, a TOF 144 h^{-1} was measured after 2 h at 25 ºC even in the absence of base. Cao and coworkers developed a system based on Pd NPs over Pyridinic-Nitrogen-Doped Carbon (Pd/CN_x).[224] Pd/$CN_{0.25}$ was a highly active system for the dehydrogenation of FA with a TOF of 5530 h^{-1} without any additive (1 M FA, 25 ºC, 1 h) and also the hydrogenation reaction with a TON of 135075 (NEt_3, 100 ºC, 6.0 MPa total pressure, H_2/CO_2= 1:1, 24 h).

Yamashita and coworkers synthesize bimetallic PdAg NPs over phenylendiamine-functionalized mesoporous silica (phenylamine-grafted PdAg/SBA-15).[196] Using this system, a TON of 874 ($NaHCO_3$, 100 ºC, 2.0 MPa total pressure, H_2/CO_2= 1:1, 24 h) was reached for hydrogenation, and a TOF of 631 h^{-1} (FA/HCO_2Na= 9:1, 75 ºC, 1 h) was obtained for dehydrogenation. The catalyst could be recovered and reused three times without loss of activity in the hydrogenation reaction. Here, the synergy in the PdAg alloy was evidenced since the monometallic Ag catalyst was not active in catalysis and the monometallic Pd was much less active than when alloyed. More recently, the same authors reported another bimetallic PdAg system supported on an amine functionalized mesoporous carbon (amine-MSC).[195] The introduction of these basic groups on the support improved the performance in both reactions of interest. DFT calculations showed that phenylamine groups near of PdAg NPs affect O-H dissociation of FA and favored the adsorption of CO_2 in hydrogenation. The TON obtained for hydrogenation was 874 ($NaHCO_3$, 100 ºC, 2.0 MPa total pressure, H_2/CO_2= 1:1, 24 h) and TOF for dehydrogenation was 5638 (FA/HCO_2Na= 9:1, 60 ºC, 1 h). The system showed reversibility for three cycles in both reactions, without any reduction in activity in consecutives utilizations. This system was also successfully tested under flow conditions using a fixed-bed reactor. The same year, Lin and coworkers employed a highly efficient formate-piperidine-adduct (FPA) for hydrogen storage with a carbon-supported palladium nano-catalyst.[225] FPA is an advantageous substrate for the generation of hydrogen since it does not involve the formation of CO and NH_3. For the hydrogenation reaction, a TOF up to 5504 h^{-1} was obtained in 70% 2-propanol solution (FA, 30 ºC, 1 h). This system was used in hydrogenation-dehydrogenation for 5 cycles and no loss of activity was observed. As previously mentioned, Yamashita and coworkers developed a bimetallic system based on PdAg NPs within a core-shell structured zeolitic imidazolate framework (ZIF-8).[197] This ZIF-8@Pd_1Ag_2@ZIF-8 system contains small NPs of 2.8 nm of size. DFT calculations showed that both Ag atoms and basic N groups present on ZIF-8 were transferring charge to Pd. A TON of 1191 was reached for the hydrogenation reaction (1 M $NaHCO_3$ aqueous solution, 100 ºC, 2.0 MPa total pressure, H_2/CO_2= 1:1, 24 h) and the activity for dehydrogenation was in the

same range (FA, 30 ºC, 2 h). The use of this core-shell structure also provided high stability to the system, making possible its recycling with no loss of activity during at least three times.

Yan and coworkers synthesized a sub-nanometer Pd–Mn clusters encaged within silicalite-1 (S-1) zeolites (PdMnx@S-1).[194] DFT studies were carried out and indicated that the addition of Mn passivated the Pd active sites, weakening the interaction with intermediates, which was favorable for FA decomposition. This is the most active dual heterogeneous system under mild conditions to date. A TON of 2151 was obtained for the hydrogenation reaction (NaOH, 80 ºC, 4.0 MPa total pressure, H_2/CO_2= 1:1, 24 h). For the dehydrogenation, a TOF value of 6860 h^{-1} was obtained (FA, 60 ºC, 40 min). Recycling experiments were carried out for hydrogenation and the catalyst maintained its activity during 5 cycles.

More recently, Zou et al. reported bimetallic PdCu NPs and PdAu NPs deposited over activated carbon (AC) that were active in both catalytic reactions using EtOH as solvent and using NEt_3 as additive.[226] PdCu/AC showed more activity than PdAu/AC. For hydrogenation, a TOF of 100 h^{-1} was obtained (110 ºC, 1.0 MPa total pressure, H_2/CO_2= 1:1, 2 h), while for dehydrogenation, the TOF reached 430 h^{-1} (FA, 80 ºC, 2 h). This system showed stability for both reactions after six cycles, but both reactions were not combined.

Very recently, Beller and coworkers developed a catalytic system based on Pd for the dehydrogenation of FA with outstanding activity.[227] Polymeric carbon nitride was employed as support and this system reach a TTON of 41395 (10 mmol FA, 2 mmol HCOONa, 10 ml tryglime, 120 ºC) during for 15 days of reaction.

1.3.2. Heterogeneous catalyst for the use of H_2 storage and release due the reversible transformation of bicarbonate and formate

FA decomposition is more favorable energetically ($\Delta G = -32.9$ kJ·mol^{-1}) than that of formate salts (*e.g.*, Na^+, K^+, NH_4^+, $\Delta G = 1$ kJ·mol^{-1}) but the decomposition of the formate/bicarbonate pair is more suitable for hydrogen storage-release under ambient conditions.[213,228] This is due to even formic

acid in non-toxic and with low-flammability under ambient conditions, it is a corrosive liquid. However, formate salts represent an alternative because they are non-acidic and non-corrosive, which make them easier to handle and transport for its application as hydrogen carriers.

Solubility is another important factor for the use of formate salts as hydrogen carrier. For example, for more commonly used formate salts based on different cations (mol salt in 100 ml H_2O, 20 ºC): K^+ (4.01) > NH_4^+ (2.26) > Na^+ (1.19).[213]

Next, some of the most efficient system will be presented. Once again, palladium-based catalysts are the most employed (Scheme 24).

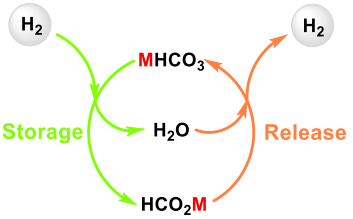

Cao, 2014, M=K
Pd/*r*GO, H_2O, 6 cycles
80 ºC, 20 min, TOF: 11299 h^{-1} (DH)
H_2 (40 bar), 100 ºC, 32 h, TON: 7088 (H)

Lin, 2015, M=NH_4
Pd/AC, H_2O, 5 cycles
80 ºC, 1.5 h, TON: 5061 (DH)
H_2 (28 bar), 20 ºC, 15 h, TON: 1769 (H)

Huan & Zhang, 2016, M=K
Pd/NMC-8, H_2O, 0 cycle
80 ºC, 1 h, TOF: 2416 h^{-1} (DH)
H_2 (60 bar), 80 ºC, 2 h, TON: 1598 (H)

Huan & Wang, 2016, M=K
Pd/*mpg*-C_3N_4, H_2O, 0 cycle
60 ºC, 5 h, 59% yield (DH)
H_2 (60 bar), 80 ºC, 1.5 h, TON: 6595 (H)

Yoon & Asefa, 2017, M=Na
Pd/PDMC, H_2O, 0 cycle
80 ºC, 2 h, TOF: 2562 h^{-1} (DH)
H_2 (40 bar), 80 ºC, 24 h, TON: 1625 (H)

Kawanami, 2018, M=K
$Pd_{0.5}Au_{0.5}$/PDA-*r*GO, 0 cycle
80 ºC, 25 min, TOF: 1630 h^{-1} (DH)
H_2 (50 bar), 50 ºC, 16 h, 94% yield (H)

Shishido, 2019, M=NH_4
PdAu/AC, H_2O, 0 cycle
40 ºC, TOF: 4200 h^{-1} (DH)
H_2 (50 bar), 60 ºC, TOF: 5820 h^{-1} (H)

Mori & Yamashita, 2020, M=Na
Ag@Pd@TiO_x/TiO_2, 0 cycle
75 ºC, 15 min, TOF: 6499 h^{-1} (DH)
H_2 (30 bar), 80 ºC, 2 h, TON: 820 (H)

Shao & Ji, 2020, M=K
Pd/N,P-C, H_2O, 0 cycle
80 ºC, 130 min, TOF: 3254 h^{-1} (DH)
H_2 (60 bar), 80 ºC, 3 h, TON: 4269 (H)

Scheme 24. Heterogeneous catalysts for the use of H_2 storage and release due the reversible transformation of bicarbonate and formate.

In 2014, Cao and coworkers employed a palladium-based system over graphite oxide nanosheets (Pd/*r*-GO).[200] This was the first heterogeneous system for the reversible dehydrogenation of formates to bicarbonates. They employed $KHCO_3$ and HCOOK salts as substrates in both reactions. The catalyst could be used for six consecutive hydrogenation-dehydrogenation cycles under mild aqueous conditions. For hydrogenation, a TON of 7088 was obtained (4.8 M $KHCO_3$, 100 ºC, 40 bar H_2, 32 h) and for dehydrogenation, the initial TOF was 11299 h^{-1} (4.8 M HCOOK, 80 ºC, 20 min).

Lin and coworkers used a palladium catalyst supported over activated carbon (Pd/AC).[96] In this case, NH_4HCO_3 and $HCOONH_4$ were used as salts. Authors selected NH_4^+ as cation due its superior solubility compared to Na^+. For K^+ and Na^+ carbonates, the activity for hydrogenation was very low (<1 in both cases). However, for NH_4^+ bicarbonate, TON was 278. This was related to the concentrations of bicarbonates: $NaHCO_3$ (0.61 M) < $KHCO_3$ (0.89 M) < NH_4HCO_3 (0.92 M). The TOF for dehydrogenation was 1769 h^{-1} (1 M NH_4HCO_3, 20 ºC, 28 bar H_2, 15 h) and for dehydrogenation TON was 5061 ($HCOONH_4$, 80 ºC, 1.5 h). This catalyst was used for five cycles of hydrogen storage and release by varying the conditions.

Zhang and coworkers employed palladium over nitrogen-doped mesoporous carbon (Scheme 25).[201] This support was synthesized through a hard template method and nitration under flow of ammonia at different temperatures. They observed that the nitrogen functionalities in the support stabilized the Pd NPs and increased the electron density.

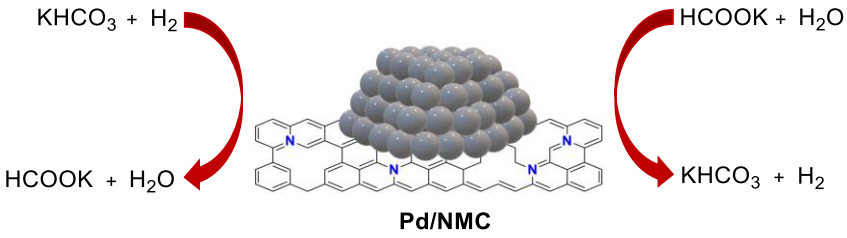

Scheme 25. Pd NPs over nitrogen-doped mesoporous carbon catalyst for reverse hydrogenation of bicarbonate and dehydrogenation of formate processes.

Catalysis was carried out in aqueous solutions and a TON of 1598 was obtained for hydrogenation (4 M $KHCO_3$, 80 ºC, 60 bar H_2, 2 h). For the reverse reaction, a TOF of 2416 h^{-1} was obtained ($KHCO_3$, 80 ºC, 1 h). In

terms of recyclability, the hydrogenation activity decreased after the first cycle but remained stable during the next cycles. For the dehydrogenation reaction, a decrease of activity was observed during the third cycle. The catalyst deactivation was attributed to the blockage of the active sites by accumulation of intermediates. Zhang and coworkers also used a system of Pd NPs over mesoporous graphitic carbon nitride (*mpg*-C_3N_4).[187] Potassium salts were used both for hydrogenation and dehydrogenation in aqueous media. TON of 6595 was measured for hydrogenation (4 M $KHCO_3$, 80 ºC, 60 bar H_2, 1.5 h) and a yield of 59% was obtained for dehydrogenation ($KHCO_3$, 60 ºC, 5 h). The catalyst was recycled six times without loss of activity, but no consecutive coupled hydrogenation-dehydrogenation experiments were reported.

One year later, Asefa and coworkers developed a system based on ultrasmall Pd NPs over N-doped carbon support (Pd/PDMC).[106] This support was synthesized using polyaniline (PANI) with colloidal silica (Scheme 26). This composite was pyrolyzed and the template then was removed, obtaining a new functionalized carbon-based material. Variations in pyrolysis temperature provided different morphologies and size of carbon spheres and, consequently, variations in Pd NPs size. In this study, a TON of 1625 was obtained for the hydrogenation reaction (1 M $NaHCO_3$, 80 ºC, 40 bar H_2, 24 h) while a TOF of 2562 h^{-1} was reached for the dehydrogenation (1 M $NaHCO_3$, 80 ºC, 2 h). This catalyst was recycled three times in hydrogenation reaction. A slight decrease in activity was observed. No combined hydrogenation/dehydrogenation cycles were carried out.

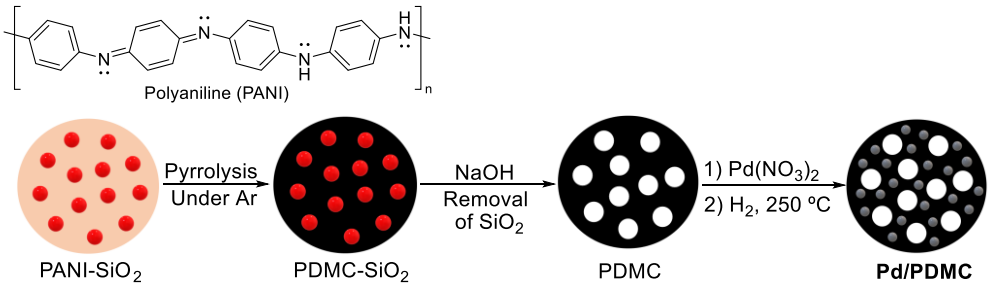

Scheme 26. Pd NPs over N-doped carbon support (Pd/PDMC) for reverse hydrogenation of bicarbonate and dehydrogenation of formate processes.

Kawanami and coworkers employed bimetallic PdAu NPs over *p*-phenilenediamine-functionalized reduced graphene oxide ($Pd_{0.5}Au_{0.5}$/PDA-

*r*GO) (Scheme 27).[72] These catalysts demonstrated to be highly active for both reactions. High yields were obtained for the hydrogenation of $KHCO_3$: 94% at 50 ºC (50 bar H_2, 16 h) and even 90% at 30 ºC. For dehydrogenation, TOFs of 1630 h^{-1} and 6980 h^{-1} was obtained for dehydrogenation of HCOOK and FA respectively (80 ºC, 25 min). This catalyst was employed in recyclability experiments for hydrogenation and deactivation of the catalyst was observed due to the loss of PDA.

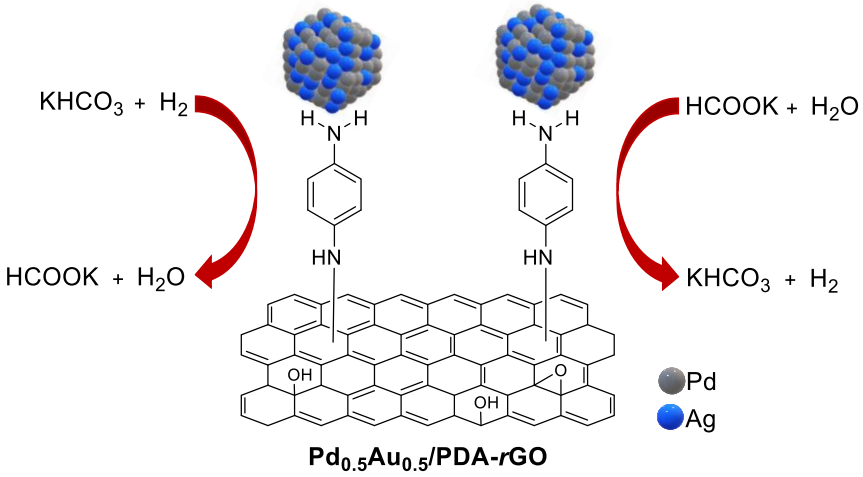

Scheme 27. PdAu NPs over p-phenilenediamine-functionalized reduced graphene oxide for reverse hydrogenation of bicarbonate and dehydrogenation of formate processes.

Another PdAu bimetallic system was reported by Shishido and coworkers using activated carbon as support.[202] Several Pd:Au ratios were tested, and the most efficient catalyst resulted using 1:1. The bimetallic catalyst demonstrated to be more active than the monometallic alone, indicating a synergistic effect. They employed NH_4HCO_3/$HCOONH_4$ and obtained a TOF of 5820 h^{-1} for the hydrogenation reaction (60 ºC, 50 bar H_2). For the dehydrogenation process, a TOF up to 4200 h^{-1} was reached (40 ºC).

In 2020, Yamashita and coworkers reported the Ag@Pd/TiO_2 catalysts with a TiO_x shell (Scheme 28).[229] The alloy between Pd and Ag appeared fundamental in this work to obtain high catalytic activity. The role of the TiO_x shell was analyzed by kinetic studies, concluding that the presence of both Ag and TiO_x shell near Pd promotes the rate-limiting C-H bond dissociation step in the dehydrogenation reaction and facilitates the adsorption and

activation of bicarbonate during the hydrogenation reaction. A TON value of 820 was obtained in hydrogenation (1 M $NaHCO_3$, 80 ºC, 30 bar H_2, 2 h). For dehydrogenation, the TOF was up to 6499 h^{-1} (75 ºC, 15 min).

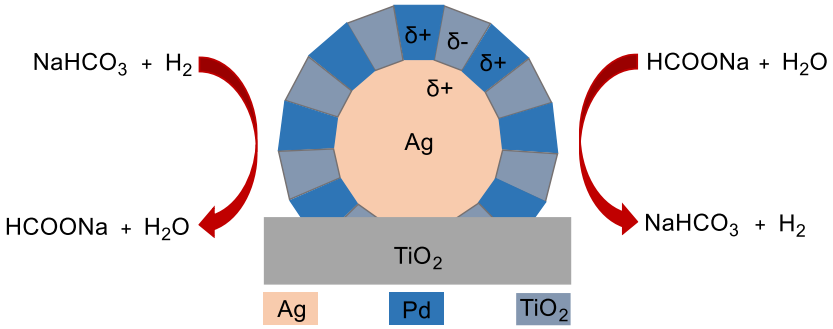

$Ag@TiO_x@Pd/TiO_2$

Scheme 28. $Ag@Pd/TiO_2$ catalysts with a TiOx shell for reverse hydrogenation of bicarbonate and dehydrogenation of formate processes.

Ji and coworkers developed monometallic Pd NPs over N- and P-co-doped carbon (Pd/N,P-C) as support which was produced by pyrolysis of a mixture of 1,10-phenanthroline and triphenylphosphine.[199] They used K^+ based salts for both reactions and obtained a TON of 4269 for the hydrogenation reaction (4 M $KHCO_3$, 80 ºC, 60 bar H_2, 3 h), while the TOF for dehydrogenation was up to 3254 h^{-1} (80 ºC, 130 min). They could recover and reuse this catalyst three times for hydrogenation and five times for dehydrogenation without loss of activity.

As previously mentioned, palladium-based catalysts predominate in these processes, either as monometallic materials or alloyed with other metals such as Au and Ag. The relevance of supports was also evidenced in various examples. Carbon-based supports modified with nitrogen increase the catalyst activity and, in most cases, also improve their stability. For H_2 storage and release reactions, very active and efficient systems were developed. However, efforts are still needed to enhance the activity and stability of catalytic systems for large scale applications.

The work described in this thesis deals with the development of new catalytic Pd-based systems for both the hydrogenation of CO_2 into formate and the use of formate in reduction processes.

1.4. References

[1] Real-time and historical CO_2 levels were obtained from the website: https://www.co2levels.org/#sources.

[2] M. Crippa, D. Guizzardi, M. Banja, E. Solazzo, M. Muntean, E. Schaaf, F. Pagani, F. Monforti-Ferrario, J. Olivier, R. Quadrelli, A. Risquez Martin, P. Taghavi-Moharamli, G. Grassi, S. Rossi, D. Jacome Felix Oom, A. Branco, J. San-Miguel-Ayanz, E. Vignati, CO_2 emissions of all world countries - Report, EUR 31182 EN, Publications Office of the European Union, Luxembourg, **2022**, doi:10.2760/730164, JRC130363.

[3] E. C. Ra, K. Y. Kim, E. H. Kim, H. Lee, K. An, J. S. Lee, *ACS Catal*. **2020**, *10*, 11318−11345.

[4] M. Aresta, Carbon *Dioxide as Chemical Feedstock*, 1st edition, Wiley-VCH Verlag GmbH & Co. KGaA, ISBN: 9783527324750, DOI:10.1002/9783527629916, **2010**.

[5] M. D. Burkart, N. Hazari, C. L. Tway, E. L. Zeitler, *ACS Catal*. **2019**, *9*, 7937−7956.

[6] X. T. Cao, D. M. Kabtamu, S. Kumar, R. S. Varma, *ACS Sustainable Chem. Eng.* **2022**, *10*, 12906−12932.

[7] M. Aresta, A. Dibenedetto, E. Quaranta, *J. Catal.* **2016**, *343*, 2−45.

[8] J. Artz, T. E. Müller, K. Thenert, J. Kleinekorte, R. Meys, A. Sternberg, A. Bardow, W. Leitner, *Chem. Rev*. **2018**, *118*, 434−504.

[9] B. Hua, C. Guild, S. L. Sui, *J. CO_2 Util.* **2013**, *1*, 18−27.

[10] B. B. A. Bediako, Q. Qian, B. Han, *Acc. Chem. Res*. **2021**, *54*, 2467−2476.

[11] Z. Li, S. Yang, H. Li, *Curr. Org. Synth.* **2022**, *19*, 187−196.

[12] C. Fang, C. Lu, M. Liu, Y. Zhu, Y. Fu, B.-L. Lin, *ACS Catal*. **2016**, *6*, 7876−7881.

[13] Z. Ye, J. Chen, *ACS Catal.* **2021**, *11*, 13983−13999.

[14] Q. Zou, J. Chen, Y. Wang, J. Gu, F. Liu, T. Zhao, *ACS Sustainable Chem. Eng*. **2021**, *9*, 16153−16162.

[15] X.-C. Chen, L. Guo, G.-H. Shi, K.-C. Zhao, Y. Lu, Y. Liu, *Mol. Catal*. **2022**, *528*, 112431.

[16] (a) X. Cui, Y. Zhang, Y. Deng, F. Shi, *Chem. Commun*. **2014**, *50*, 189−191; (b) X. Cui, X. Dai, Y. Zhang, Y. Deng, F. Shi, *Chem. Sci.* **2014**, *5*, 649; (c) T. Witoon, T. Permsirivanich, W. Donphai, A. Jaree, M. Chareonpanich, *Fuel Process. Technol*. **2013**, *116*, 72−78; (d) G. Bonura, F. Arena, G. Mezzatesta, C. Cannilla, L. Spadaro, F. Frusteri, *Catal. Today* **2011**, *171*, 251−256; (e) X. Cui, Y. Zhang, Y. Deng, F. Shi, *Chem. Commun*. **2014**, *50*, 13521−13524.

[17] Q. Zhang, X.-T. Lin, N. Fukaya, T. Fujitani, K. Sato, J.-C. Choi, *Green Chem*. **2020**, *22*, 8414−8422.

[18] W. Lin, H. Cheng, Q. Wu, C. Zhang, M. Arai, F. Zhao, *ACS Catal*. **2020**, *10*, 3285−3296.

[19] P. Ju, J. Chen, A. Chen, L. Chen, Y. Yu, *ACS Sustainable Chem. Eng*. **2017**, *5*, 2516−2528.

[20] Q. Zhang, X.-T. Lin, N. Fukaya, T. Fujitani, K. Sato, J.-C. Choi, *Green Chem*. **2020**, *22*, 8414−8422.

[21] (a) Y. Li, X. Fang, K. Junge, M. Beller, *Angew. Chem. Int. Ed*. **2013**, *52*, 9568−9571; (b) K. Beydoun, T. vom Stein, J. Klankermayer, W. Leitner, *Angew. Chem. Int. Ed*. **2013**, *52*, 3496−9557; (c) Y. Li, I. Sorribes, T. Yan, K. Junge, M. Beller, *Angew. Chem. Int. Ed*. **2013**, *52*, 12156−12160; (d) K. Beydoun, G. Ghattas, K. Thenert, J. Klankermayer, W. Leitner*, Angew. Chem. Int. Ed*. **2014**, 53, 11010−11014.
[22] (a) K. Kon, S. M. A. H. Siddiki, W. Onodera, K.-i Shimizu, *Chem. Eur. J*. **2014**, *20*, 6264−6267; (b) X. Cui, X. Dai, Y. Zhang, Y. Deng, F. Shi, *Chem. Sci*. **2014**, *5*, 649−655; (c) X.-L. Du, G. Tang, H.-L. Bao, Z. Jiang, X.-H. Zhong, D. S. Su, J.-Q. Wang, *ChemSusChem* **2015**, *8*, 3489−3496; (d) X. Su, W. Lin, H. Cheng, C. Zhang, Y. Li, T. Liu, B. Zhang, Q. Wu, X. Yu, F. Zhao, *RSC Adv*. **2016**, *6*, 103650; (e) T. Toyao, S. M. A. H. Siddiki, Y. Morita, T. Kamachi, A. S. Touchy, W. Onodera, K. Kon, S. Furukawa, H. Ariga, K. Asakura, K. Yoshizawa, K. Shimizu, *Chem. Eur. J.* **2017**, *23*, 14848−14859; (f) M. Tamura, A. Miura, Y. Gu, Y. Nakagawa, K. Tomishige, *Chem. Lett*. **2017**, *46*, 1243−1246; (g) K. Liu, Z. Zhao, W. Lin, Q. Liu, Q. Wu, R. Shi, C. Zhang, H. Cheng, M. Arai, F. Zhao, *ChemCatChem* **2019**, *11*, 3919−3926.
[23] (a) J. R. Cabrero-Antonino, R. Adam, V. Papa, M. Beller, *Nat. Commun*. **2020**, *11*, 3893; (b) J. R. Cabrero-Antonino, R. Adam, M. Beller, *Angew. Chem. Int. Ed*. **2019**, *58*, 12820−12838.
[24] Q. Liu, L. Wu, R. Jackstell, M. Beller, *Nat. Commun*. **2015**, *6*, 5933.
[25] (a) S. Van de Vyver, Y. Román-Leshkov, Catal. Sci. Technol. **2013**, 3, 1465−1479; (b) M. Limbach, *Advances in Organometallic Chemistry*; Pérez, P. J., Ed.; Academic Press, **2015**; Vol. 63, pp 175−202.
[26] A. S. Lindsey, H. Jeskey, *Chem. Rev*. **1957**, *57*, 583−620.
[27] National Academies of Sciences, Engineering, and Medicine. *Gaseous Carbon Waste Streams Utilization: Status and Research Needs*; The National Academies Press: Washington, DC, **2019**.
[28] (a) S. Wang, G. Dua, C. Xi, *Org. Biomol. Chem*. **2016**, *14*, 3666; (b) T. G. Ostapowicz, M. Schmitz, M. Krystof, J. Klankermayer, W. Leitner, *Angew. Chem. Int. Ed.* **2013**, *52*, 12119−12123; (c) F. Manjolinho, M. Arndt, K. Gooßen, L. J. Gooßen, *ACS Catal*. **2012**, *2*, 2014−2021; (d) Y. Zhang, S. N. Riduan, *Angew. Chem. Int. Ed*. **2011**, *50*, 6210−6212; (e) L. Pavlovic, J. Vaitla, A. Bayer, K. H. Hopmann, *Organometallics* **2018**, *37*, 941−948; (f) T. Zhang, J. Zhong, Z. Wu, *J. Energy Chem*. **2021**, *59*, 572−580; (g) L. Feng, X. Li, B. Liu, E. Vessally, *J. CO_2 Util*. **2020**, *40*, 101220; (h) L. Zhang, Z. Hou, *Curr. Opin. Green Sustain. Chem*. **2017**, *3*, 17−21.
[29] A. Álvarez, A. Bansode, A. Urakawa, A. V. Bavykina, T. A. Wezendonk, M. Makkee, J. Gascon, F. Kapteijn, *Chem. Rev.* **2017**, *117*, 9804−9838.
[30] G. Centi, E. A. Quadrelli, S. Perathoner, *Energy Environ. Sci*. **2013**, *6*, 1711−1731.
[31] A. Álvarez, M. Borges, J. J. Corral-Pérez, J. G. Olcina, L. Hu, D. Cornu, R. Huang, D. Stoian, A. Urakawa, *ChemPhysChem* **2017**, *18*, 3135−3141.
[32] P. Davies, F. F. Snowdon, G. W. Bridger, D. O. Hughes, P. W. Young, U. K. Patent 1,010,871 (to ICI), **1965**.
[33] A. Y. Rozovskii, *Russ. Chem. Rev*. **1989**, *58*, 41−56.

[34] D. Gao, W. Li, H. Wang, G. Wang, R. Cai, *Trans. Tianjin Univ*. **2022**, *28*, 245−264.
[35] S. Zhang, Z. Wu, X. Liu, K. Hua, Z. Shao, B. Wei, C. Huang, H. Wang, Y. Sun, *Top. Catal*. **2021**, *64*, 371−394.
[36] X. Zhang, G. Zhang, C. Song, X. Guo, *Front. Energy Res*. **2021**, *8*, 1−16.
[37] J. Zhong, X. Yang, Z. Wu, B. Liang, Y. Huang, T. Zhang, *Chem. Soc. Rev*. **2020**, *49*, 1385−1413.
[38] K. Stangeland, H. Li, Z. Yu, *Energ. Ecol. Environ.* **2020**, *5*, 4, 272−285.
[39] J. Wang, G. Li, Z. Li, C. Tang, Z. Feng, H. An, H. Liu, T. Liu, C. Li, *Sci. Adv*. **2017** *3*, 10, e1701290.
[40] J. Hu, L. Yu, J. Deng, Y. Wang, K. Cheng, C. Ma, Q. Zhang, W. Wen, S. Yu, Y. Pan, J. Yang, H. Ma, F. Qi, Y. Wang, Y. Zheng, M. Chen, R. Huang, S. Zhang, Z. Zhao, J. Mao, X. Meng, Q. Ji, G. Hou, X. Han, X. Bao, Y. Wang, D. Deng, *Nat. Catal*. **2021**, *4*, 242−250.
[41] L. Wang, W. Zhang, X. Zheng, Y. Chen, W. Wu, J. Qiu, X. Zhao, X. Zhao, Y. Dai, J. Zeng, *Nat. Energy* **2017**, *2*, 869−876.
[42] Y. Chen, S. Choi, L. T. Thompson, *ACS Catal*. **2015**, *5*, 1717−1725.
[43] J.-L. Dubois, K. Sayama, H. Arakawa, *Chem. Lett*. **1992**, *21*, 1115−1118.
[44] W.-J. Shen, K.-W. Jun, H.-S. Choi, K.-W Lee, *Korean J. Chem. Eng*. **2000**, *17*, 210−216.
[45] (a) Y. Zhu, S. A. Tjokro Rahardjo, C. Valkenburt, L. J. Snowden-Swan, S. B. Jones, M. A. Machinal, *Techno-Economic Analysis for the Thermochemical Conversion of Biomass to Liquid Fuels*; Pacific Northwest National Laboratory: Richland, WA, **2011**; (b) M. Fazlollahnejad, M. Taghizadeh, A. Eliassi, G. Bakeri, *Chin. J. Chem. Eng*. **2009**, *17*, 630−634; (c) M. Farsi, R. Eslamloueyan, A. Jahanmiri, *Chem. Eng. Process*. **2011**, 50, 85−94.
[46] K.-W. Jun, K. S. Rama Rao, M.-H. Jung, K.-W. Lee, *Bull. Korean Chem. Soc*. **1998**, *19*, 466−470.
[47] N. Yan, K. Philippot, *Curr. Opin. Chem. Eng*. **2018**, *20*, 86−92.
[48] (a) Y. Sun, S. M. Campbell, J. H. Lunsford, G. E. Lewis, D. Palke, L. M. Tau, *J. Catal.* **1993**, *143*, 32−44; (b) N.-Y. Topsøe, K. Pedersen, E. G. Derouane, *J. Catal*. **1981**, *70*, 41−52.
[49] M. Stöcker, *Micropor. Mesopor. Mater*. **1999**, *29*, 3−48.
[50] M. Xu, J. H. Lunsford, D. W. Goodman, A. Bhattacharyya, *Appl. Catal. A* **1997**, *149*, 2, 289−301.
[51] (a) I. Son-Ki, B. Se-Won, P. Young-Kwon, J. Jong-Ki, *CO_2 Hydrogenation over Copper-Based Hybrid Catalysts for the Synthesis of Oxygenates. In Utilization of Greenhouse Gases*; American Chemical Society: Washington, DC, **2003**; Vol. 852, pp 183−194; (b) Q. Ge, Y. Huang, F. Qiu, C. Zhang, *J. Nat. Gas Chem*. **1999**, *8*, 280−285; (c) G. Bonura, M. Cordaro, L. Spadaro, C. Cannilla, F. Arena, F. Frusteri, *Appl. Catal. B* **2013**, 140−141, 16−24.
[52] C. S. Chen, J. H. Lin, J. H. You, C. R. Chen, *J. Am. Chem. Soc*. **2006**, *128*, 15950−15951.

[53] A. Goguet, F. Meunier, J. Breen, R. Burch, M. Petch, A. Faurghenciu, *J. Catal*. **2004**, *226*, 382−392.
[54] W. Wang, S. Wang, X. Ma, J. Gong, *Chem. Soc. Rev*. **2011**, *40*, 3703−3727.
[55] J. Guo, H. Lou, H. Zhao, D. Chai, X. Zheng, *Appl. Catal. A* **2004**, *273*, 75−82.
[56] S. Corthals, J. Van Nederkassel, J. Geboers, H. De Winne, J. Van Noyen, B. Moens, B. Sels, P. Jacobs, *Catal. Today* **2008**, *138*, 28−32.
[57] J. R. Rostrup-Nielsen, J. H. B. Hansen, *J. Catal.* **1993**, *144*, 38−49.
[58] M. C. Bradford, M. A. Vannice, *Catal. Rev.: Sci. Eng*. **1999**, *41*, 1−42.
[59] S. Rönsch, J. Schneider, S. Matthischke, M. Schlüter, M. Götz, J. Lefebvre, P. Prabhakaran, S. Bajohr, *Fuel* **2016**, *166*, 276−296.
[60] (a) A. Karelovic, P. Ruiz, *J. Catal*. **2013**, *301*, 141−153; (b) S. Sharma, Z. Hu, P. Zhang, E. W. McFarland, H. Metiu, *J. Catal*. **2011**, *278*, 297−309; (c) Y. Guo, S. Mei, K. Yuan, D.-J. Wang, H.-C. Liu, C.-H. Yan, Y.-W. Zhang, *ACS Catal*. **2018**, *8*, 6203−6215; (d) J. H. Kwak, L. Kovarik, J. Szanyi, *ACS Catal*. **2013**, *3*, 2094−2100; (e) S. Rahmani, M. Rezaei, F. Meshkani, *J. Ind. Eng. Chem*. **2014**, *20*, 1346−1352 (f) C. Vogt, E. Groeneveld, G. Kamsma, M. Nachtegaal, L. Lu, C. J. Kiely, P. H. Berben, F. Meirer, B. M. Weckhuysen, *Nat. Catal*. **2018**, *1*, 127−134; (g) C. Vogt, M. Monai, E. B. Sterk, J. Palle, A. E. M. Melcherts, B. Zijlstra, E. Groeneveld, P. H. Berben, J. M. Boereboom, E. J. M. Hensen, F. Meirer, I. A. W. Filot, B. M. Weckhuysen, *Nat. Commun*. **2019**, 10, 5330; (h) H. H. Shin, L. Lu, Z. Yang, C. J. Kiely, S. McIntosh, *ACS Catal*. **2016**, *6*, 2811−2818; (i) A. Parastaev, V. Muravev, E. Huertas Osta, A. J. F. van Hoof, T. F. Kimpel, N. Kosinov, E. J. M. Hensen, *Nat. Catal*. **2020**, *3*, 526−533.
[61] J. H. Kwak, L. Kovarik, J. Szanyi, *ACS Catal.* **2013**, *3*, 11, 2449−2455.
[62] H. C. Wu, Y. C. Chang, J. H. Wu, J. H. Lin, I. K. Lin, C. S. Chen, *Catal. Sci. Technol*. **2015**, *5*, 4154−4163.
[63] C. Hernández Mejía, C. Vogt, B. M. Weckhuysen, K. P. de Jong, *Catal. Today* **2020**, *343*, 56−62.
[64] R.-P. Ye, J. Ding, W. Gong, M. D. Argyle, Q. Zhong, Y. Wang, C. K. Russell, Z. Xu, A. G. Russell, Q. Li, M. Fan, Y.-G. Yao, *Nat. Commun*. **2019**, *10*, 5698.
[65] G. Prieto, *ChemSusChem* **2017**, *10*, 1056−1070.
[66] Z. Li, J. Wang, Y. Qu, H. Liu, C. Tang, S. Miao, Z. Feng, H. An, C. Li, *ACS Catal.* **2017**, *7*, 8544−8548.
[67] P. Gao, S. Dang, S. Li, X. Bu, Z. Liu, M. Qiu, C. Yang, H. Wang, L. Zhong, Y. Han, Q. Liu, W. Wei, Y. Sun, *ACS Catal*. **2018**, *8*, 571−578.
[68] L. Xiong, S. Liu, Y. Men, L. Li, X. Niu, K. Guo, J. Xu, W. An, J. Wang, Y. Cong, *J. Environ. Chem. Eng*. **2022**, *10*, 108407.
[69] W.-H. Wang, X. Feng, M. Bao, T*ransformation of Carbon Dioxide to Formic Acid and Methanol*, SpringerBriefs in Green Chemistry for Sustainability, **2017**.
[70] J. Hietala, A. Vuori, P. Johnsson, I. Pollari, W. Reutemann, H. Kieczka, Formic Acid in Ullmann's Encyclopedia of Industrial Chemistry; Wiley-VCH Verlag GmbH & Co. KGaA: Weinheim, Germany, **2016**.

[71] J. Ohi, *J. Mater. Res.* **2005**, *20*, 12, 3180−3187.
[72] H. Zhong, M. Iguchi, M. Chatterjee, T. Ishizaka, M. Kitta, Q. Xu, H. Kawanami, *ACS Catal*. **2018**, *8*, 5355−5362.
[73] J. H. Lee, J. Ryu, J. Y. Kim, S.-W. Nam, J. H. Han, T.-H. Lim, S. Gautam, K. H. Chae, C. W. Yoon, *J. Mater. Chem. A* **2014**, *2*, 9490−9495.
[74] W.-H. Wang, Y. Himeda, *Hydrogenation In Recent Advances in Transition Metal-Catalysed Homogeneous Hydrogenation of Carbon Dioxide in Aqueous Media*; Karamé, I., Ed.; InTechOpen, **2012**.
[75] Y.-P. Zhang, J.-H. Fei, Y.-M. Yu, X.-M. Zheng, *Catal. Commun.* **2004**, *5*, 643−646.
[76] P. Mondal, P. Bhanja, R. Khatun, A. Bhaumik, D. Das, Sk. M. Islam, *J. Colloid Interface Sci.* **2017**, *508*, 378−386.
[77] H. Stephen, T. Stephen, Vol. I, *Solubilities of inorganic and organic compounds*, Pergamon Press New York, Part I and II, **1963**.
[78] M. S. Maru, S. Ram, J. H. Adwani, R. S. Shukla, *ChemistrySelect* **2017**, *2*, 3823−3830.
[79] Y. Himeda, N. Onozawa-Komatsuzaki, H. Sugihara, K. Kasuga, *Organometallics* **2007**, *26*, 702−712.
[80] K. Rohmann, J. Kothe, M. W. Haenel, U. Englert, M. Hölscher, W. Leitner, *Angew. Chem. Int. Ed*. **2016**, *55*, 8966−8969.
[81] S. Moret, P. J. Dyson, G. Laurenczy, *Nat. Commun*. **2014**, *5*, 4017.
[82] C. Fink, S. Katsyuba, G. Laurenczy, *Phys. Chem. Chem. Phys.* **2016**, *18*, 10764−10773.
[83] N. M. Simon, M. Zanatta, F. P. dos Santos, M. C. Corvo, E. J. Cabrita, J. Dupont, *ChemSusChem* **2017**, *10*, 4927−4933.
[84] J. X. Mao, J. A. Steckel, F. Yan, N. Dhumal, H. Kim, K. Damodaran, *Phys. Chem. Chem. Phys*. **2016**, *18*, 1911−1917.
[85] Y. Wu, Y. Zhao, H. Wang, B. Yu, X. Yu, H. Zhang, Z. Liu, *Ind. Eng. Chem. Res*. **2019**, *58*, 6333−6339.
[86] Z. Zhang, S. Hu, J. Song, W. Li, G. Yang, B. Han, *ChemSusChem* **2009**, *2*, 234−238.
[87] Z. Zhang, Y. Xie, W. Li, S. Hu, J. Song, T. Jiang, B. Han, *Angew. Chem. Int. Ed*. **2008**, *47*, 1127−1129.
[88] M. Besnard, M. I. Cabaço, F. V. Chávez, N. Pinaud, P. J. Sebastião, J. A. P. Coutinho, J. Mascetti, Y. Danten, *J. Phys. Chem. A* **2012**, *116*, 4890−4901.
[89] M. I. Qadir, A. Weilhard, J. A. Fernandes, I. de Pedro, B. J. C. Vieira, J. C. Waerenborgh, J. Dupont, *ACS Catal*. **2018**, *8*, 1621−1627.
[90] A. Weilhard, M. I. Qadir, V. Sans, J. Dupont, *ACS Catal.* **2018**, *8*, 1628−1634.
[91] M. Zanatta, A.-L. Girard, G. Marin, G. Ebeling, F. P. dos Santos, C. Valsecchi, H. Stassen, P. R. Livotto, W. Lewis, J. Dupont, *Phys. Chem. Chem. Phys.* **2016**, *18*, 18297.

[92] W. Leitner, E. Dinjus, F. Gaßner, *Aqueous Phase Organometallic Catalysis. Concepts and Applications* (Eds.: B. Cornils, W. A. Herrmann), Wiley-VCH, Weinheim, **1998**, p. 486.
[93] J. Klankermayer, S. Wesselbaum, K. Beydoun, W. Leitner, *Angew. Chem. Int. Ed*. **2016**, *55*, 7296−7343.
[94] S. Ogo, R. Kabe, H. Hayashi, R. Harada, S. Fukuzumi, *Dalton Trans.* **2006**, 4657−4663.
[95] J. Su, M. Lu, H. Lin, *Green Chem*. **2015**, *17*, 2769−2773.
[96] J. Su, L. Yang, M. Lu, H. Lin, *ChemSusChem* **2015**, *8*, 813−816.
[97] T. Wang, D. Ren, Z. Huo, Z. Song, F. Jin, M. Chen, L. Chen, *Green Chem*. **2017**, *19*, 716−721.
[98] D. Wei, X. Shi, P. Sponholz, H. Junge, M. Beller, *ACS Cent. Sci*. **2022**, *8*, 1457−1463.
[99] J. Sá, G. D. Arteaga, R. A. Daley, J. Bernardi, J. A. Anderson, *J. Phys. Chem. B* **2006**, *110*, 17090−17095.
[100] D. Preti, C. Resta, S. Squarcialupi, G. Fachinetti, *Angew. Chem. Int. Ed*. **2011**, *50*, 12551−12554.
[101] J. J. Anderson, D. J. Drury, J. E. Hamlin, A. G. Kent, WO 8602066, **1986**.
[102] M. J. Green, A. R. Lucy, M. Kitson, S. J. Smith, EP 0329337, **1989**.
[103] T. Schaub, R. A. Paciello, *Angew. Chem. Int. Ed*. **2011**, *50*, 7278−7282.
[104] H. Song, N. Zhang, C. Zhong, Z. Liu, M. Xiao, H. Gai, *New J. Chem*. **2017**, *41*, 9170−9177.
[105] P. Albers, J. Pietsch, S. F. Parker, *J. Mol. Catal. A Chem*. **2001**, *173*, 275−286.
[106] K. Koha, M. Jeon, D. M. Chevrier, P. Zhang, C. W. Yoon, T. Asefa, *Appl. Catal. B: Environ*. **2017**, *203*, 820−828.
[107] (a) P. G. Jessop, T. Ikariya, R. Noyori, *Chem. Rev*. **1995**, *95*, 2, 259−272; (b) P. G. Jessop, Y. Hsiao, T. Ikariya, R. Noyori, *J. Am. Chem. Soc*. **1996**, *118*, 344−355; (c) P. G. Jessop, F. Joó, C.-C. Tai, *Coord. Chem. Rev*. **2004**, *248*, 2425−2442; (d) Y. Himeda, *Eur. J. Inorg. Chem*. **2007**, 3927−3941; (e) C. Federsel, R. Jackstell, M. Beller, *Angew. Chem. Int. Ed*. **2010**, *49*, 6254−6257.; (f) W.-H. Wang, Y. Himeda, J. T. Muckerman, G. F. Manbeck, E. Fujita, *Chem. Rev*. **2015**, *115*, 12936−12973; (g) A. K. Singh, S. Singh, A. Kumar, *Catal. Sci. Technol*. **2016**, *6*, 12−40; (h) K. Dong, R. Razzaq, Y. Hu, K. Ding, *Top. Curr. Chem*. **2017**, *375*, 23.
[108] S. Chatterjee, I. Dutta, Y. Lum, Z. Lai, K.-W. Huang, *Energy Environ. Sci*. **2021**, *14*, 1194−1246.
[109] Y. Inoue, H. Izumida, Y. Sasaki, H. Hashimoto, *Chem. Lett*. **1976**, *5*, 8, 863−864.
[110] (a) Y. Musashi, S. Sakaki, *J. Am. Chem. Soc*. **2000**, *122*, 3867−3877; (b) S. Bontemps, L. Vendier, S. Sabo-Etienne, *Angew. Chem., Int. Ed*. **2012**, *51*, 1671−1674; (c) N. M. Rezayee, C. A. Huff, M. S. Sanford, *J. Am. Chem. Soc*. **2015**, *137*, 1028−1031; (d) R. Kuriki, K. Sekizawa, O. Ishitani, K. Maeda, *Angew. Chem. Int. Ed*. **2015**, *54*, 2406−2409; (e) J. Kothandaraman, A. Goeppert, M. Czaun, G. A. Olah, G. K. S. Prakash, *J. Am. Chem. Soc.* **2016**, *138*, 778−781; (f) Z. Li, T. M.

Rayder, L. Luo, J. A. Byers, C. Tsung, *J. Am. Chem. Soc*. **2018**, *140*, 8082−8085; (g) C. A. Huff, M. S. Sanford, *ACS Catal*. **2013**, *3*, 2412−2416; (h) G. A. Filonenko, M. P. Conley, C. Copéret, M. Lutz, E. J. M. Hensen, E. A. Pidko, *ACS Catal*. **2013**, *3*, 2522−2526; (i) J. Elek, L. Nádasdi, G. Papp, G. Laurenczy, F. Joó, *Appl. Catal. A: Gen*. **2003**, *255*, 59−67; (j) G. A. Filonenko, R. van Putten, E. N. Schulpen, E. J. M. Hensen, E. A. Pidko, *ChemCatChem* **2014**, *6*, 1526−1530; (k) M. Scott, B. B. Molinos, C. Westhues, G. Francik, W. Leitner, *ChemSusChem* **2017**, *10*, 1085−1093; (l) S. Sanz, A. Azua, E. Peris, *Dalton Trans*. **2010**, *39*, 6339−6343; (m) P. Munshi, A. D. Main, J. C. Linehan, C.-C. Tai, P. G. Jessop, *J. Am. Chem. Soc*. **2002**, *124*, 7963−7971; (n) C. Yin, Z. Xu, S.-Y. Yang, S. M. Ng, K. Y. Wong, Z. Lin, C. P. Lau, *Organometallics* **2001**, *20*, 1216−1222; (o) T.-T. Thai, B. Therrien, G. Süss-Fink, *J. Organomet. Chem*. **2009**, *694*, 3973−3981; (p) H. Horváth, G. Laurenczy, A. Kathó, *J. Organomet. Chem*. **2004**, *689*, 1036−1045.

[111] (a) F. Hutschka, A. Dedieu, M. Eichberger, R. Fornika, W. Leitner, *J. Am. Chem. Soc*. **1997**, *119*, 4432−4443; (b) A. Anaby, M. Feller, Y. Ben-David, G. Leitus, Y. Diskin-Posner, L. J. Shimon, D. Milstein, *J. Am. Chem. Soc*. **2016**, *138*, 9941−9950; (c) Q. Qian, J. Zhang, M. Cui, B. X. Han, *Nat. Commun*. **2016**, *7*, 11481; (d) C. M. Jens, M. Scott, B. Liebergesell, C. G. Westhues, P. Schäfer, G. Franciò, K. Leonhard, W. Leitner, A. Bardow, *Adv. Synth. Catal*. **2019**, *361*, 307−316.

[112] (a) J. F. Hull, Y. Himeda, W. H. Wang, B. Hashiguchi, R. Periana, D. J. Szalda, J. T. Muckerman, E. Fujita, *Nat. Chem*. **2012**, *4*, 383−388; (b) R. Tanaka, M. Yamashita, K. Nozaki, *J. Am. Chem. Soc*. **2009**, *131*, 14168−14169; (c) T. J. Schmeier, G. E. Dobereiner, R. H. Crabtree, N. Hazari, *J. Am. Chem. Soc*. **2011**, *133*, 9274−9277; (d) C. Liu, J. Xie, G. Tian, W. Li, Q. L. Zhou, *Chem. Sci*. **2015**, *6*, 2928−2931; (e) B. An, L. Zeng, M. Jia, Z. Li, Z. Lin, Y. Song, Y. Zhou, J. Cheng, C. Wang, W. B. Lin, *J. Am. Chem. Soc*. **2017**, *139*, 17747−17750; (f) R. Kanega, N. Onishi, D. J. Szalda, M. Z. Ertem, J. T. Muckerman, E. Fujita, Y. Himeda, *ACS Catal*. **2017**, *7*, 6426−6429; (g) A. Kumar, S. Semwal, J. Choudhury, *ACS Catal*. **2019**, *9*, 3, 2164−2168; (h) W.-H. Wang, J. T. Muckerman, E. Fujita, Y. Himeda, *ACS Catal*. **2013**, *3*, 856−860; (i) A. Azua, S. Sanz, E. Peris, *Chem. Eur. J*. **2011**, *17*, 3963−3967; (j) Y. Maenaka, T. Suenobu, S. Fukuzumi, *Energy Environ. Sci*. **2012**, *5*, 7360; (k) S.-M. Lu, Z. Wang, J. Li, J. Xiao, C. Li, *Green Chem*. **2016**, *18*, 4553−4558; (l) R. Puerta-Oteo, M. Hölscher, M. V. Jiménez, W. Leitner, V. Passarelli, J. J. Pérez-Torrente, *Organometallics* **2018**, *37*, 684−696.

[113] K. Mori, T. Sano, H. Kobayashi and H. Yamashita, *J. Am. Chem. Soc*. **2018**, *140*, 8902−8909.

[114] X. Zhang, G. Liu, K. Meiwes-Broer, G. Gantefor and K. Bowen, *Angew. Chem. Int. Ed*. **2016**, *55*, 9644−9647.

[115] Y. Jiang, O. Blacque, T. Fox and H. Berke, *J. Am. Chem. Soc*. **2013**, *135*, 7751−7760.

[116] Q. Liu, X. Yang, L. Li, S. Miao, Y. Li, Y. Q. Li, X. Wang, Y. Huang and T. Zhang, *Nat. Commun*. **2017**, *8*, 1407.

[117] K. Sordakis, C. Tang, L. K. Vogt, H. Junge, P. J. Dyson, M. Beller, G. Laurenczy, *Chem. Rev.* **2018**, *118*, 372−433.
[118] S. Wesselbaum, U. Hintermair, W. Leitner, *Angew. Chem. Int. Ed*. **2012**, *51*, 8585−8588.
[119] A. Weilhard, S. P. Argent, V. Sans, *Nat. Commun.* **2021**, *12*, 231.
[120] T. Singh, S. Jalwal, S. Chakraborty, *Asian J. Org. Chem*. **2022**, *11*, e202200330.
[121] C. Ziebart, C. Federsel, P. Anbarasan, R. Jackstell, W. Baumann, A. Spannenberg, M. Beller, *J. Am. Chem. Soc.* **2012**, *134*, 20701−20704.
[122] F. Bertini, N. Gorgas, B. Stöger, M. Peruzzini, L. F. Veiros, K. Kirchner, L. Gonsalvi, *ACS Catal*. **2016**, *6*, 2889−2893.
[123] A. Z. Spentzos, C. L. Barnes, W. H. Bernskoetter, *Inorg. Chem.* **2016**, *55*, 8225−8233.
[124] B. G. Schieweck, N. F. Westhues, J. Klankermayer, *Chem. Sci*. **2019**, *10*, 6519−6523.
[125] M. V. Vollmer, J. Ye, J. C. Linehan, B. J. Graziano, A. Preston, E. S. Wiedner, C. C. Lu, *ACS Catal*. **2020**, *10*, 2459−2470.
[126] K. Chaudhary, M. Trivedi, D. T. Masram, A. Kumar, G. Kumar, A. Husain, N. P. Rath, *Dalton Trans*. **2020**, *49*, 2994−3000.
[127] D. Wei, R. Sang, P. Sponholz, H. Junge, M. Beller, *Nat. Energy*, **2022**, *7*, 438−447.
[128] Z. T. Hlatshwayo, J. G. Doremus, P. L. McGrier, *ChemCatChem* **2022**, *14*, e202200783.
[129] L. Le-Quang, M. Stanbury, S. Chardon-Noblat, J.-M. Mouesca, V. Maurel, J. Chauvin, *Chem. Commun*. **2019**, *55*, 13598−13601.
[130] P. Bhanja, A. Modak, A. Bhaumik, *Chem. Eur. J*. **2018**, *24*, 7278−7297.
[131] Y. Liu, W. Zhou, W. L. Teo, K. Wang, L. Zhang, Y. Zeng, Y. Zhao, *Chem*. **2020**, *6*, 3172−3202.
[132] X. Li, Q. Su, K. Luo, H. Li, G. Li, Q. Wu, *Mater. Lett*. **2021**, *282*, 128704.
[133] Z. Xu, N. D. McNamara, G. T. Neumann, W. F. Schneider, J. C. Hicks, *ChemCatChem* **2013**, *5*, 1769−1771.
[134] N. D. McNamara, J. C. Hicks, *ChemSusChem* **2014**, *7*, 1114−1124.
[135] K. Park, G. H. Gunasekar, N. Prakash, K-D. Jung, S. Yoon, *ChemSusChem* **2015**, *8*, 3410−3413.
[136] G. H. Gunasekar, D. Hyuna, P. Natarajana, K.-D. Jung, S. Yoona, *Catal. Today* **2016**, *265*, 52−55.
[137] A. V. Bavykina, E. Rozhko, M. G. Goesten, T. Wezendonk, B. Seoane, F. Kapteijn, M. Makkee, J. Gascon, *ChemCatChem* **2016**, *8*, 2217−2221.
[138] G. H. Gunasekar, K. Park, V. Ganesan, K. Lee, N.-K. Kim, K.-D. Jung, S. Yoon, *Chem. Mater*. **2017**, *29*, 6740−6748.
[139] G. H. Gunasekar, K. Park, H. Jeong, K.-D. Jung, K. Park, S. Yoon, *Catalysts* **2018**, *8*, 295.
[140] G. H. Gunasekar, J. Shin, K.-D. Jung, K. Park, S. Yoon, *ACS Catal*. **2018**, *8*, 4346−4353.

[141] G. H. Gunasekar, S. Yoon, *J. Mater. Chem. A* **2019**, *7*, 14019−14026.
[142] Y. Kuwahara, Y. Fujie, H. Yamashita, *ChemCatChem* **2017**, *9*, 1906−1914.
[143] H.-K. Lo, I. Thiel, C. Copéret, *Chem. Eur. J*. **2019**, *25*, 9443−9446.
[144] J. J. Corral-Pérez, A. Billings, D. Stoian, A. Urakawa, *ChemCatChem* **2019**, *11*, 4725−4730.
[145] K.-R. Oh, G.-N. Yun, K.-D. Kim, Y.-J. Cheong, C. Yoo, F. Prihatno, H.-Y. Jang, A. H. Valekar, G.-Y. Cha, M. Lee, J. Jung, Y.-U. Kwon, Y. K. Hwang, *Chem. Mater*. **2022**, *34*, 8153−8162.
[146] Y.-M. Yu, Y.-P. Zhang, J.-H. Fei, X.-M. Zheng, *Chinese J. Chem*. **2005**, *23*, 977−982.
[147] Y.-M. Yu, J.-H. Fei, Y.-P. Zhang, X.-M. Zheng, *Chinese J. Chem*. **2006**, *24*, 840−844.
[148] Y.-M. Yu, J.-H. Fei, Y.-P. Zhang, X.-M. Zheng, *J. Fuel Chem. Technol*. **2006**, *34*, 6, 700−705.
[149] Y.-P. Zhang, J.-H. Fei, Y.-M. Yu, X.-M. Zheng, *Catal. Lett*. **2004**, *93*, 231−234.
[150] V. Srivastava, *Open Chem*. **2018**, *16*, 853−863.
[151] Z.-Z. Yang, H. Zhang, B. Yu, Y. Zhao, G. Ji, Z. Liu, *Chem. Commun*. **2015**, *51*, 1271−1274.
[152] G. H. Gunasekar, K.-D. Jung, S. Yoon, *Inorg. Chem*. **2019**, *58*, 3717−3723.
[153] C. Wu, F. Irshad, M. Luo, Y. Zhao, X. Ma, S. Wang, *ChemCatChem* **2019**, *11*, 1256−1263.
[154] R. Sun, A. Kann, H. Hartmann, A. Besmehn, P. J. C. Hausoul, R. Palkovits, *ChemSusChem* **2019**, *12*, 3278−3285.
[155] B. Chen, M. Dong, S. Liu, Z. Xie, J. Yang, S. Li, Y. Wang, J. Du, H. Liu, B. Han, *ACS Catal*. **2020**, *10*, 8557−8566.
[156] K. Mori, T. Taga, H. Yamashita, *ACS Catal*. **2017**, *7*, 3147−3151.
[157] D. A. Bulushev, J. R.H. Ross, *Catal. Rev*. **2018**, *60*, 4, 566−593.
[158] G. H. Gunasekar, K. Park, K.-D. Jung, S. Yoon, *Inorg. Chem. Front*. **2016**, *3*, 882−895.
[159] A. A. Olajire, *J. CO_2 Util*. **2018**, *24*, 522−547.
[160] G. Bredig, S. R. Carter, *Ber. Dtsch. Chem. Ges*. **1914**, 47, 541−545.
[161] M. W. Farlow, H. Adkins, *J. Am. Chem. Soc*. **1935**, *57*, 2222−2223.
[162] R. Sun, Y. Liao, S.-T. Bai, M. Zheng, C. Zhou, T. Zhang, B. F. Sels, *Energy Environ. Sci*. **2021**, *14*, 1247−1285.
[163] M. Liu, Y. Xu, Y. Meng, L. Wang, H. Wang, Y. Huang, N. Onishi, L. Wang, Z. Fan, Y. Himeda, *Adv. Energy Mater*. **2022**, *12*, 2200817.
[164] D. Preti, S. Squarcialupi, G. Fachinetti, *ChemCatChem* **2012**, *4*, 469−471.
[165] G. A. Filonenko, W. L. Vrijburg, E. J.M. Hensen, E. A. Pidko, *J. Catal*. **2016**, *343*, 97−105.
[166] (a) A. Ciftci, D. A. J. M. Ligthart, P. Pastorino, E. J. M. Hensen, *Appl. Catal. B* **2013**, *130−131*, 325−335; (b) P. Liu, E. J. M. Hensen, *J. Am. Chem. Soc.* **2013**, *135*, 14032−14035; (c) P. Liu, C. Li, E. J. M. Hensen, *Chem. Eur. J.* **2012**, *18*,

12122−12129; (d) P. Liu, Y. Guan, R. A. van Santen, C. Li, E. J. M. Hensen, *Chem. Commun*. **2011**, *47*, 11540−11542; (e) A. E. Saunders, M. B. Sigman, B. A. Korgel, *J. Phys. Chem. B* **2004**, *108*, 193−199; (f) R. Sharma, G. P. Holland, V. C. Solomon, H. Zimmermann, S. Schiffenhaus, S. A. Amin, D. A. Buttry, J. L. Yarger, *J. Phys. Chem. C* **2009**, *113*, 16387−16393; (g) P. M. Shem, R. Sardar, J. S. Shumaker-Parry, *Langmuir* **2009**, *25*, 13279−13283.

[167] C.-L. Chiang, K.-S. Lin, H.-W. Chuang, C.-M. Wu, *Int. J. Hydrog. Energy* **2017**, *42*, 23647−23663.

[168] C.-L. Chiang, K.-S. Lin, H.-W. Chuang, *J. Clean. Prod*. **2018**, *172*, 1957−1977.

[169] H. Reymond, J. J. Corral-Pérez, A. Urakawa, P. R. von Rohr, *React. Chem. Eng*. **2018**, *3*, 912−919.

[170] C. Hao, S. Wang, M. Li, L. Kang, X. Ma, *Catal. Today* **2011**, *160*, 184−190.

[171] N. Liu, R. Du, W. Li, *Adv. Mater. Res*. **2013**, *821−822*, 1330−1335.

[172] N. Liu, J. Lei, M. Li, P. Wang, *Adv. Mater. Res*. **2014**, *881−883*, 283−286.

[173] W. Zhang, S. Wang, Y. Zhao, X. Ma, *Fuel Process. Technol*. **2018**, *178*, 98−103.

[174] P. R. Upadhyay, V. Srivastava, *RSC Adv*. **2016**, *6*, 42297.

[175] P. Upadhyay, V. Srivastava, *Catal. Lett*. **2016**, *146*, 12−21.

[176] V. Srivastava, *Catal. Lett*. **2014**, *144*, 1745−1750.

[177] P. R. Upadhyay, V. Srivastava, *Catal. Lett*. **2017**, *147*, 1051−1060.

[178] V. Srivastava, *Catal. Lett*. **2014**, *144*, 12, 2221−2226.

[179] S. K. Kabra, E. Turpeinen, M. Huuhtanen, R. L. Keiski, G. D. Yadav, *Chem. Eng. J.* **2016**, *285*, 625−634.

[180] M. S. Maru, S. Ram, R. S. Shukla, N.-ul H. Khan, *Mol. Catal.* **2018**, *446*, 23−30.

[181] S. J. Louis Anandaraj, L. Kang, S. DeBeer, A. Bordet, W. Leitner, *Small* **2023**, 2206806.

[182] L. T. M. Nguyen, H. Park, M. Banu, J. Y. Kim, D. H. Youn, G. Magesh, W. Y. Kim, J. S. Lee, *RSC Adv*. **2015**, *5*, 105560.

[183] H. Park, J. H. Lee, E. H. Kim, K. Y. Kim, Y. H. Choi, D. H. Youn, J. S. Lee, *Chem. Commun*. **2016**, *52*, 14302−14305.

[184] C. Mondelli, B. Puértolas, M. Ackermann, Z. Chen, J. Pérez-Ramírez, *ChemSusChem* **2018**, *11*, 2859−2869.

[185] H. Wiener, J. Blum, H. Feilchenfeld, Y. Sasson, N. Zalmanov, *J. Catal*. **1988**, *110*, 1, 184−190.

[186] E. González, C. Marchant, C. Sepúlveda, R. García, I. T. Ghampson, N. Escalona, J. L. García-Fierro, *Appl. Catal. B: Environ*. **2018**, *224*, 368−375.

[187] X. Shao, J. Xu, Y. Huang, X. Su, H. Duan, X. Wang, T. Zhang, *AlChE J.* **2016**, *62*, 2410−2418.

[188] L.-C. Lee, X. Xing, Y. Zhao*, ACS Appl. Mater. Interfaces* **2017**, *9*, 38436−38444.

[189] Y. Zhou, Y. Huang, B. Jin, X. Luo, Z. Liang, *Ind. Eng. Chem. Res*. **2019**, *58*, 44−52.

[190] X. Shao, X. Miao, X. Yu, W. Wang, X. Ji, *RSC Adv*. **2020**, *10*, 9414.

[191] Z. Zhang, L. Zhang, M. J. Hülsey, N. Yan, *Mol. Catal*. **2019**, *475*, 110461.

[192] J. Zhang, W. Liao, H. Zheng, Y. Zhang, L. Xia, B.-T. Teng, J.-Q. Lu, W. Huang, Z. Zhang, *J. Catal.* **2022**, *405*, 152−163.
[193] Q. Sun, X. Fu, R. Si, C.-H. Wang, N. Yan, *ChemCatChem* **2019**, *11*, 5093−5097.
[194] Q. Sun, B. W. J. Chen, N. Wang, Q. He, A. Chang, C.-M. Yang, H. Asakura, T. Tanaka, M. J. Hülsey, C.-H. Wang, J. Yu, N. Yan, *Angew. Chem. Int. Ed*. **2020**, *59*, 20183−20191.
[195] S. Masuda, K. Mori, Y. Futamura, H. Yamashita, *ACS Catal*. **2018**, *8,* 2277−2285.
[196] K. Mori, S. Masuda, H. Tanaka, K. Yoshizawa, M. Chee, H. Yamashita, *Chem. Commun.* **2017**, *53*, 4677−4680.
[197] M. Wen, K. Mori, Y. Futamura, Y. Kuwahara, M. Navlani-García, T. An, H. Yamashita, *Nature* **2019**, *9*, 15675.
[198] K. Mori, A. Konishi, H. Yamashita, *J. Phys. Chem. C* **2020**, *124*, 11499−11505.
[199] X. Shao, X. Miao, T. Zhang, W. Wang, J. Wang, X. Ji, *ACS Appl. Nano Mater*. **2020**, *3*, 9209−9217.
[200] Q.-Y. Bi, J.-D. Lin, Y.-M. Liu, X.-L. Du, J.-Q. Wang, H.-Y. He, Y. Cao, *Angew. Chem. Int. Ed*. **2014**, *53*, 13583−13587.
[201] F. Wang, J. Xu, X. Shao, X. Su, Y. Huang, T. Zhang, *ChemSusChem* **2016**, *9*, 246−251.
[202] K. Nakajima, M. Tominaga, M. Waseda, H. Miura, T. Shishido, *ACS Sustainable Chem. Eng*. **2019**, *7*, 6522−6530.
[203] G. Yang, Y. Kuwahara, S. Masuda, K. Mori, C. Louis, H. Yamashita, *J. Mater. Chem. A* **2020**, *8*, 4437−4446.
[204] Y. Kuwahara, Y. Fujie, T. Mihogi, H. Yamashita, *ACS Catal*. **2020**, *10*, 6356−6366.
[205] L. Xu, T. Cui, J. Zhu, X. Wang, M. Ji, *New J. Chem*. **2021**, *45*, 6293−6300.
[206] P. Patel, S. Nandi, M. S. Maru, R. I. Kureshy, N.-ul H. Khan, *J. CO_2 Util*. **2018**, *25*, 310−314.
[207] P. H. Pandey, H. S. Pawar, *J. CO_2 Util*. **2020**, *41*, 101267.
[208] Y. Zhao, T. Wang, X. Wang, R. Hao, H. Wang, *Chem. Eng. J.* **2018**, *347*, 860−869.
[209] Y. Zhao, T. Wang, Y. Wang, R. Hao, H. Wang, Y. Han, *J. Ind. Eng. Chem.* **2019**, *77*, 291−302.
[210] X.-P. Fu, L. Peres, J. Esvan, C. Amiens, K. Philippot, N. Yan, *Nanoscale* **2021**, *13*, 8931.
[211] K. Philippot, B. Chaudret, *C. R. Chim*. **2003**, *6*, 1019−1034.
[212] M. Wang, J. Zhang, N. Yan, *Front. Chem*. **2013**, *1*, 1−8.
[213] D. Wei, X. Shi, R. Qu, K. Junge, H. Junge, M. Beller, *ACS Energy Lett.* **2022**, *7*, 3734−3752.
[214] R. Williams, R. S. Crandall, A. Bloom, *Appl. Phys. Lett.* **1978**, *33*, 381−383.
[215] J. Eppinger, K.-W. Huang, *ACS Energy Lett*. **2017**, *2*, 188−195.
[216] F. Joó, *ChemSusChem* **2008**, *1*, 805−808.
[217] S. Enthaler, J. von Langermann, T. Schmidt, *Energy Environ. Sci*. **2010**, *3*, 1207−1217.
[218] B. Zaidman, H. Wiener, Y. Sasson, *Int. J. Hydrog. Energy* **1986**, *11*, 341−347.

[219] R. Qu, K. Junge, M. Beller, *Chem. Rev*. **2023**, *123*, 1103−1165.
[220] A. Kann, H. Hartmann, A. Besmehn, P. J. C. Hausoul, R. Palkovits, *ChemSusChem* **2018**, *11*, 1857−1865.
[221] A. Kipshagen, J. C. Baums, H. Hartmann, A. Besmehn, P. J. C. Hausoul, R. Palkovits, *Catal. Sci. Technol*. **2022**, *12*, 5649−5656.
[222] K. Park, G. H. Gunasekar, S.-H. Kim, H. Park, S. Kim, K. Park, K.-D. Jung, S. Yoon, *Green Chem*. **2020**, *22*, 1639−1649.
[223] S. Schlussel, S. Kwon, *Korean J. Chem. Eng.* **2022**, *39*, 11, 2883−2895.
[224] Q.-Y. Bi, J.-D. Lin, Y.-M. Liu, H.-Y. He, F.-Q. Huang, Y. Cao, *Angew. Chem. Int. Ed.* **2016**, *55*, 11849−11853.
[225] M. Lu, J. Zhang, Y. Yao, J. Sun, Y. Wang, H. Lin, *Green Chem*. **2018**, *20*, 4292−4298.
[226] L. Zou, Q. Liu, Q. Zhang, Z. Zhu, Y. Huang, Z. Liang, *Ind. Eng. Chem. Res*. **2022**, *61*, 2455−2468.
[227] Z. Chen, C. A. M. Stein, R. Qu, N. Rockstroh, S. Bartling, J. Weiß, C. Kubis, K. Junge, H. Junge, M. Beller, *ACS Catal*. **2023**, *13*, 4835−4841.
[228] K. Grubel, H. Jeong, C. W. Yoon, T. Autrey, *J. Energy Chem*. **2020**, *41*, 216−224.
[229] S. Masuda, Y. Shimoji, K. Mori, Y. Kuwahara, H. Yamashita, *ACS Appl. Energy Mater*. **2020**, *3*, 5819−5829.

UNIVERSITAT ROVIRA I VIRGILI
EFFICIENT VALORIZATION OF CO2 INTO FORMATE THROUGH NANOCATALYSIS
María Dolores Fernández Martínez

CHAPTER 2

Objectives

UNIVERSITAT ROVIRA I VIRGILI
EFFICIENT VALORIZATION OF CO2 INTO FORMATE THROUGH NANOCATALYSIS
María Dolores Fernández Martínez

The environmental issues arising from the high concentration of CO_2 in the atmosphere are nowadays regarded as critical and have triggered much interest in research towards the development of non-fossil-based feedstocks. In this context, despite its inertness, CO_2 has become a very attractive C1 source to obtain fuels and chemicals. Among the potential transformations, the hydrogenation of CO_2 into formic acid and derivatives have become a priority in view of the recent progress made in the production of H_2 *via* water splitting. Moreover, the development of catalytic systems that could be active in both the hydrogenation of CO_2 into formic acid derivatives and in their dehydrogenation to use them in reduction reactions is of high interest.
The general objective of this thesis is the development of efficient catalytic systems for the hydrogenation of CO_2 into formates and for the dehydrogenation of the formate products in reduction reactions.

Inspired by the state-of-the-art described in Chapter 1, the specific objectives of this work were defined as follow:

- **Objective 1: Development of efficient ligand-capped palladium heterogeneous catalysts for the hydrogenation of CO_2 into formates**

  Chapter 3 describes the preparation of a series of Pd based nanocatalysts stabilized by phosphine and NHC-ligands and supported onto inorganic solids, and their application in the CO_2 hydrogenation into formates. The first part of this chapter deals with the synthesis of the Pd NPs *via* the organometallic approach, including the utilization of various ligands and supports, and the characterization of the resulting materials. The second part of the chapter describes the catalytic testing of these materials and their recycling.

- **Objective 2: Study of the mechanism of CO_2 hydrogenation into formates using ligand-capped Pd NPs by DFT calculations**

  Chapter 4 explores the structural and electronic properties of two of the ligand-caped Pd catalysts described in Chapter 3 using a **Pd_{55}** NP model and how they affect their performance in the hydrogenation of CO_2 into formate. In the first part of this chapter, the more favorable adsorption

modes of the PPh_3 and PTA ligands over Pd NP were determined, as well as the degree of coverage involved when these ligands are used as NP stabilizers. In the second part of the chapter, the interactions between bicarbonate and the Pd surface was investigated.

- **Objective 3: Enhancement of the activity and stability of TiO_2 supported PPh_3-capped palladium nanocatalysts in the CO_2 hydrogenation into formates through modifications by organic molecules.**

Chapter 5 describes the modifications of TiO_2 supported PPh_3-capped palladium catalysts by organosilanes and organophosphonic acids following two approaches: the modification of the TiO_2 support prior to Pd NP deposition and the modification of the previously synthesized PPh_3-capped Pd catalyst supported on TiO_2. In the first part of this chapter, the preparation of two series of catalytic materials is detailed, together with their characterization. In the second part of this chapter, these materials were tested in the CO_2 hydrogenation into formates and their catalytic performance compared with that of the reference catalyst in terms of activity and reusability.

- **Objective 4: Evaluation of the catalytic performance of the PPh_3-capped Pd catalyst on TiO_2 in the reduction of nitroaromatics and related cascade reactions using potassium formate reducing agent.**

Chapter 6 briefly explores the performance of **Pd-PPh_3/TiO_2** in the reduction of nitrophenols and nitroarenes and in the direct reductive amination of aldehydes using potassium formate as reducing agent.

CHAPTER 3

Hydrogenation of CO_2 into formates by ligand-capped palladium heterogeneous catalysts

UNIVERSITAT ROVIRA I VIRGILI
EFFICIENT VALORIZATION OF CO2 INTO FORMATE THROUGH NANOCATALYSIS
María Dolores Fernández Martínez

3.1. Introduction

The environmental issues arising from the high concentration of CO_2 in the atmosphere are nowadays regarded as critical and have triggered much interest in research towards the development of non-fossil-based feedstocks. In this context, despite its inertness, CO_2 has become a very attractive C1 source to obtain fuels and chemicals.[1] However, commercially, the transformation of CO_2 into chemicals is currently limited to the production of urea,[2] polycarbonates,[3] salicylic acid,[4] methanol[1c,5] and carboxylic acids.[6] Among the potential transformations of CO_2, its hydrogenation into formic acid and derivatives (Figure 1) have become a priority in view of the recent progress made in the production of H_2 *via* water splitting.[7]

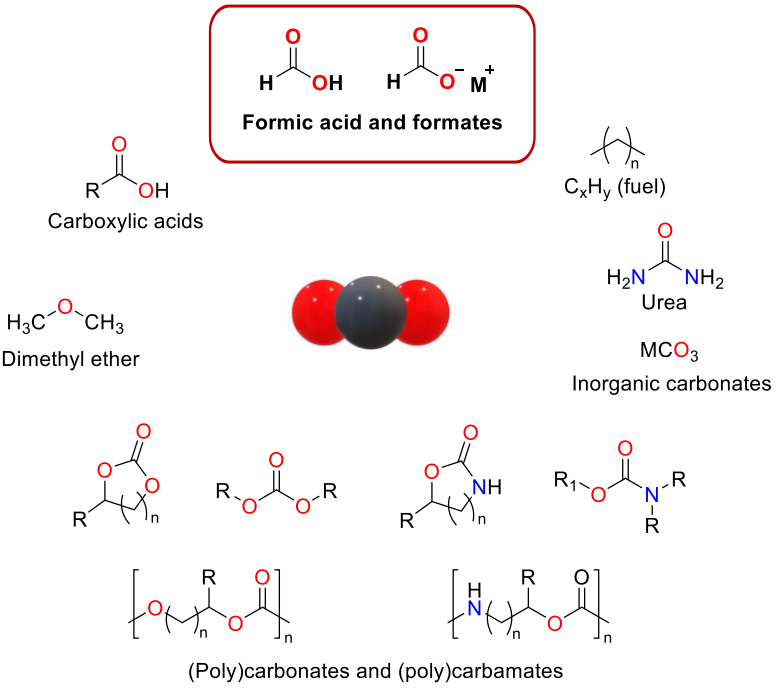

Figure 1. High-added value products obtained from CO_2.

Indeed, formic acid presents high hydrogen storage capacity and stability and provides a way to store CO_2 in a chemically stable form, giving rise to CO_2 mediated hydrogen energy cycle.[8]

However, the harsh conditions usually required made the design of efficient and reusable catalysts for this transformation very challenging.

As previously mentioned in Section 1.2.1. of Chapter 1, several highly active homogeneous catalysts were described for the transformation of CO_2 into formic acid/formates.[9,10]

On the other hand, heterogenized[11] and heterogeneous[12] catalysts are usually less active but provide advantages in term of handling and separation for subsequent recycling and reuse. However, if the reaction is performed in the gas phase, high temperatures are usually required and the most interesting products such as HCOOH and MeOH are thermodynamically disfavored.[13] In aqueous phase, the reaction becomes slightly exothermic due to solvation effects and is even more favorable under alkaline conditions. In this process, the pH is a crucial parameter due to the low solubility of CO_2 in water, the type of base used, the temperature and the pressure of CO_2 and H_2. The hydrogenation of CO_2 under basic conditions or from the hydrogenation of carbonates or bicarbonates has several advantages over the HCO_2H/CO_2 system since it allows the release of H_2 without producing CO.

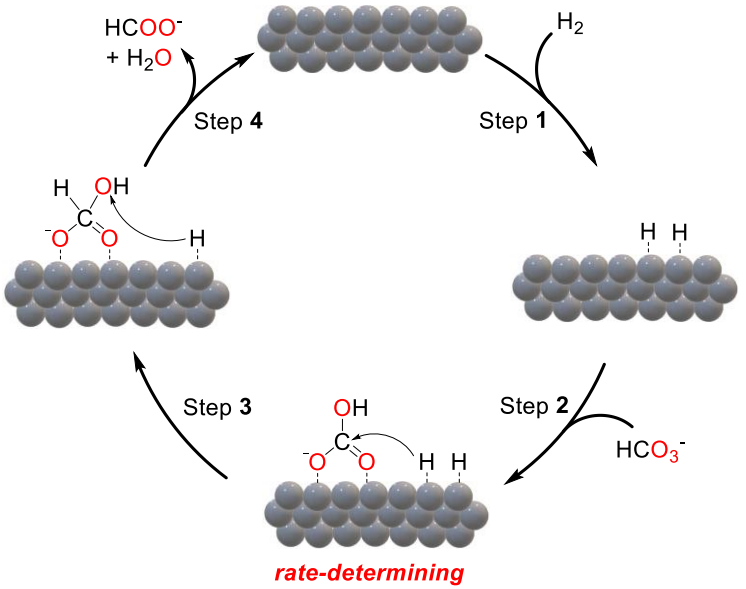

Scheme 1. Mechanism of hydrogenation of CO_2 in basic media.

The heterogeneous process involves the adsorption and activation of HCO_3^-/CO_2 in solution, the adsorption and dissociation of H_2 and the formation and desorption of formate over the catalyst (Scheme 1), which in turn are mainly

dependent on the number of catalytic active sites, the electron density at the metal and the interactions between active sites and chemical intermediates. As a result, it was reported that the particle size of the catalysts and the electron density at the metal are key factors for the activity in this reaction.[14] Among the metals reported, Pd was described as one of the most active metals for the production of formic acid/formate[8b,15] and the combination of Pd with other metals such as Au,[8b,16] Ag,[17] and Ni also revealed efficient for this transformation.[18] The choice of the support in this reaction is also important and for instance, Pd catalysts on carbon based supports such as reduced graphene oxide (*r*GO), N-doped carbon (N-C) or mesoporous graphitic carbon nitride (*g*-C_3N_4) revealed very efficient for the hydrogenation of bicarbonates to formates.[16,19] For instance, Shishido and coworkers reported a TOF of 5820 h^{-1} based on the Pd on surface using 10Au1Pd@AC catalyst under 50 bar of H_2 and using NH_4HCO_3 as base.[16] Zhang and coworkers reported a TON of 6595 for Pd on surface of the system Pd@*mpg*-C_3N_4 under 60 bar of H_2 and using $KHCO_3$ as base (Scheme 2).[19]

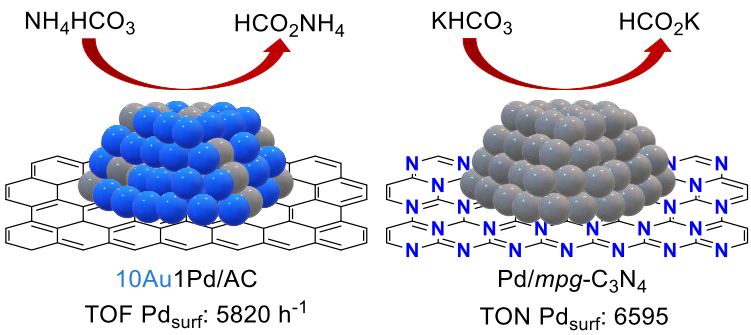

Scheme 2. Hydrogenation of bicarbonate to formate using carbon supported Pd based systems.

In 2018, Mori et al. reported the highly efficient CO_2 hydrogenation using Pd based catalysts supported onto TiO_2.[17c] In this study, they showed that using bimetallic Pd/Ag nanoparticles, isolated and electron-rich Pd atoms are created and enhance the electronegativity of the dissociated hydride species, resulting in superior catalytic performance. Using the Pd@Ag/TiO_2 catalyst, they obtained a TON of 2496. This value increased to 14839 when authors calculated it using the number of Pd surface atoms obtained by pulsed CO

adsorption measurements (Figure 2). This TON was obtained under 20 bar of pressure (CO_2:H_2, 1:1) and using $NaHCO_3$ as base.

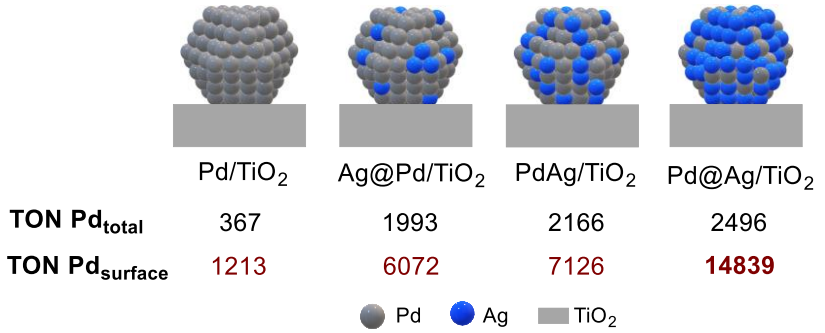

Figure 2. Comparison of the catalytic activities of a series of supported PdAg catalysts with different surface compositions during the CO_2 hydrogenation to formate.

In this work, the preparation of heterogeneous CO_2 hydrogenation catalysts based on palladium nanoparticles supported on TiO_2 is reported. The decomposition of an organometallic precursor was performed under H_2 in the presence of various ligand stabilizers to control the surface composition and the size of the nanoparticles. Indeed, comparison with other methods such as chemical reduction or wetness impregnation reduction, this organometallic approach initially developed by Philippot and Chaudret yields nanoparticles with a clean surface that do not require activation at high temperature.[20,21] Here, phosphorus based ligands and a *N*-heterocyclic carbene were used as capping agents for Pd nanoparticles and the effect on their catalytic performance in the hydrogenation of CO_2 into formate was particularly looked at.

3.2. Results and Discussion

3.2.1. Synthesis and characterization of ligand-stabilized Pd NPs supported over TiO_2

The effect of the ligands on the properties of the resulting nanoparticles such as size, dispersion and morphology were first evaluated using TiO_2 as support. Catalysts were prepared with a nominal loading of 4 wt% Pd over TiO_2. The general procedure and the ligands used in the synthesis are described in Scheme 3.

In a common experiment, TiO_2 was first dried in an oven at 100 ºC overnight. The metal precursor and the ligand (0.1 equiv. in the case of bidentate ligand, 0.5 equivalent for NHC ligand) were weighted in the glove box and charged in a Fischer-Porter bottle. Then, support and solvent (THF, 100 ml) were added, the Fischer-Porter was closed, purged with hydrogen several times and then charged with 3 bar of H_2. The mixture was then heated at 60 ºC and stirred at 700 rpm overnight. After the reaction, the mixture was cooled to room temperature and re-entered in the glove box. Samples for TEM analysis were prepared by deposition of five drops of the reaction crude onto a copper grid. The rest of the reaction crude was concentrated and washed several times with hexane. The catalyst was dried under vacuum during several hours.

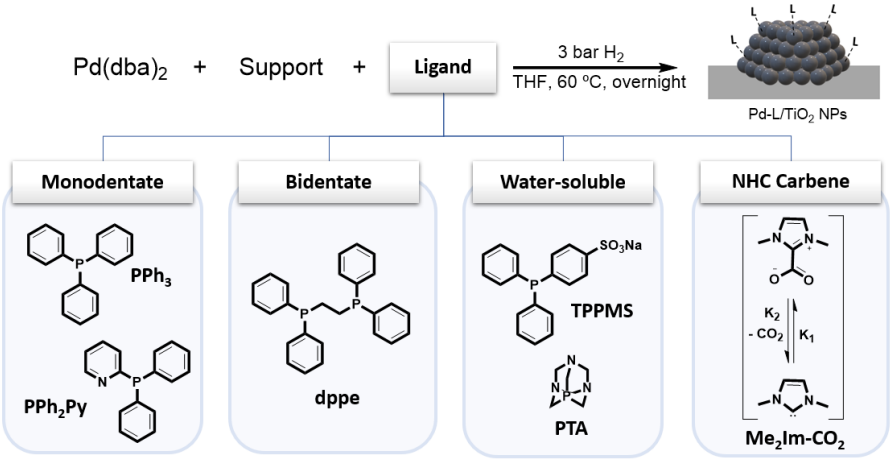

Scheme 3. General procedure for the synthesis of supported Pd-NPs in the presence of ligands.

Various phosphines were used such as triphenylphosphine (PPh_3),[22] which was previously reported as an essential additive for the reduction of CO_2 to FA with heterogeneous catalyst,[14b,23] diphenyl-2-pyridylphosphine (PPh_2Py) and water soluble phosphines such as 1,3,5-triaza-7-phosphaadamantane (PTA) and 3-(diphenylphosphino) benzenesulfonic acid sodium salt (TPPMS) that were previously reported using molecular catalysts.[24,25] The *N*-heterocyclic carbene (NHC) precursor 1,3-dimethylimidazolium-2-carboxylate ($Me_2Im\text{-}CO_2$), previously utilized by our group for the synthesis of mono- and bimetallic nanoparticles,[26] was also tested.

In all cases, highly crystalline small nanoparticles with spherical shape were obtained. In the presence of ligands, the size of the nanoparticles was in the range 2-3 nm with narrow distributions (Table 1, Figure 3). In contrast, when no ligand was used in the synthesis, the nanoparticles displayed a diameter of 5.4 nm with a broad size distribution (Table 1, Entry 7). This clearly indicated the strong stabilizing ability of these ligands and their importance to form small and well-defined NPs under these conditions. The smallest nanoparticles (*ca*. 2 nm) were obtained using water-soluble phosphines (PTA and TPPMS; Table 1, Entries 3 and 4). Chaudret and co-workers reported the synthesis of Ru and Pt nanoparticles with this ligand and demonstrated that the coordination of PTA to NPs occurs through the P atom.[27]

Table 1. Characterization data for TiO_2 supported Pd NPs stabilized by different ligands.[a]

Entry	Ligand	Particle size (nm)	ICP (Pd wt%)
1	PPh_3	2.37 ± 0.19	3.98
2	PPh_2Py	2.47 ± 1.30	3.07
3	PTA	1.92 ± 0.91	2.97
4	TPPMS	2.02 ± 1.57	2.99
5	$Me_2Im\text{-}CO_2$	2.83 ± 1.38	3.12
6	dppe	2.31 ± 0.82	3.00
7[b]	-	5.36 ± 2.83	4.09
8[c]	PPh_3	2.25 ± 0.91	3.31

[a]Synthesis conditions: Pd 4 wt% (metal precursor $Pd(dba)_2$), 0.2 equiv. of ligand (except for dppe and NHC: 0.1 equiv. and 0.5 equiv.), 1 g of TiO_2, 200 ml THF, 3 bar H_2, 60 ºC, overnight. [b]In absence of ligand. [c]Using 0.4 equiv. of ligand per Pd.

The NPs stabilized with dppe, PPh_3, PPh_2Py and the NHC revealed slightly larger. When the PPh_3:Pd ratio was increased from 0.2 to 0.4 (Entry 1 *vs*. Entry 8), no significant differences were observed in terms of mean diameter, although the distribution was slightly broader. In terms of metal content, the particles stabilized with PTA and TPPMS exhibited the lowest Pd contents and those synthesized in the absence of ligand, the largest.

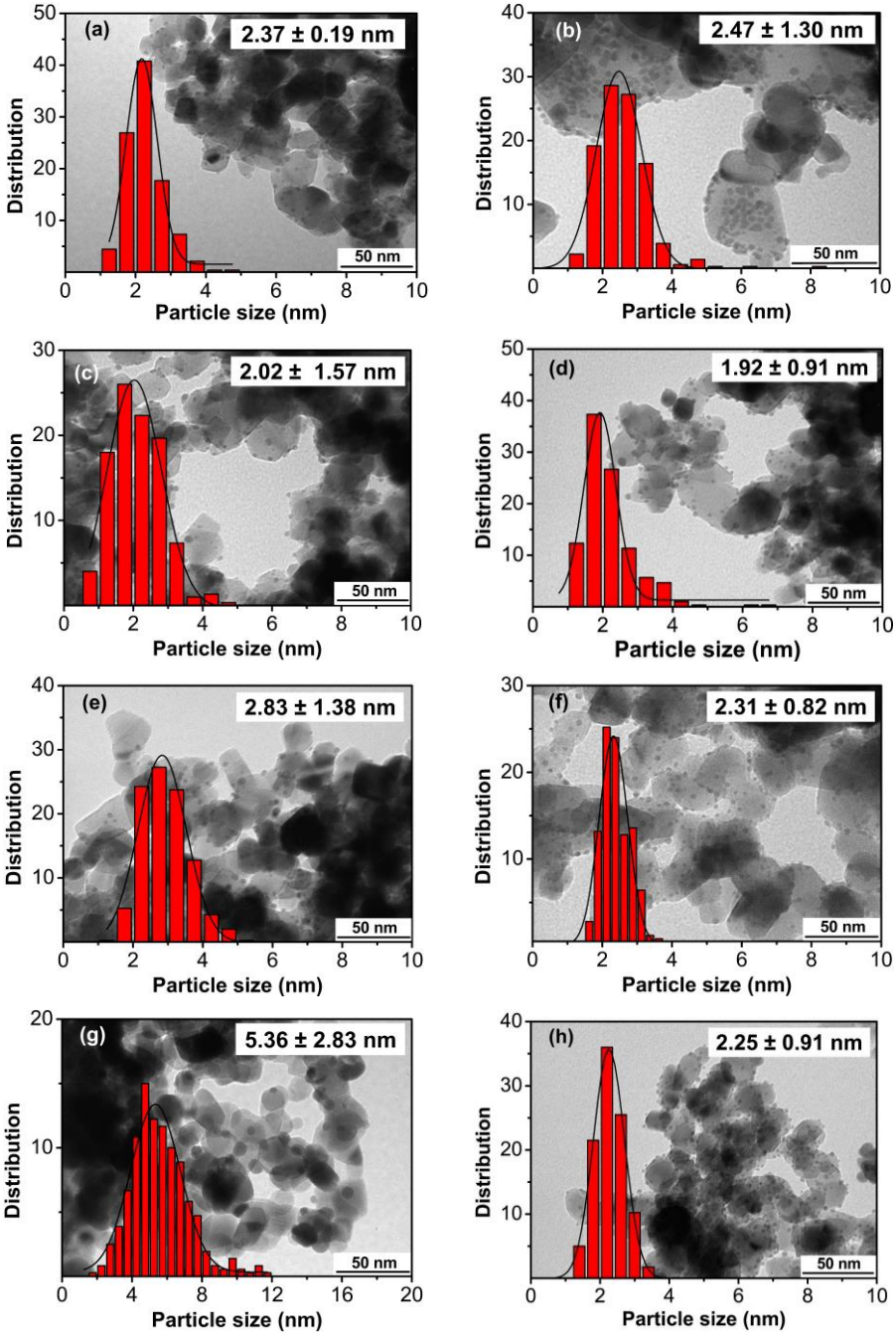

Figure 3. TEM images of Pd-NPs supported over TiO_2 and stabilized with PPh_3 (a), PPh_2Py (b), TPPMS (c), PTA (d), $Me_2Im\text{-}CO_2$ (e), dppe (f), without stabilizer (g) and with 0.4 eq of PPh_3 (h).

Some of these catalysts were also characterized by HR-TEM. For **Pd-Pd-PPh$_3$/TiO$_2$** highly crystalline nanoparticles were found (Figure 4 (b)). Additionally, the presence of P at the surface of the nanoparticles was confirmed by EDX (Figure 4 (c)).

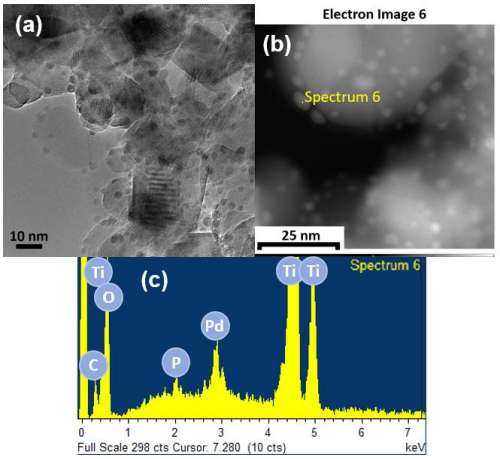

Figure 4. HR-TEM (a), SEM-EDX and HR-HAADF STEM analyses (b) and (c) of the **Pd-PPh$_3$/TiO$_2$** catalyst.

Other catalysts were also characterized by HR-TEM (Figure 5) and the observed sizes are similar to those obtained by TEM. When PTA was used as ligand for the synthesis of supported NPs (Figure 5 (a)), EDX mapping confirmed the presence of Pd and P at the NP surface. The system synthesized in the absence of ligand, **Pd/TiO$_2$** (Figure 5 (b)), presented larger NPs as was previously observed.

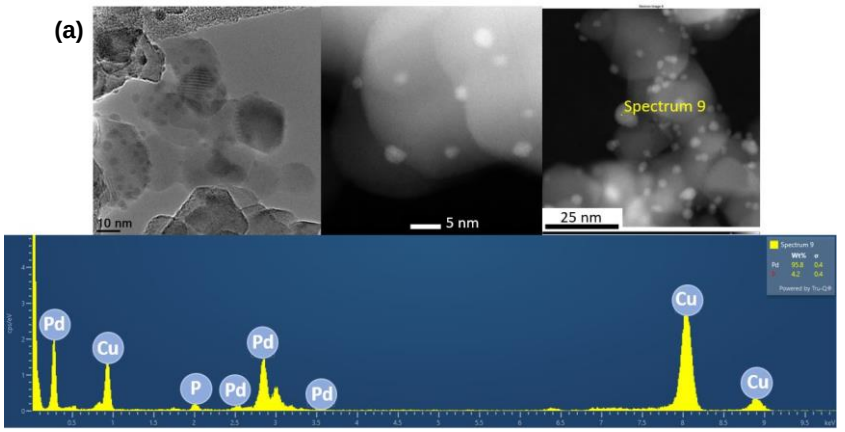

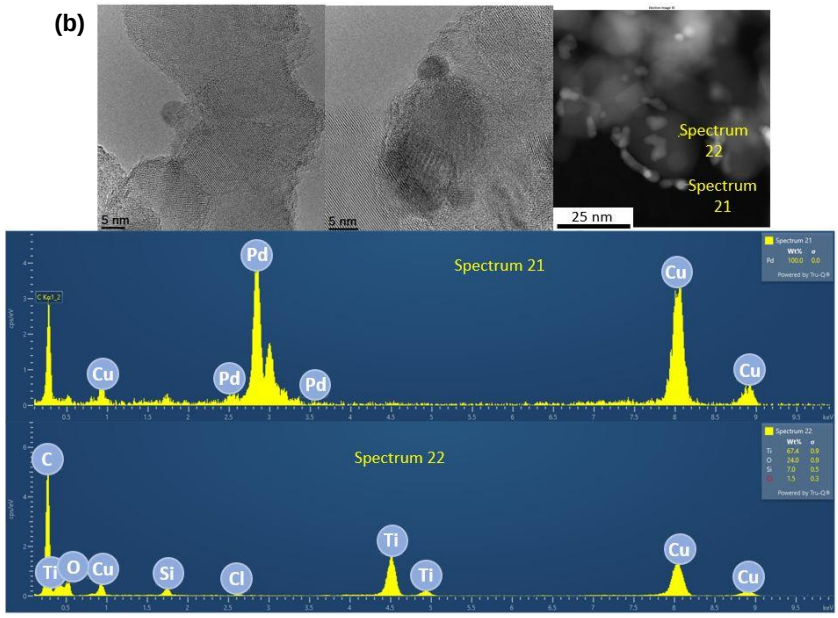

Figure 5. HR-TEM, SEM-EDX and HR-HAADF STEM analyses of **Pd-PTA/TiO_2** (a) and **Pd/TiO_2** (b) catalysts.

XRD analysis of **Pd-PPh_3/TiO_2** did not reveal information about the crystalline structure of the supported nanoparticles due to the high crystallinity of the TiO_2 support and the small size of the nanoparticles (Figure 6).

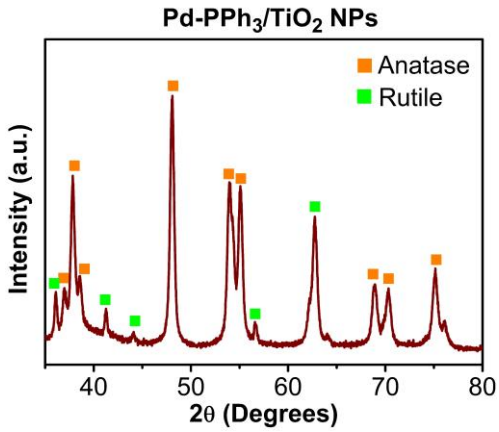

Figure 6. XRD of the catalyst **Pd-PPh_3/TiO_2**.

Next, the TiO_2 support and the TiO_2-supported Pd NPs were analyzed by TGA. For the support (Figure 7 (a)), a first weight lost was observed at T < 200 ºC and assigned to absorbed water, while the subsequent weight lost

between 200-600 ºC correspond to -OH on the surface of TiO_2 nanoparticles.[28] The TGA experiments carried out for every **Pd-ligand/TiO_2** system (Figure 7 (b)) synthesized shows differences between samples but did not reveal clear quantitative information about the content of organic material corresponding to the different ligands. This could be due to the very small proportion of organics compared with the total mass of the catalyst.

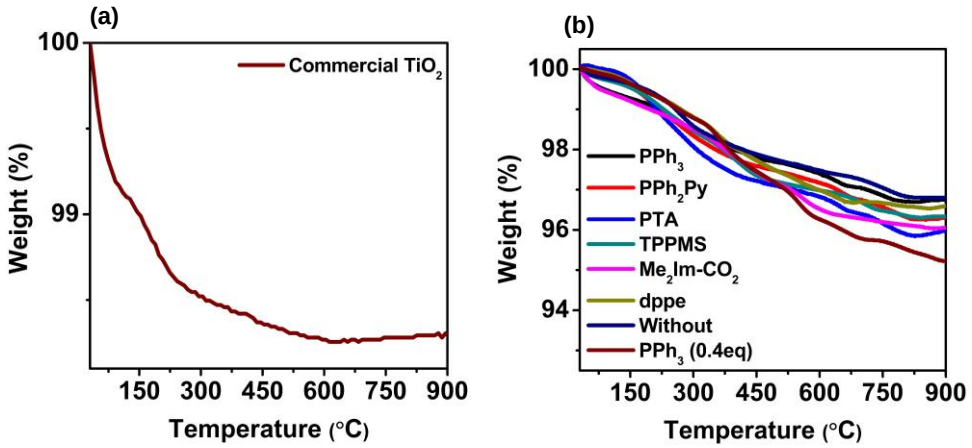

Figure 7. TGA plots for TiO_2 (a) and comparative image of TGA of Pd NPs stabilized with different ligands and supported over TiO_2 (b).

XPS analysis of the Pd nanoparticles stabilized with PPh_3 (Figure 8 (b)) evidenced that mainly zero valent Pd was present at the surface of TiO_2-supported NPs, although some $Pd^{\delta+}$ was detected (12.5%). Using reported methods, the percentage of $Pd^{\delta+}$ at the NP surface was calculated to be *ca.* 20% (Table 2).[29,30,31] The presence of P from the ligand was confirmed, as previously observed by EDX mapping.

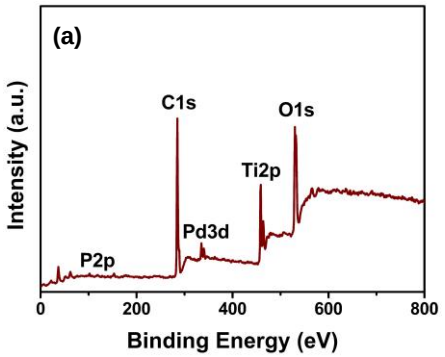

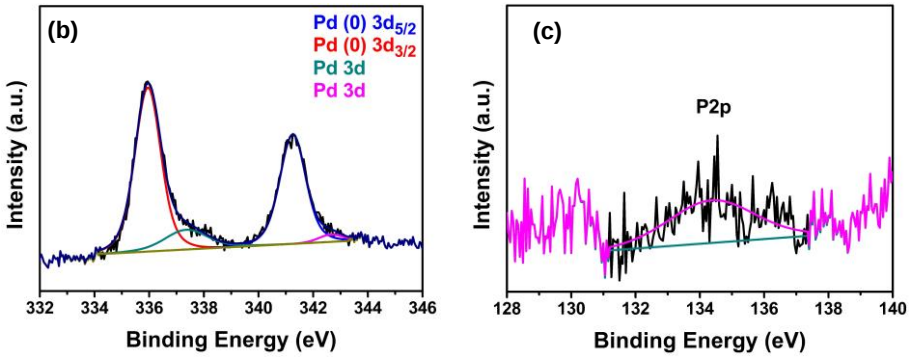

Figure 8. XPS spectra of **Pd-PPh$_3$/TiO$_2$** NPs.

Therefore, with this methodology, a series of small and well defined ligand-capped Pd NPs supported on TiO_2 was obtained.

Table 2. Percentage of the total particle surface which is oxidized for **Pd-PPh$_3$/TiO$_2$** NPs using reported methods.[29,30,31]

Method	N_t[a]	N_s[b]	N_s/N_t (%)	$Pd^{\delta+}$ in surface (%)
De Vries	284	166	58	21
Magic Numbers	303	160	53	24
VHH[c]	284	161	57	24

Average particle size measured by TEM: 2.37 nm. $Pd^{\delta+}$ detected by XPS: 12.5%. [a]N_t: Number of total atoms. [b]N_s: Number of surface atoms. [c]VHH: Van Hardevel Hartod method.

The presence of the ligands clearly influenced the size and size distribution of the synthesized nanoparticles. Moreover, the steric and electronic properties of these ligands also affected the size of the resulting NPs, although to a smaller extent.

3.2.2. Synthesis and characterization of PPh$_3$-stabilized Pd colloidal NPs

Colloidal Pd NPs stabilized with PPh_3 were also synthesized to obtain further information about these catalysts (Scheme 4).[32] These colloidal NPs exhibited a very small size (1.90 ± 0.57 nm) (Figure 9 (a)) which is in accordance to data obtained by HR-TEM (Figure 9 (b) and (c)). These colloidal NPs were thus slightly smaller than their analogues supported onto TiO_2.

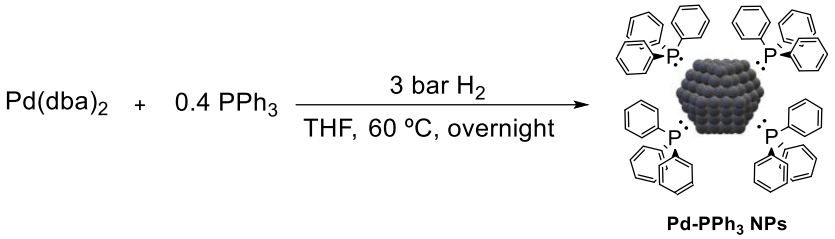

Scheme 4. Synthesis of colloidal nanoparticles stabilized nanoparticles with PPh_3.

Some agglomerations were sometimes detected when samples were prepared after isolation of the catalyst, and not directly from the crude. In terms of composition, only Pd and P are present in the sample (Figure 9 (e)).

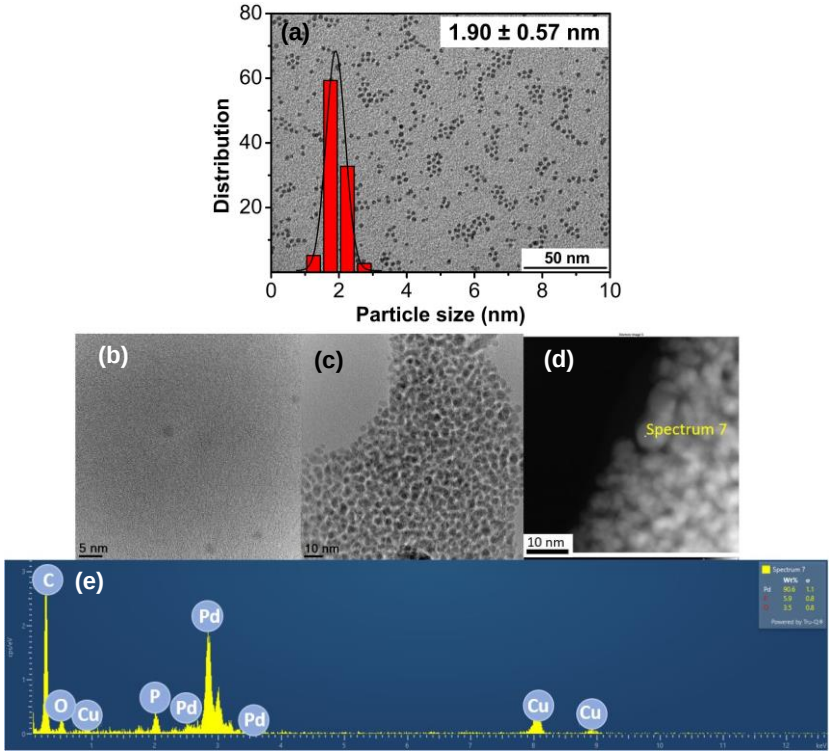

Figure 9. TEM image (a), HR-TEM (b), (c) and SEM-EDX and HR-HAADF STEM analyses (c) and (d) of colloidal **Pd-PPh_3** NPs.

XRD analysis of the corresponding colloidal nanoparticles was performed, the diffraction pattern observed indicated *fcc* packing of the Pd NPs (Figure 10).

To obtain some information on the ligand coverage at the surface of the synthesized nanoparticles, thermogravimetric analysis (TGA) of the colloidal NPs was performed (Figure 11).

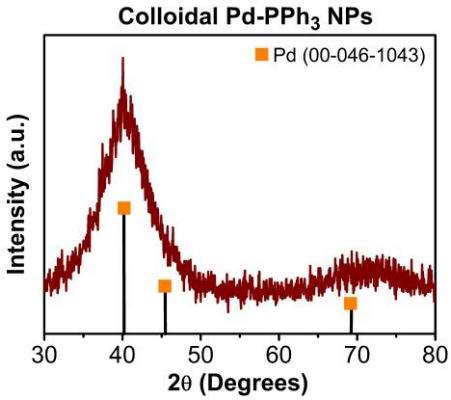

Figure 10. DRX of the colloidal **Pd-PPh$_3$** NPs.

A weight loss was observed at low temperature, attributed to the remaining solvent from the synthesis. A second weight loss was detected in the range of 150-300 ºC. This agrees with the temperature range expected for PPh_3 loss. This weight loss was of 25%. These colloidal **Pd-PPh$_3$** NPs were analyzed by NMR after its isolation and a small amount of hydrogenation product of dba was detected. This compound must also account for the weight loss observed.

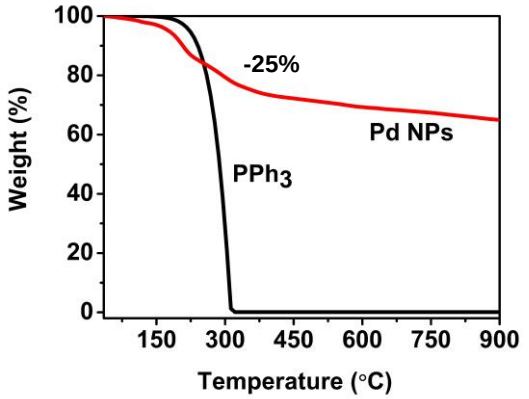

Figure 11. TGA plot of colloidal nanoparticles stabilized with PPh_3.

XPS analysis of this system also evidenced that mainly zero valent Pd present at the surface (Figure 12), although some $Pd^{\delta+}$ was detected (16%).

Using reported methods, the percentage of $Pd^{\delta+}$ at the NP surface was calculated to be *ca*. 23% (Table 3).[29,30,31]

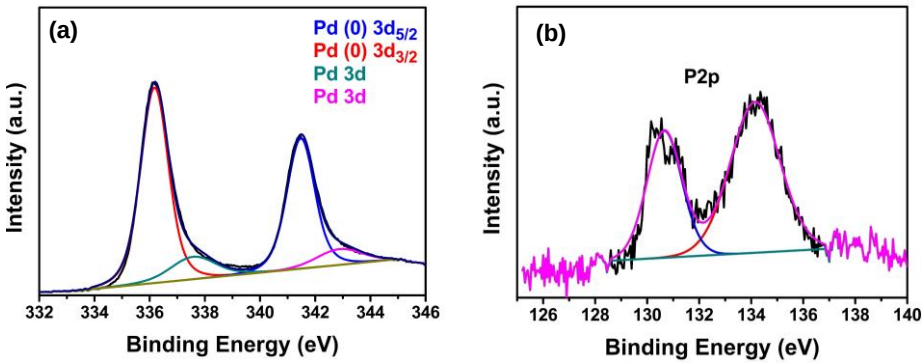

Figure 12. XPS spectra of colloidal palladium nanoparticles stabilized with PPh_3.

Table 3. Percentage of the total surface of the particle which is oxidized for colloidal nanoparticles stabilized with PPh_3 using reported methods.[29,30,31]

Method	N_t[a]	N_s[b]	N_s/N_t (%)	$Pd^{\delta+}$ in surface (%)
De Vries	147	103	70	23
Magic Numbers	155	96	62	26
VHH[c]	147	94	64	25

Average particle size measured by TEM: 1.90 nm. $Pd^{\delta+}$ detected by XPS: 16.0%. [a]N_t: Number of total atoms. [b]N_s: Number of surface atoms. [c]VHH: Van Hardevel Hartod method.

These data are in agreement with those calculated for the Pd-PPh_3 NPs supported on TiO_2. The synthesis of these NPs therefore confirm the *fcc* packing of Pd NPs stabilized by PPh_3.

3.2.3. Synthesis and characterization of PPh_3-stabilized Pd NPs supported over supports of different nature

Next, a second series of catalysts was synthesized using different supports such as metal oxides (TiO_2, CeO_2, Al_2O_3) and carbon-based supports (COF TpPa-1,[33] *g*-C_3N_4 and CNTs) using PPh_3 as stabilizing ligand (Scheme 5). In all cases, small and highly crystalline nanoparticles with spherical shape were obtained. The mean diameters of the corresponding Pd NPs varied between 2.3 and 3.5 nm depending on the support (Table 4 and Figure 13). When

CNTs, COF TpPa-1, TiO_2, CeO_2 and Al_2O_3 were used, the diameter of the resulting Pd NPs was in the range 2-3 nm, while slightly larger nanoclusters were formed using carbon nitride.

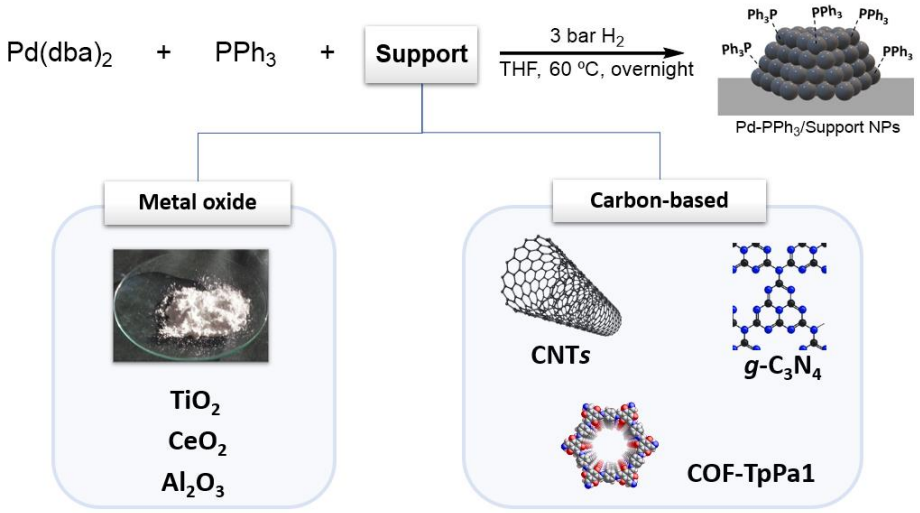

Scheme 5. General procedure for the synthesis of Pd-PPh_3 NPs in the presence of supports of different nature.

Interestingly, previous reports on Pd NPs supported onto COF TpPa-1 described the formation of particles with a diameter of 7 ± 3 nm.[34] Here, in the presence of PPh_3, the size of the NPs obtained onto the same support was *ca*. 2.3 nm, thus again indicating that the use of ligands leads to the formation of smaller and better defined Pd catalysts.

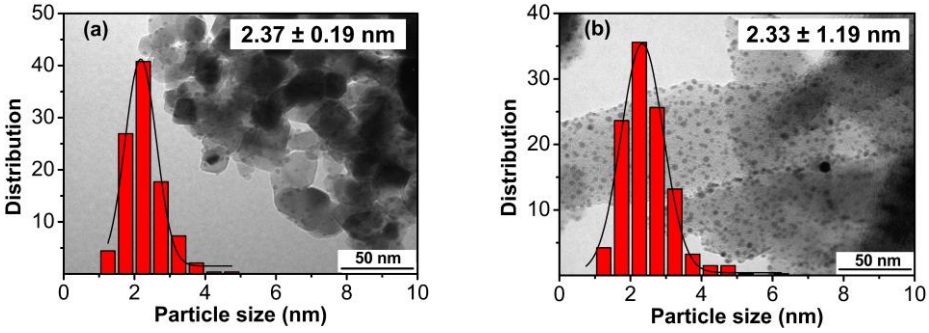

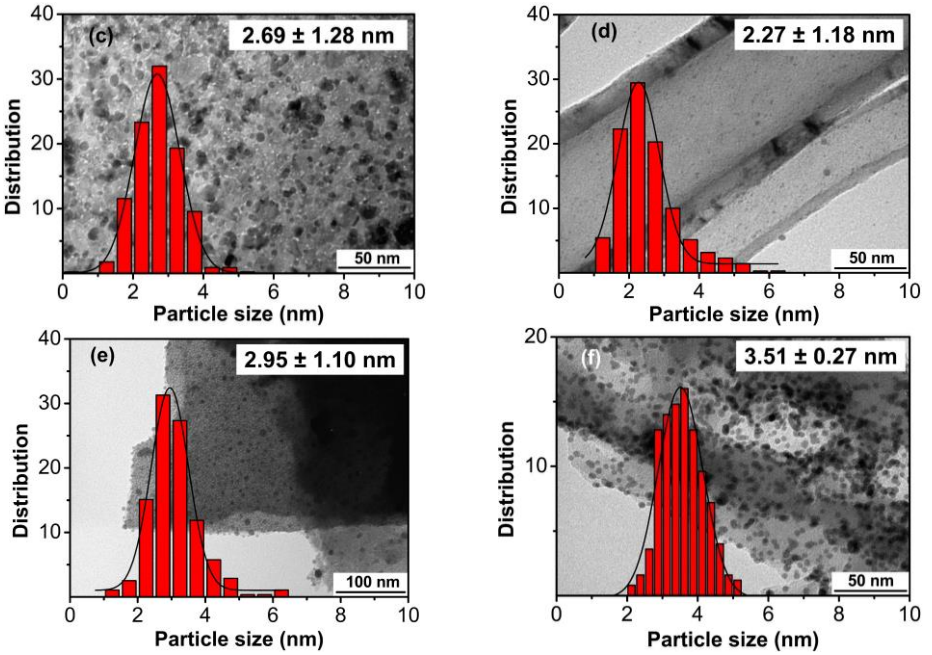

Figure 13. TEM images of Pd-NPs stabilized with PPh_3 and supported over TiO_2 (a), COF TpPa-1 (b), CeO_2 (c), CNTs (d), basic Al_2O_3 (e) and *g*-C_3N_4 (f).

Table 4. Characterization data Pd NPs catalysts stabilized by PPh_3 onto different supports.[a]

Entry	Support	Particle size (nm)	ICP (Pd wt%)
1	TiO_2	2.37 ± 0.19	3.98
2	CeO_2	2.69 ± 1.28	2.33
3	Al_2O_3	2.95 ± 1.10	3.32
4	CNTs	2.27 ± 1.18	2.55
5	COF TpPa-1	2.33 ± 1.19	2.09
6	*g*-C_3N_4	3.51 ± 0.27	3.07
7[b]	-	1.90 ± 0.57	-

[a]Synthesis conditions: Pd 4 wt% (metal precursor $Pd(dba)_2$), 0.2 equiv. of the corresponding ligand, 1 g of corresponding support, 200 ml THF, 3 bar H_2, 60 ºC, overnight. [b]In absence of support.

ICP analysis (Table 4) revealed a metal content of 2.09% for the COF TpPa-1 supported catalyst while the TiO_2 based material exhibited a content very

close to the nominal value (3.98%). The two supports with the lowest metal content were organic in nature.

Therefore, a strong effect of the support on the size of the Pd NPs was observed, probably due to the strength of the corresponding metal-support interactions.

3.2.4. CO_2 hydrogenation into formate

Initial catalytic experiments were carried out at 80 ºC in water with 4 M $KHCO_3$ and a total pressure of 36 bar (CO_2/H_2= 1) using both sets of synthesized Pd NPs as catalysts using 1,4-dioxane as internal standard.

The results obtained using TiO_2 supported catalysts bearing various ligands are summarized in Table 5.

Table 5. Effect of the ligand in the CO_2 hydrogenation to formate.[a]

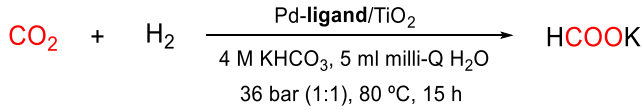

Entry	Ligand	TON[b]	TOF (h^{-1})[c]
1	PPh_3	876	58
2	PPh_2Py	700	47
3	PTA	385	26
4	TPPMS	701	47
5	Me_2Im-CO_2	506	34
6	Without	572	38
7	dppe	856	57
8	PPh_3 (0.4 equiv.)	868	58

[a]Reaction conditions: 20 mg of palladium supported nanoparticles catalyst stabilized with PPh_3, 5 ml milli-Q H_2O, $KHCO_3$ (4 M), 80 ºC, pTotal= 36 bar, $p(CO_2) = p(H_2)$, 15 h. [b]TON= mmol formate/mmol total of Pd, calculated by NMR using 1,4-dioxane as internal standard. [c]TOF= TON/t(h).

Turnover numbers obtained varied from 385 for the PTA capped catalyst (Entry 3) up to 876 (Entry 1) for that synthesized in the presence of PPh_3. It is noteworthy that when the catalytic experiments were performed using the catalysts synthesized in the presence of 0.4 equiv. of PPh_3, the activity

remained practically unchanged (Entry 8). The catalysts stabilized by the bidentate ligand dppe also provided high catalytic activity (TON= 856) while those containing PPh_2Py and TPPMS presented intermediate catalytic activities (TON= *ca.* 700, entries 2 and 4). Nanoparticles without ligand and those stabilized with NHC provided TON values somewhat lower (Entries 5 and 6).

Based on these results, it was concluded that the catalytic activity was not directly related with the size of the NPs (Figure 14) since the smallest NPs (PTA) provided the lowest TON value while the largest NPs (synthesized in the absence of ligand) exhibited an intermediate activity. In this series, the most active catalysts were those stabilized by PPh_3 and dppe. Recently, Staiger et al.[35] used different phosphines as additives for the synthesis of colloidal Pd NPs for semi-hydrogenation of alkynes. In their case, the results with PPh_3, compared with bulkier phosphines, provided the highest catalytic selectivity, which was explained by the steric inhibition of the active sites at the particle surface.

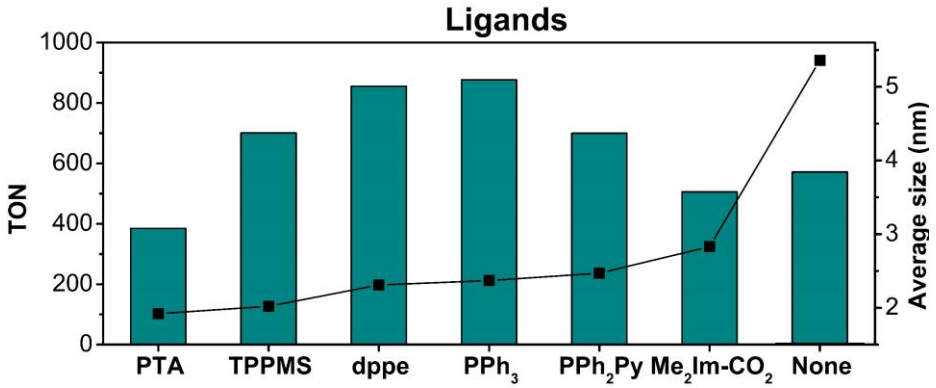

Figure 14. Effect of ligand on the size of NPs and catalytic activity for the hydrogenation of CO_2.

It should be noted that low catalytic activity was obtained using the NPs stabilized with NHC ligand, which could be due the stronger interaction between Pd and the ligand that reduced the number of active sites during catalysis. In the ligand-free nanoparticles, despite a more available surface, the activity was lower compared to most catalysts stabilized by phosphine ligands, which could be attributed to the size of the NPs and/or some electronic effect induced by the ligands. Surprisingly, when the nanoparticles

containing PTA, which exhibited the smallest size, were used, the lowest catalytic activity was obtained. This could be due to the blocking of surface active sites by the ligand and/ or a fast catalyst deactivation. For other water-soluble ligand (TPPMS) the activity was higher. For PPh_2Py, the catalytic activity was very similar to that of TPPMS.

Therefore, the variations observed in catalytic activity could not be related with the size of the nanoparticles obtained during the catalyst preparation, but with the electronic and steric properties that the ligands confer to the active phase.

Next, the effect of the support was evaluated in the CO_2 hydrogenation to formate under basic conditions. The results are summarized in Table 6.

Table 6. Effect of the support in CO_2 hydrogenation to formate.[a]

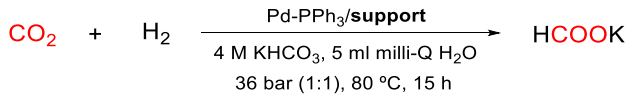

Entry	Support	TON[b]	TOF (h^{-1})[c]
1	TiO_2	876	58
2	CeO_2	243	16
3	CNTs	15	-
4	Al_2O_3	284	19
5	COF TpPa-1	321	21
6	*g*-C_3N_4	465	31
7	*Unsupported*	7	-

[a]Reaction conditions: 20 mg of palladium supported nanoparticles catalyst stabilized with PPh_3, 5 ml milli-Q H_2O, $KHCO_3$ (4 M), 80 ºC, pTotal= 36 bar, $p(CO_2) = p(H_2)$, 15 h. [b]TON= mmol formate/mmol total of Pd, calculated by NMR using 1,4-dioxane as internal standard. [c]TOF= TON/t(h).

Among the series, the highest activity was obtained using the TiO_2-based catalyst (Table 6, Entry 1, Figure 15). All the other supports provided much lower activities. For other metal oxides such as Al_2O_3, the TON values were below 300 (Entries 2 and 4). In the case of carbon-based supports, the highest activity was achieved using *g*-C_3N_4 (TON= 465, entry 6), followed by

COF TpPa-1 (TON= 321) while very low activity was obtained with catalysts supported on CNTs and colloidal nanoparticles.

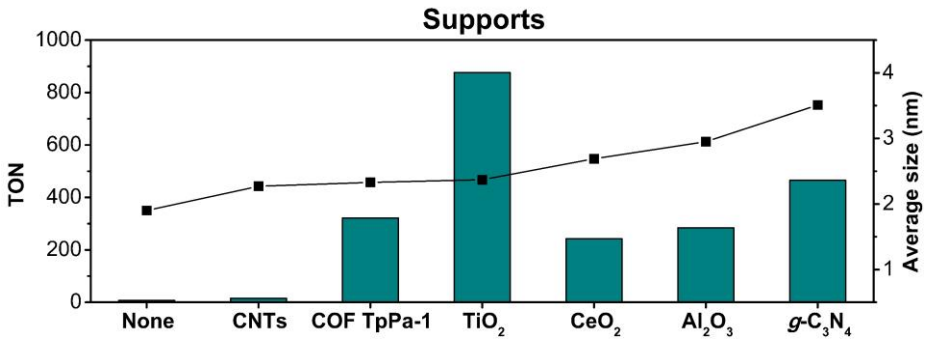

Figure 15. Effect of the support in the catalytic activity as a function of NP size for the hydrogenation of CO_2.

Comparing the results obtained with metal oxides, these results are in agreement with a previous report by Mori et al.[17c] that described TiO_2 based catalysts were more efficient than those on CeO_2. Regarding the size of the nanoparticles, in these two catalysts (2.37 ± 0.19 nm *vs.* 2.69 ± 1.28 nm, Figure 13 (a) and (c), Table 6), values are similar.

However, the metal content was higher (3.98 ± 0.03 wt% Pd) for **Pd-PPh$_3$/TiO$_2$** than for **Pd-PPh$_3$/CeO$_2$** (2.33 wt%), which could indicate a stronger metal-support interaction between Pd and TiO_2. Within the series, the lowest activity was observed for the **Pd-PPh$_3$/COF** TpPa-1 system (Table 6, Entry 5). This result could be explained by some stability issue of this support under basic conditions, as previously described,[33] although in another report, Pd catalysts supported on COF TpPa-1 were previously reported and no stability issues were indicated.[34]

These results thus highlight the importance of metal-support interactions to reach high catalytic activity in this reaction.

As previously mentioned, the base plays a fundamental role in the thermodynamics of this process. At pH 6-9, the true substrate of the reaction is not CO_2, but bicarbonate (HCO_3^-) since CO_2 dissolved in water shows a pH-dependent equilibrium between the HCO_3^- species (pKa_1= 6.35 at 25 ºC) and CO_3^{2-} (pKa_2= 10.33).[36] It was previously reported that the hydrogenation of carbonates is more difficult than that of bicarbonates in aqueous

solutions.[15c] Consequently, by increasing the pH, the balance changes from bicarbonate to carbonate, thus decreasing the yield to formate. Furthermore, the pH of the solution can influence the stability of metal hydrides.[37]
In this study, various organic and inorganic bases such as NEt_3, KOH, $KHCO_3$ and $NaHCO_3$ were tested (Table 7 and Figure 16).

Table 7. Effect of the nature of the base in CO_2 hydrogenation to formate.[a]

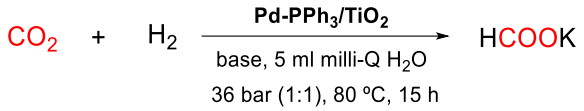

Entry	Base, 1 M	TON[b]	TOF (h^{-1})[c]
1	$NaHCO_3$	242	0.31
2	$KHCO_3$	319	0.41
3	KOH	229	0.29
4	NEt_3	6	0.42
5	None	9	0.57

[a]Reaction conditions: 20 mg **Pd-PPh3/TiO2** NPs, 5 ml milli-Q H_2O, 80 ºC, pTotal= 36 bar, $p(CO_2) = p(H_2)$, 15 h. [b]TON= mmol formate/mmol total of Pd, calculated by NMR using 1,4-dioxane as internal standard. [c]TOF= TON/t(h).

In the absence of base (Table 7, Entry 5), hardly any catalytic activity was observed. When NEt_3 was used (Table 7, Entry 4), low activity was obtained, probably due to the low solubility of this base in the reaction medium.

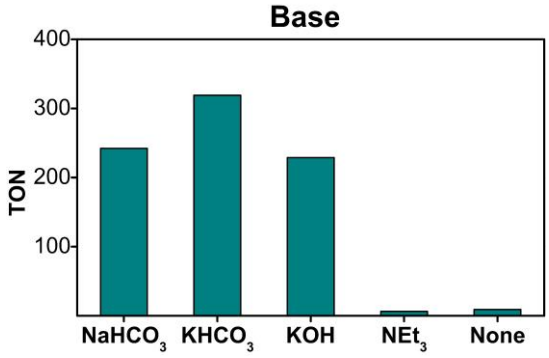

Figure 16. Effect of the base in the catalytic activity for the hydrogenation of CO_2.

When bicarbonates were used, high catalytic activity was reached with $KHCO_3$ compared with that obtained with $NaHCO_3$ (Table 7, Entry 2 *vs*. Entry 1). Similar effect was previously reported.[36]

Indeed, the cation can affect the balance between carbonate and bicarbonate. Moreover, $KHCO_3$ provides a higher concentration of HCO_3^- than $NaHCO_3$ in solution.[8b,15c,38] Using KOH, (Table 7, Entry 3), the catalytic activity was similar to that obtained using $NaHCO_3$.

The concentration of the base also proved important as TON values increased at higher base concentrations (Table 8).

Table 8. Effect of the concentration of the base in CO_2 hydrogenation to formate.[a]

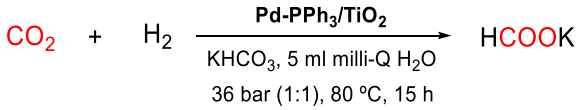

Entry	[$KHCO_3$], M	TON[b]	TOF (h^{-1})[c]
1	0.5	69	5
2	1	319	21
3	2	402	27
4	4	877	58

[a]Reaction conditions: 20 mg **Pd-PPh$_3$/TiO$_2$** NPs, 5 ml milli-Q H_2O, 80 ºC, pTotal= 36 bar, $p(CO_2) = p(H_2)$, 15 h. [b]TON= mmol formate/mmol total of Pd, calculated by NMR using 1,4-dioxane as internal standard. [c]TOF= TON/t(h).

The results described a volcano plot that could be explained by the lower solubility of CO_2 at higher temperature and/or the lower stability of the catalysts at T > 60 ºC. In terms of total pressure, upon increasing from 9 to 18, 24 up to 36 bar of CO_2, (Figure 17 (a)), the catalytic activity continuously increased. In terms of partial pressures (Figure 17 (b)), the ratio pCO_2:pH_2 1:2 provided the highest activity with a TON value of 1145. When the reaction temperature was optimized, the highest activity was obtained at 60 ºC (Figure 17 (c)). When the reaction was monitored over time (Figure 17 (d)), TOF values up to *ca*. 150 h^{-1} were obtained at early reaction times (1-2 h). At longer reaction times, TOF values decreased and after 15 h of reaction, the TOF values reached a maximum of *ca*. 70 h^{-1}. This value remained constant at

longer reaction times, thus indicating the deactivation of the catalyst under these conditions.

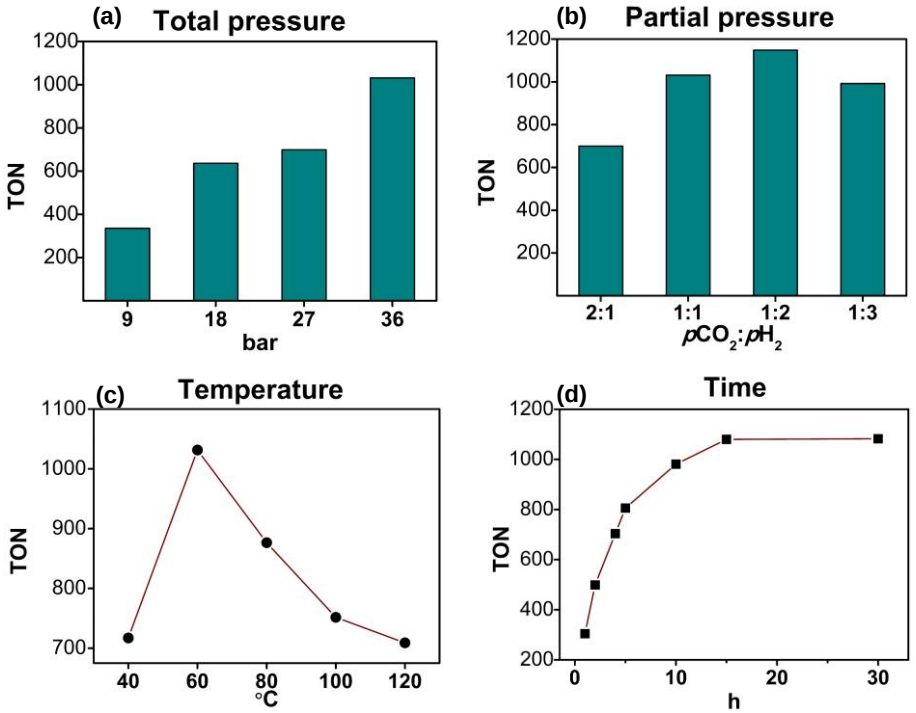

Figure 17. Variation of TON values as a function of (a) total pressure, (b) partial pressures, (c) temperature and (d) time in the hydrogenation of CO_2 using **Pd-PPh$_3$/TiO$_2$** as catalyst.

For comparison with reported catalytic performance, an important aspect to be mentioned is the calculation of the TON values. In this work, the TON is calculated as mol of formate divided by total mol of Pd, which is obtained by ICP. But in some studies, TON is calculated in a different way. Su et al.[38] calculated TON using the dispersion of metal atoms on the support surface. These values are calculated from the CO chemisorption analysis. Dispersion value obtained in this study for Pd/AC is 23.3% at 5 wt% of metal loading. Mori et al.[17c] also uses this approximation and TON values strongly increase when only Pd surface atoms are taken into account. In their case, the TON increased from 2496 to 14839 using dispersion obtained by CO chemisorption. In this context chemisorption with pulses of CO and also H_2 was performed with some of our catalysts. Several tests were performed, but

this technique was not compatible with the use of ligands due to the range of temperature required (between 200 to 500 ºC), and the results obtained were not conclusive.

Another way of calculating TON was proposed by Louis Anandaraj et al.[39] Surface atoms were estimated from the NPs diameter, calculating the volume of the NPs and the volume of the shell containing the first layer of Pd atoms (atomic radius of Pd: 140 pm). Using this approximation, the TON values were calculated for our systems bearing different ligands (Figure 18).

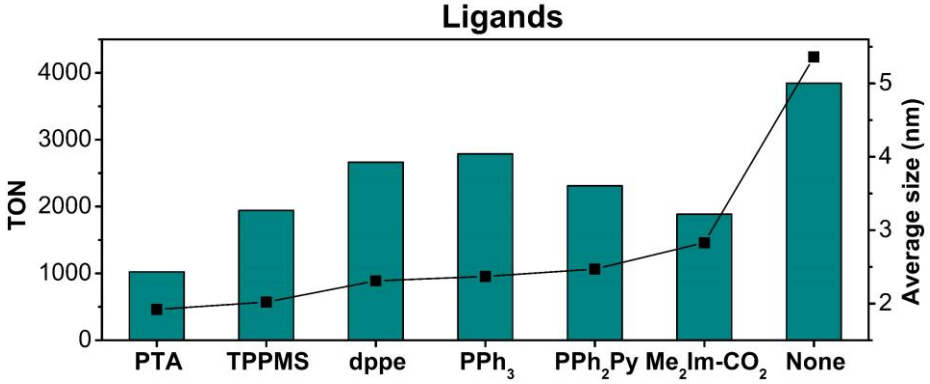

Figure 18. Effect of ligand on the size of NPs and catalytic activity for the hydrogenation of CO_2 with TON calculated in accordance at Pd surface atoms (%).

Another way to calculate Pd on surface is based on the use of De Vries[29,30] model which was used in this chapter to calculate the % of oxidized Pd at the surface. With this approximation TON follows the same trend that previously (Figure 19).

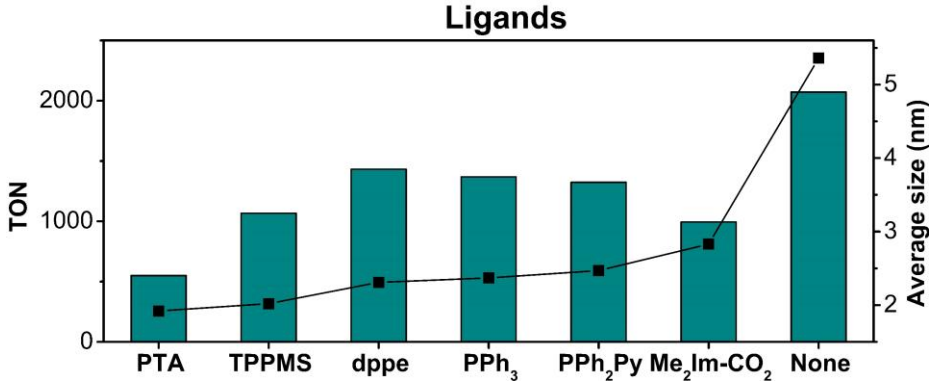

Figure 19. Effect of ligand on the size of NPs and catalytic activity for the hydrogenation of CO_2 with TON calculated with De Vries Method.

For the calculation of TON by Pd on surface through these approximations, the highest activity was obtained by **Pd/TiO_2**, the catalyst with the largest particle size. Since these NPs present less surface atoms compared with the total number of Pd atoms.

However, using these are approximations for our systems, several variables are ignored such as the presence of the support (so not all the surface is exposed) and the ligand (it could cover part of the surface of Pd).

In this section, all previously synthesized catalysts were tested in the hydrogenation of CO_2 to formate. The results obtained demonstrate the effect of the ligand employed and of the support. However, there is not a direct correlation between size and activity. **$Pd\text{-}PPh_3/TiO_2$** revealed the most active system with a TON of 1032 (TOF of 69 h^{-1}, [HCOOK]= 1.1 mol/l) under mild conditions of pressure and temperature (36 bar (pCO_2:pH_2= 1), 60 ºC, 15 h).

3.2.5. Catalyst recycling tests

A recyclability experiment was performed under optimized conditions using the TiO_2-supported Pd catalysts synthesized in the presence of PPh_3. After each catalytic test, the catalyst was recovered by centrifugation, washed three times with milli-Q water and dried. Then, the catalyst was redispersed in water, and fresh $KHCO_3$ and 1,4-dioxane were added. The procedure was repeated three times.

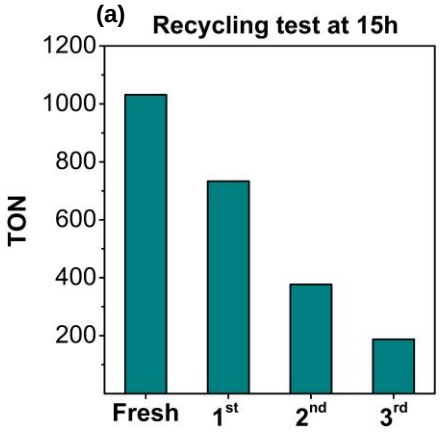

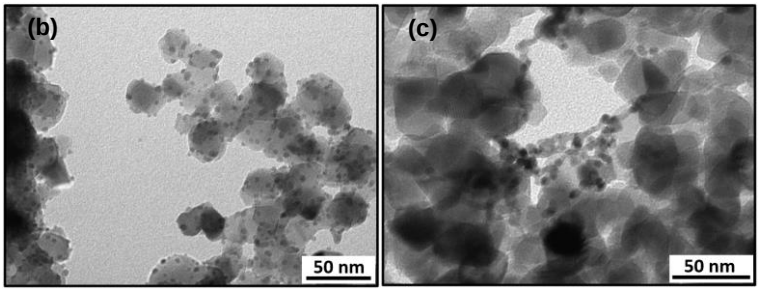

Figure 20. Recycling results using the catalyst **Pd-PPh$_3$/TiO$_2$** (a) and TEM images before catalysis (b) and after catalysis (c) with NPs on the order of 6 nm NPs (b) and agglomerates (c). Conditions: 20 mg of **Pd-PPh$_3$/TiO$_2$** catalyst, 5 ml milli-Q H_2O, $KHCO_3$ (4 M), pTotal= 36 bar, p(CO_2) = p(H_2), 60 ºC. TON= mmol formate/mmol total of Pd, calculated by NMR using 1,4-dioxane as internal standard.

However, a decrease in catalytic activity was observed after each run (Figure 20 (a)). TEM images of the catalyst (Figure 20 (b) and 20 (c)) after the third recovery revealed that the NPs had considerably increased in size (*ca*. 6 nm) and in some regions, agglomeration was also detected. Similar results were reported by Mori et al. for the system PdAg/TiO_2.[40] To avoid such agglomerations in catalysis, the use of ligands, polymers or surfactants were previously reported.[41]

ICP measurements of the catalytic solutions were performed but no Pd could be detected, indicating that no Pd leaching had occurred. It was therefore concluded that sintering of the Pd NPs was responsible of the decrease in catalytic activity during these experiments.

Other methods for recycling were carried out:

- Filtration using a Nylon membrane was tested instead of centrifugation but no differences were observed.
- Recycling with isolation of the catalyst was also performed after 1 h of reaction (Figure 21). However, a decrease in activity was also observed, probably due to the deactivation of catalyst even at early reaction times.

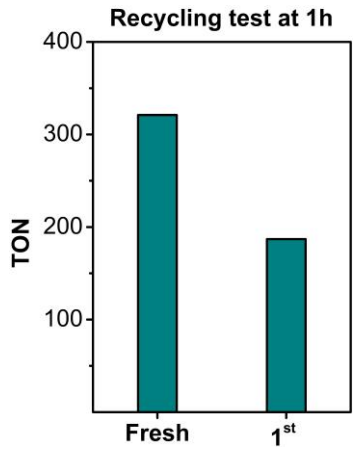

Figure 21. Recycling results using the catalyst **Pd-PPh$_3$/TiO$_2$** at 1 h.

Recycling was also performed using **Pd-NHC/TiO$_2$** NPs. Due to the strong interaction of NHC with Pd, it was thought that agglomeration could be avoided.

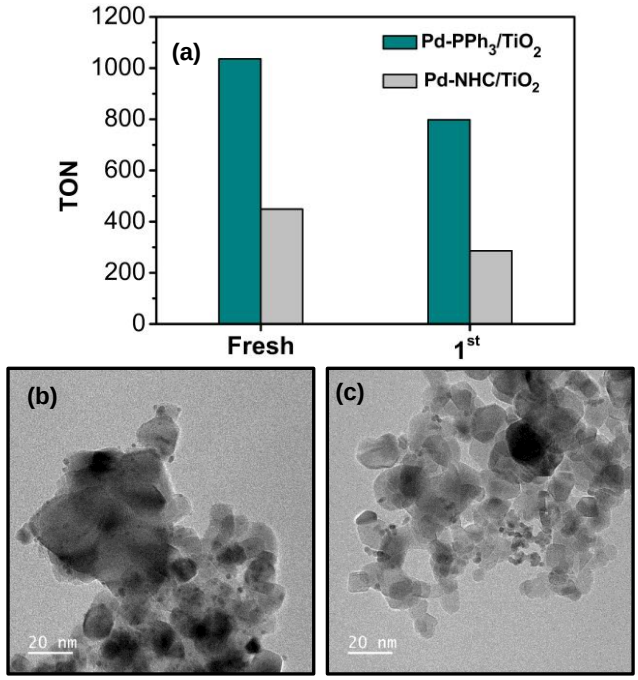

Figure 22. Comparison of recycling experiments between **Pd-PPh$_3$/TiO$_2$** and **Pd-NHC/TiO$_2$** (a) and TEM images before (b) and after catalysis (c) with **Pd-NHC/TiO$_2$** NPs. Conditions: 20 mg of **Pd-NHC/TiO$_2$** catalyst, 5 ml milli-Q H_2O, $KHCO_3$ (4 M),

pTotal= 36 bar, p(CO_2) = p(H_2), 60 ºC. TON= mmol formate/mmol total of Pd, calculated by NMR using 1,4-dioxane as internal standard.

However, similarly to the results obtained with the NPs stabilized by PPh_3, a strong decrease in activity (*ca*. 36%) was observed after the first cycle (Figure 22 (a)). TEM analysis of the spent catalyst again revealed an increasing in NP size and agglomerations (Figure 22 (b) and (c)).

3.3. Conclusions

Novel catalysts based on ligand-capped Pd NPs supported on various materials were prepared using the organometallic approach and the following conclusions could be drawn:

- Variations on the ligand employed on synthesis showed that water-soluble ligads provides smaller sizes.
- When no ligand was employed on the synthesis, the highest particle size (*ca*. 5 nm) was obtained.
- ICP reuslts showed lower Pd content when water-soluble phosphines were employed.
- EDX and XPS analysis on **Pd-PPh_3/TiO_2** confirmed the presence of P at the NP surfaces.
- Colloidal **Pd-PPh_3** NPs were synthesized to provide more information about crystallinity and amount of ligand present on the sample.
- Supports of different nature were also employed and small and crystalline Pd NPs were obtained in all cases.
- The activity of these systems was evaluated in the hydrogenation of CO_2 to formate. The results revealed that the size of the nanoparticles could not be directly correlated with their catalytic performance and the interactions between the nanoparticles and the support appeared to be critical to the catalyst activity.
- The **Pd-PPh_3/TiO_2** catalytic system reached a TON of 1032 (TOF of 69 h^{-1}, [HCOOK]= 1.1 mol/l) under mild conditions of pressure and temperature (36 bar (pCO_2:pH_2= 1), 60 ºC, 15 h).
- Initial recycling study revealed unsuccessful and current efforts are focused on support modification to limit sintering and enhance catalytic activity of these catalysts.

3.4. Experimental section

Materials and Methods

Metal precursors $Pd(dba)_2$, CeO_2 and TiO_2 (Titanium (IV) oxide nanopowder, 21 nm primary particle size (TEM), ≥ 99.5% trace metals basis) supports were purchased from Sigma-Aldrich and used without any further purification. Covalent Organic Framework TpPa-1 was synthesized following a reported procedure.[33] Carbon Nanotubes were purchased too (CNTs (PR-24-XT-LHT, PYROGRAP®)). Graphitic carbon nitride (*g*-C_3N_4) was synthesized according to the literature.[42,43] Ligands used for the stabilization of the nanoparticles were commercial and purchased from Sigma-Aldrich, except 1,3-dimethylimidazolium-2-carboxylate (Me_2Im-CO_2), which synthesis was previously reported by our group.[26] All solvents were dried from a solvent purification system (SPS) and deoxygenated. Tetrahydrofuran was further dried by refluxing in the presence of sodium/acetophenone. Milli-Q water was employed in catalytic experiments. Any other solvent or reagent employed was reagent grade. Hydrogen (5.0) was purchased from Carburos Metálicos and CO_2 (5.3) was purchased from Abelló Linde. All the synthesis were performed using Schlenk techniques under Argon and glovebox using nitrogen as inert gas. The syntheses of nanoparticles were carried in Fischer-Porter bottles and catalytic tests were performed in a stainless steel high-pressure reactor Hel CAT-7 (7 x 10 ml).

Characterization techniques

Transmission Electron Microscopy (TEM)

Measurements were performed at the “Unitat de Microscopia dels Serveis de Recursos Cientifics I Tècnics de la Universitat Rovira i Virgili” in Tarragona with JEOL 1011 electron microscope operated at 100 kV with resolution of 3 Å. The samples were prepared by deposition of several drops of the reaction crude onto a copper grid. The particles size distributions were determined by a manual analysis. At least 300 particles on a given grid were measured to obtain a statistical size distribution and mean diameter.

Environmental Scanning Electron Microscope (ESEM)

The equipment used was FEI ESEM Quanta 600 from “Unitat de Microscopia dels Serveis de Recursos Cientifics I Tècnics de la Universitat Rovira i Virgili”

in Tarragona. This microscope has an integrated analysis system OXFORD INSTRUMENTS. Energy-dispersive X-ray spectroscopy (EDX) analysis was carried out using this technique (BSED detector and HV (20 kV)).

Field Emission Scanning Electron Microscope (FESEM)

The microscope used for FESEM analysis was Themo Scientific Scios2. from "Unitat de Microscopia dels Serveis de Recursos Cientifics I Tècnics de la Universitat Rovira i Virgili" in Tarragona.

X-ray Diffraction (XRD)

XRD measurements were made using a Siemens D5000 diffractometer (Bragg-Brentano parafocusing geometry and vertical θ-θ goniometer) fitted with a curved graphite diffracted-beam monochromator, incident and diffracted-beam Soller slits, a 0.06º receiving slit and scintillation counter as a detector. The angular *2θ* diffraction range was between 30 and 80º. The data were collected with an angular step of 0.05º at 12 s per step and sample rotation. A low background Si(510) wafer was used as sample holder. $Cu_{k\alpha}$ radiation was obtained from a copper X-ray tube operated at 40 kV and 30 mA. Measurements were performance in "Servei de Recursos Cientifics I Tècnics de la Universitat Rovira i Virgili" in Tarragona.

Inductively Coupled Plasma-Optical Emission Spectrometry (ICP-OES)

The inductively coupled plasma-optical emission spectrometer ICP-OES ARCOS FHS16 employed is in "Servei de Recursos Cientifics I Tècnics de la Universitat Rovira i Virgili" in Tarragona. The digestion of samples was made employing aqua regia in Milestone Ethos Easy Advanced microwave digestion system. Quantification of metals is performed by comparison with the respective calibration curve constructed in the range of 0-20 ppm.

Nuclear Magnetic Resonance (NMR)

The equipment used were Bruker Avance Neo 400 with probe Smart (PI HR-400-S1-BBF/H/D-5.0-Z SP N) and sample case of 24 positions VARIAN Varian NMRSYS 400 (reverse probe 5 mm Auto-X 1H/31P-15N, probe 5mm autoswitchable PFG and 5 mm probe One Probe). Measurements were performed in "Servei de Recursos Cientifics I Tècnics de la Universitat Rovira

i Virgili" in Tarragona. Dry and deoxygenated 1,4-dioxane was used as internal standard for catalytic experiments.

Thermogravimetric Analysis (TGA)

Thermogravimetric analysis experiments were carried out with a Mettler Toledo TGA2 thermo-balance equipped with a gas flow system. For a typical TGA experiment, a small amount of sample (5-10 mg) was placed in an alumina crucible and heated at a rate of 10°C/min in N_2 atmosphere (50 ml/min) within a temperature range of 30-900°C.

High Resolution Transmission Electron Microscopy (HR-TEM)

The morphology, crystallographic information and chemical analysis of the Pd nanoparticles were studied by Transmission electron microscopy in Advanced Microscopy Laboratory at Instituto de Nanociencia of the Universidad of Zaragoza.

High resolution TEM (HRTEM) imaging of the nanoparticles was performed in an image-corrected FEI Titan 60-300 operated at 300 kV and equipped with a S-FEG and a Cs CETCOR corrector for the objective lens from CEOS, providing a point resolution in TEM mode below 1 Å, and a bottom mounted 2 K × 2 K Ultrascan CCD camera from Gatan.

Scanning transmission electron microscopy (STEM) imaging and EDS were carried out in a probe-corrected FEI Titan 60–300 operated at 300 kV and equipped with a high brightness X-FEG and a Cs CETCOR corrector for the condenser system to provide sub-angstrom probe size. In order to analyze the chemical composition of the materials, X-ray Energy Dispersive Spectra (EDS) were obtained with an Ultim Max detector (Oxford Instruments).

TEM specimens were prepared by placing a drop of a Tetrahydrofuran (THF) solution containing the NPs onto a holey carbon coated copper micro-grid.

X-ray Photoelectron Spectroscopy (XPS)

XPS measurements were performed at room temperature with a SPECS PHOIBOS 150 hemispherical analyzer (SPECS GmbH, Berlin, Germany)) in a base pressure of 5 x 10-10 mbar using monochromatic Al K alpha radiation (1486.74 eV) as excitation source operated at 300 W. The energy resolution as measured by the FWHM of the Ag3d5/2 peak for a sputtered silver foil was

0.62 eV. The spectra were calibrated with respect to the C1s at 285.0 eV. Measurements were carried out in the Fundació Institut Català de Nanociència i Nanotecnologia (ICN2). The XPS data were curve-resolved using the CASAXPS software after Shirley background subtraction. The spectra were fitted with the minimum number of peaks needed to reproduce the spectral features.

CO Chemisorption

CO measurements were performed with a Micromeritics AutoChem HP in the Institut de Recerca en Energia de Catalunya (IREC). Two difference types of chemisorption with pulses of CO and chemisorption of H_2 were performed using different conditions.

- CO chemisorption with reduction with H_2 at 500 ºC: He 50 ml/min, 10 min, H_2 with T ramp to 500 ºC 1 ºC/min, dwell 180 min, He dwell 60 min, T ramp to 40 ºC 10 ºC/min, dwell 30 min and CO pulses (10% CO on He) at 40 ºC.
- CO chemisorption with reduction with 12% H_2 on Ar at 250 ºC: He 50 ml/min, 30 min, H_2 with T ramp to 250 ºC 1 ºC/min, dwell 60 min, 12% H_2/Ar 50 ml/min, dwell 60 min, He at T ramp to 40 ºC 10 ºC/min, dwell 30 min and CO pulses (10% CO on He) at 35 ºC.
- CO chemisorption with reduction with 12% H_2 on Ar at 100 ºC: He 50 ml/min, 5 min, 12% H_2/Ar 50 ml/min, T ramp to 100 ºC 1 ºC/min, dwell 30 min, He at T ramp to 40 ºC 10 ºC/min, dwell 30 min and H_2 pulses (12% H_2 on Ar) at 40 ºC.

Synthesis and characterization of PPh_3 stabilized Pd NPs supported over TiO_2

In a common experiment, TiO_2 was first dried in an oven at 100 ºC overnight. The metal precursor and the ligand (0.1 equiv. in the case of bidentate ligand, 0.5 equivalent for NHC ligand) were weighted in the glove box and charged in a Fischer-Porter bottle. Then, support and solvent (THF, 100 ml) were added, the Fischer-Porter was closed, purged with hydrogen several times and then charged with 3 bar of H_2. The mixture was then heated at 60 ºC and stirred at 700 rpm overnight. After the reaction, the mixture was cooled to room temperature and re-entered in the glove box. Samples for TEM analysis

were prepared by deposition of five drops of the reaction crude onto a copper grid. The rest of the reaction crude was concentrated and washed several times with hexane. The catalyst was dried under vacuum during several hours.

Catalytic experiments for CO_2 reduction to formate

Stainless steel high-pressure reactor HEL CAT-7 (7 x 10 ml) was charged with TiO_2 supported palladium nanoparticles (20 mg), 20 mg of 1,4-dioxane and 5 ml of a 4 M base solution employing milli-Q water. The reactor was first flushed with 3 cycles of hydrogen to remove the air. Then, the reactor was charged with 10 bar of H_2 and heated at 40 ºC under stirring for twenty minutes. At this point, the reactor was depressurized, purged several times with CO_2 and charged with 18 bar of CO_2 and let under stirring for 20 minutes. Then, the reactor was charged with 18 bar of H_2 (1:1, CO_2:H_2) and heated to reach the temperature under 600 rpm of stirring. The experiment was left 15 h and after this time, the reactor was allowed to cool in an ice bath. When the reactor was cooled, it was depressurized and opened.. A small amount of the sample was centrifuged and 100 µl of supernatant were analysed by NMR using D_2O as deuterated solvent.

Catalytic activity was evaluated through Turn Over Number (eq. 1) and Turn Over Frequency calculations (eq. 2):

$$\mathrm{TON} = \frac{\text{mmol formate formed}}{\text{mmol active palladium atoms}} \quad (\text{eq. } 1)$$

$$\mathrm{TOF}\ (\mathrm{h}^{-1}) = \frac{\mathrm{TON}}{\text{time (h)}} \quad (\text{eq. } 2)$$

The amount of formate was obtained from NMR using 1,4-dioxane as Internal Standard. A calibration curve was previously constructed to obtain the Response Factor (Figure S1). Potassium formate was the only product obtained in all catalytic experiments (Figure S2).

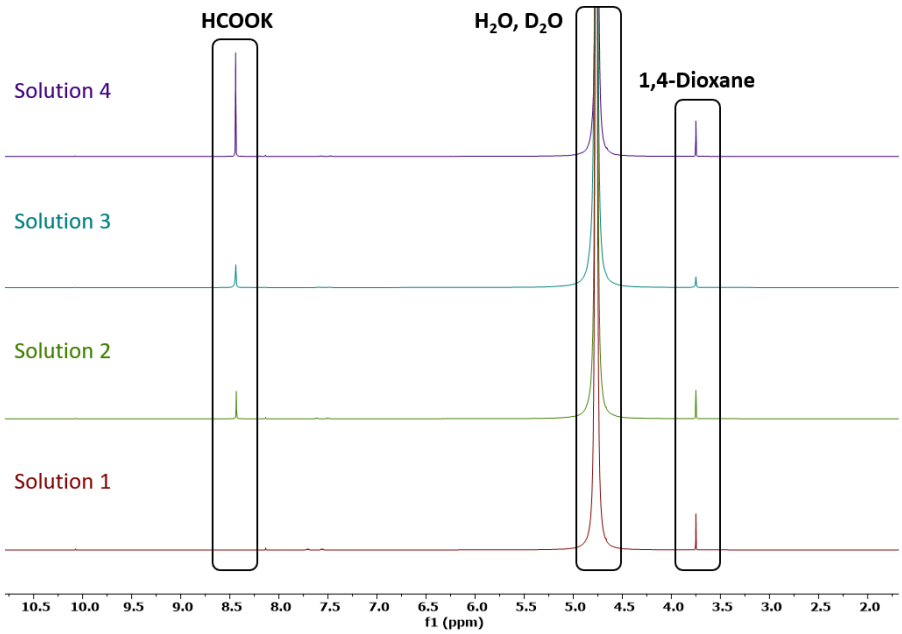

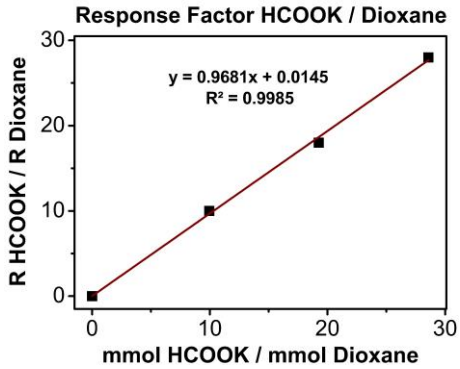

Figure S1. Calibration of NMR with 1,4-dioxane as internal standard.

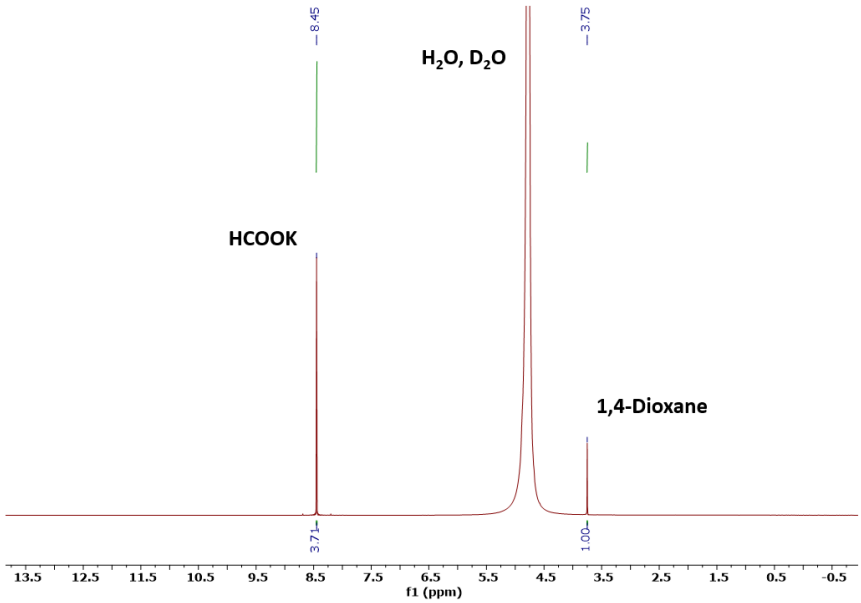

Figure S2. Representative NMR spectra of the hydrogenation of CO_2 to potassium formate using 1,4-dioxane as internal standard.

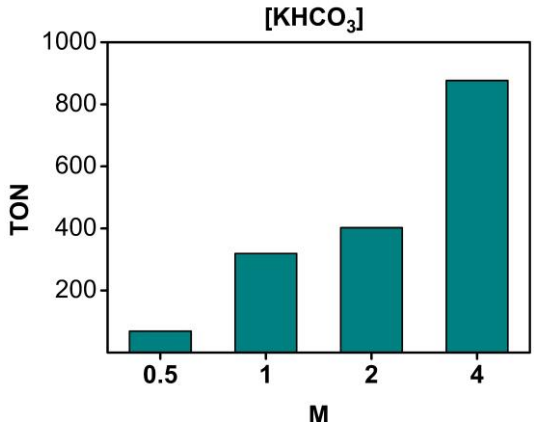

Figure S3. Effect of the concentration of the base in CO_2 hydrogenation to formate.

Table S1. Effect of the additive in CO_2 hydrogenation to formate.[a]

Entry	[$KHCO_3$], M	Additive	TON[b]	TOF (h^{-1})[c]
1	1	Without	319	21
2	1	KBF_4	348	23
3	1	KOAc	386	26
4	4	Without	877	58

5	4	KBF_4	822	55
6	4	KOAc	672	45

[a]Reaction conditions: 20 mg **Pd-PPh$_3$/TiO$_2$** NPs, 5 ml milli-Q H_2O, $KHCO_3$, 80 ºC, pTotal= 36 bar, p (CO_2) = p(H_2), 15 h. [b]TON= mmol formate/mmol total of Pd, calculated by NMR using 1,4-dioxane as internal standard. [c]TOF= TON/t(h).

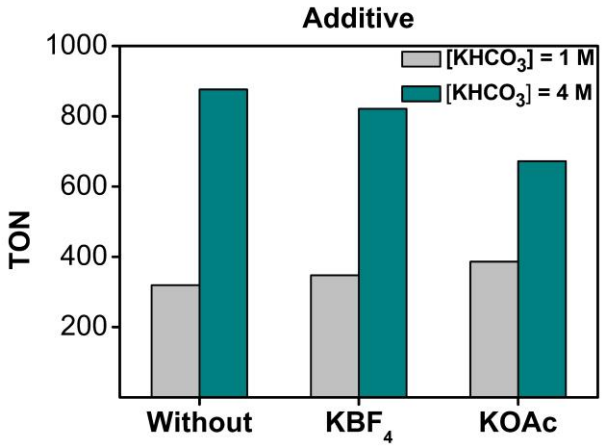

Figure S4. Effect of the additive in CO_2 hydrogenation to formate.

Table S2. Effect of the temperature in CO_2 hydrogenation to formate.[a]

Entry	Temperature (ºC)	TON[b]	TOF (h^{-1})[c]
1	40	717	48
2	60	1031	69
3	80	877	58
4	100	752	50
5	120	709	47

[a]Reaction conditions: 20 mg of **Pd-PPh$_3$/TiO$_2$** NPs, 5 ml milli-Q H_2O, $KHCO_3$ (4 M), pTotal=36 bar, p (CO_2) = p(H_2), 15 h. [b]TON= mmol formate/mmol total of Pd, calculated by NMR using 1,4-dioxane as internal standard. [c]TOF= TON/t(h).

Table S3. Effect of the total pressure in CO_2 hydrogenation to formate.[a]

Entry	Pressure (bar)	TON[b]	TOF (h^{-1})[c]
1	9	336	22
2	18	637	42
3	27	699	47

4	36	1031	69

[a]Reaction conditions: 20 mg of **Pd-PPh$_3$/TiO$_2$** NPs, 5 ml milli-Q H_2O, $KHCO_3$ (4 M), 60 ºC, p (CO_2) = p(H_2), 15 h. [b]TON= mmol formate/mmol total of Pd, calculated by NMR using 1,4-dioxane as internal standard. [c]TOF= TON/t(h).

Table S4. Effect of the partial pressures in CO_2 hydrogenation to formate.[a]

Entry	P (bar)	pCO_2 (bar)	pH_2 (bar)	TON[b]	TOF (h^{-1})[c]
1	36	18	18	1031	69
2	36	24	12	700	47
3	36	12	24	1145	76
4	36	9	27	992	66
5	36	0	36	882	59

[a]Reaction conditions: 20 mg of **Pd-PPh$_3$/TiO$_2$** NPs, 5 ml milli-Q H_2O, $KHCO_3$ (4 M), 60 ºC, pTotal= 36 bar, 15 h. [b]TON= mmol formate/mmol total of Pd, calculated by NMR using 1,4-dioxane as internal standard. [c]TOF= TON/t(h).

Table S5. Effect of time in CO_2 hydrogenation to formate.[a]

Entry	Time (h)	TON[b]	TOF (h^{-1})[c]
1	1	154	154
2	2	295	148
3	5	683	137
4	10	736	74
5	15	1031	69
6	30	1052	35
7	45	1056	23

[a]Reaction conditions: 20 mg of **Pd-PPh$_3$/TiO$_2$** NPs, 5 ml milli-Q H_2O, $KHCO_3$ (4 M), 60 ºC, pTotal= 36 bar, p (CO_2) = p(H_2). [b]TON= mmol formate/mmol total of Pd, calculated by NMR using 1,4-dioxane as internal standard. [c]TOF= TON/t(h).

Equations for the calculation of Pd on surface by Su et al.[38] (eq. 3) and by Louis Anandaraj et al.[39] (eq. 4 to 6):

$$\mathrm{TON} = \frac{\text{mmol formate formed}}{\text{total mmol of palladium atoms x D (\%)}} \qquad (\text{eq. } 3)$$

$$\text{TON} = \frac{\text{mmol formate formed}}{\text{total mmol of Pd x \% surface Pd}} \quad (\text{eq. } 4)$$

$$V_{NPs} = \frac{4}{3}\pi \text{ x } r_{NPs}^3 \quad (\text{eq. } 5)$$

$$V_{Shell} = \frac{4}{3}\pi \text{ x } (r_{NPs}^3 - (r_{NPs} - r_{at(Pd)})^3 \quad (\text{eq. } 6)$$

Table S6. Catalytic activity calculated with Pd on surface using different ligands for CO_2 hydrogenation to formate.[a]

Ligand	Size (nm)[b]	V_T (nm^3)[c]	V_s (nm^3)[d]	%Pd[e]	TON[f]	TOF (h^{-1})[g]
PPh_3	2.37	6.97	2.19	31.42	2788	186
PPh_2Py	2.47	7.89	2.39	30.29	2311	154
PTA	1.92	3.71	1.40	37.68	1022	68
TPPMS	2.02	4.32	1.56	36.09	1942	129
Me_2Im-CO_2	2.83	11.87	3.19	26.84	1885	126
Without	5.36	80.63	11.99	14.87	3846	256
dppe	2.31	6.45	2.07	32.13	2663	178
PPh_3[h]	2.25	5.96	1.96	32.88	2660	177

[a]Reaction conditions: 20 mg of palladium supported nanoparticles catalyst stabilized with PPh_3, 5 ml milli-Q H_2O, $KHCO_3$ (4 M), 80 ºC, pTotal= 36 bar, $p(CO_2) = p(H_2)$, 15 h. [b]Particle size measured by TEM. [c]Total volume of NP. [d]Shell volume. [e]Pd on surface of the NP. [f]TON= mmol formate/mmol total of Pd x % surface Pd, calculated by NMR using 1,4-dioxane as internal standard. [g]TOF= TON/t(h). [h]0.4 equiv. of PPh_3.

Table S7. Catalytic activity calculated with Pd on surface (De Vries Model)[29,30] using different ligands for CO_2 hydrogenation to formate.[a]

Ligand	Size (nm)[b]	N_t[c]	N_s[d]	N_s/N_t(%)	TON[e]	TOF (h^{-1})[f]
PPh_3	2.37	284	166	58.43	1369	91
PPh_2Py	2.47	322	182	56.40	1324	88
PTA	1.92	151	105	69.66	550	37
TPPMS	2.02	176	117	66.82	1067	71
Me_2Im-CO_2	2.83	484	242	50.12	994	66

Without	5.36	3291	922	28.01	2072	138
dppe	2.31	263	157	59.72	1432	95
PPh_3[h]	2.25	243	149	61.07	1402	93

[a]Reaction conditions: 20 mg of palladium supported nanoparticles catalyst stabilized with PPh_3, 5 ml milli-Q H_2O, $KHCO_3$ (4 M), 80 ºC, pTotal= 36 bar, $p(CO_2) = p(H_2)$, 15 h. [b]Particle size measured by TEM. [c]Total atoms of NP. [d]Pd on surface. [e]TON= mmol formate/mmol total of Pd x % surface Pd, calculated by NMR using 1,4-dioxane as internal standard. [f]TOF= TON/t(h). [g]0.4 equiv. of PPh_3.

3.5. References

[1] (a) G. Centi, S. Perathoner, *Catal. Today* **2009**, *148*, 191−205; (b) G. Centi, E. A. Quadrelli, S. Perathoner, *Energy Environ. Sci*. **2013**, *6*, 1711−1731; (c) A. Dibenedetto, A. Angelini, P. Stufano, *J. Chem. Technol. Biotechnol.* **2014**, *89*, 334−353.

[2] P. Styring, D. Jansen, H. de Coninck, H. Reith, K. Armstrong, Carbon Capture and Utilisation in the green economy, Centre for Low Carbon Futures, **2011**, http://co2chem.co.uk/carbon-captureand-utilisation-inthe-green-economy.

[3] S. Ghazali-Esfahani, H. Song, E. Păunescu, F. D. Bobbink, H. Liu, Z. Fei, G. Laurenczy, M. Bagherzadeh, N. Yan, P. J. Dyson, *Green Chem*. **2013**, *15*, 1584−1589.

[4] E. Alper, O. Yuksel Orhan, *Petroleum* **2017**, *3*, 109−126.

[5] (a) M. Kurtz, N. Bauer, C. Büscher, H. Wilmer, O. Hinrichsen, R. Becker, S. Rabe, K. Merz, M. Driess, R. A. Fischer, M. Muhler, *Catal. Lett*. **2004**, *92*, 49−52; (b) S. Vukojevic, O. Trapp, J.-D. Grunwaldt, C. Kiener, F. Schüth, *Angew. Chem. Int. Ed*. **2005**, *44*, 7978−7981; (c) C. He, G. Tian, Z. Liu, S. Feng, *Org. Lett*. **2010**, *12*, 649−651; (d) S. Wesselbaum, V. Moha, M. Meuresch, S. Brosinski, K. M. Thenert, J. Kothe, T. V. Stein, U. Englert, M. Holscher, J. Klankermayer, W. Leitner, *Chem. Sci*. **2015**, *6*, 693−704.

[6] M. Siebert, M. Seibicke, A. F. Siegle, S. Kräh, O. Trapp, *J. Am. Chem. Soc*. **2019**, *141*, 334−341.

[7] M. Ni, M. K. H. Leung, D. Y. C. Leung, K. Sumathy, *Renew. Sust. Energ. Rev.* **2007**, *11*, 401−425.

[8] (a) J. Ohi, *J. Mater. Res*. **2005**, *20*, 3180−3187; (b) J. H. Lee, J. Ryu, J. Y. Kim, S.-W. Nam, J. H. Han, T.-H. Lim, S. Gautam, K. H. Chaec, C. W. Yoon, *J. Mater. Chem. A* **2014**, *2*, 9490−9495; (c) H. Zhong, M. Iguchi, M. Chatterjee, T. Ishizaka, M. Kitta, Q. Xu, H. Kawanami, *ACS Catal.* **2018**, *8*, 5355−5362.

[9] P. Upadhyay, V. Srivastava, *PESD* **2016**, *10*, 13−34.

[10] (a) J. Klankermayer, S. Wesselbaum, K. Beydoun, W. Leitner, *Angew. Chem. Int. Ed*. **2016**, *55*, 7296−7343; (b) A. Weilhard, M. I. Qadir, V. Sans, J. Dupont, *ACS Catal.* **2018**, *8*, 1628−1634; (c) A. Weilhard, S. P. Argent, V. Sans, *Nat. Commun.* **2021**, *12*, 231; (d) R. Tanaka, M. Yamashita, K. Nozaki, *J. Am. Chem. Soc*. **2009**, *131*,

14168−14169; (e) M. V. Vollmer, J. Ye, J. C. Linehan, B. J. Graziano, A. Preston, E. S. Wiedner, C. C. Lu, *ACS Catal*. **2020**, *10*, 2459−2470; (f) A. Z. Spentzos, C. L. Barnes, W. H. Bernskoetter, *Inorg. Chem.* **2016**, *55*, 8225−8233; (g) B. G. Schieweck, N. F. Westhues, J. Klankermayer, *Chem. Sci*. **2019**, *10*, 6519−6523; (h) D. Wei, R. Sang, P. Sponholz, H. Junge, M. Beller, *Nat. Energy* **2022**, *7*, 438−447.

[11] (a) G. H. Gunasekar, J. Shin, K.-D. Jung, K. Park, S. Yoon, *ACS Catal*. **2018**, *8*, 4346−4353; (b) Z. Zhang, Y. Xie, W. Li, S. Hu, J. Song, T. Jiang, B. Han, *Angew. Chem. Int. Ed*. **2008**, *47*, 1127–1129; (c) H.-K. Lo, C. Copéret, *ChemCatChem* **2019**, *11*, 430−434.

[12] (a) R.-P. Ye, J. Ding, W. Gong, M. D. Argyle, Q. Zhong, Y. Wang, C. K. Russell, Z. Xu, A. G. Russell, Q. Li, M. Fan, Y.-G. Yao, *Nat. Commun*. **2019**, *10*, 5698; (b) D. Preti, C. Resta, S. Squarcialupi, G. Fachinetti, *Angew. Chem. Int. Ed.* **2011**, *50*, 12551−12554; (c) C. Hao, S. Wang, M. Li, L. Kang, X. Ma, *Catal. Today* **2011**, *160*, 184−190; (d) D. A. Bulushev, J. R. H. Ross, *Catal. Rev. Sci. Eng*. **2018**, *60*, 566−593.

[13] (a) L. Fan, Y. Sakaiya, K. Fujimoto, *Appl. Catal. A* **1999**, *180*, L11−L13; (b) A. García-Trenco, A. Regoutz, E. R. White, D. J. Payne, M. S. P. Shaffer, C. K. Williams, *Appl. Catal. B* **2018**, *220*, 9−18.

[14] (a) K. Zhou, Y. Li, *Angew. Chem. Int. Ed.* **2012**, *51*, 602−613; (b) L. I. Zhang, M. X. Zhou, A. Q. Wang, T. Zhang, *Chem. Rev.* **2019**, *120*, 683−733.

[15] (a) H. Park, J. H. Lee, E. H. Kim, K. Y. Kim, Y. H. Choi, D. H. Younb, J. S. Lee, *Chem. Commun*. **2016**, *52*, 14302−14305; (b) X. Shao, X. Miao, X. Yu, W. Wang, X. Ji, *RSC Adv*. **2020**, *10*, 9414−9419; (c) J. Su, M. Lu, H. Lin, *Green Chem*. **2015**, *17*, 2769−2773; (d) W.-H. Wang, X. Feng, M. Bao, *Transformation of CO_2 to Formic Acid or Formate Over Heterogeneous Catalysts*, Chapter 3, **2017**, 43–52, Online ISBN 978-981-10-3250-9.

[16] K. Nakajima, M. Tominaga, M. Waseda, H. Miura, T. Shishido, *ACS Sustainable Chem. Eng*. **2019**, *7*, 6522−6530.

[17] (a) Y. Kuwahara, Y. Fujie, T. Mihogi, H. Yamashita, *ACS Catal*. **2020**, *10*, 6356−6366; (b) G. Yang, Y. Kuwahara, S. Masuda, K. Mori, C. Louis, H. Yamashita, *J. Mater. Chem. A* **2020**, *8*, 4437−4446; (c) K. Mori, T. Sano, H. Kobayashi, H. Yamashita, *J. Am. Chem. Soc*. **2018**, *140*, 8902−8909.

[18] L. T. M. Nguyen, H. Park, M. Banu, J. Y. Kim, D. H. Youn, G. Magesh, W. Y. Kima, J. S. Lee, *RSC Adv*. **2015**, *5*, 105560−105566.

[19] X. Shao, J. Xu, Y. Huang, X. Su, H. Duan, X. Wang, T. Zhang, *AIChE J.* **2016**, *62*, 2410−2418.

[20] K. Philippot, B. Chaudret, *C. R. Chim*. **2003**, *6*, 1019−1034.

[21] A. Balanta, C. Godard, C. Claver, *Chem. Soc. Rev*. **2011**, *40*, 4973−4985.

[22] Y. Zhang, J. Feia, Y. Yua, X. Zheng, *Catal. Lett*. **2004**, *93*, 231−234.

[23] (a) W. Zhang, S. Wang, Y. Zhao, X. Ma, *Fuel Process. Technol*. **2018**, *178*, 98−103; (b) V. Srivastava, *Catal. Lett.* **2014**, *144*, 2221−2226; (c) P. R. Upadhyay, V. Srivastava, *RSC Adv*. **2016**, *6*, 42297−42306; (d) Z.-Z. Yang, H. Zhang, B. Yu, Y.

Zhao, G. Ji, Z. Liu, *Chem. Commun*. **2015**, *51*, 1271−1274; (e) S. Wang, S. Hou, C. Wu, Y. Zhao, X. Ma, *Chin. Chem. Lett*. **2019**, *30*, 398−402.
[24] (a) S. Wesselbaum, U. Hintermair, W. Leitner, *Angew. Chem. Int. Ed*. **2012**, *51*, 8585−8588; (b) P. G. Jessop, F. Joó, C.-C. Tai, *Coord. Chem. Rev*. **2004**, *248*, 2425−2442; (c) S. Moret, P. J. Dyson, G. Laurenczy, *Nat. Commun*. **2014**, *5*, 4017; (d) J. Elek, L. Nádasdi, G. Papp, G. Laurenczy, F. Joó, *Appl. Catal. A* **2003**, *255*, 59−67.
[25] K. J. Fisher, E. C. Alyea, N. Shahnazarian, *Phosphorus, Sulfur, Silicon Relat. Elem*. **1990**, *48*, 37−40.
[26] (a) M. Díaz de los Bernardos, S. Pérez-Rodríguez, A. Gual, C. Claver, C. Godard, *Chem. Commun*. **2017**, *53*, 7894−7897; (b) D. A. Lomelí-Rosales, J. A. Delgado, M. Díaz de los Bernardos, S. Pérez-Rodríguez, A. Gual, C. Claver, C. Godard, *Chem. Eur. J.* **2019**, *25*, 8321−8331.
[27] P.-J. Debouttière, Y. Coppel, A. Denicourt-Nowicki, A. Roucoux, B. Chaudret, K. Philippot, *Eur. J. Inorg. Chem*. **2012**, 1229−1236.
[28] X. W. Li, R. G. Song, Y. Jiang, C. Wang, D. Jiang, *Appl. Surf. Sci.* **2013** *276*, 761−768.
[29] C. Rangheard, C. de Julián Fernández, P.-H. Phua, J. Hoorn, L. Lefort, J. G. de Vries, *Dalton Trans*. **2010**, *39*, 8464−8471.
[30] B. K. Teo, N. J. A. Sloane, *Inorg. Chem.* **1985**, *24*, 4545−4558.
[31] V. Hardevel, V. Hartog, *Surf. Sci*. **1969**, *15*, 189−230.
[32] (a) E. Ramirez, S. Jansat, K. Philippot, P. Lecante, M. Gomez, A. M. Masdeu-Bultó, B. Chaudret, *J. Organomet. Chem*. **2004**, *689*, 4601–4610; (b) S. U. Son, Y. Jang, K. Y. Yoon, E. Kang, T. Hyeon, *Nano Lett*. **2004**, *4*, 6, 1147-1151; (c) J. Cookson, *Platin. Met. Rev*. **2012**, *56*, 2, 83–98.
[33] S. Kandambeth, A. Mallick, B. Lukose, M. V. Mane, T. Heine, R. Banerjee, *J. Am. Chem. Soc*. **2012**, *134*, 19524−19527.
[34] P. Pachfule, M. K. Panda, S. Kandambeth, S. M. Shivaprasad, D. D. Díaz, R. Banerjee, *J. Mater. Chem. A* **2014**, *2*, 7944−7952.
[35] L. Staiger, T. Kratky, S. Günther, O. Tomanek, R. Zbořil, R. W. Fischer, R. A. Fischer, M. Cokoja, *ChemCatChem* **2021**, *13*, 227−234.
[36] T. Wang, D. Ren, Z. Huo, Z. Song, F. Jin, M. Chen, L. Chen, *Green Chem*. **2017**, *19*, 716−721.
[37] J. Sá, G. D. Arteaga, R. A. Daley, J. Bernardi, J. A. Anderson, *J. Phys. Chem. B* **2006**, *110*, 17090−17095.
[38] J. Su, L. Yang, M. Lu, H. Lin, *ChemSusChem* **2015**, *8*, 813−816.
[39] S. J. Louis Anandaraj, L. Kang, S. DeBeer, A. Bordet, W. Leitner, *Small* **2023**, 2206806.
[40] K. Mori, A. Konishi, H. Yamashita, *J. Phys. Chem*. *C* **2020**, *124*, 11499−11505.
[41] M. T. Reetz, W. Helbig, S. A. Quaiser, U. Stimming, N. Breuer, R. Vogel, *Science* **1995**, *267*, 367−369.

[42] H. A. Bicalho, R. D. F. Rios, I. Binatti, J. D. Ardisson, A. J. Howarth, R. M. Lago, A. P. C. Teixeira, *J. Hazard. Mater.* **2020**, *400*, 123310.
[43] X. Wang, K. Maeda, A. Thomas, K. Takanabe, G. Xin, J. M. Carlsson, K. Domen, M. Antonietti, *Nat. Mater.* **2009**, *8*, 76−80.

CHAPTER 4

Preliminary DFT studies of the mechanism of CO_2 hydrogenation into formates using ligand-capped Pd NPs

UNIVERSITAT ROVIRA I VIRGILI
EFFICIENT VALORIZATION OF CO2 INTO FORMATE THROUGH NANOCATALYSIS
María Dolores Fernández Martínez

4.1. Introduction

The work described in this chapter aims to gain more insight into the mechanism of the CO_2 hydrogenation into formate catalyzed by ligand-capped Pd NPs based on the results described in Chapter 3. Indeed, these results indicated that particle size was not the main parameter to explain the catalytic performance of these catalysts and it was thought that Density Functional Theory (DFT) calculations could help improving our understanding of the properties of these nanocatalysts. However, such catalysts are complex systems, hard to be described accurately because of the large number of metal atoms present,[1,2] and contain ligands that are partially mobile. Moreover, these systems are not easy to characterize experimentally. For these reasons, efforts are being made to use first-principles studies that work hand in hand with experimental methods for a better understanding of metallic nanoparticles with adsorbed ligands.[3,4]

4.1.1. Ligand-capped nanocatalysts studied by DFT

Several examples of modelized metal NPs (Au,[5,6] Rh,[7] Ru,[8,9,10,11,12,13,14] Pt[15,16] and Pd[17,18]) containing ligands of different nature were reported.

López et al. developed a model of 55-atom nanocluster of Au (Au_{55}) and covered by 27 Ph_2PO ligands (metal-ligand ratio of 1.56:1)[5] based on the range of experimental results obtained by van Leeuwen and coworkers.[19] These Au NPs stabilized by secondary phosphine oxides (SPOs) were used in the chemoselective hydrogenation of acrolein and other *α,β*-unsaturated aldehydes (Figure 1). The AuNP-SPO interface enables the heterocyclic cleavage of H_2 molecule and the addition to the aldehyde C=O bond is kinetically favorable to form the corresponding alcohol. This occurred *via* a concerted transition state stabilized by dipolar interactions in a four-member ring structure in which the presence of ligand is essential. A year later, in 2018, López and co-workers reported the modelization and study of a 1,10-phenantrholine functionalized Au (111) surface (Figure 1).[6] This model was used to better understand the properties of Au NPs supported onto TiO_2 and embedded in a nitrogen-doped carbon (Au@N-doped carbon/TiO_2), which was utilized in the selective hydrogenation of structurally diverse alkynes. The graphenization of the ligand ensured the fixation of the golds NPs under the

reaction conditions. The good performance of these catalysts were correlated with a frustrated Lewis pair interface formed by the combination of Au and N atoms from the N-doped carbon. DFT confirmed that these interfaces can serve as a basic site to promote the heterolytic activation of H_2 under very mild conditions.

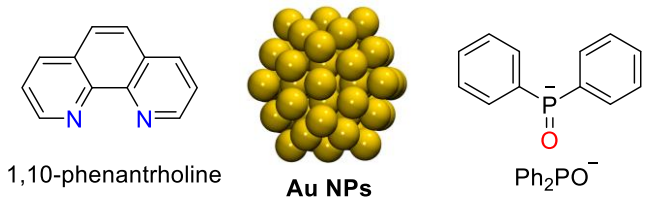

Figure 1. Examples of ligand-containing Au NPs modelized by DFT.

Very recently, Castillón and coworkers reported the use of Ru and Rh NPs stabilized by bulky NHC ligands as catalysts for the selective H/D exchange in phosphines using D_2 as the deuterium source (Figure 2).[7]

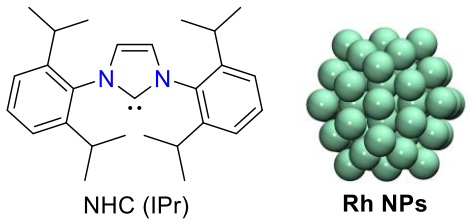

Figure 2. Example of NHC ligand used with Rh NPs modelized by DFT.

A combined experimental and computational study revealed that H/D exchange proceeded preferentially *via* C−H bond activation at nanoparticle edges. The importance of the ligand was highlighted by a comparison between NHC decorated Rh_{55}NP and the naked Rh_{55} NPs for the selective H/D exchange in P(*o*-tolyl)$_3$ phosphine, for which the ligands decorating the NPs prevent the strong adsorption through the P-atom, allowing interactions with the phosphine substituents. Several coordination modes and possible C-H activations paths were studied, revealing a strong influence of the phosphine structure on the selectivity.

For ligand-stabilized Ru NPs, various studies were reported with ligands of different nature. For instance, in 2011, Chaudret and coworkers studied computationally the system based on Ru NPs of 1.8 nm stabilized by NHC

ligands and accommodating 1.5 hydride per surface Ru.[8] When 1,3-bis(2,6-diisopropylphenyl)imidazol-2-ylidene was used as ligand to stabilize Ru NPs, 8 ligand molecules could be present on the NP's surfaces. The results obtained with this ligand were compared with those with N,N-di(tert-butyl)imidazol-2-ylidene, another NHC ligand presented distinct adsorption mode over the Ru surface due to steric effects (Figure 3).

Other Ru based systems employing NHC as ligand for the deuteration and tritiation of oxazole, imidazole, triazole and carbazole substructures.[9] The model used for the DFT study was based on a 0.5 nm Ru cluster with 1.4 H atoms per Ru surface atom ($Ru_{13}H_{17}$).[10] This system provided a deeper understanding of C-H and N-H activation processes occurring at the surface of metallic nanoclusters. Martínez-Prieto et al. studied a system based on Pt NPs for hydrogenation reactions using zwitterionic amidinates.[11] The DFT calculations were carried out using a Ru_{55} (of *ca.* 1 nm) model containing 1.6 hydride per ruthenium surface atom (Figure 3). The largest number of ligand molecules adsorbed onto the Ru_{55} surface was 6, which corresponded to Ru NPs stabilized with 0.1 equiv. of the ligand. The possible coordination modes of the ligands were also analyzed, concluding that the most stable mode was through the two nitrogen atoms of the amidinate to two adjacent Ru-atoms with a binding energy of -47.9 kcal·mol^{-1}.

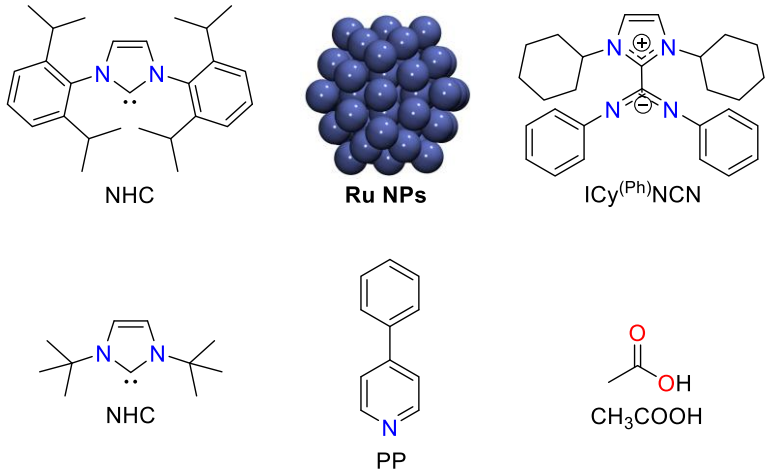

Figure 3. Example of ligands used for the stabilization of Ru NPs and studied by DFT.

Another ligand employed on the stabilization of nanoparticles that were modelized by Poteau and coworker was ethanoic acid as example of a carboxylic acid (Figure 3).[13] The optimal surface composition determined by DFT calculations appeared to be *ca.* [0.4–0.6] H/Ru_{surf} and 0.4 ethanoate/Ru_{surf}. Ethanoate is the species which is truly is adsorbed onto the surface of Ru. The interaction mode of ethanoate with the surface plays a crucial role in determining the availability of hydrogen atoms on the surface. These findings were further validated by comparing them with experimental results. The authors conducted an in-depth investigation of this particular system in relation to its potential application in the Hydrogen Evolution Reaction (HER).

Sala and coworkers also reported Ru NP catalysts for the HER reaction but in which 4-phenylpyridine (PP) acted as ligand.[14] They used a Ru_{55} cluster with 53 atoms of H (0.96 $H:Ru_{total}$ ratio, 1.2 $H:Ru_{surf}$ ratio) for the DFT study (Figure 3). With this ligand, two coordination modes can compete: the σ-donation of the nitrogen lone pair and an aromatic π-to-metal surface interaction (η^6 from both phenyl rings) were. This latter type of coordination revealed a more stable interaction. Depending on these, the number of PP that can be accommodated on the Ru surface could change. The saturation of the Ru_{55} surface was reached with 11 PPs in this model (0.27 PP/Ru_{surf}) with the coadsorption of 9 σ-PPs and 2 π-PPs molecules.

Pd-based system were also modelized and studied on the presence of ligands by DFT calculations.[17,18]

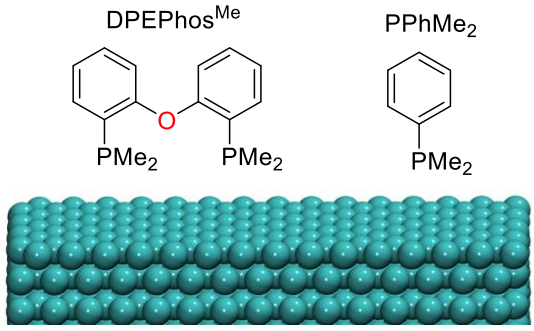

Figure 4. Ligands employed with Pd (111) surface and modelized by DFT.

In 2018, Ortuño and López modelized a phosphine-decorated Pd (111) surface for the selective conversion of biomass-derived substrates (Figure 4).[17] The ligands DPEPhos^{Me} and $PPhMe_2$ were employed and induced distinct effects on the Pd system for the decarbonylation of fatty acids to produce linear α-olefins. When the monodentate $PPhMe_2$ ligand was used, the formation of self-assembled monolayers that completely passivate the metal surface was observed, in line with the poor activity observed experimentally.[20] However, when the bidentate DPEPhos^{Me} ligand was used, the creation of cavities that enhance selectivity was revealed, which caused rapid product release and precluded undesired side reactions. Moreover, this ligand prevented catalyst deactivation due to the flexibility of the phosphine arms that promotes CO desorption, reducing surface poisoning. This study showed how activity and selectivity can be modulated by the nature of the ligands employed even for heterogeneous catalysts. More recently, Villa and coworkers studied the effect of the presence of ligands on isolated Pd ions and on Pd NPs.[18] But, as a model of Pd nanostructure, a (100) surface was employed and aminopropanol was the selected ligand. The preferential coordination of aminopropanol through the NH group was confirmed by combination of experimental and computational techniques. Through this interaction, the aminopropanol ligand could control the particle shape through the selective blocking of Pd (100) facets, which promotes the growth on the Pd (111) facets.

These reports thus confirmed the importance of ligands in metallic NP systems, both for their synthesis and their catalytic performance. The combination of experimental and computational work thus constitutes a very useful tool to increase our knowledge of these complex systems. In this chapter, atomistic computational models will be explored for different ligand-decorated Pd NPs. These models will be used to understand the observed effects of the ligand on CO_2 hydrogenation catalysis.

4.1.2. Mechanistic studies for the hydrogenation of CO_2 to formates

The catalytic hydrogenation of CO_2 to formic acid and formate is a reaction that was also studied computationally in recent years.[21]

The CO_2 transformation into formic acid was computationally characterized for several systems such as single-atom catalysts (SACs) based on Cu,[22] Co,[23] Ni and Fe;[24] surfaces of Ni[25] or Au[26] and bimetallic Pd-Cu clusters.[27]
For the production of formate, SACs were also studied by computational means[28] and the analysis of mono- and bimetallic nanoparticles and small bimetallic clusters was also reported.[29,30]
Noble-metal free NiFe NPs were modeled by Mu and coworkers for the hydrogenation of HCO_3^- to formate and CO.[29] The models for these NPs consisted in 13 atoms and bimetallic $Ni@Ni_{12}Fe$ (where a Ni atom is exposed on the surface) and $Fe@Ni_{12}$ (where Fe atom is exposed on the Ni surface) were tested to highlight the importance of the second element and its distribution in the system. Two pathways were analyzed for each system, depending on whether the attack of H takes place at the C (Figure 5, pathway 1) or at one of the O (Figure 5, pathway 2) of the bicarbonate species. For both $Ni@Ni_{12}Fe$ and $Fe@Ni_{12}$, the attack to the C atom was energetically preferred and $Fe@Ni_{12}$ provided a lower energy barrier compared to $Ni@Ni_{12}Fe$, resulting in a superior catalytic activity.

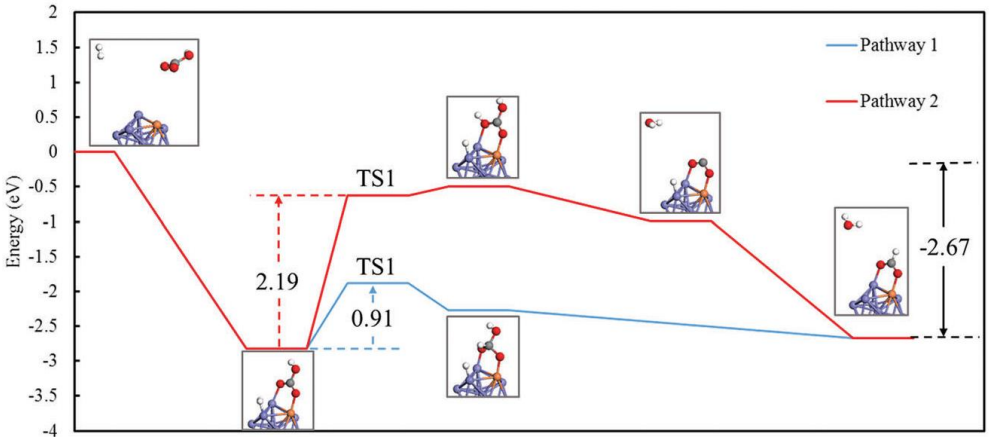

Figure 5. Energy profile of HCO_3^- reduction to formate by $Fe@Ni_{12}$ nanoclusters. Reproduced from reference 29 with permission from the Royal Society of Chemistry.

A very active Au-based system for the CO_2 hydrogenation to formate was studied by Zhang and coworkers.[30] Experimentally, the Au NPs were synthesized over previously modified SiO_2 with APTES and a Schiff-base. Nanoclusters, single atoms and Au NPs larger than 2 nm were obtained.

Depending on the synthetic procedure, variations in size and distributions were observed. The authors studied the reaction mechanism by computational methods with a closed packed cuboctahedral Au_{55} cluster of *ca.* 1.2 nm of size accommodated with an alkyl-imine Schiff base (Figure 6). The H_2 dissociation occurs on the low-coordinated corners of Au_{55} (TS-1). CO_2 molecule is captured as a zwitterionic intermediate on the gold surface. At this point, one of the activated H atoms can attack the C atom to form a formate intermediate (TS2) with a barrier of 1 eV. This is the rate-determining step. The second H addition produces formic acid (TS3), which is desorbed from the metallic surface and forms the formate adduct with NEt_3.

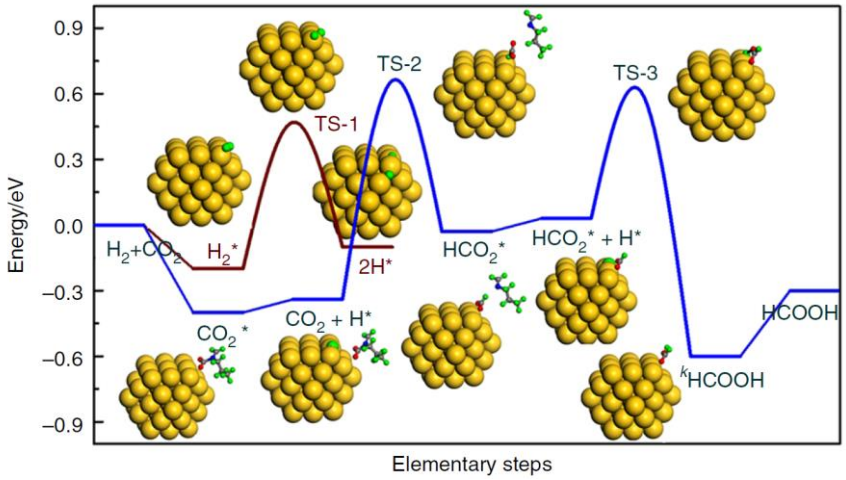

Figure 6. Free energy diagram for CO_2 hydrogenation over the Au/SiO_2-Schiff catalyst. Reproduced from reference 30.

Most examples for the hydrogenation of CO_2 to formate in basic medium were reported for PdAg bimetallic NPs.[31,32,33,34] In 2017, Mori et al. developed a phenylamine-functionalized mesoporous silica supported PdAg nanoparticles for reversible hydrogenation of CO_2 and H_2 release.[31] But only the decomposition of formic acid to produce H_2 was studied by DFT, employing a Pd (111) surface aiming at understanding the observed activity improvement in the presence of an amine. More recently, the same group reported another PdAg based catalyst for both the hydrogenation of CO_2 and the H_2 release from the product employing a phenylamine-functionalized mesoporous carbon support.[32] $Pd_{11}Ag_{11}$ cluster was the selected model for

the alloy, where the bottom two layers were fixed and the top layer was allowed to relax during optimizations. The study of the mechanism was carried out in the absence and in the presence of the amine, to determine its effect on catalysis (Figure 7).

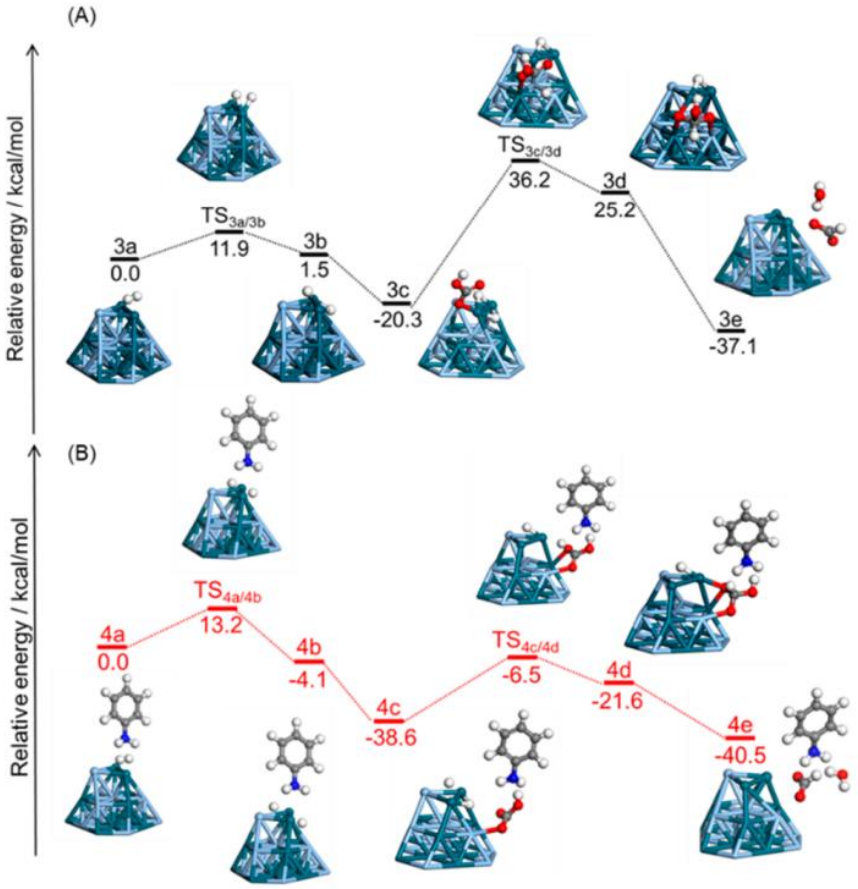

Figure 7. Mechanistic study of hydrogenation of CO_2 in the absence (A) and in the presence (B) of phenylamine. Reproduced from reference 32. Copyright 2018 American Chemical Society.

The hydrogenation of CO_2 started by dissociation of H_2 to produce metal-hydride species, followed by the adsorption of HCO_3^- species formed in the basic medium. Then, the attack of one of the activated H takes place at the C of the bicarbonate. Formate is obtained together with H_2O, thus regenerating the active species. In the absence of amine (Figure 7 (A)), the rate determining step in the attack of H to HCO_3^- with a barrier of 56.5

kcal·mol^{-1} (2.45 eV). However, in the presence of the amine (Figure 7 (B)), the barrier corresponding to this TS was much lower, 32.1 kcal·mol^{-1} (1.39 eV). The interaction of the HCO_3^- with the phenylamine molecules through N−H···O hydrogen bonding revealed to play an important role in the formation of the intermediate.

This group also reported a PdAg based system supported on TiO_2 for the hydrogenation of CO_2 to formate.[33] In this report, the DFT calculations focused on the role of Ag. They employed Pd_{22}, $Pd_{11}Ag_{11}$, and Pd_6Ag_{16} clusters as models (Figure 8).

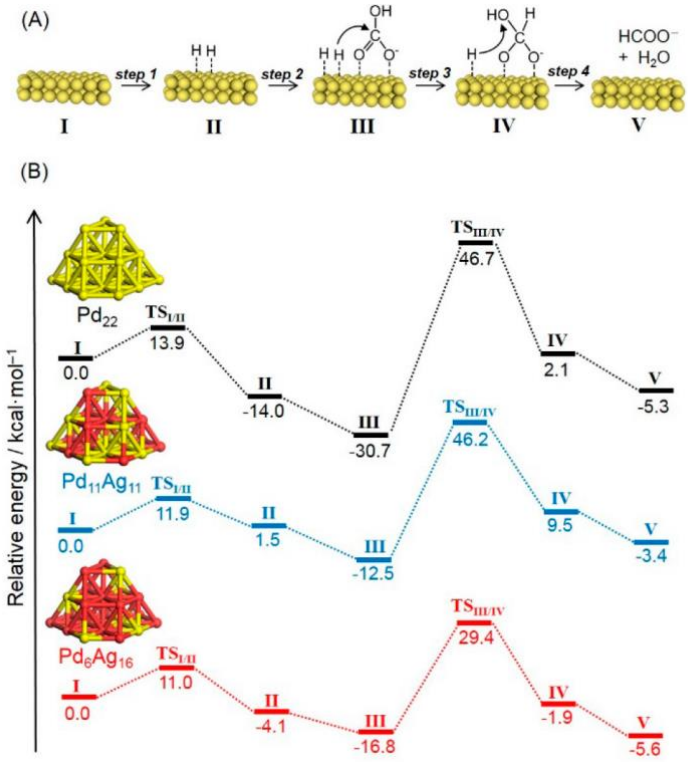

Figure 8. Possible reaction mechanism (A) and potential energy profiles (B) for CO_2 hydrogenation using clusters of different composition. Reproduced from reference 33. Copyright 2018 American Chemical Society.

The rate determining step was again the attack of an activated H from the surface at the bicarbonate C atom. When the Ag content increased, the energy for the associated TS decreased (from 3.36 eV for Pd_{22} to 0.55 eV for Pd_6Ag_{16}). Calculations on a Ag_{22} cluster were also performed and revealed

that Ag did not participate in the catalytic cycle as an active center. By DFT calculations of Muliken atomic charges, it was determined that the role of Ag was to donate electron density to Pd. Therefore, it was concluded that the presence of Ag in the alloy improved the catalytic activity of the system through electronic effect.

Other recent works on PdAg NPs over supports of different nature by the same authors highlighted the importance of an amine in the medium and the role of Ag as part of the alloy.[34]

To conclude, a series of metallic NPs modelized and studied by DFT were presented. The relevance of the ligands for the stabilization of these systems and their role on catalysis was highlighted. However, to date, all DFT mechanistic studies on the hydrogenation of CO_2 to formate were performed on naked metal cluster and the study of ligand decorated nanocatalysts for this reaction remains unexplored.

In this following sections, preliminary results obtained using DFT calculations on the interactions between two phosphine ligands and the Pd NP surface (using an icosahedral **Pd_{55}** model) are described as well as an exploration of the interactions between catalytic intermediates and the Pd nanocatalyst.

The work described in this chapter was carried out in collaboration with Profs. Jordi Carbó and Josep M. Ricart of the Universitat Rovira I Virgili.

4.2. Results and discussion

4.2.1. Exploring the composition and adsorption modes of ligand-stabilized Pd_{55} nanoclusters

4.2.1.1. Interaction of PPh_3 and PTA with Pd_{55} NPs

This study consists in the modelization of Pd NPs using models containing 55 atoms of Pd with an icosahedral shape. The size of these **Pd_{55}** NPs is 1.06 nm. Even if these models are smaller than those obtained experimentally on Chapter 3, they were selected to reduce the computational cost.

The models employed in this study are represented in Figure 9. On the left, naked **Pd_{55}** NP is displayed, while on the right part, hydrogen atoms were included in the structure to give the **$Pd_{55}H_{28}$** NP system, given the experimental method employed for the synthesis of Pd NPs[35] with H_2 as reductant.

The presence of mobile and reactive hydrides over metallic NPs surface was previously demonstrated for Ru systems.[36,37] Here, 28 atoms of hydrogen were disposed randomly over the surface (0.5 H:Pd_{total} ratio, 0.7 H:Pd_{surf} ratio). This number was selected based on previous reports on Ru NPs.[38]

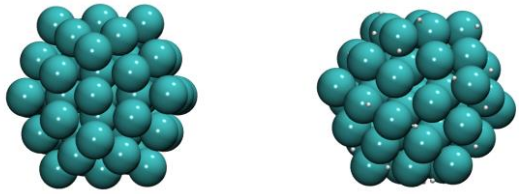

Figure 9. Modelized **Pd_{55}** (left) and **$Pd_{55}H_{28}$** (right) NPs. Atoms: white, H; cyan, Pd.

After optimization of the system, all of them were coordinated through an μ^3-H mode (coordinated to three Pd atoms).

The PPh_3 and PTA ligands were selected as stabilizers for the NPs under study (Figure 10). In the previous chapter, the highest catalytic activity was obtained using Pd-NPs stabilized with PPh_3 while the NPs stabilized by the PTA ligand provided the less active system in the hydrogenation of CO_2 to formate, despite their small size.

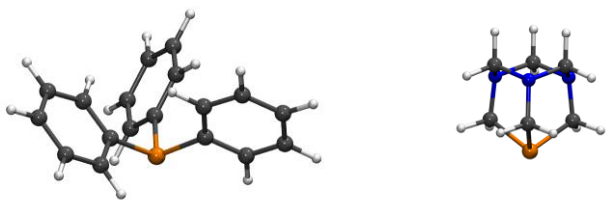

Figure 10. PPh_3 (left) and PTA (right) ligands modelized for the adsorption over **Pd_{55}** and **$Pd_{55}H_{28}$** NPs. Atoms: white, H; grey, C; blue, N; orange, P.

Different adsorption modes of these two ligands over **Pd_{55}** and **$Pd_{55}H_{28}$** NPs were analyzed (Figure 11). The four modes examined were: Top, in which the P atom from the ligand is adsorbed over a Pd located on one of the vertex of the NP; Edge where P is located over a centered Pd of one Edge of the cluster; Hollow in which P is located over a hole between three Pd neighbors present on a face of the NP; Ring oriented where one of the aromatic rings from the PPh_3 ligand is interacting with one of the faces of the NP. For Top, Edge and Ring oriented, the initial Pd-P distance was 2.5 Å. For Hollow, the

initial Pd-P distance was lower than in the other three modes of adsorption because using a longer distance, the P ended up adsorbed in a bridge position, that is, between two palladium atoms located at the NP edge.

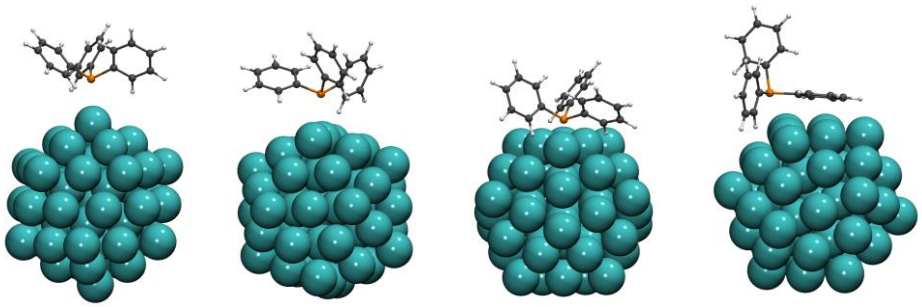

Figure 11. Possible adsorption modes of PPh_3 on **Pd_{55}** NP (Top, Edge, Hollow and Ring orientation). Atoms: white, H; grey, C; orange, P; cyan, Pd.

Table 1 summarizes the results obtained for the different adsorption modes studied for PPh_3. The adsorption modes of PPh_3 over **Pd_{55}** NP are presented in Entries 1 to 4. An adsorption energy (E_{ads}) of -1.27 eV and a final Pd-P distance of 2.24 Å were obtained for the Top interaction (Entry 1). When the Edge interaction was looked at (Entry 2), a lower energy (-1.60 eV) was obtained. However, in the final geometry, two C atoms from one of the aromatic rings of the ligand are interacting with one Pd atom located on the vertex of the cluster (C-Pd distance of 2.26 and 2.27 Å), resulting in a short distance between the P atom and another Pd (with 2.24 and 2.94 Å). For the Hollow interaction (Entry 3), an energy of -1.38 eV was obtained. The P atom was located in a bridge position, between two Pd atoms with Pd-P distances of 2.24 and 2.87 Å. Again, the interaction of two atoms from one of the aromatic rings of the ligand with another Pd atom was observed (C-Pd distances of 2.30 and 2.31 Å). Furthermore, an additional interaction between a C of another ring and the surface (C-Pd distance of 2.31 Å) was detected. For the Ring orientation (Entry 4), an energy of -2.43 eV was obtained. The P atom that was initially located over one of the Pd atoms of the Edge, resulted in the final geometry to be over two Pd atoms (Pd-P distance of 2.22 and 2.89 Å). One of the rings from PPh_3 approximated the face of the cluster, with six C atoms interacting with three Pd atoms at distances between 2.14-2.33 Å. Two C atoms from another ring interact with one Pd atom at distances of 2.25 and 2.37 Å. The final geometry is represented in Figure 12 (left).

Table 1. Possible adsorption modes, energies (eV) and Pd-P distances (Å) of PPh_3 on **Pd_{55}** NPs without hydrides (top) and with hydrides (bottom) on the surface.

Entry	System	Interaction	E_{ads} (eV)[a]	d Pd-P (Å)
1	**Pd_{55}**	Top	-1.27	2.24
2	**Pd_{55}**	Edge	-1.60	2.24, 2.94
3	**Pd_{55}**	Hollow	-1.38	2.24, 2.87
4	**Pd_{55}**	Ring	-2.43	2.22, 2.89
5	**$Pd_{55}H_{28}$**	Top	-1.83	2.26
6	**$Pd_{55}H_{28}$**	Edge	-2.16	2.25, 2.99
7	**$Pd_{55}H_{28}$**	Hollow	-1.94	2.26, 2.78
8	**$Pd_{55}H_{28}$**	Ring	-1.96	2.32

[a] $E_{ads} = E_{PPh_3@NP} - (E_{NP} + E_{PPh_3})$.

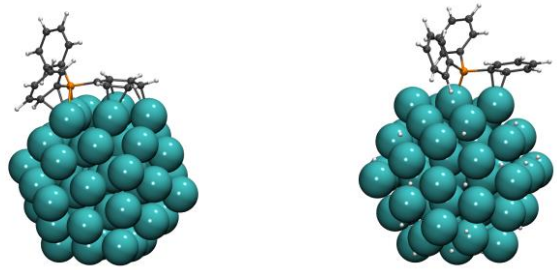

Figure 12. Most stable adsorption modes of PPh_3 on **Pd_{55}** NP (left) and **$Pd_{55}H_{28}$** NP (right). Atoms: white, H; grey, C; orange, P; cyan, Pd.

The results for adsorption of PPh_3 over **$Pd_{55}H_{28}$** NP are summarized in Entries 5 to 8. For the adsorption on Top position (Entry 5), the E_{ads} obtained was −1.83 eV with a final Pd-P distance of 2.26 Å. The Edge interaction (Entry 6) provided an E_{ads} of -2.16 eV with the P atom located between two Pd of the NP edge with distances of 2.25 and 2.99 Å. Two C atoms of one ring interact with a Pd atom at 2.32 and 2.36 Å (Figure 12, right). For the Hollow position (Entry 7), the obtained E_{ads} was -1.94 eV with the P atom interacting with two Pd atoms at 2.26 and 2.78 Å. Two aromatic rings interact with the Pd surface by one C (C-Pd distance of 2.40 Å) and by two C atoms (2.28 and 2.35 Å). For the Ring oriented interaction (Entry 8), the obtained Eads was -1.96 eV

(Pd-P distance of 2.32 Å) with six C from the ring interacting with the Pd surface with C-Pd distances in the range 2.23−2.48 Å.

No relevant differences in adsorption energies were therefore observed when hydrogen atoms were present at the **Pd_{55}** surface, although it should be noted that slightly higher adsorption energies were obtained, except for the Ring mode. For **PPh_3@Pd_{55}**, the most stable adsorption mode was the Ring orientation, while for **PPh_3@$Pd_{55}H_{28}$**, the Edge orientation was more stable. In most cases, interactions of several C atoms from the aromatic rings of the ligand with the Pd surface were observed. When six C atoms are interacting (η^6-phenyl interactions), sp^3 hybridization increased and as a result, the H atoms were not located in the Ph plane. These interactions were accompanied by the η^2 interactions of C from another aromatic ring.

Table 2. Possible adsorption modes and energies (eV) and Pd-P distances (Å) of PTA through P atom on **Pd_{55}** NPs without hydrides (top) and with hydrides (bottom) on the surface.

Entry	System	Interaction	E_{ads} (eV)[a]	d Pd-P (Å)
1	**Pd_{55}**	Top	-1.32	2.21
2	**Pd_{55}**	Edge	-1.26	2.21
3	**Pd_{55}**	Hollow-center	-1.12	2.48-2.52
4	**$Pd_{55}H_{28}$**	Top	-1.87	2.23
5	**$Pd_{55}H_{28}$**	Edge	-1.73	2.24
6	**$Pd_{55}H_{28}$**	Hollow	-1.94	2.23
7	**$Pd_{55}H_{28}$**	Hollow-center	-1.77	2.45-2.75

[a] $E_{ads} = E_{PTA@NP} - (E_{NP} + E_{PTA})$.

The interactions between the Pd surface and the PTA ligand were also studied. With this ligand, the adsorption could occur through the P or the N atom. The results for P adsorption over **Pd_{55}** and **$Pd_{55}H_{28}$** NPs are presented in Table 2. In Entries 1 to 3, the results for **PTA@Pd_{55}** are presented. For the Top interaction (Entry 1), the obtained E_{ads} was -1.32 eV with a Pd-P distance of 2.21 Å. For the Edge interaction (Entry 2), the E_{ads} was -1.26 eV with the same Pd-P distance. For the Hollow-center interaction (Entry 3), for which the P atom is located at the center of a face, between three Pd atoms, the

obtained E_{ads} was -1.12 eV and the P interacted with the three surrounding Pd atoms with Pd-P distances between 2.48-2.52 Å.

The results obtained for the interactions between PTA and **$Pd_{55}H_{28}$** NP are displayed in Entries 4 to 7. For the Top interaction (Entry 4), the obtained E_{ads} was -1.87 eV (d Pd-P= 2.23 Å). For the Edge interaction (Entry 5), an E_{ads} of -1.73 eV was obtained with Pd-P distance of 2.24 Å. The Hollow interaction (Entry 6) provided an E_{ads} of -1.94 eV and Pd-P distance of 2.23 Å. The final geometry contained the P atom over only one Pd atom (Figure 13, right), not between three as in the initial structure. For the Hollow-center interaction (Entry 7), the E_{ads} was -1.77 eV and Pd-P distances were in the range 2.45-2.75 Å.

Therefore, in this case, when hydrogen atoms are included, higher interaction energies were obtained. For **PTA@Pd_{55}**, the Top interaction was the most stable (Figure 13, left), while for **PTA@$Pd_{55}H_{28}$**, the most favourable interaction was the Hollow one (Figure 13, right).

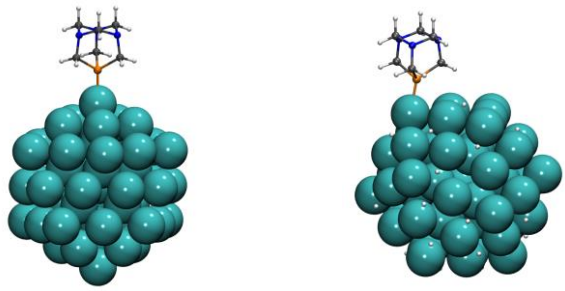

Figure 13. More stable adsorption modes of PTA through P atom on **Pd_{55}** NP (left) and **$Pd_{55}H_{28}$** NP (right). Atoms: white, H; grey, C; orange, P; blue, N; cyan, Pd.

When PTA was employed as ligand with coordination through P, no additional interactions were observed.

When N was the atom interacting with Pd surface, several positions were studied. Figure 14 shows the interaction through 1 N atom.

Table 3 summarizes the results obtained for the adsorption of PTA trough N atoms on **Pd_{55}** and **$Pd_{55}H_{28}$** systems.

In general, lower E_{ads} were obtained compared with those obtained with the interactions through the P atom (Table 2).

Table 3. Possible adsorption modes and energies (eV) of PTA through N atom on **Pd_{55}** NPs without hydrides (top) and with hydrides (bottom) on the surface.

Entry	System	Interaction	E_{ads} (eV)[a]	d Pd-N (Å)
1	**Pd_{55}**	Top	-0.52	2.14
2	**Pd_{55}**	Top[b]	-0.25	2.17
3	**Pd_{55}**	Edge	-0.22	2.17
4	**Pd_{55}**	Hollow	-0.43	3.58-3.63
5	**$Pd_{55}H_{28}$**	Top	-1.10	2.50
6	**$Pd_{55}H_{28}$**	Top[b]	-0.85	2.22
7	**$Pd_{55}H_{28}$**	Edge	-0.93	2.21
8	**$Pd_{55}H_{28}$**	Hollow	-0.27	3.60-3.75

[a]$E_{ads} = E_{PTA@NP} - (E_{NP} + E_{PTA})$. [b]Interaction of three N atoms present in PTA ligand orientated to Pd atom.

These results are in agreement with experimental work previously reported by Philippot and coworkers.[39] In terms of distances, when hydrogen atoms are present, higher distances are observed.

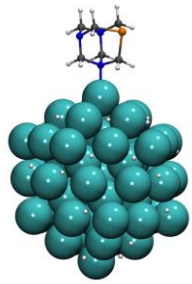

Figure 14. Example of adsorption mode of PTA through one N atom on **$Pd_{55}H_{28}$** NP. Atoms: white, H; grey, C; orange, P; blue, N; cyan, Pd.

In this section, the optimization of different Pd NP systems in the absence (**Pd_{55}** NP) and in the presence of hydrogen atoms on the surface (**$Pd_{55}H_{28}$**) were performed. The adsorption of two ligands of different nature (PPh_3 and PTA) was investigated in different positions (Top, Edge, Hollow and Ring oriented). For the PPh_3 coordination over **Pd_{55}**, the adsorption energy was slightly higher than for **$Pd_{55}H_{28}$**, except for the Ring oriented interaction. In

this latter case, C atoms from the phenyl substituents of the ligand are interacting with Pd surface atoms (η^6-phenyl interactions). These interactions were accompanied by the η^2 interaction of C from other aromatic ring. However, for **PPh_3@$Pd_{55}H_{28}$** the most stable adsorption mode is Edge, although in the final structure, the P atom is interacting with two Pd atoms from the surface and an η^2 interaction between two C atoms from one of the aromatic rings with the surface was again observed.

In conclusion for the adsorption of PPh_3, the π system of the aromatic rings interact with the Pd-NPs surface, which is higher when no hydrogen atoms are over the NP surface. When PTA is used as ligand, the presence of hydrogen atoms at the surface also promotes a stabilization of the system. This was observed when both, P and N, are the atoms from PTA which interact with the Pd surface. P adsorption is more energetically favorable than N adsorption. Top is the preferred mode of interaction, even when PTA is adsorbed *via* the P atom and the initial geometry was Hollow, the system resulted in a pseudo-top position. For PTA, no interactions between the carbon backbone and the Pd surface were observed. Finally, comparing both ligands, for PPh_3, the largest E_{ads} were -2.43 eV for **Pd_{55}** system and -2.16 eV for **$Pd_{55}H_{28}$** NP, resulting in a more favorable adsorption than for PTA, for which the largest E_{ads} was -1.32 eV with **Pd_{55}** and -1.94 eV with **$Pd_{55}H_{28}$** NPs. In terms of Pd-P distances for these ligands, no significant different were observed.

4.2.1.2. Analysis of the coverage of Pd_{55} NPs by PPh_3 and PTA phosphine ligands

With the results of the adsorption of one molecule of ligand (PPh_3 and PTA) in hand, the coverage of the surface by these ligands was studied for **$Pd_{55}H_{28}$**. These calculations aimed at determining the maximum number of ligands that can cover the surface of the NPs. First, the coverage of **nPPh_3@$Pd_{55}H_{28}$** was looked at with the ligand in Top position. Despite that this was not the most stable configuration for 1 PPh_3 system, this coordination mode was used for the surface coverage by more molecules of ligand. The results obtained for PPh_3 are summarized in Table 4. Different energies were analyzed: E_{ads}, corresponding to the adsorption energy that was employed in previous tables;

average E_{ads}, which correspond to the E_{ads} divided by the number of PPh_3 adsorbed molecules; and finally, the total E_{ads} variation, which is the total E_{ads} for the obtained system minus the energy of the system with one less phosphine. This latter E_{ads} variation corresponds to the energy cost of adding a new phosphine to the system with respect to the previous one.

Table 4. Effect of PPh_3 coverage oon **$Pd_{55}H_{28}$** NP adsorption energies for Top interaction. Energies in eV.

n PPh_3	E_{ads} (eV)[a]	Av. E_{ads} (eV)[b]	Total E_{ads} variation (eV)[c]
1	-1.83	-	-
2	-3.31	-1.66	-1.49
3	-4.83	-1.61	-1.52
4	-6.43	-1.61	-1.60
5	-7.85	-1.57	-1.42
6	-9.56	-1.59	-1.71
7	-10.90	-1.56	-1.34
8	-12.28	-1.53	-1.38
9	-13.78	-1.53	-1.49
10	-15.25	-1.53	-1.48
11	-16.81	-1.53	-1.55
12	-18.20	-1.52	-1.39
13	-18.08	-1.39	0.12

[a] $E_{ads} = E_{PPh_3@Pd_{55}H_{28}} - (E_{Pd_{55}H_{28}} + E_{PPh_3})$. [b] Average $E_{ads} = E_{ads}/nPPh_3$.
[c] Total E_{ads} variation $= E_{nPPh_3@Pd_{55}H_{28}} - (E_{(n-1)PPh_3@Pd_{55}H_{28}} + E_{PPh_3})$.

It can thus be observed how E_{ads} increase when adding up to 12 PPh_3 molecules. However, when the 13th is added on Edge position (there are only 12 Top positions, which means 12 vertexes on the NP), the E_{ads} only slightly increased (from -18.20 eV at 12 PPh_3 to -18.08 eV at 13 PPh_3). This increase of energy is more significant on Av. E_{ads} and on total E_{ads} variation. On this last, the energy is even positive (0.12 eV). These results therefore indicate

that the maximum of PPh_3 molecules that can be adsorbed on Top position over **$Pd_{55}H_{28}$** NP are 12 (one for every vertex).

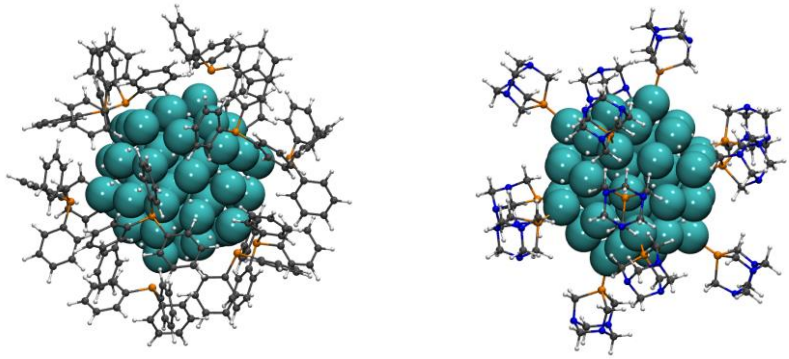

Figure 15. 3D representation of Top **$12PPh_3@Pd_{55}H_{28}$** (left) and **$13PTA@Pd_{55}H_{28}$** (right) structures. Atoms: white, H; grey, C; orange, P; blue, N; cyan, Pd.

Next, the coverage of Pd surface was investigated with PTA ligands on Top position, as previously performed by PPh_3. For PTA, for 13 PTA molecules (12 PTA molecules on Top position and 1 on Edge), the Average E_{ads} and Total E_{ads} variations were still negative (-1.60 and -1.43 eV, respectively). This thus indicated that a higher coverage by this ligand is more energetically favourable than for PPh_3. This was attributed to the smaller size of this ligand and therefore to lower steric hindrance between surface ligands (Figure 15). Cone angle of PTA is reported as 103º, relatively small for a phosphine. For PPh_3 is 145º.[40]

The same calculations were performed for the adsorption of PPh_3 over **$Pd_{55}H_{28}$** in Edge position (Table 5), which demonstrated to be the more energetically favored in the previous section. When up to 6 PPh_3 molecules were included, E_{ads} decreased. However, when the 7th molecule was added, a high increase in energy was observed (from -9.63 eV for 6 PPh_3 to -1.01 eV with 7 PPh_3). Moreover, for Average E_{ads}, an energy increase was observed at each step, but with 7 PPh_3, this decrease became much more noticeable. This was also confirmed by analysis the variation of total E_{ads}, which, for 6 PPh_3 molecules, was still negative (-1.27 eV) but when the 7th PPh_3 molecule was included, the total E_{ads} was positive and high. Although the calculation converged, the obtained structure collapsed due to the proximity between the

last PPh_3 included with another. For this reason, the corresponding value has been omitted.

Table 5. Effect of **nPPh_3@$Pd_{55}H_{28}$** NP coverage on its adsorption energies for Edge interaction. Energies in eV.

n PPh_3	E_{ads} (eV)	Av. E_{ads} (eV)[a]	Total E_{ads} variation (eV)[b]
1	-2.16	-	-
2	-3.65	-1.83	-1.49
3	-5.01	-1.67	-1.36
4	-6.85	-1.71	-1.84
5	-8.36	-1.67	-1.51
6	-9.63	-1.67	-1.27
7	-1.01	-0.14	-

[a]$E_{ads} = E_{PPh_3@Pd_{55}H_{28}} - (E_{Pd_{55}H_{28}} + E_{PPh_3})$. [b]Average $E_{ads} = E_{ads}/nPPh_3$.
[c]Total E_{ads} variation $= E_{nPPh_3@Pd_{55}H_{28}} - (E_{(n-1)PPh_3@Pd_{55}H_{28}} + E_{PPh_3})$.

It was therefore concluded that for PPh_3 in Edge position, the maximum number of molecules that can cover the surface is 6 (Figure 16). This number is half that previously obtained for Top position.

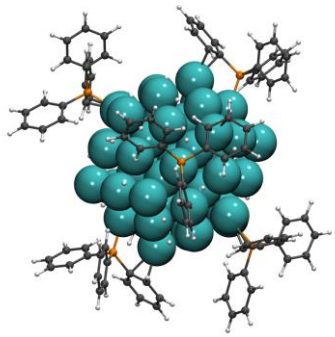

Figure 16. 3D representation of Edge **6PPh_3@$Pd_{55}H_{28}$**. Atoms: white, H; grey, C; orange, P; cyan, Pd.

The results obtained in this section therefore indicate that the coverage of the Pd NPs is higher when the PTA ligand is the NP stabilizer than when PPh_3 is used. A lower availability of the Pd surface in Pd-PTA NPs is therefore

expected than when the Pd-PPh_3 catalyst is used, which could explain the lower activity of the Pd-PTA system in catalysis.

4.2.2. Exploring the interactions of catalytic intermediates with phosphine-stabilized Pd_{55}

4.2.2.1. Interaction of carbonate and bicarbonate with Pd_{55}

In this section, the DFT results concerning the interactions of the Pd surface with bicarbonate and carbonate species are presented as under basic conditions, bicarbonate is expected to be the real substrate of the hydrogenation of CO_2, although carbonate was also previously considered.[41] Several interaction modes of bicarbonate were analyzed and are represented (Figure 17).

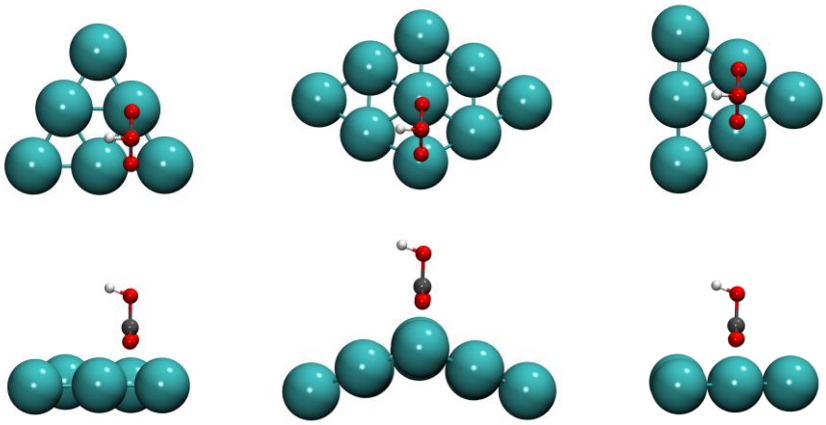

Figure 17. Different interaction modes of bicarbonate with **Pd_{55}** NP surface from the top and from the side view: Edge-Bridge (E-B) on the left, Edge-Vertex (E-V) on the center and Edge-Edge (E-E) in the right. Atoms: white, H; grey, C; red, O; cyan, Pd.

In all cases, bicarbonate is adsorbed in a bridge configuration through two oxygen atoms. On the left, the top and side views of the interaction of oxygen atoms from bicarbonate on Edge and Bridge (E-B) with respect to two Pd atoms from the surface (one of the faces of the NP) are displayed. The Bridge denomination is used when one oxygen is over a bond between two Pd atoms. In the center of the figure, the Edge-Vertex interaction (E-V) is represented, with the bicarbonate located over one edge and one vertex Pd atoms of the NP. Finally, on the right, the Edge-Edge (E-E) interaction is

displayed in which both oxygen atoms are located directly over two Pd atoms situated on the edges of one of the NP facets.
The results concerning the interaction of both bicarbonate and carbonate with **Pd_{55}**, **$Pd_{55}H_{28}$** and **$nPPh_3@Pd_{55}H_{28}$** NPs are presented in Table 6.

Table 6. Interaction modes and energies (eV) of bicarbonate (top) and carbonate (bottom) with **Pd_{55}**, **$Pd_{55}H_{28}$** and **$nPPh_3@Pd_{55}H_{28}$** NPs based systems.

Entry	System	I_{final}[a]	E_{rel} (eV)	d Pd-O (Å)
1	**Pd_{55}**	E-V[b]	-0.25	2.08, 2.15
2	**Pd_{55}**	E-E[c]	-0.06	2.14, 2.15
3	**$Pd_{55}H_{28}$**	E-V	-0.44	2.12-2.13
4	**$Pd_{55}H_{28}$**	E-B[d]	-0.25	2.24, 2.23, 2.38
5	**$5PPh_3@Pd_{55}H_{28}$**	E-V	+0.39	2.17, 2.26
6	**$5PPh_3@Pd_{55}H_{28}$**	E-V	-0.15	2.10, 2.21
7	**$5PPh_3@Pd_{55}H_{28}$**	E-V	-0.28	2.11, 2.17
8	**Pd_{55}**	E-V	+1.00	1.99, 2.02
9	**Pd_{55}**	E-E	+1.22	2.03, 2.03
10	**$Pd_{55}H_{28}$**	E-V	+1.13	2.03, 2.04
11	**$Pd_{55}H_{28}$**	E-B	+1.23	2.06, 2.17, 2.26
12	**$5PPh_3@Pd_{55}H_{28}$**	E-V	+1.83	2.05, 2.10
13	**$5PPh_3@Pd_{55}H_{28}$**	E-B	+1.16	2.07, 2.09, 2.32
14	**$4PPh_3@Pd_{55}H_{28}$**	E-V	+1.108	1.99, 2.07
15	**$4PPh_3@Pd_{55}H_{28}$**	E-B	+1.111	2.07, 2,10, 2.31

[a]Interaction initial and final. [b]Interaction E-V: Edge-Vertex. [c]Interaction E-E: Edge-Edge. [d]Interaction E-B: Edge-Bridge.

Relative energies (E_{rel}) are calculated on base of the whole system and taking as references the computed energies for H_2O, H_2 and CO_2. No solvent was included in this preliminary study because of the computational cost. H_2O, H_2

and CO_2 were used as molecules of reference since in VASP calculations, charges are balanced to give a neutral total system, which is not the case here since hydrides are present at the surface of the Pd NPs and bicarbonate and carbonate are also charges species. The adsorption of bicarbonate and carbonate molecules over metallic surfaces were previously reported and no significant differences were observed whether a negative charge was introduced or not.[42] The initial charge it is not expected to affect parameters such as geometry.[43] The results obtained for interactions of bicarbonate are displayed in Entries 1-7. When the E-V interaction of bicarbonate with **Pd_{55}** NP was initially considered (Entry 1), the optimization provided a Pd-O distance of 2.08 and 2.15 Å, in agreement with reported values.[42] When the E-E interaction was looked at (Entry 2), the resulting Pd-O distances were 2.14 and 2.15 Å. When the E-E and E-V interactions of bicarbonate were studied using the **$Pd_{55}H_{28}$** NP system the final geometry was maintained after optimization for E-V (Entry 3), but for E-E, optimization resulted in a final geometry corresponding to a E-B interaction (Entry 4) with longer Pd-O distances (2.24, 2.23 and 2.38 Å).

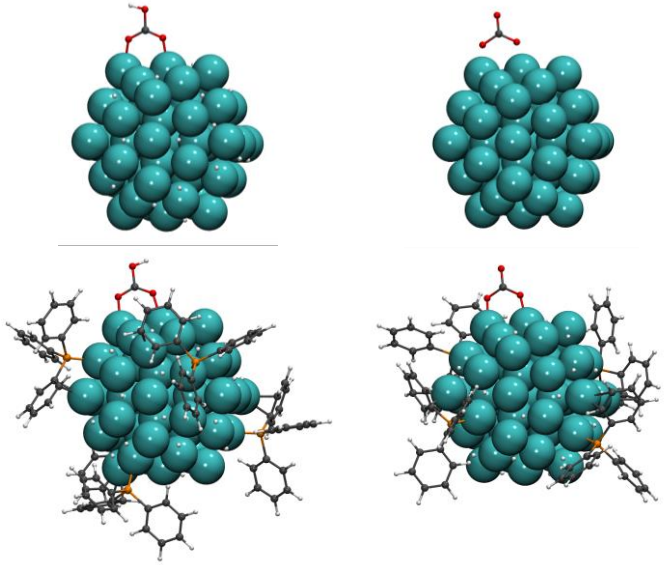

Figure 18. Most stable interactions of bicarbonate corresponding to systems from Entry 3 (left, up) and Entry 7 (left, down) and carbonate corresponding to systems from Entry 8 (right, up) and Entry 14 (right, down). Atoms: white, H; grey, C; red, O; cyan, Pd.

When the interactions of bicarbonate with **5PPh$_3$@Pd$_{55}$H$_{28}$** were analyzed (Entries 5 to 7), the calculations converged to a final E-V interaction with similar Pd-O distances (2.10-2.26 Å) (Figure 18, left-down).

The results obtained for carbonate interactions with different Pd NP systems are presented in Entries 8 to 15. In all cases, these interactions were less stable than in the case of bicarbonate. It is noteworthy that the most stable hydride containing system for carbonate interactions was **4PPh$_3$@Pd$_{55}$H$_{28}$** (Figure 18, right-down), a system in which PPh_3 was present.

For bicarbonate, the most stable interactions for all systems were E-V. The **Pd$_{55}$H$_{28}$** system gave the most stable interaction (Entry 3) with a E_{rel} of -0.44 eV (Figure 18, left-up). Therefore, in this case, the presence of ligands does not seem to have a positive effect.

For carbonate, **Pd$_{55}$** system gave the most stable interaction (Entry 8) with a E_{rel} of +1.00 eV. When **Pd$_{55}$** and **Pd$_{55}$H$_{28}$** are employed, same E-V final interaction mode is preferred. However, in the presence of PPh_3 molecules, the E-B interaction mode was more energetically favorable when 5 PPh_3 are present (Entry 13). When 4 PPh_3 are located over the **Pd$_{55}$H$_{28}$** NP, the difference between E-V and E-B is small, although slightly more favorable for the E-V mode.

In conclusion, bicarbonate adsorption over **Pd$_{55}$**, **Pd$_{55}$H$_{28}$** and **nPPh$_3$@Pd$_{55}$H$_{28}$** NPs systems resulted in lower relative energies (E_{rel}) than for carbonate, in agreement with previously reported experimental works.[44]

4.2.2.2. Interaction of the reaction intermediate with Pd NPs

Based on the results obtained in the previous section, bicarbonate was selected as a substrate to study the mechanism of hydrogenation of CO_2 to formate using the **Pd$_{55}$H$_{28}$** NP system.

In the first step of this study, no ligand was included to limit the computational cost. One hydrogen atom close to bicarbonate molecule will be the responsible of the attack on the C atom of bicarbonate molecule. This step was reported to be rate-determining for other systems.[29,34a] Starting from the system **Pd$_{55}$H$_{28}$** hydrogen atoms are present on the system and it is equivalent to have some hydrides at the first step reported as the dissociative adsorption of H_2 molecule over the metallic surface[34c] and one of them it is going to be used for the attack of C present on the surface of **Pd$_{55}$H$_{28}$**. Figure

19 shows the closest H atoms present on the surface of **Pd_{55}** NP which are available for the attack at the C atom. Even if the mechanism of hydrogenation of bicarbonate to formate can theoretically proceed *via* another pathway in which H can attack one of the O atoms of the bicarbonate, previous reports demonstrated that it was less energetically favorable.[33,45] Therefore, the H attack at C was selected as the pathway to explore.

After several attempts to determine which H is the most suitable for the attack, the H atom indicated in Figure 19 was selected. Prior to the attack, the migration of this H atom from the initial position (left image) to the closest position near bicarbonate molecule (right image) were optimized.

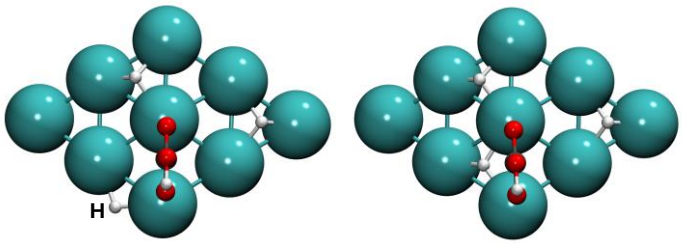

Figure 19. Migration of one H over the surface of **$Pd_{55}H_{28}$** NP. On the left, initial position; on the right, final position. Atoms: white, H; grey, C; red, O; cyan, Pd.

One of the surface H atom as closest to the C atom as possible was chosen for the initial geometry to proceed for the H attack to get the reaction intermediate. After optimization, the geometry obtained is represented in Figure 20. The C atom adopts a tetrahedral conformation and the relative energy obtained for this process was 1.88 eV, which agrees with reported values.[29,32] The C-H distance was 1.108 Å and the C-OH one was 1.41 Å while the other C-O distances were 1.39 and 1.40 Å. The O-Pd distances were 1.97 and 1.99 Å.

From this geometry, many efforts were made to find the transition state corresponding to this reaction step. First, Nudged Elastic Band (NEB) method[46] was employed, freezing part of the structure to lower the computational cost. One of the images obtained have a E_{rel} of 2.12 eV compared to the initial state which is an stimation of the barrier for this process. For this structure, H atom is slightly near of C (1.115 Å) compared with the initial image.

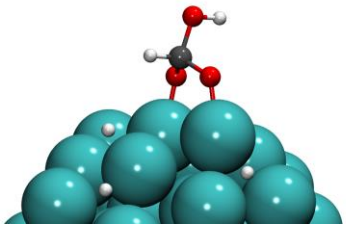

Figure 20. Intermediate formed by H attack to C from bicarbonate molecule adsorbed over **Pd_{55}** NP. Atoms: white, H; grey, C; red, O; cyan, Pd.

Using this structure as reference, three imaginary frequencies were found, two of them with a low value (of the order of 100 cm^{-1}). But, the third imaginary frequency was 842.8 cm^{-1} and corresponds to the movement of H that interacts with C atom, so this frequency could be attributed to the transition state. Due to lack of time, no further work could be conducted to date but this study will be performed in the near future.

4.2.3. Future work

In the near future, this study will be completed with the introduction of the ligands in the model and the determination of the energy profile for each system to analyze the catalytic results that were experimentally obtained and described in Chapter 3. The effect of the support will also be looked at (Figure 21).

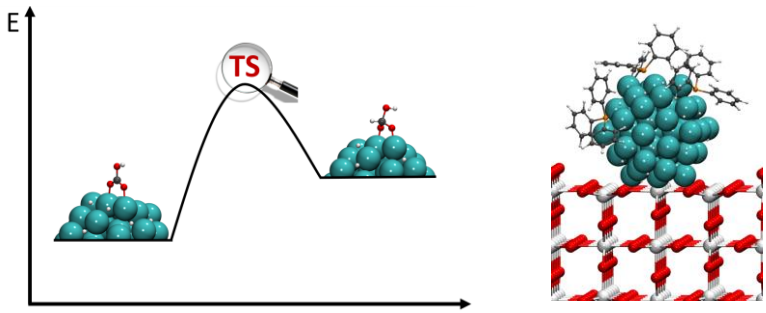

Figure 21. Proposed future work which include mechanistic studies for the hydrogenation of bicarbonate to formate and the metal-support interaction. Atoms: white, H; grey, C; orange, P; cyan, Pd; red, O; off-white, Ti.

4.3. Conclusions

PPh_3- and PTA-decorated Pd NPs were studied by means of DFT calculations exploring different phosphine adsorption modes, ligand coverage and interactions of carbonate and bicarbonate species. This study aimed at getting insights into the hydrogenation reactions described in Chapter 3. The most remarkable conclusions obtained were:

- The most stable adsorption of PPh_3 at the **Pd_{55}** surface takes place through the P atom and additional interactions of the carbon atoms from the aromatic rings in η^6 or η^2 fashions were also detected.
- For PTA, adsorption through the P atom is preferred to the interaction *via* the nitrogen atom.
- Lower energies of adsorption were obtained for PPh_3 than for PTA, which translates into a higher stabilization of the system when this ligand is used.
- Higher degree of coverage of the NP was observed for PTA than for PPh_3. This makes the surface less available for interactions with the substrates in catalysis.
- Bicarbonate adsorption at the NP surface is more stable than carbonate.

4.4. Computational details

All quantum mechanics static calculations were performed using the Vienna ab initio simulation package 5.3.5 (VASP) program[47] within spin polarized density functional theory (DFT) approximation.[48] The exchange correlation functional used was the Perdew-Burke-Ernzenhof (PBE).[49] The core electrons were described within the projector augmented wave (PAW) approach[50] and the valence states were expanded in a plane-wave basis set with an energy cut-off of 400 eV. In all cases, as the real system is not periodic, a single special k-point (Γ k-point) has been used to sample the first Brillouin zone. Geometry convergence criterion was reached when all forces were smaller than 0.01 $eV \cdot Å^{-1}$, whereas the convergence criterion for the wave function minimization was set at 10^{-5} eV. **Pd_{55}** clusters were placed in

the center of a unit cell of 30 x 30 x 30 Å^3, with a vacuum space between NPs of neighbor periodic images of, at least, 10 Å to avoid possible interactions. Adsorption energies (E_{ads}) for ligands were calculated with the formula (eq. 1):

$$E_{ads} = E_{ligand@NP} - (E_{NP} + E_{ligand}) \quad \text{(eq. 1)}$$

Average E_{ads} for PPh_3 were calculated with the formula (eq. 2):

$$Av.E_{ads} = E_{ads}/nPPh_3 \quad \text{(eq. 2)}$$

where n is the number of PPh_3 molecules. Total E_{ads} variation for PPh_3 was calculated by eq. 3:

$$E_{nPPh_3@Pd_{55}H_{28}} - (E_{(n-1)PPh_3@Pd_{55}H_{28}} + E_{PPh_3}) \quad \text{(eq. 3)}$$

Relatives energies (E_{rel}) for bicarbonate was calculated with the formula (eq. 4):

$$E_{rel} = E_{NP-HCO_3} + 1/2E_{H_2}) - (E_{NP} + E_{CO_2} + H_{H_2O}) \quad \text{(eq. 4)}$$

and for carbonate (eq. 5):

$$E_{rel} = E_{NP-CO_3} + E_{H_2}) - (E_{NP} + E_{CO_2} + H_{H_2O}) \quad \text{(eq. 5)}$$

4.5. References

[1] A. Heuer-Jungemann, N. Feliu, I. Bakaimi, M. Hamaly, A. Alkilany, I. Chakraborty, A. Masood, M. F. Casula, A. Kostopoulou, E. Oh, K. Susumu, M. H. Stewart, I. L. Medintz, E. Stratakis, W. J. Parak, A. G. Kanaras, *Chem. Rev*. **2019**, *119*, 4819−4880.

[2] K. Philippot, A. Roucoux, *Nanoparticles in Catalysis: Advances in Synthesis and Applications*, **2021**, WILEY-VCH GmbH.

[3] L. Cusinato, I. del Rosal, R. Poteau, *Dalton Trans*. **2017**, *46*, 378.

[4] M. A. Ortuño, N. López, *Catal. Sci. Technol*. **2019**, *9*, 5173−5185.

[5] N. Almora-Barrios, I. Cano, P. W. N. M. van Leeuwen, N. López, *ACS Catal*. **2017**, *7*, 3949−3954.

[6] J. L. Fiorio, R. V. Gonçalves, E. Teixeira-Neto, M. A. Ortuño, N. López, L. M. Rossi, *ACS Catal*. **2018**, *8*, 3516−3524.

[7] F. Martinez-Espinar, A. Salom-Català, E. Bresó-Femenia, C. Claver, F. Baletto, J. M. Ricart, B. Chaudret, J. J. Carbó, C. Godard, S. Castillon, *Inorg. Chem*. **2023**, *62*, 4570−4580.

[8] P. Lara, O. Rivada-Wheelaghan, S. Conejero, R. Poteau, K. Philippot, B. Chaudret, *Angew. Chem. Int. Ed*. **2011**, *50*, 12080−12084.

[9] V. Pfeifer, M. Certiat, D. Bouzouita, A. Palazzolo, S. Garcia-Argote, E. Marcon, D.-A. Buisson, P. Lesot, L. Maron, B. Chaudret, S. Tricard, I. del Rosal, R. Poteau, S. Feuillastre, G. Pieters, *Chem. Eur. J*. **2020**, *26*, 4988−4996.

[10] (a) C. Taglang, L. M. Martínez-Prieto, I. del Rosal, L. Maron, R. Poteau, K. Philippot, B. Chaudret, S. Perato, A. S. Lone, C. Puente, C. Dugave, B. Rousseau,

G. Pieters, *Angew. Chem. Int. Ed*. **2015**, *54*, 10474−10477; (b) N. Rothermel, D. Bouzouita, T. Röther, I. del Rosal, S. Tricard, R. Poteau, T. Gutmann, B. Chaudret, H.-H. Limbach, G. Buntkowsky, *ChemCatChem* **2018**, *10*, 4243−4247.

[11] L. M. Martínez-Prieto, I. Cano, A. Márquez, E. A. Baquero, S. Tricard, L. Cusinato, I. del Rosal, R. Poteau, Y. Coppel, K. Philippot, B. Chaudret, J. Cámpora, P. W. N. M. van Leeuwen, *Chem. Sci.* **2017**, *8*, 2931.

[12] (a) I. del Rosal, M. Mercy, I. C. Gerber, R. Poteau, *ACS Nano* **2013**, *7*, 11, 9823−9835; (b) L. Cusinato, L. M. Martínez-Prieto, B. Chaudret, I. del Rosal, R. Poteau, *Nanoscale* **2016**, *8*, 10974.

[13] R. González-Gómez, L. Cusinato, C. Bijani, Y. Coppel, P. Lecante, C. Amiens, I. del Rosal, K. Philippot, R. Poteau, *Nanoscale* **2019**, *11*, 9392.

[14] J. Creus, S. Drouet, S. Suriñach, P. Lecante, V. Collière, R. Poteau, K. Philippot, J. García-Antón, X. Sala, *ACS Catal*. **2018**, *8*, 11094−11102.

[15] S. Tuokko, P. M. Pihko, K. Honkala, *Angew. Chem.* **2016**, *128*, 1702−1706.

[16] J. Navarro-Ruiz, D. Cornu, N. López, *J. Phys. Chem. C* **2018**, *122*, 25339−25348.

[17] M. A. Ortuño, N. López, *ACS Catal*. **2018**, *8*, 6138−6145.

[18] S. Campisi, C. Beevers, A. Nasrallah, C. R. A. Catlow, C. e. Chan-Thaw, M. Manzoli, N. Dimitratos, D. J. Willock, A. Roldan, A. Villa, *J. Phys. Chem*. *C* **2020**, *124*, 4781−4790.

[19] I. Cano, M. A. Huertos, A. M. Chapman, G. Buntkowsky, T. Gutmann, P. B. Groszewicz, P. W. N. M. van Leeuwen, *J. Am. Chem. Soc.* **2015**, *137*, 7718−7727.

[20] A. Chatterjee, V. R. Jensen, *ACS Catal.* **2017**, *7*, 2543−2547.

[21] (a) M. Liu, Y. Xu, Y. Meng, L. Wang, H. Wang, Y. Huang, N. Onishi, L. Wang, Z. Fan, Y. Himeda, *Adv. Energy Mater*. **2022**, *12*, 2200817; (b) Y. Li, S. H. Chan, Q. Sun, *Nanoscale* **2015**, *7*, 8663.

[22] J. Ma, H. Gong, T. Zhang, H. Yu, R. Zhang, Z. Liu, G. Yang, H. Sun, S. Tang, Y. Qiu, *Appl. Surf. Sci.* **2019**, *488*, 1−9.

[23] M. D. Esrafili, B. Nejadebrahimi, *Appl. Surf. Sci.* **2019**, *475*, 363−371.

[24] K. Homlamai, T. Maihom, S. Choomwattana, M. Sawangphruk, J. Limtrakul, *Appl. Surf. Sci.* **2020**, *499*, 143928.

[25] (a) E. Vesselli, L. De Rogatis, X. Ding, A. Baraldi, L. Savio, L. Vattuone, M. Rocca, P. Fornasiero, M. Peressi, A. Baldereschi, R. Rosei, G. Comelli, *J. Am. Chem. Soc*. **2008**, *130*, 11417−11422; (b) G. Peng, S. J. Sibener, G. C. Schatz, S. T. Ceyer, M. Mavrikakis, *J. Phys. Chem. C* **2012**, *116*, 3001−3006; (c) G. Peng, S.J. Sibener, G. C. Schatz, M. Mavrikakis, *Surf. Sci*. **2012**, *606*, 1050−1055.

[26] X. Lv, G. Lu, Z.-Q. Wang, Z.-N. Xu, G.-C. Guo, *ACS Catal*. **2017**, *7*, 4519−4526.

[27] (a) G. Liu, P. Poths, X. Zhang, Z. Zhu, M. Marshall, M. Blankenhorn, A. N. Alexandrova, K. H. Bowen, *J. Am. Chem. Soc*. **2020**, *142*, 7930−7936; (b) D. Chattaraj, C. Majumder, *Phys. Chem. Chem. Phys*. **2023**, *25*, 2584−2594.

[28] X. Su, X.-F. Yang, Y. Huang, B. Liu, T. Zhang, *Acc. Chem. Res*. **2019**, *52*, 656−664 and references *therein*.

[29] L. Gong, J.-J. Chen, Y. Mu, *Phys. Chem. Chem. Phys*. **2017**, *19*, 28344−28353.

[30] Q. Liu, X. Yang, L. Li, S. Miao, Y. Li, Y. Li, X. Wang, Y. Huang, T. Zhang, *Nat. Commun*. **2017**, *8*, 1407.
[31] K. Mori, S. Masuda, H. Tanaka, K. Yoshizawa, M. Che, H. Yamashita, *Chem. Commun*. **2017**, *53*, 4677−4680.
[32] S. Masuda, K. Mori, Y. Futamura, H. Yamashita, *ACS Catal*. **2018**, *8*, 2277−2285.
[33] K. Mori, T. Sano, H. Kobayashi, H. Yamashita, *J. Am. Chem. Soc*. **2018**, *140*, 8902−8909.
[34] (a) M. Wen, K. Mori, Y. Futamura, Y. Kuwahara, M. Navlani-García, T. An, H. Yamashita, *Sci. Rep*. **2019**, *9*, 15675; (b) S. Masuda, K. Mori, Y. Kuwahara, H. Yamashita, *J. Mater. Chem. A* **2019**, *7*, 16356−16363; (c) K. Mori, A. Konishi, H. Yamashita, *J. Phys. Chem. C* **2020**, *124*, 11499−11505.
[35] K. Philippot, B. Chaudret, *C. R. Chim*. **2003**, *6*, 1019−1034.
[36] T. Pery, K. Pelzer, G. Buntkowsky, K. Philippot, H.-H. Limbach, B. Chaudret, *ChemPhysChem* **2005**, *6*, 605−607.
[37] N. Rothermel, H.-H. Limbach, I. del Rosal, R. Poteau, G. Mencia, B. Chaudret, G. Buntkowsky, T. Gutmann, *Catal. Sci. Technol.* **2021**, *11*, 4509−4520.
[38] J. García-Antón, M. Rosa Axet, S. Jansat, K. Philippot, B. Chaudret, T. Pery, G. Buntkowsky, H.-H. Limbach, *Angew. Chem. Int. Ed*. **2008**, *47*, 2074−2078.
[39] P.-J. Debouttière, Y. Coppel, A. Denicourt-Nowicki, A. Roucoux, B. Chaudret, K. Philippot, *Eur. J. Inorg. Chem*. **2012**, 1229−1236.
[40] A. D. Phillips, L. Gonsalvi, A. Romerosa, F. Vizza, M. Peruzzini, *Coord. Chem. Rev*. **2004**, *248*, 955−993.
[41] T. Wang, D. Ren, Z. Huo, Z. Song, F. Jin, M. Chen, L. Chen, *Green Chem*. **2017**, *19*, 716−721.
[42] A. Berná, A. Rodes, J. M. Feliu, F. Illas, A. Gil, A. Clotet, J. M. Ricart, *J. Phys. Chem. B* **2004**, *108*, 17928−17939.
[43] (a) A. Markovits, M. García-Hernández, J. M. Ricart, F. Illas, *J. Phys. Chem. B* **1999**, *103*, 509; (b) P. Paredes Olivera, E. M. Patrito, *Electrochim. Acta* **1998**, *44*, 1247; (c) S. A. Wasileski, M. J. Weaver, *J. Electroanal. Chem*. **2002**, *524*, 219.
[44] J. Su, M. Lu, H. Lin, *Green Chem*. **2015**, *17*, 2769−2773.
[45] C. S. He, L. Gong, J. Zhang, P. P. He, Y. Mu, *J. CO_2 Util*. **2017**, *19*, 157−164.
[46] G. Mills, H. Jónsson, *Phys. Rev. Lett*. **1994**, *72*, 7, 1124−1127.
[47] (a) G. Kresse, J. Hafner, *Phys. Rev. B* **1993**, *47*, 558; (b) G. Kresse, J. Furthmüller, *Comput. Mat. Sci*. **1996**, *6*, 15−50; (c) G. Kresse, J. Furthmüller, *Phys. Rev. B* **1996**, *54*, 11169.
[48] (a) P. Hohenberg, W. Kohn, *Phys. Rev*. **1964**, *136*, 864−871; (b) W. Kohn, L. J. Sham, *Phys. Rev*. **1965**, *140*, 1133−1138.
[49] J. P. Perdew, K. Burke, M. Ernzerhof, *Phys. Rev. Lett*. **1996**, *77*, 3865.
[50] G. Kresse, D. Joubert, *Phys. Rev. B* **1999**, *59*, 1758.

CHAPTER 5

Modifications of TiO_2 supported PPh_3-capped palladium nanocatalysts in the CO_2 hydrogenation into formates

UNIVERSITAT ROVIRA I VIRGILI
EFFICIENT VALORIZATION OF CO2 INTO FORMATE THROUGH NANOCATALYSIS
María Dolores Fernández Martínez

5.1. Introduction

Heterogeneous catalysts have become a crucial part of many industrial activities, such as organic synthesis, oil refining, and pollution control.[1] Modern heterogeneous catalysts consist of several elements in precise proportions.[1c] Currently, heterogeneous catalysts are optimized for the greatest reaction rate, which in turn results in optimal selectivity.[1b,1c,1d] It is possible to improve the heterogeneous catalyst activity by modifying the support using approaches such as nanotechnology and nanoscience or controlling the pore structure.[1e,1f,2] For heterogeneous catalysis, the problem of catalyst separation and recovery from the reaction mixture are addressed by the utilization of supports such as Al_2O_3, TiO_2, ZrO_2, ZnO, among others, to immobilize the active phase.[1f]

Indeed, the catalyst is ideally dispersed on a suitable support to stabilize the metal nanoparticles, obtain optimal performance and minimize the amount of costly metal.[1b,1f] However, the catalyst support may sometimes exert a structural effect, brought about by textural and active phase-linked effect. Thus, the support in heterogeneous catalysts must retain its specific properties, such as porosity, surface area, dispersion, selectivity, and activity.[3,4] The morphology and pore size of the selected support materials play an important role in enhancing the heterogeneous catalyst's stability and performance.[3d]

In Chapter 3, supports of different nature (metal oxides and carbon based) were tested in Pd-catalyzed hydrogenation of CO_2 to formate and notable differences were observed.

In the design of new catalysts, the appropriate metal-support interactions (MSI) must be obtained and their tuning can be achieved through adjustments of either the composition and/or morphology of support and active phase or through the modifications their surface (Figure 1).[5,6] However, changes in composition and morphology can affect this nature.[7] Surface modifications can enhance steric control or provide hydrophilic/hydrophobic character that can be suitable for the target substrates and catalysis media.[8]

As previously mentioned in Chapter 1, TiO_2 is one of most efficient supports for heterogenous catalysts in the hydrogenation of CO_2 to formate.[9] Here, surface modification of TiO_2 support and treatment of composite by overlay

deposition was carried out to improve the catalytic performance of the catalysts described in Chapter 3.

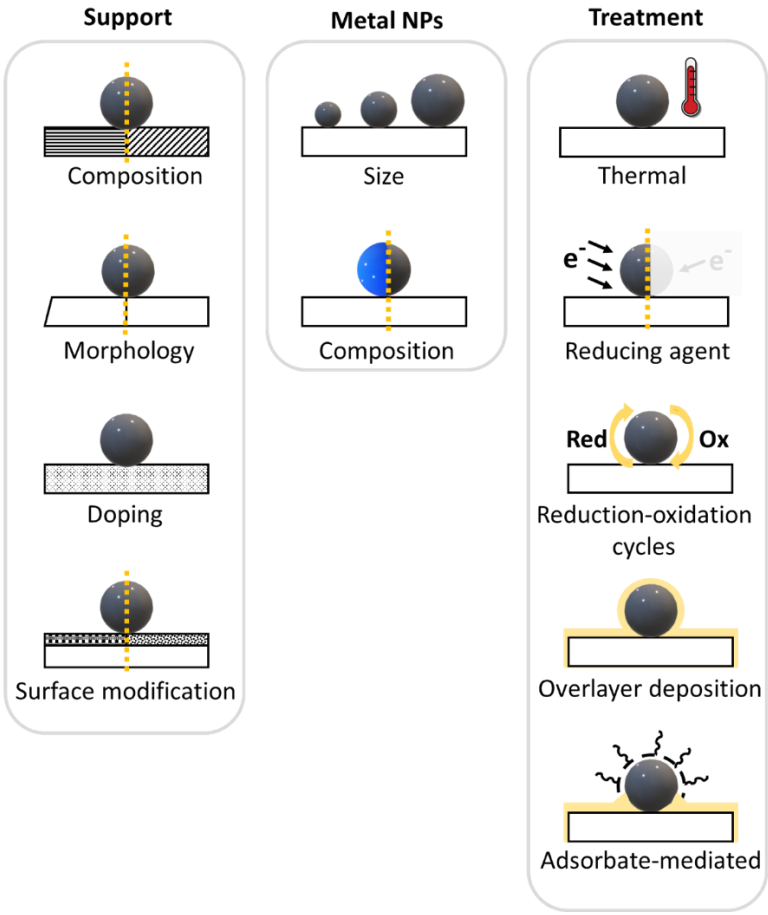

Figure 1. Main Metal-Support Interactions (MSI) in which both support and metallic nanoparticles are involved.

In this area, the use of organic self-assembled monolayers (SAMs) is one of the most used methods.[10,11] These organic modifiers can act as spacers between NPs to avoid sintering and improve stability/recyclability of the catalyst (Figure 2). Moreover, depending on the functional groups in these modifiers, the catalyst activity can be enhanced through interactions with the substrate.[12] These groups could also confer a hydrophobic or hydrophilic character to the system and as such, also favor catalyst substrate interactions.[13]

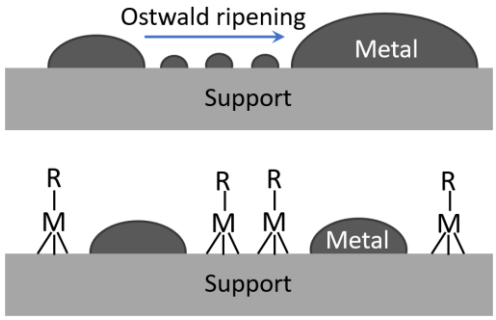

Figure 2. Improvement of resistance to sintering with the introduction of a modifier (M).

Modification of carbon-based and silica supports with organic molecules were previously reported for the design of functionalized surfaces. Such modifications were used to cover metallic nanoparticles with alkylic chain[14] or with groups containing amine functionalities[15] to produce catalytic materials for CO_2 hydrogenation into formate.

Organosilanes are one of the most commonly used molecules to modify supports and constitute a type of inorganic/organic hybrid materials (Scheme 1).

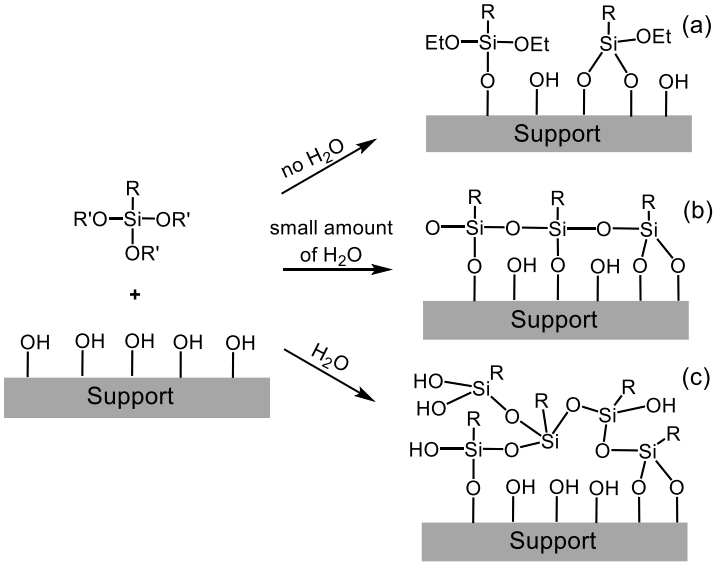

Scheme 1. Schematic representation of silanization process using APTES as organosilane molecule involved. (a) in absence of H_2O, only Si-O-support partial monolayer is formed; (b) controlled amount of H_2O, Si-O-support + Si-O-Si dense monolayer is formed and (c) in excess of H_2O few Si-O-M multilayer is formed.

These molecules are represented by the formula $R_nSiX_{(4-n)}$ with n= 1, 2, or 3 where R is an organic group linked to Si *via* a Si-C bond and X is a hydrolysable organic group (such as ethoxy or chloro).[16] Aminoalkylsilanes, such as (3-aminopropyl)triethoxysilane (APTES), is one of the most commonly reported organosilane.[17] Modification occurs through silanization, which is a process that covers a surface such as metal oxide with chloro or alkoxysilane.[18] Using APTES, this process starts with the hydrolysis of the ethoxy groups that is catalyzed by water, leading to the formation of silanols (Scheme 1). Depending on the amount of water, layers can interact with each other in different ways, giving rise to a non-homogeneous coverage of the TiO_2 surface.[19]

Then, the APTES silanols will condense with the surface -OH to form a monolayer. The way in which APTES is attached to the TiO_2 surface have been object of discussion in literature. There are several possibilities (Figure 3) depending on whether its anchoring takes place through Si or NH_2 groups.

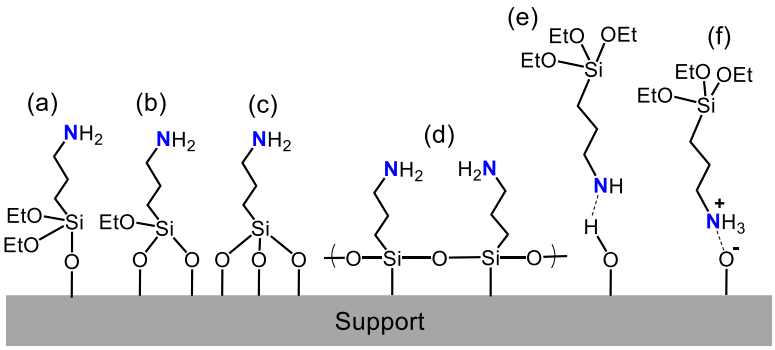

Figure 3. Possible interactions of APTES and TiO_2.

The most accepted chemisorption of APTES onto TiO_2, based on both experimental and theoretical studies, implies one or two Si−O−Ti bonds.[17,20] Sometimes, APTES was used directly over metallic nanoparticles for their stabilization and functionalization.[21] It is believed that the amine group present in APTES does not only provide an additional stabilization for the particles but can also have an effect in catalysis where an acidic molecule such as CO_2 is involved.[22]

Liu et al. reported that APTES directly participates in the synthesis of a protonated Schiff-base which covers Au NPs during the dehydrogenation of FA into CO_2 and H_2.[23] Later, the same authors developed a new Au based catalyst for the hydrogenation of CO_2 into formic acid in which SiO_2 was modified by APTES and a Schiff-base.[24] In both samples (using APTES and Schiff-base), the catalysts contained nanoclusters, single atoms and Au NPs larger than 2 nm. Depending on the synthetic procedure, variations in size and distributions were observed. For the hydrogenation of CO_2, small sub-nanoclusters were more efficient than nanoparticles and single-atom based catalysts. NEt_3 was present in the medium, and hydrogenation occurred through the CO_2 route rather than bicarbonate. The authors studied the reaction mechanism by computational methods and showed that an adduct is formed due to the introduction of a Schiff-base (Scheme 2). The TON reached by these catalysts was 14470 over 12 h at 90 ºC.

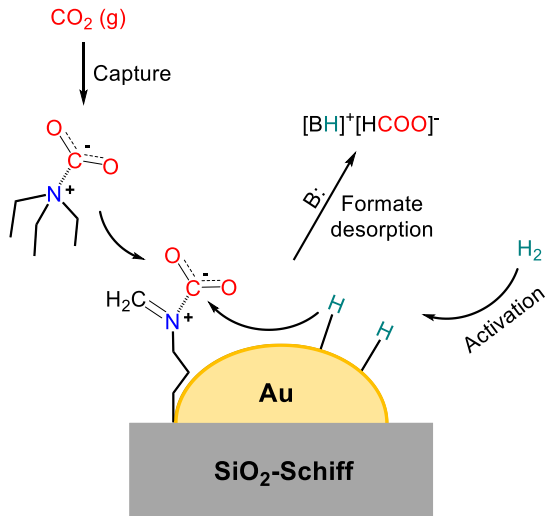

Scheme 2. Proposed mechanism for the hydrogenation of CO_2 to formate Shiff-base modified Au catalyst.

The same year, Mori et al. reported PdAg NPs supported over amine-funcionalized mesoporous silica for the reversible CO_2 hydrogenation and release of H_2.[25] They tested various organosilanes containing amine groups and in the CO_2 hydrogenation (and formate dehydrogenation), the catalyst

containing the aniline group exhibited the PdAg NPs with the smallest size (3.9 nm) and revealed the most active. (Scheme 3).

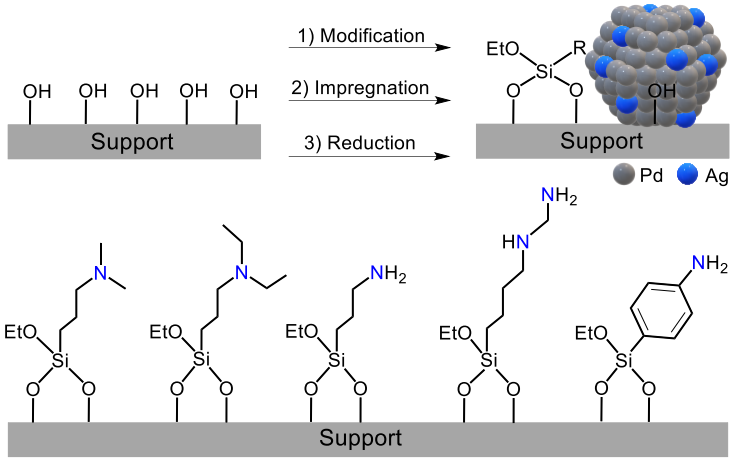

Scheme 3. Different organosilanes employed in modification of SBA-15 support before PdAg NPs synthesis.

The authors carried out DFT calculations to further determine the role of the amine functionality and observed that the presence of amine affects the O-H dissociation of FA and favored the adsorption of CO_2 in hydrogenation. In terms of recyclability, the catalyst could be recovered and reused for three runs without loss of activity nor changes in structure.

Srivastava reported the preparation of Ru NPs supported over various amine organosilane modified SBA-15 mesoporous silica and their application as catalyst in the hydrogenation of CO_2 into formic acid.[26] Primary, secondary and tertiary amines were tested and the use of the primary amine provided the highest catalytic activity. Moreover, a strong effect on the catalyst stability was observed. When organosilanes bearing secondary and tertiary amines were used, a large decrease in catalytic activity was observed after the 3rd run. However, when a primary amine group was present, no decrease was observed before the 5th run.

Ionic Liquids (ILs) constitute another type of interesting molecules for support modification[27] and materials of different nature such as mesoporous silica, zeolites, polymers, clays, carbon-based or metal oxides were modified using ILs.[28] Materials resulting from the deposition of ILs over heterogeneous support materials are called supported ionic liquid phase (SILP) systems

(Figure 4). Depending on whether the ILs are physiosorbed or chemisorbed, the amount of molecules and the material stability can vary (Figure 4). Chemisorption is usually preferred due to the stability of strong covalent bonds. In these materials, the properties of the initial ILs usually remain unaltered (interaction between cation and anion).[28] Thus, SILPs can be used for the synthesis of catalysts based on metallic nanoparticles since with this type of support, NPs are stabilized by both the electrostatic interactions with ILs (as for free ILs) and by metal-support interactions.[29]

Although the most common SILP systems are based on SiO_2,[30,31] TiO_2 based catalysts can also be synthesized directly in the presence of ILs by conventional methods,[32] or by first modifying the TiO_2 support with ILs prior to NP deposition.[27,33]

For instance, Menhert et al. covalently anchored 1-*n*-butyl-3-[3-(triethoxysilanyl)propyl]-4,5-dihydroimidazolium over a silica surface for application in the Rh hydroformylation of 1-hexene.[34]

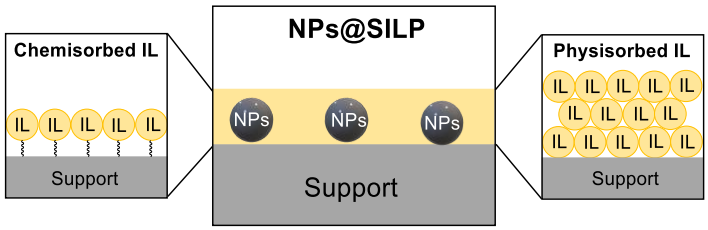

Reduced quantities of ILs
Enhanced NP stability and activity
Improved mass transport into IL phase
Implementation in continuous flow processes

Figure 4. Chemisorption and physisorption of Supported-Ionic Liquids (SILPs) example.

The silanization reaction of ILs was studied using solid-state ^{29}Si NMR to determine whether one, two or three O atoms are attached to the surface of oxide supports.[35] Other techniques such as TGA, scanning electron microscopy (SEM) and FT-IR were also used to quantify the amount of deposited IL over the support, to study the morphology of the material and for the qualitative identification of the organic functional groups present in the material, respectively.[36]

For catalytic reactions involving CO_2, the interactions between IL and CO_2 depend on the anion. For instance, when basic anions such as acetate in combination with 1,3-dialkylimidazolium are used, interactions with CO_2 can be enhanced.[37] As such, this type of ILs were used in the hydrogenation of CO_2 to formic acid.[38]

In recent years, Leitner and co-workers reported the preparation of metallic nanoparticles in ionic liquids covalently grafted onto SiO_2 by silanization.[35,39,40,41,42] Monometallic Rh[39] NPs and bimetallic systems such as CoRh[40] and FeRu[41] were applied in different catalytic processes.[35] These nanoparticles were synthesized using the organometallic approach[43] and in general, imidazolium-based supported ionic liquids were employed. Various systems were developed by tuning the parameters of these imidazolium-based SILPs such as the alkyl spacer, the anion and the *N*-alkyl chain length (Figure 5). The nature of the anion affects the IL hydrophobic (NTf_2^-, for example) or hydrophilic character (*e.g.* OT_f^-) and thus influence the catalytic outcome of various catalytic reactions.

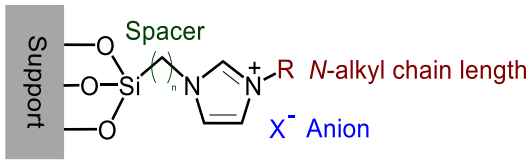

Figure 5. Specific groups used to tune the IL properties in imidazolium-based SILPs.

Ru NPs[42] were also reported by the same authors for the hydrogenation of CO_2 to formate. Very recently, Leitner and co-worked reported a Ru-based catalyst supported over imidazolium-based SILP for the hydrogenation of CO_2 into formate in the presence of NEt_3 (Scheme 4).[44] The authors first covalently modified the SiO_2 surface with ILs *via* silanization while the synthesis of the Ru NPs was performed in a second step. Small NPs were obtained (0.8-2.9 nm). Modifications of the alkyl chain and anion resulted very important to modulate their properties, which revealed to affect their catalytic performance. These modifications resulted in an increase of the TON by 2 or 10-fold when compared with unmodified Ru/SiO_2 catalyst at 60 bar total pressure (CO_2:H_2= 1:2, 100 °C, and NEt_3:H_2O solvent system). Indeed, the introduction of an ammonium sulfonate group in the alkyl chain dramatically

increased the catalyst activity (TON up to 16100 per surface Ru atoms). Using H/D exchange experiments, the authors determined that the modification favored the desorption of formate from the catalyst surface.

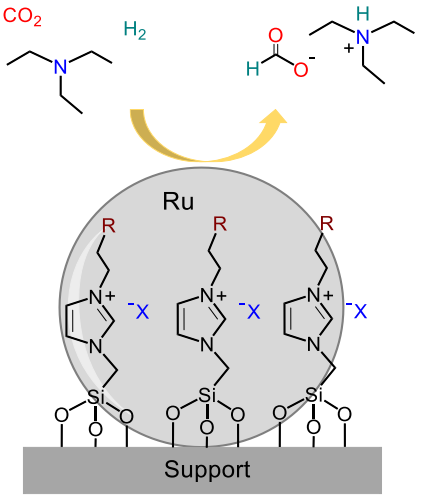

Scheme 4. Ru NPs supported in imidazolium-based SILPs for hydrogenation of CO_2 to formate.

In this work, the Ru@SILP(Bu-NTf_2) catalyst was tested in recycling experiments. After several cycles, a significant loss of activity was observed, which was attributed to the leaching of IL from the support due to the use of NEt_3 + H_2O as solvent system. When the same catalyst was tested in the presence of DCM as cosolvent, a lower TON was observed, but was maintained for several cycles.

Using a completely distinct synthesis, other authors reported Pd NPs supported over poly(ionic liquid)s (PILs) for the hydrogenation of CO_2 into formic acid.[45] The presence of abundant N atoms in the PILs favored the anchoring of the Pd NPs. Moreover, a strong hydrophobicity was conferred to the system by the bis(trifluoromethanesulfonyl)amide anion ([NTf_2^-], with high affinity with CO_2. Using this catalytic system, a TOF of 1190 h^{-1} was obtained in the presence of NEt_3 aqueous solution (100 ºC, 4.0 MPa total pressure, H_2/CO_2= 1:1, 1 h) and good recyclability was observed during several runs.[45a]

Organophosphonic acids (PAs) constitute another common type of molecules used for the modification of support surfaces. These $RPO(OH)_2$ compounds were especially used to modify metal oxide surfaces.[46]

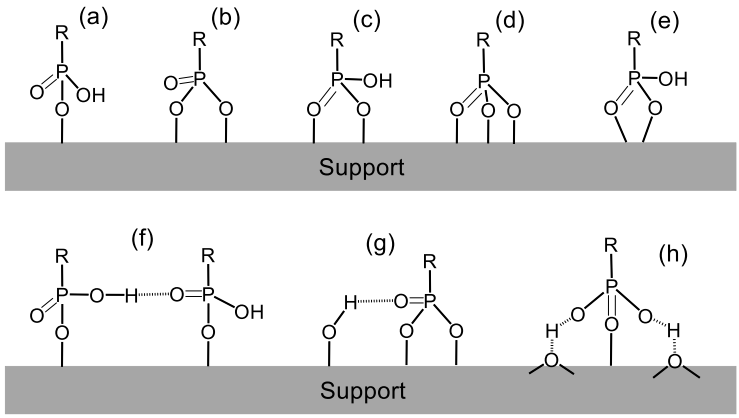

Figure 6. Binding modes of interactions between PAs and TiO_2. Monodentate (a), brinding bidentate (b) and (c), brinding tridentate (d), chelating bidentate (e) and additional hydrogen-bonding interactions (f), (g) and (h).

There are two possible ways for the binding of these species onto oxide surfaces: by coordination of P=O with a surface Lewis acid or by condensation of P-OH with surface -OH groups.

The interaction of PAs with TiO_2 could be monodentate, bidentate and tridentate (Figure 6). However, Brodard-Severac et al.[47] employed SAMs of ^{17}O-enriched phosphonic acids chemisorbed on TiO_2 and only observed bridging modes. They also suggested that mono-, bi- and tridentate coordination could be taking place from the detection of P–O–Ti, P=O, and P–OH groups. Others discarded the homocondensation between several PAs.[48]

Moreover, when PAs are used for surface modification, an additional annealing or aging treatment is necessary. Generally, after formatting of SAMs (introduction of metal oxide into a diluted PA solution), the composite is removed from solution and annealed at ≈ 120°C. This produce condensation reactions to form strong bonds between PAs and metal oxide.[11] Several studies about PAs coverage of TiO_2 were reported[49] and DFT calculations were performed to investigate the effect of tail functional group.[50] Although the binding of organophosphonic acids at the metal–metal-oxide

interface often remains unclear, the functional groups located in the alkyl chain were shown to have an effect on the activity and stability of the corresponding catalysts.[51] One example of the influence such a functional group was reported by Medlin and coworkers.[52] In this work, Pd and Pt nanoparticles were synthesized and supported onto TiO_2 and Al_2O_3. In this case, the use of organophosphonic acid resulted essential to the selectivity of the reaction. Variations in the chain length and functional groups were tested and affected the interactions with the acidic CO_2 molecule. Deposition of PAs with NH_2 group had two positive effects: to consume acidic OH groups at TiO_2 surface and favor interaction with CO_2. Methylphosphonic acid provided excellent selectivity (up to ≈ 99% at conversions near 50%) for CO_2 reduction to CO. However, when no modification was made, full hydrogenation of CO_2 into CH_4 was observed. The improvement due to PA was attributed to the promotion of CO_2 adsorption and facile desorption of CO, preventing CO poisoning.

In the work presented in this chapter, modifications of the TiO_2 support/catalyst were carried out with the previously mentioned molecules with Si and P as anchoring atoms. The newly prepared materials were characterized and tested in the catalytic hydrogenation of CO_2 into formate. The effect of these modifications on the activity and recyclability of these catalyst was particularly looked at.

5.2. Results and Discussion

The objective of the work described in this chapter was to improve the metal-support interaction between palladium NPs and TiO_2 through modifications by organic molecules to solve the recyclability issue reflected in the Chapter 3 of this thesis.

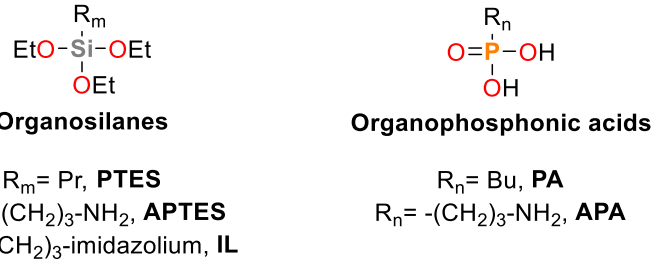

Figure 7. Representation of molecules of different nature used in TiO_2 modification.

For this purpose, two different approaches were developed for the catalyst modification using triethoxysilanes (TESs) and organophosphonic acids (PAs) (Figure 7).

In the first approach, the TiO_2 support was first modified prior to Pd NP deposition whereas in the second approach, the Pd NPs were initially supported onto TiO_2 and the modifiers were reacted subsequently (Scheme 5).

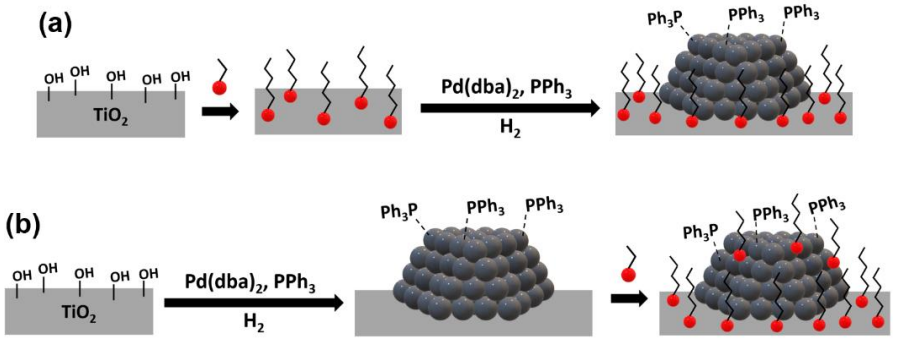

Scheme 5. Deposition of modifier on a support before synthesize metal catalyst (reverse deposition) (a) and deposition of modifier on a previously synthesized supported metal catalyst (b).

This study aimed at comparing the robustness of the linkage of the modifiers through different atoms (Si or P) and evaluate the effect of the group located at the end of the modifier chain. In the case of ILs, different anions were used to evaluate the effect of their hydrophilic or hydrophobic character.

5.2.1. Synthesis and characterization of modified TiO_2 supports

The first approach consisted in an initial modification of the support prior to the deposition of the metal nanoparticles. In the literature, this approach is known as the reverse deposition.[52] In the following sections, the modifications of the TiO_2 support by TESs and PAs are described, followed by deposition of the Pd NPs.

5.2.1.1. Synthesis and characterization of modified TiO_2 with $RSi(OEt)_3$ modifiers (R= Pr, $-(CH_2)_3-NH_2$, $-(CH_2)_3$-imidazolium)

The synthesis of TiO_2 modified with $RSi(OEt)_3$ was carried out following literature procedures (Figure 8).[20b,53]

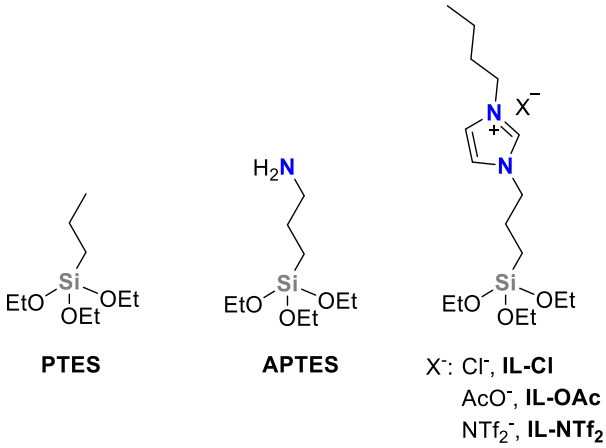

Figure 8. Organosilane modifiers used in this study.

In a typical synthesis, when PTES and APTES were used as modifier, the reaction with TiO_2 was performed in a EtOH:H_2O solution or absolute EtOH. For ILs, TiO_2 was added to a solution of ILs in toluene, water or EtOH:H_2O mixture. The mixture was then centrifuged and the solid was recovered and washed several times with H_2O and EtOH. Finally, the white solid was dried under vacuum for several hours.

In view of the variety of conditions used form the modifications of support by organosilanes, an optimization of synthesis parameters such as concentration of APTES, APTES/TiO_2 ratio, temperature and time was initially performed (Table 1).

To evaluate the results of these syntheses, the samples were analised by FT-IR and TGA. FT-IR analysis was first carried out to confirm that the reaction of condensation between hydroxyl groups on TiO_2 surface and silanol groups had taken place. The regions where functional groups of interest could be detected are summarized in Figure 9. In the region between 960 and 910 cm^{-1}, the bands corresponding to Ti-O-Si appears.[54] These signals can overlap with the Ti-O-Ti band, which is a broad band that appaears on the range *ca.* 900-400 cm^{-1}. Condensation between silanols groups can be identified by detection of a Si-O-Si stretching band at 1070 cm^{-1} and an asymmetric Si-O-Si stretching band at 1160 cm^{-1}.[17] In the region of 1250-1200 cm^{-1}, a band corresponding to Si-CH_2-R is expected.

Table 1. Optimization of synthesis conditions for TiO_2 modified with organosilanes, $RSi(OEt)_3$.[a]

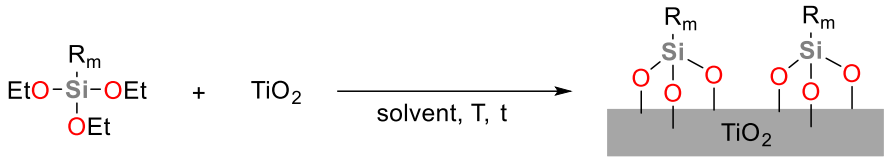

R_m= Pr, **PTES**
R_m= -$(CH_2)_3$-NH_2, **APTES**
R_m= -$(CH_2)_3$-imidazolium, **IL**

PTES@TiO_2
APTES@TiO_2
IL-X@TiO_2

Entry	[C], M	mmol/mg TiO_2	T (ºC)	Code
1	0.13	0.013	r.t.	**PTES@TiO_2-1**
2	0.01	0.003	r.t.	**APTES@TiO_2-2**
3	0.13	0.013	r.t.	**APTES@TiO_2-3**
4	1	0.01	r.t.	**APTES@TiO_2-4**
5[b]	1	0.005	120	**APTES@TiO_2-5**
6	4	0.02	r.t.	**APTES@TiO_2-6**
7[b]	4	0.02	120	**APTES@TiO_2-7**
8[c]	0.022	0.0009	80	**IL-Cl@TiO_2-8**
9[d]	0.12	0.01	110	**IL-Cl@TiO_2-9**
10[d]	0.13	0.013	110	**IL-NTf_2@TiO_2-10**
11[e]	0.013	0.0013	80	**IL-OAc@TiO_2-11**
12[e]	0.13	0.013	80	**IL-OAc@TiO_2-12**

[a]Synthesis conditions: TiO_2 was added to a previously prepared solution of (A)PTES on mixture EtOH:milli-Q H_2O (95:5 v/v) and reacted at r.t. overnight. [b]For 120 ºC reaction, the reaction was performed in an autoclave during 4 h using EtOH as solvent. [c] Suspension of 2 g of TiO_2 in 80 ml of milli-Q H_2O was added to a previously prepared solution of IL-Cl in 2 ml of milli-Q H_2O. The mixture was stirred at 80 ºC during 12 h. [d] TiO_2 (500 mg) was added to a solution of IL-Cl in dry toluene and stirred at reflux overnight. [e]TiO_2 was added to a solution of IL-OAc in EtOH:milli-Q H_2O mixture (95:5 v/v) and was heated at 80 ºC overnight.

Due to the presence of alkyl groups in the samples, bands corresponding to -CH_2 bending and -CH_2 stretching, are usually detected between 1470-1420 and 3000-2850 cm^{-1} are usually detected.[36] When an amine group is included in the material, two bands corresponding to C-N stretching (*ca*. 1360 cm^{-1})

and to N-H bending (*ca*. 1600 cm^{-1}) are also expected.[55] This latter appears at similar wavenumber than those due to -OH bending from hydroxyl group at the TiO_2 surface.

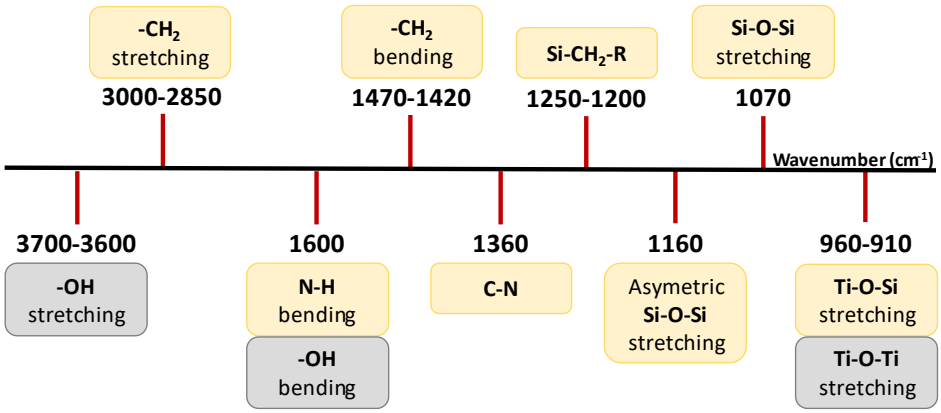

Figure 9. Organosilane modifiers used in this study.

FT-IR spectra of modified samples and commercial TiO_2 are displayed in Figure 10. For commercial TiO_2, 3 bands were observed: a broad band at 3700–2600 cm^{-1} corresponding to O-H stretching vibrations, a band located at *ca*. 1630 cm^{-1} attributed to the molecular water bending mode based on previous reports,[53] and a very broad band at *ca.* 900 cm^{-1} corresponding to the Ti-O-Ti stretching. For **PTES@TiO$_2$-1**, new bands at 1040 and 1240 cm^{-1} were detected, indicating the presence of the modifier in the sample. Moreover, bands corresponding to -CH_2 stretching vibrations were observed. Bands corresponding to -OH from TiO_2 were still detected, indicating that the coverage of the support surface was uncomplete. Bands between 2400-2269 cm^{-1} that also appear in TiO_2 spectrum were attributed to the presence of CO_2. For **APTES@TiO$_2$-2**, apart from the bands detected in the previous sample, a new band was detected at 1558 cm^{-1} and attributed to C-N stretching confirmed the presence of the amine group at the end of the alkyl chain.

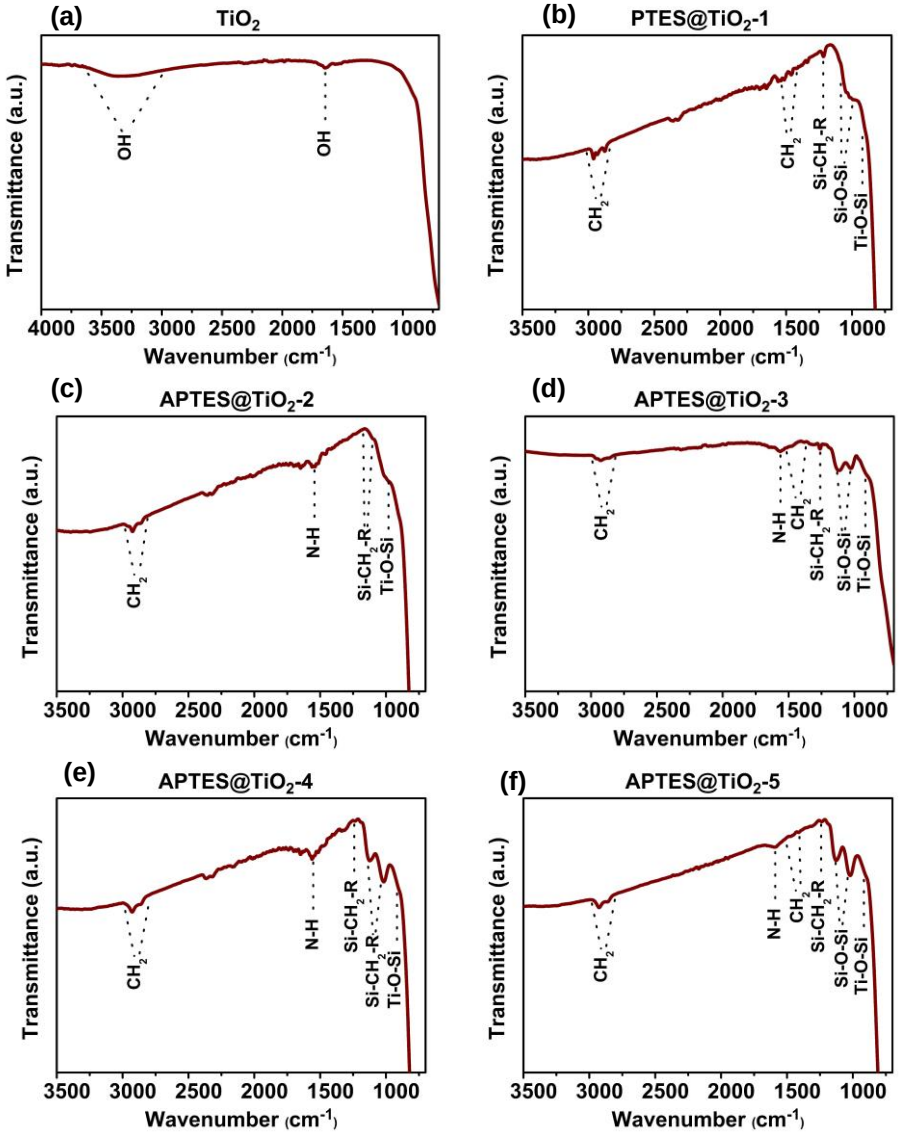
(a)
TiO2
OH
OH
Transmittance (a.u.)
4000 3500 3000 2500 2000 1500 1000
Wavenumber (cm-1)
(b)
PTES@TiO2-1
CH2
CH2
Si-CH2-R
Si-O-Si
Ti-O-Si
Transmittance (a.u.)
3500 3000 2500 2000 1500 1000
Wavenumber (cm-1)
(c)
APTES@TiO2-2
CH2
N-H
Si-CH2-R
Ti-O-Si
Transmittance (a.u.)
3500 3000 2500 2000 1500 1000
Wavenumber (cm-1)
(d)
APTES@TiO2-3
CH2
N-H
CH2
Si-CH2-R
Si-O-Si
Ti-O-Si
Transmittance (a.u.)
3500 3000 2500 2000 1500 1000
Wavenumber (cm-1)
(e)
APTES@TiO2-4
CH2
N-H
Si-CH2-R
Si-CH2-R
Ti-O-Si
Transmittance (a.u.)
3500 3000 2500 2000 1500 1000
Wavenumber (cm-1)
(f)
APTES@TiO2-5
CH2
N-H
CH2
Si-CH2-R
Si-O-Si
Ti-O-Si
Transmittance (a.u.)
3500 3000 2500 2000 1500 1000
Wavenumber (cm-1)

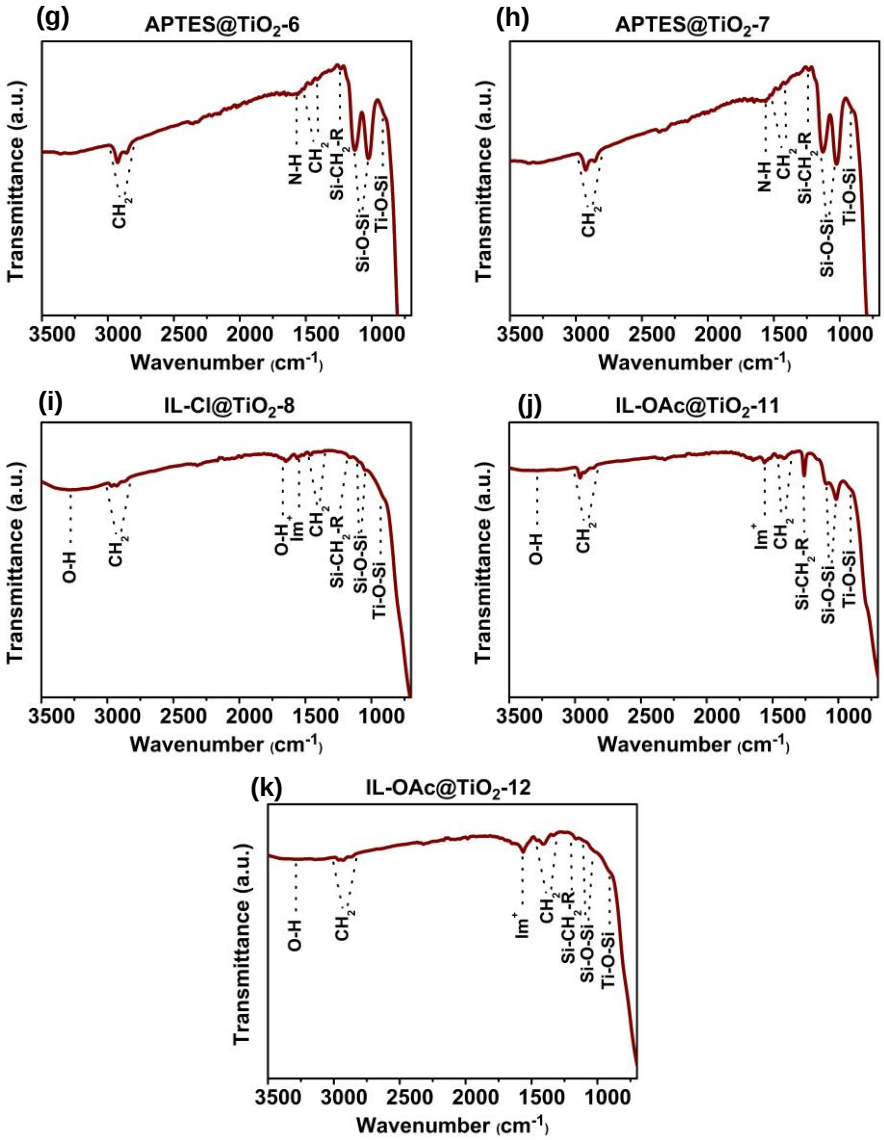

Figure 10. FT-IR of different TiO_2 modified with organosilanes, $RSi(OEt)_3$.

For all samples in which APTES was used to modify TiO_2, bands corresponding to presence of the normal vibration frequencies of the functional groups appear and increase in intensity when a higher amount of APTES and temperature was employed in synthesis. For **APTES@TiO₂-3**, a shoulder at 910 cm^{-1} was detected and attributed to Ti-O-Si stretching. Moreover, in the FTIR spectra of the samples **APTES@TiO₂-3**-

APTES@TiO_2-7 (in which mmol APTES/mg TiO_2 is higher than 0.015), the band at 1635 cm^{-1} corresponding to the -OH bending was not detected and the band between 3700-3600 cm^{-1} for -OH stretching on TiO_2 was much less intense for **APTES@TiO_2-5**, **APTES@TiO_2-6**, **APTES@TiO_2-7**, indicating a high coverage of the TiO_2 surface by APTES.

In the FT-IR spectra of **IL-Cl@TiO_2-8**, **IL-OAc@TiO_2-11** and IL-**OAc@TiO_2-12** (Figure 10), bands at 911 (Ti-O-Si), 1162-1019 (Si-O-Si), 1264-1245 (Si-CH_2-R), 1486-1408 (-CH_2) and 2985-2841 (-CH_2) cm^{-1} were detected in agreement with previously reported values for 1130-1000 (Si-O-Si), 1250-1200 (Si-CH_2-R), 1470-1420 (-CH_2) and 3000-2850 (-CH_2) cm^{-1} for ionic liquid-functionalized porous amorphous silica.[36] Bands at 1566 and 1400 cm^{-1} corresponding to imidazolium ring stretch were also detected.[56] Moreover, bands between 3250–3000cm^{-1} were also present in the spectra. These bands could be attributed to the imidazolium ring C–H stretch.[56] However, due to the similarity in wavelengths for the band for -OH stretching on the support, the presence of -OH group could not be discarded.

These systems were also characterized by TGA (Figure 11) to obtain information about the amount of organosilanes over the TiO_2. In commercial TiO_2, a weight loss was observed at low temperature (< 200 ºC) and associated to the loss of water. For the rest of samples, weight losses in the same temperature range were also detected. For the modified TiO_2 samples, a new weight loss located between 200 and 450 ºC was detected and attributed to the loss of anchored organosilanes.

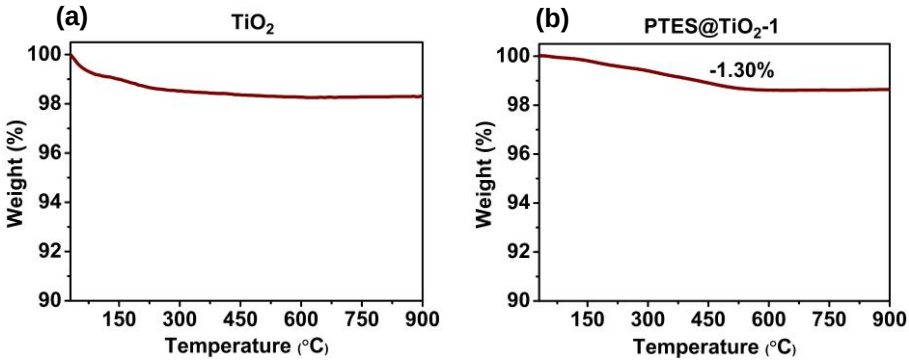

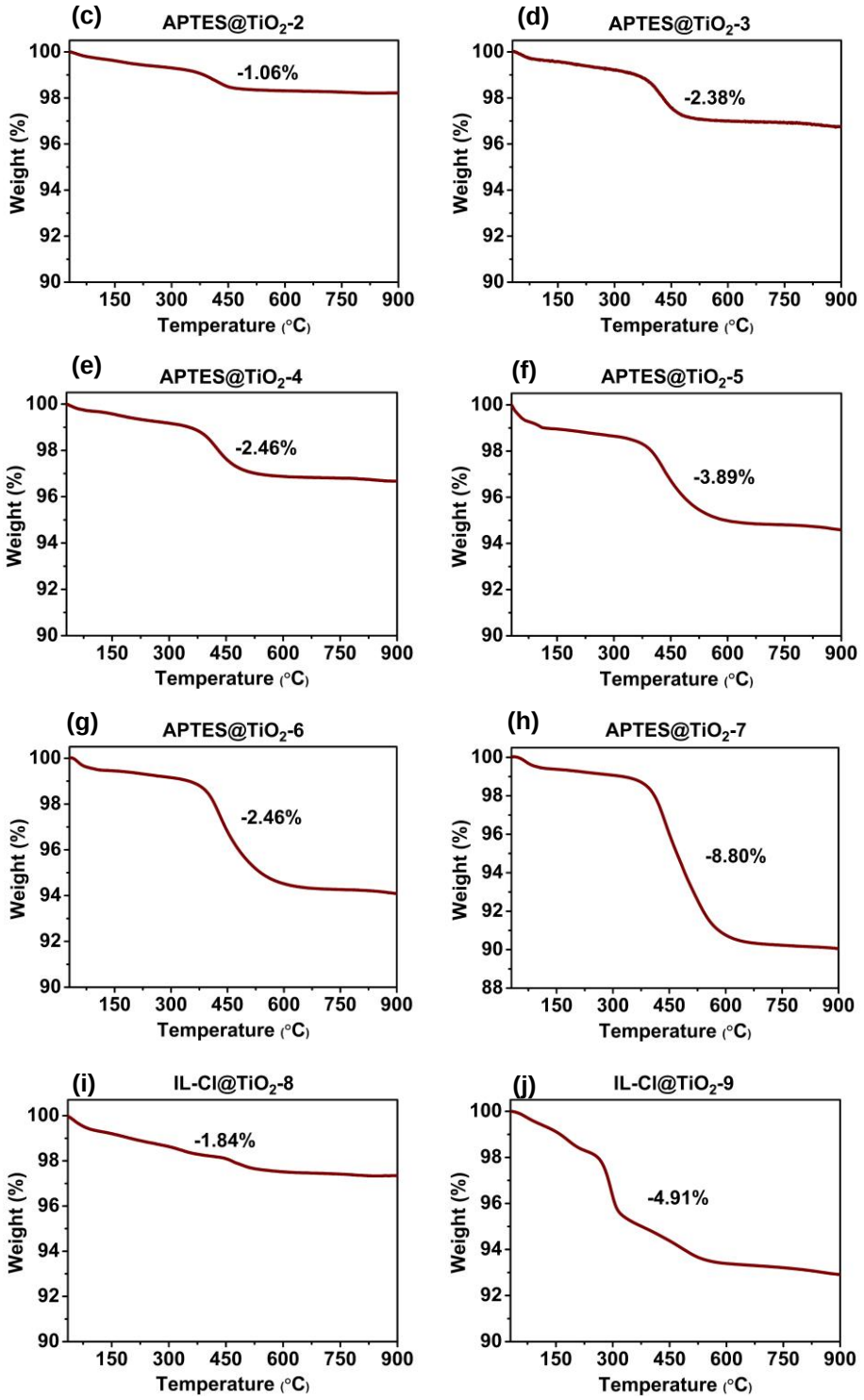
(c)
APTES@TiO2-2
-1.06%
(d)
APTES@TiO2-3
-2.38%
(e)
APTES@TiO2-4
-2.46%
(f)
APTES@TiO2-5
-3.89%
(g)
APTES@TiO2-6
-2.46%
(h)
APTES@TiO2-7
-8.80%
(i)
IL-Cl@TiO2-8
-1.84%
(j)
IL-Cl@TiO2-9
-4.91%
Weight (%)
Temperature (°C)

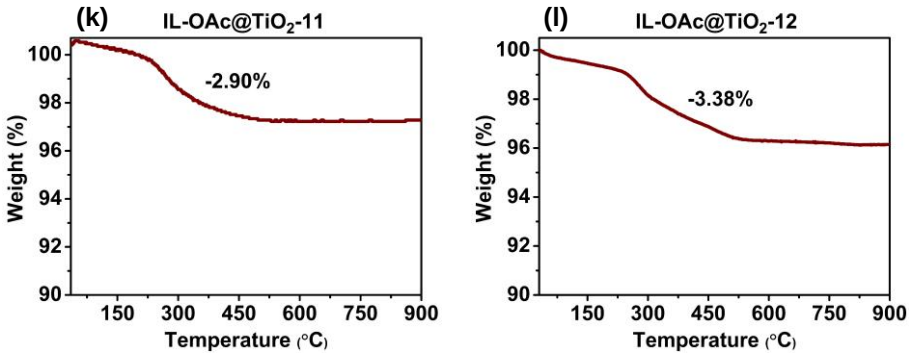

Figure 11. TGA of different TiO_2 modified with organosilanes, $RSi(OEt)_3$.

The TGA data obtained for these materials are summarized in Table 2. For **PTES@TiO_2-1** (Entry 1), a weight loss of 1.30% was observed. When APTES was employed to modify TiO_2, the weight losses observed ranged between 1 and *ca*. 9% (Entry 2 to Entry 7).

Table 2. Weight losses measured by TGA in TiO_2 modified with organosilanes, $RSi(OEt)_3$.

Entry	System	Weight loss (%)
1	**PTES@TiO_2-1**	1.30
2	**APTES@TiO_2-2**	1.06
3	**APTES@TiO_2-3**	2.38
4	**APTES@TiO_2-4**	2.46
5	**APTES@TiO_2-5**	3.89
6	**APTES@TiO_2-6**	2.46
7	**APTES@TiO_2-7**	8.80
8	**IL-Cl@TiO_2-8**	1.84
9	**IL-Cl@TiO_2-9**	4.91
10	**IL-NTf_2@TiO_2-10**	*
11	**IL-OAc@TiO_2-11**	2.90
12	**IL-OAc@TiO_2-12**	3.38

*Not determined

These results indicated that the temperature applied during the synthesis played an important role. Comparing the data obtained for **APTES@TiO_2-3, APTES@TiO_2-4 and APTES@TiO_2-6** (Entries 3 and 4 *vs*. Entry 6), for which the concentration and the mmol APTES/mg TiO_2 ratios were varied, but all reactions were performed at room temperature, very similar weight losses were measured (*ca*. 2.4%). In contrast, when the synthesis temperature was increased to 120 ºC in EtOH (**APTES@TiO_2-5** *vs*. **APTES@TiO_2-7**, Entries 5 and 7), increasing the mmol APTES/mg TiO_2 ratio from 0.005 to 0.02 resulted in an increase in weight loss from 3.89 to 8.80% respectively. This result indicated that the reactivity of the organosilane modifier might be limited by the temperature even when concentration and the mmol APTES/mg TiO_2 ratios are varied. However, it is noteworthy that distinct solvent systems were used for these syntheses and could play a role in the difference in reactivity observed. When the TiO_2 support was modified with TESs containing an IL, higher weight loss was measured when the synthesis was performed in the presence of larger amounts of modifier (Entry 8 *vs*. Entry 9 and Entry 11 *vs*. Entry 12).

From these results, it was concluded that a variety of supports was successfully prepared using organosilanes, $RSi(OEt)_3$, as modifiers (R= Pr, -$(CH_2)_3$-NH_2, -$(CH_2)_3$-imidazolium). FT-IR analysis confirmed the presence of these modifiers at the surface of the TiO_2 supports and TGA provided quantitative information about these systems, indicating that the temperature employed during the synthesis largely influences the coverage of the support surface by the modifier.

5.2.1.2. Synthesis and characterization of modified TiO_2 with $RPO(OH)_2$ modifiers (R= Bu, -$(CH_2)_3$-NH_2)

Organophosphonic acids (PAs) containing a butyl chain or a 3-propylamine group were also used as modifiers (Figure 12). The materials synthesized and the conditions used for their synthesis are summarized in Table 3. The preparations were carried out using a modifier concentration of 0.01 M at room temperature. After reaction, an additional annealing or aging treatment of the material at 120 ºC was performed in some cases. This produces condensation reactions to form strong bonds between PAs and metal oxide.[11]

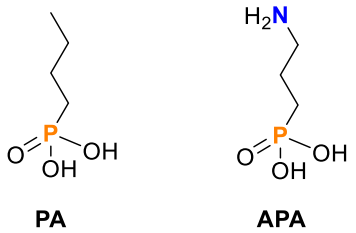

Figure 12. Organophosphonic acids modifiers used in this study.

Table 3. Characterization data for TiO_2 modified with PAs in different conditions.[a]

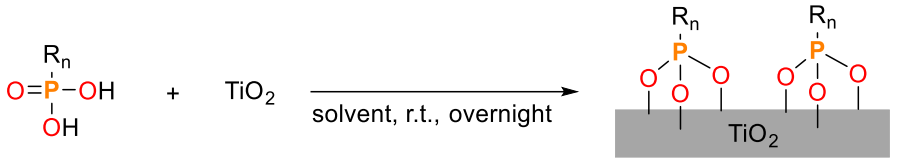

R_n= Bu, **PA**
R_n= -$(CH_2)_3$-NH_2, **APA**

PA@TiO_2
APA@TiO_2

Entry	[C], M	mmol/mg TiO_2	T (ºC)	Code
1	0.01	0.003	r.t.	**PA@TiO_2-1**
2[b][c]	0.01	0.003	r.t.	**APA@TiO_2-2**
3[b]	0.01	0.003	r.t.	**APA@TiO_2-3**

[a]Synthesis conditions: TiO_2 was added to a solution of 10 mM of butylphosphonic acid (PA) in THF and the mixture was stirred at r.t. overnight. [b]Synthesis in milli-Q H_2O. [c]Thermal treatment was not made for this modified support a difference of the others.

FT-IR analysis of **PA@TiO_2-1** was performed to confirm the reactivity of this type of modifier under these conditions (Figure 13).

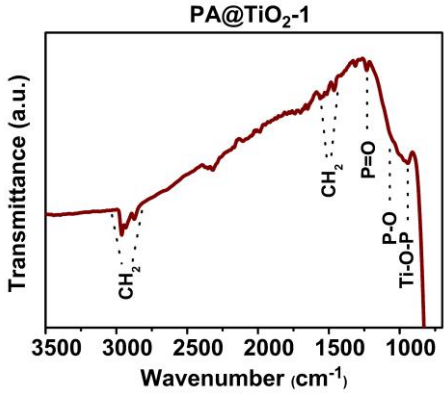

Figure 13. FT-IR spectrum of **PA@TiO_2-1**.

Bands between 3000 and 2850 cm^{-1} corresponding to -CH_2 stretching were readily detected. Moreover, bands at 946 and 1228 cm^{-1} were attributed to Ti-O-P and P=O, respectively, based on literature reports.[57] Another signal at 1153 cm^{-1} was tentatively ascribed to P-O stretching. These results therefore confirmed the anchoring of this type of modifier onto the TiO_2 surface.
TGA analysis was performed on the 3 newly synthesized materials (Figure 14 and Table 4).

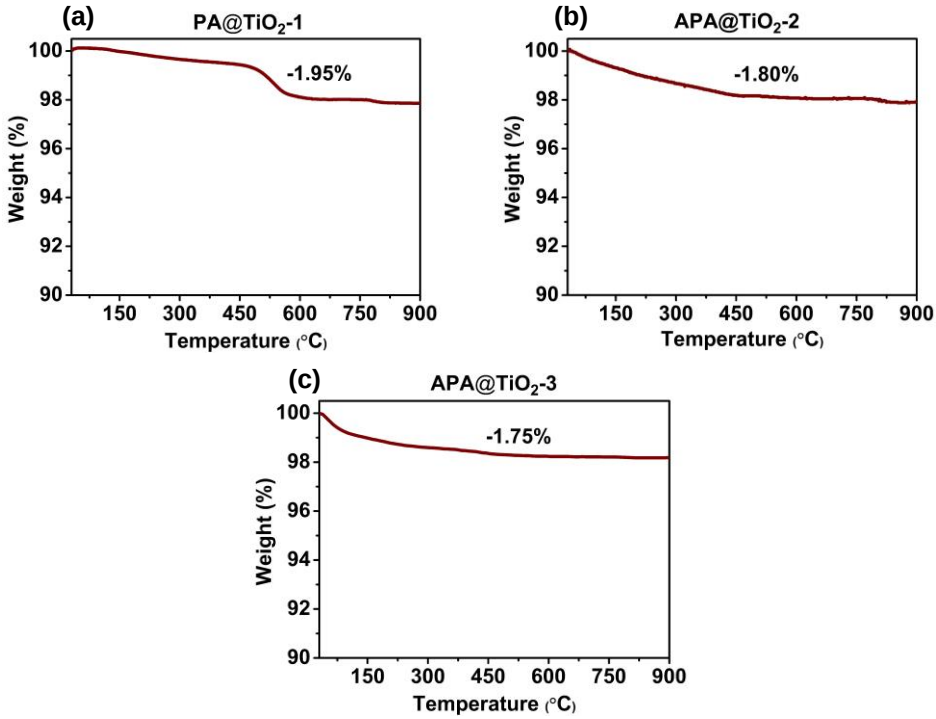

Figure 14. TGA of TiO_2 modified with NH_2-PA without aging step (a), NH_2-PA with aging step (b) and PA (c).

In all cases, the overall weight losses were similar (1.75-1.95%), although it is noteworthy that the weight loss for **PA@TiO_2-1** was sharp at a temperature of *ca.* 500 ºC while in the cases of samples **PA@TiO_2-2** and **PA@TiO_2-3**, a continuous loss was observed between 100 and *ca*. 450 ºC. The similarity in % weight loss indicated that the presence of the NH_2 group did not affect the deposition of the modifier at the TiO_2 surface and that the aging step does not affect the amount of NH_2-PA deposited over TiO_2 (Figure 14).

Table 4. Weight loss measured by TGA in TiO_2 modified with organophosphonic acids, PAs.

Entry	System	Weight loss (%)
1	**PA@TiO_2-1**	1.95
2	**APA@TiO_2-2**[a]	1.80
3	**APA@TiO_2-3**	1.75

[a]Thermal treatment was not made for this modified support a difference of the others.

In this section, modifications of TiO_2 with different organophosphonic acids (PAs) were described. FT-IR and TGA analyses indicated that the synthetic procedure was successful and that no significant differences in coverage was evident using the two distinct PAs.

5.2.2. Synthesis and characterization of supported PPh_3-capped Pd NPs over modified TiO_2

In this section, the synthesis of Pd NPs with PPh_3 as ligand was carried out over the modified TiO_2 supports previously described (Scheme 6). The synthesis of nanoparticles was performed was performed by decomposition of $Pd(dba)_2$ in THF at room temperature under H_2 pressure. A nominal loading of 4 wt% was aimed.

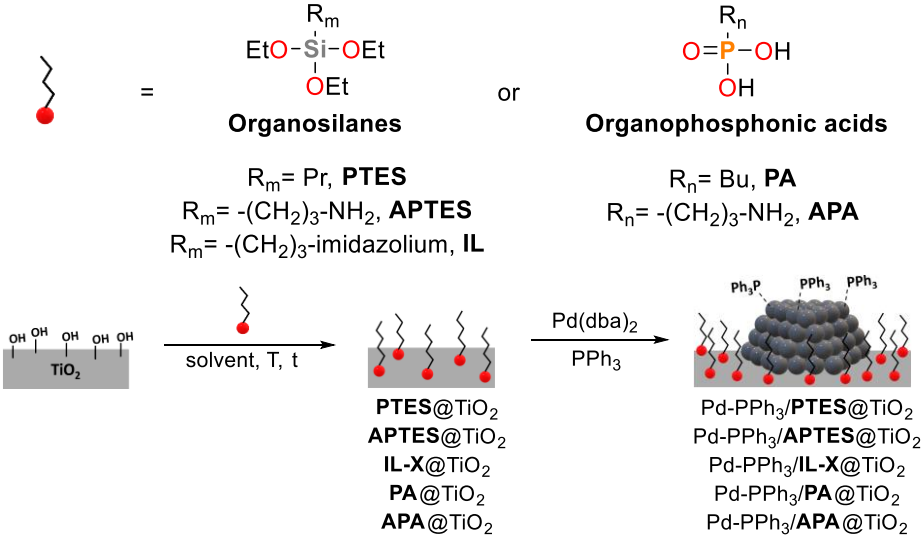

Scheme 6. Synthesis of nanoparticles stabilized with PPh_3 supported over modified-TiO_2.

The newly prepared systems were characterized by TEM, HR-TEM, ICP, XPS, FT-IR and TGA. TEM images of the newly synthesized materials are displayed in Figure 15. In all cases, small and crystalline Pd NPs were formed.

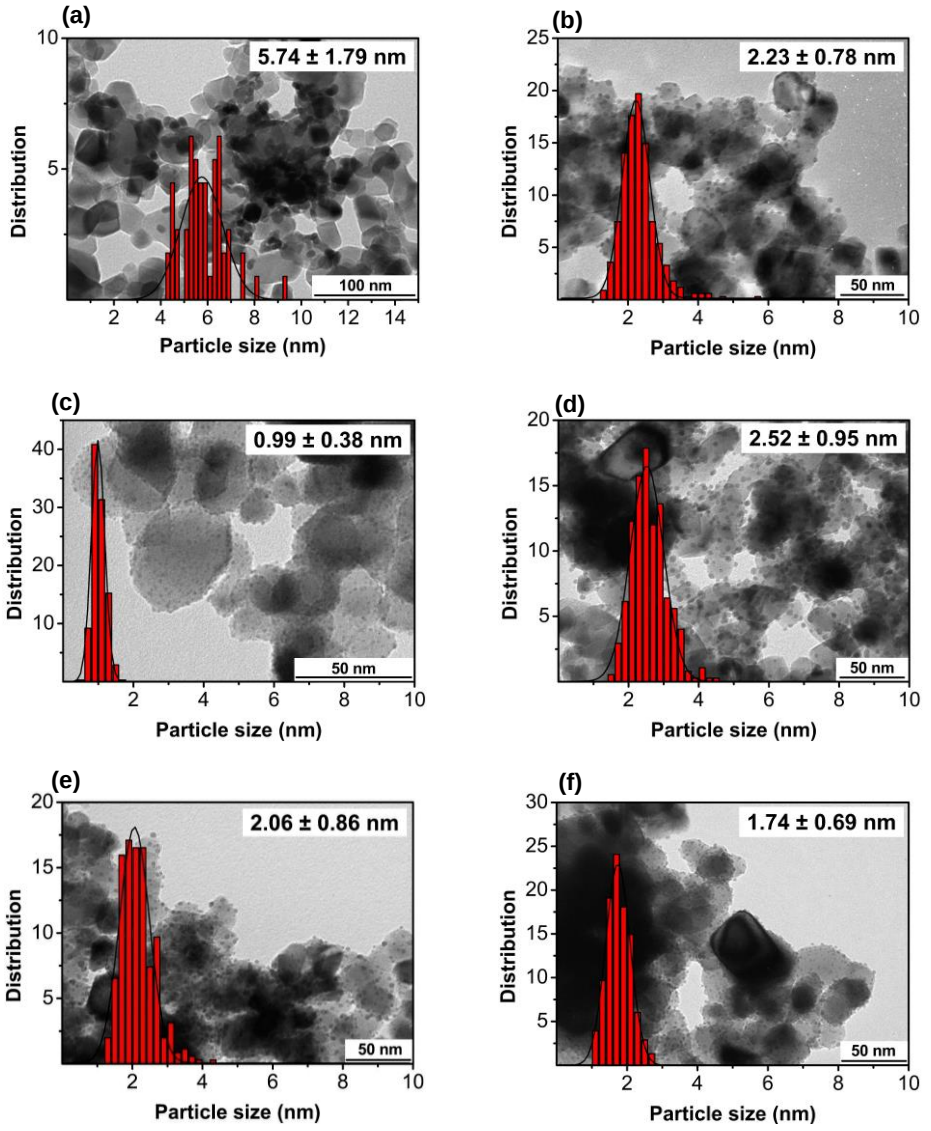

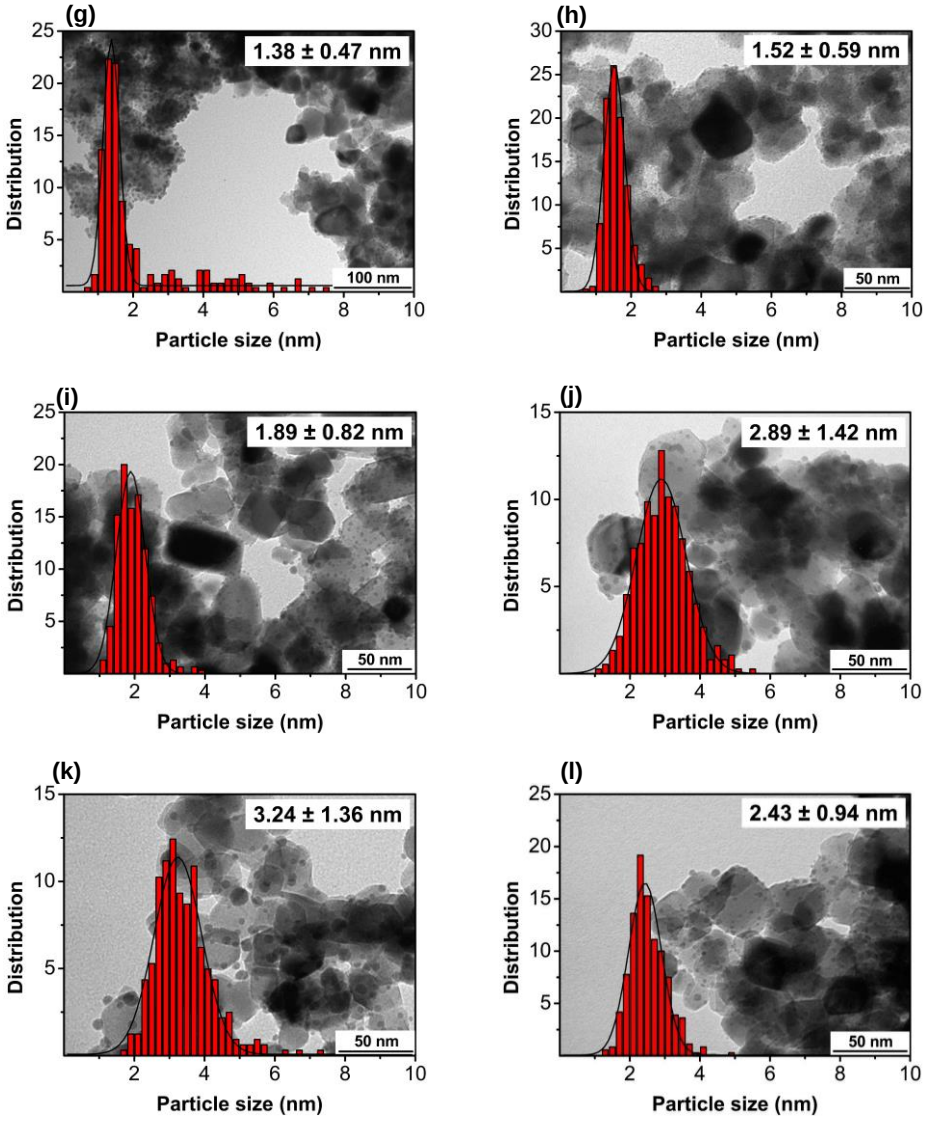
(g)
1.38 ± 0.47 nm
100 nm
(h)
1.52 ± 0.59 nm
50 nm
(i)
1.89 ± 0.82 nm
50 nm
(j)
2.89 ± 1.42 nm
50 nm
(k)
3.24 ± 1.36 nm
50 nm
(l)
2.43 ± 0.94 nm
50 nm
Distribution
Particle size (nm)

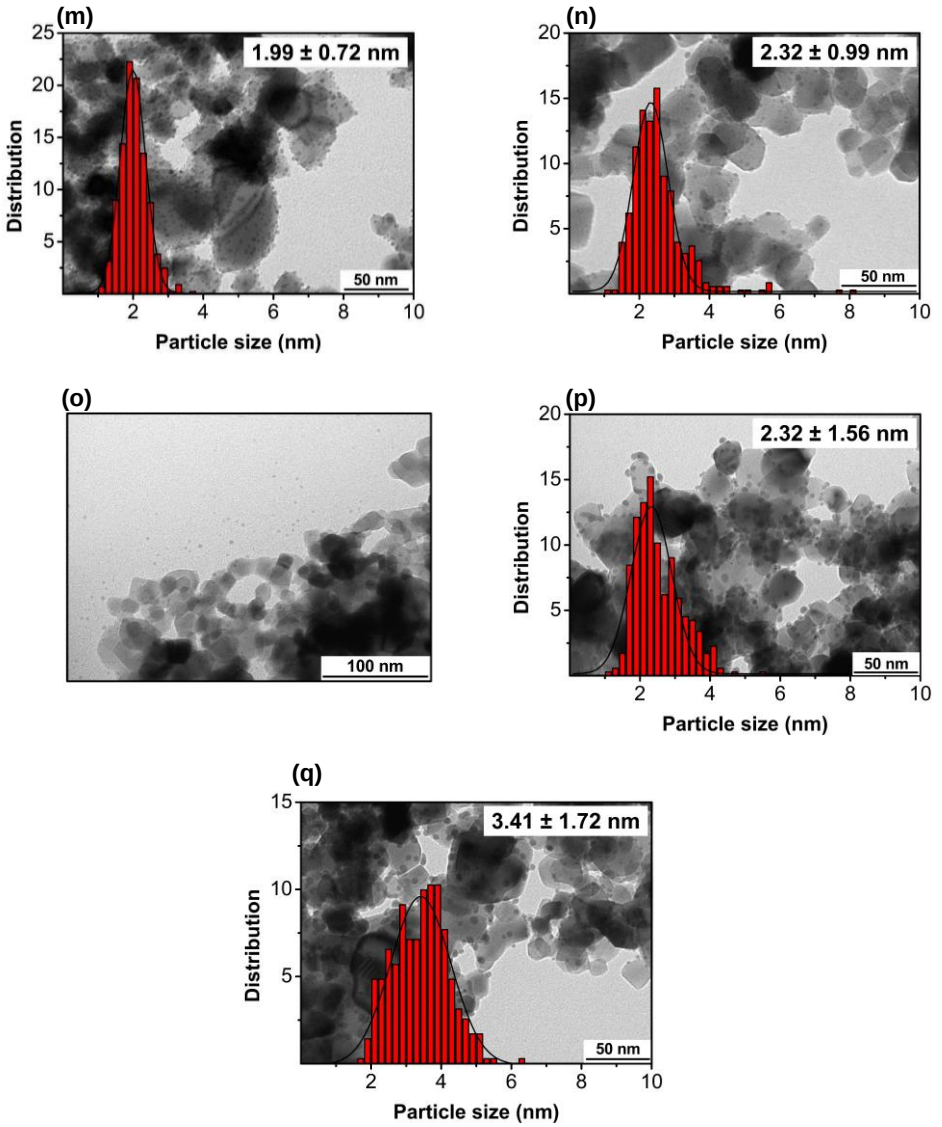

Figure 15. TEM images of **Pd-PPh$_3$/PTES@TiO$_2$-1** (a), **Pd-PPh$_3$/APTES@TiO$_2$-2** (b), **Pd-PPh$_3$/APTES@TiO$_2$-3** (c), **Pd/APTES@TiO$_2$-3** (d), **Pd-PPh$_3$/APTES@TiO$_2$-4** (e), **Pd-PPh$_3$/APTES@TiO$_2$-5** (f), **Pd-PPh$_3$/APTES@TiO$_2$-6** (g), **Pd-PPh$_3$/APTES@TiO$_2$-7** (h), **Pd-PPh$_3$/IL-Cl@TiO$_2$-8** (i), **Pd-PPh$_3$/IL-Cl@TiO$_2$-9** (j), **Pd-PPh$_3$/IL-NTf$_2$@TiO$_2$-10** (k), **Pd-PPh$_3$/IL-OAc@TiO$_2$-11** (l), **Pd-PPh$_3$/IL-OAc@TiO$_2$-12** (m), **Pd/IL-OAc@TiO$_2$-12** (n), **Pd-PPh$_3$/PA@TiO$_2$-1** (with aging step) (o), **Pd-PPh$_3$/APA@TiO$_2$-2** (without aging step) (p), **Pd-PPh$_3$/APA@TiO$_2$-3** (with aging step) (q).

The sizes and distributions obtained from TEM measurements and ICP results are summarized in Table 5.

Table 5. Characterization data for **Pd-PPh$_3$@TESs/TiO$_2$** and **Pd-PPh$_3$@PAs/TiO$_2$** NPs using different conditions.[a]

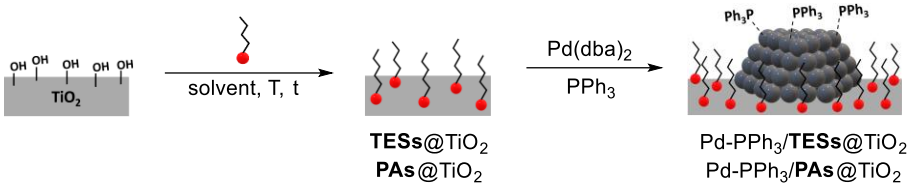

TESs@TiO$_2$
PAs@TiO$_2$

Pd-PPh$_3$/**TESs**@TiO$_2$
Pd-PPh$_3$/**PAs**@TiO$_2$

Entry	System	Size (nm)[b]	Pd wt%[c]	P wt%[c]
1	**Pd-PPh$_3$/PTES@TiO$_2$-1**	5.75 ± 1.79	3.46	0.18
2	**Pd-PPh$_3$/APTES@TiO$_2$-2**	2.23 ± 0.78	2.75	0.19
3	**Pd-PPh$_3$/APTES@TiO$_2$-3**	2.04 ± 1.05	3.07	-
4[d]	**Pd/APTES@TiO$_2$-3**	2.52 ± 0.95	3.36	-
5	**Pd-PPh$_3$/APTES@TiO$_2$-4**	2.06 ± 0.86	3.51	0.17
6	**Pd-PPh$_3$/APTES@TiO$_2$-5**	1.74 ± 0.69	3.20	-
7	**Pd-PPh$_3$/APTES@TiO$_2$-6**	1.38 ± 0.47	3.26	-
8	**Pd-PPh$_3$/APTES@TiO$_2$-7**	1.52 ± 0.59	3.34	-
9	**Pd-PPh$_3$/IL-Cl@TiO$_2$-8**	1.89 ± 0.82	3.25	-
10	**Pd-PPh$_3$/IL-Cl@TiO$_2$-9**	2.80 ± 1.42	3.35	-
11	**Pd-PPh$_3$/IL-NTf$_2$@TiO$_2$-10**	3.24 ± 1.36	2.60	-
12	**Pd-PPh$_3$/IL-OAc@TiO$_2$-11**	2.43 ± 0.94	3.17	0.17
13	**Pd-PPh$_3$/IL-OAc@TiO$_2$-12**	1.99 ± 0.74	3.58	-
14[d]	**Pd/IL-OAc@TiO$_2$-12**	2.32 ± 0.99	3.60	-
15[e]	**Pd-PPh$_3$/PA@TiO$_2$-1**	Out of support	3.29	-
16[f]	**Pd-PPh$_3$/APA@TiO$_2$-2**	2.32 ± 1.56	3.38	0.57
17[e]	**Pd-PPh$_3$/APA@TiO$_2$-3**	3.41 ± 1.72	3.29	-

[a]Synthesis conditions: Pd 4 wt% (metal precursor Pd(dba)$_2$), 0.2 eq. of PPh$_3$, previously synthesized TESs/TiO$_2$ or PAs/TiO$_2$, THF, 3 bar H$_2$, 60 ºC, overnight. [b]Determined by TEM. [c]Determined by ICP. [d]In absence of PPh$_3$. [e]With aging. [f]Without aging.

When PTES was the TiO_2 modifier, which contain an alkyl chain without further functionalization, the resulting NPs exhibited a size of 5.75 nm with a broad distribution (Entry 1). Some agglomerations of Pd-NPs were also observed. In this material, a Pd loading of 3.46 wt% was measured by ICP. The presence of phosphorus from the ligand (PPh_3) and silicon (from PTES) were also detected by EDS mapping. When TiO_2 modified with APTES were employed as support (Entries 2-7), the Pd NPs sizes ranged from 1.38 nm (Entry 3) to 2.52 nm (Entry 2) while the Pd content was between 2.75% and 3.51 wt%. The difference in Pd NP size observed for the PTES modified support and those modified with APTES clearly indicated the role of the amine function in the NP stabilization. The largest NPs (Entry 4) were obtained when the synthesis was performed in the absence of PPh_3, indicating that this ligand also played a role in the NP stabilization, although to a much lesser extent than the amine group from the support.

When the support was stabilized by organosilanes containing an IL moiety (Entries 9 - 14), particles sizes between 1.89 (Entry 9) and 3.24 nm (Entry 10) were measured while the Pd loadings spanned from 2.60 (Entry 11) to 3.60 wt% (Entry 14). Interestingly, for the materials **Pd-PPh_3/IL-Cl@TiO_2-8** and **Pd-PPh_3/IL-Cl@TiO_2-9** (Entries 9 and 10), which contain TiO_2 modified by the same organosilane but which differ by the loading of organosilane at the support surface, a relevant difference in size was observed (1.89 *vs*. 2.8 nm) while the Pd loading was not affected (3.25 *vs*. 3.35 wt%). However, due to the broad distribution of both sets of nanoparticles, no clear conclusion could be drawn. Interestingly, using these modifiers, when the synthesis of **Pd-PPh_3/IL-OAc@TiO_2-12** (Entry 13 *vs*. Entry 14) was repeated in the absence of PPh_3, no relevant differences in size nor Pd loading was observed, indicating that the ligand was not playing an important in the Pd NP stabilization when the IL-containing modifiers were used.

When the PA containing an unfunctionalized alkyl chain was used for the modification of the support (Entry 15), some large Pd agglomerations were observed and nanoparticles were detected away from the support (and thus a large proportion of the support was observed without Pd NPs) (Figure 15). This indicated that using this modified support, the NP stabilization was not efficient. When the PA containing an amine group was used as support

modifier (Entry 16 and Entry 17), the sizes of the resulting Pd NPs were 2.32 and 3.41 nm while similar Pd contents were obtained by ICP (*ca*. 3.3 wt%). Both samples revealed Pd NPs with broad distributions. For the material **Pd-PPh_3/APA@TiO_2-2**, the P content was also determined and a value of 0.57 wt% was obtained, confirming that the phosphine ligand remained after the synthesis (Entry 16).

These results therefore indicated that when organosilanes (TESs) were used to modify TiO_2, the NP stabilization was efficient, resulting in smaller Pd-NPs with narrower distributions than for PA-modified supports. This could be due to a higher affinity of Si to Ti. However, in terms of Pd loading, no relevant differences were observed. The presence of functional groups in the TESs modifiers also revealed to affect the NP stabilization since the materials containing an organosilane with a simple alkyl chain (Entry 1) provided larger Pd NPs with broader distribution than with TESs containing either an amine function or an imidazolium group (Entry 2 to Entry 13).

The support synthesized with higher concentrations of APTES provided in most cases smaller nanoparticles (except for 0.13 M, Entry 3). An opposite effect was observed when IL-containing modifiers were used (Entries 9 and 10). Moreover, when imidazolium containing modifiers were used, the nature of the anions affected the size and distribution of the resulting NPs. Indeed, when an hydrophobic anion was used (NTf_2^-), larger nanoparticles were obtained (Entry 11) compared with those synthesized using the hydrophilic ILs (Cl^- and OAc^-). Similar trend was observed for Ru NPs by Bordet et al.[39a] Moreover, a lower Pd content was measured lower for **Pd-PPh_3/IL-NTf_2@TiO_2-10**.

FT-IR analysis was performed on **Pd-PPh_3/@TiO_2-3** (Figure 16). Comparison of the FT-IR spectra before (Figure 16 (a)) and after deposition of Pd-PPh_3 NPs (Figure 16 (c)), revealed no differences and it was therefore concluded that no structural changes took place during this step. TGA analysis was also performed on this material (Figure 16 (b) and (d)). Prior to Pd deposition, a weight loss of 2.38% was observed whereas a weight loss of *ca*. 6% was determined after the synthesis of Pd NPs. The presence of other organic materials (solvent, residues from Pd precursor decomposition, PPh_3, etc.) might explain this result.

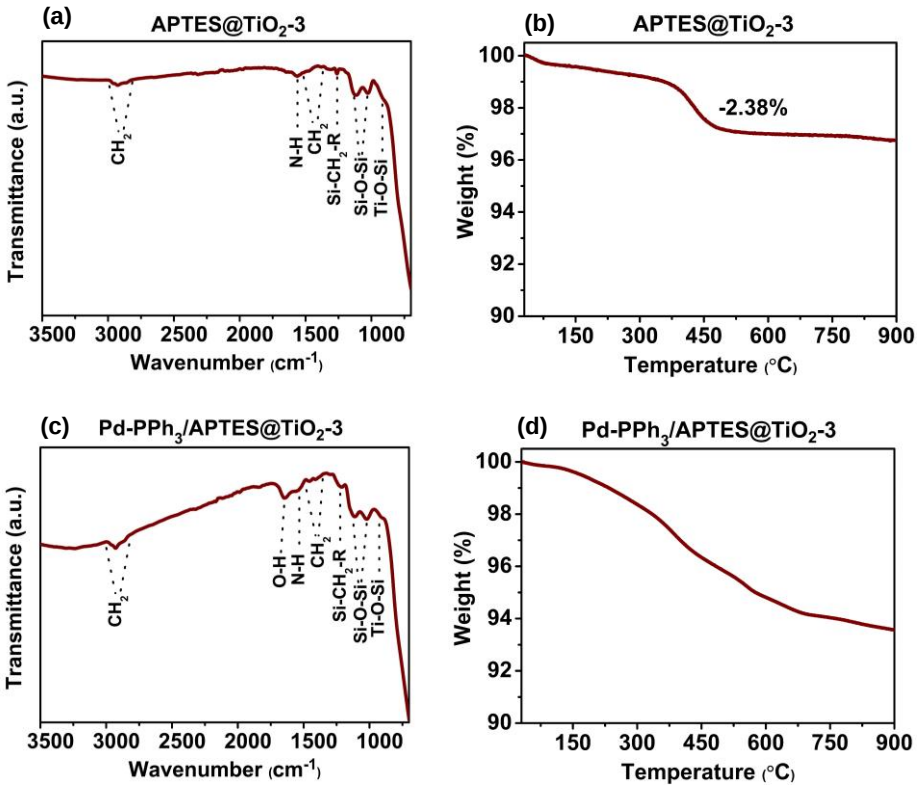

Figure 16. FT-IR spectra and TGA before (a), (b) and after (c), (d) synthesis of Pd-NPs in **Pd-PPh$_3$/@TiO$_2$-3** system.

The material **Pd-PPh$_3$/APTES@TiO$_2$-2** was also analyzed by HR-TEM (Figure 17). EDS mapping was performed to obtain additional information about the content of this sample. Figure 17 (c) shows the presence of Si at the surface of TiO_2 which demonstrates the presence of APTES.

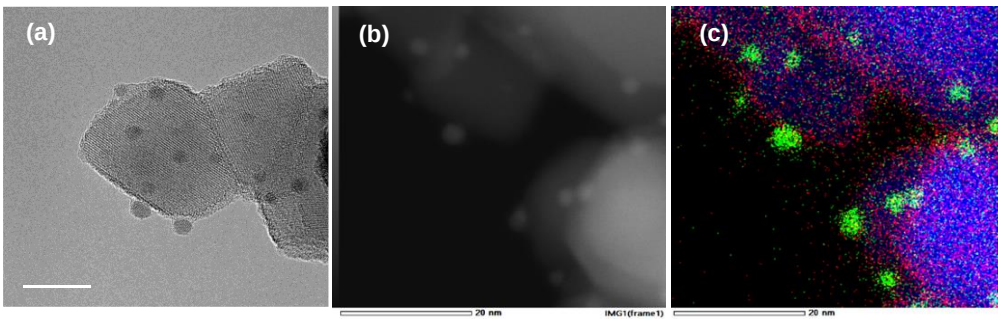

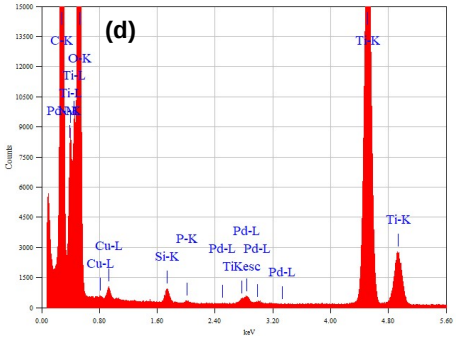

Figure 17. (a) HR-TEM image, (b) HR-HAADF STEM, (c) EDS mapping overlay (green, Pd; red, Si; blue, Ti), (d) spectrum of **Pd-PPh$_3$/APTES@TiO$_2$-2**.

The catalyst **Pd/APTES@TiO$_2$-3**, synthesized in the absence of ligand, was also analyzed by HR-TEM (Figure 18).

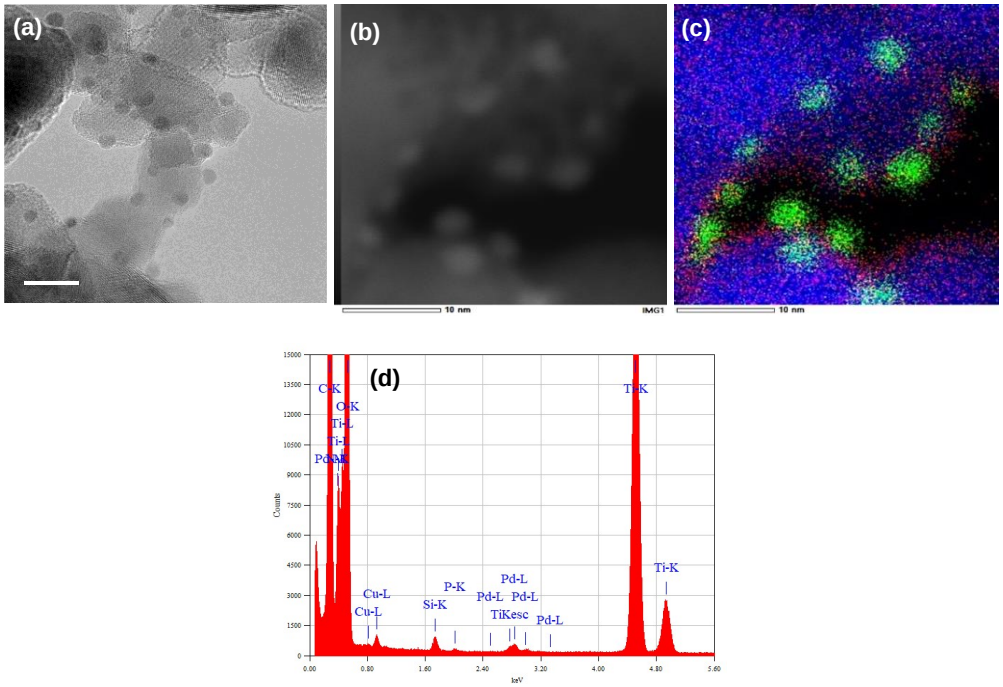

Figure 18. (a) HR-TEM image, (b) HR-HAADF STEM, (c) EDS mapping overlay (green, Pd; red, Si; blue, Ti), (d) spectrum of **Pd/APTES@TiO$_2$-3**.

For this catalyst, the same edge of Si is appreciated (Figure 18 (c)).
The catalyst **Pd-PPh$_3$/IL-Cl@TiO$_2$-8** containing a support modified by IL was also analysed by HR-TEM and EDS (Figure 19).

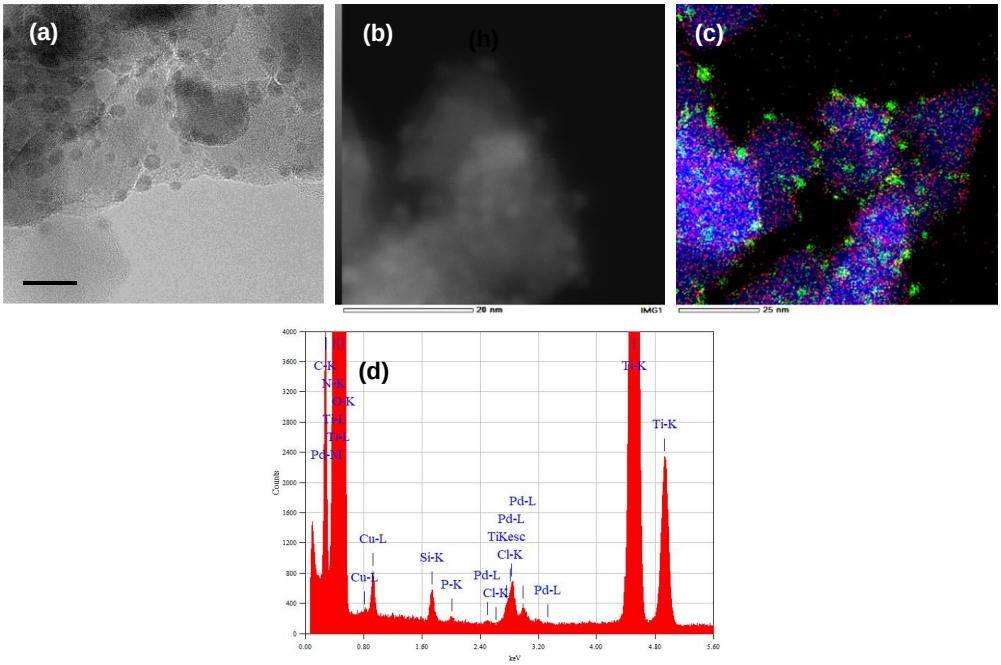

Figure 19. (a) HR-TEM image, (b) HR-HAADF STEM, (c) EDS mapping overlay (green, Pd; red, Si; blue, Ti), (d) spectrum of **Pd-PPh$_3$/IL-Cl@TiO$_2$-8**.

Due to the low concentration of IL-Cl employed for synthesis of this catalyst, the layer of Si around TiO_2 was narrow. The presence of P was also observed, indicating that the ligand remained on the NPs.

The material **Pd-PPh$_3$/APA@TiO$_2$-3**, containing TiO_2 modified by PAs was analyzed by HR-TEM (Figure 20). Small agglomerations were observed by HR-HAADF STEM (Figure 20 (b)). Phosphorus was detected over the support and over the Pd NPs due to the presence of NH_2-PA and PPh_3.

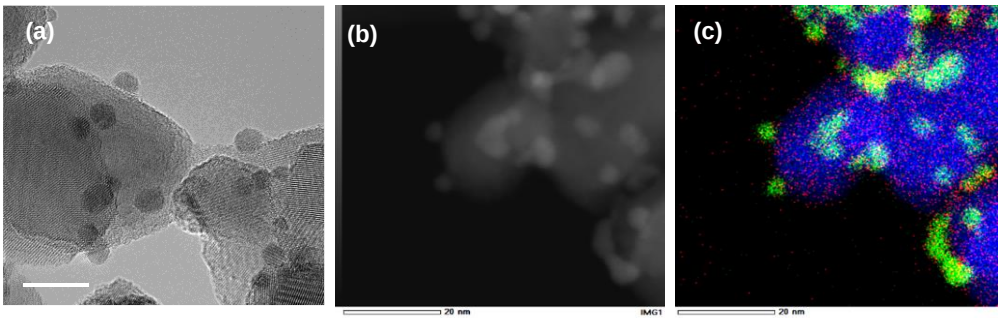

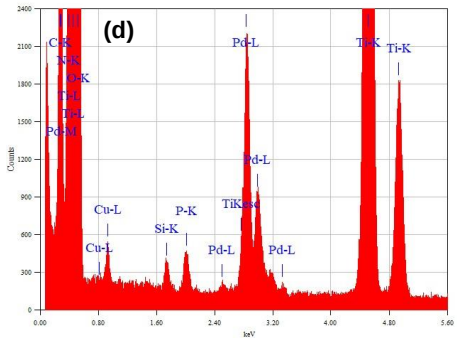

Figure 20. (a) HR-TEM image, (b) HR-HAADF STEM, (c) EDS mapping overlay (green, Pd; red, P; blue, Ti), (d) spectrum of **Pd-PPh$_3$/APA@TiO$_2$-3**.

XPS was also employed for the analysis of some of the synthesized **Pd-PPh$_3$/mod@TiO$_2$-x** catalysts (Figure 21). The data obtained were compared with those of the unmodified **Pd-PPh$_3$/TiO$_2$** catalyst. All the spectra were referenced using the C1s signal and set at 285.0 eV. Presence of Si2p, N1s and P2p for **Pd-PPh$_3$/IL-Cl@TiO$_2$-8** catalyst and N1s and P2p for **Pd-PPh$_3$/APA@TiO$_2$-3** were detected.

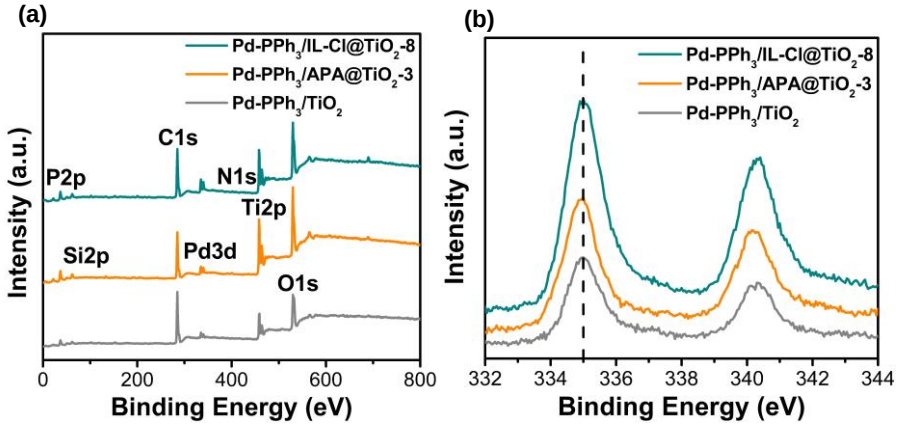

Figure 21. Stacked XPS image of overview (a) and Pd3d high resolution spectra (b) for the newly synthesized catalysts.

For Pd3d, they were compared with the unmodified **Pd-PPh$_3$/TiO$_2$** catalyst (Figure 21 (b)). No significant differences are observed for Pd BEs (335.0 eV). The relative amount of Pd$^{\delta+}$ also revealed different for samples (Table 6). In unmodified **Pd-PPh$_3$/TiO$_2$**, a value of 12.5% was measured (Entry 1), which was attributed the manipulation of the sample during analysis.

Table 6. XPS results for different **Pd-PPh$_3$/mod@TiO$_2$-x** catalyst and **Pd-PPh$_3$/TiO$_2$**.

Entry	System	Pd$^{\delta+}$ (%)
1	**Pd-PPh$_3$/TiO$_2$**	12.5
2	**Pd-PPh$_3$/IL-Cl@TiO$_2$-8**	11.6
3[a]	**Pd-PPh$_3$/APA@TiO$_2$-3**	7.8

[a]With aging step.

This value is on the same range that obtained for **Pd-PPh$_3$/IL-Cl@TiO$_2$-8** (Entry 2) and **Pd-PPh$_3$/APA@TiO$_2$-3** catalysts with an amount of 11.6 and 7.8% of Pd$^{\delta+}$, respectively.

To conclude, the synthesis and characterization of a series of different catalyst based on PPh$_3$-capped Pd NPs were successfully carried out using supports that were previously modified. The results obtained are summarized as follow:

- Several families of modifiers were used and variables such as the presence of a functional group on the modifiers, the concentration of modifier, the temperature of synthesis, etc. were evaluated.
- These materials were analised by TEM. When organosilanes were employed on the synthesis of catalysts, smaller sized of Pd NPs were obtained compared with organophosphonic acids.
- At higher concentrations of APTES, smaller NPs were obtained.
- For ILs, when smaller concentrations were employed for the synthesis of the modified TiO$_2$, the size of the Pd NP was smaller.
- The absence of -NH$_2$ group on organosilanes and organophosphonic acids influences the structure/composition of the materials. In the absence of -NH$_2$ groups, large, unsupported NPs and agglomerations were observed.
- There are no significant differences in composition between samples according to ICP analysis.
- Some of them were further characterized by FT-IR, TGA, HR-TEM and XPS, allowing to have more information about these new materials.

5.2.3. Synthesis and characterization of systems based on deposition of modifier over TiO_2 supported PPh_3-capped Pd NPs

In this section, a new series of catalysts was synthetized using TESs and PAs modifiers that were deposited over previously synthesized **Pd-PPh_3/TiO_2** material (Scheme 7). The newly prepared systems were mainly characterized by TEM and ICP, additional information was obtained from FT-IR, TGA, HR-TEM and XPS analyses for some representative examples.

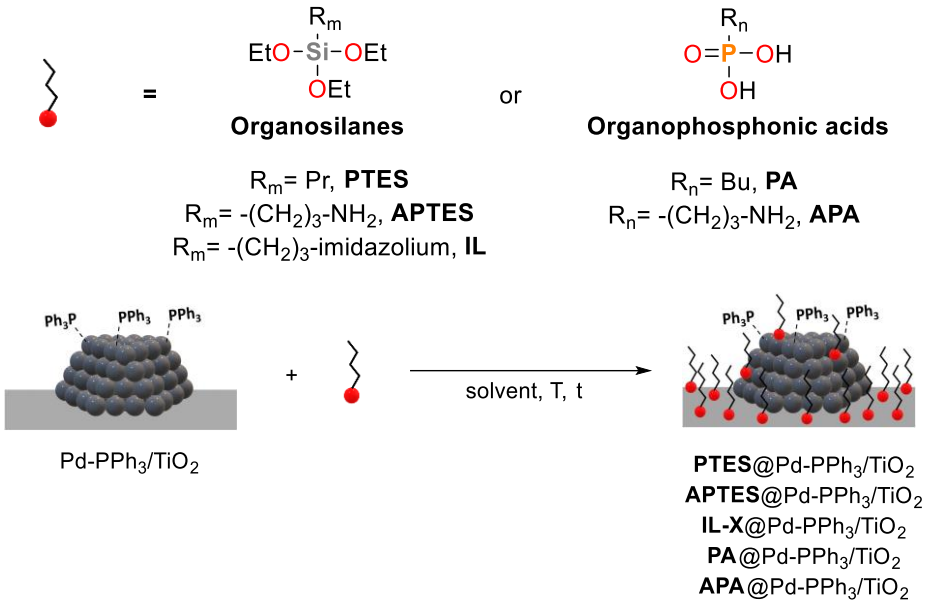

Scheme 7. Deposition of TESs and PAs modifiers over previously synthesized Pd-PPh_3 supported over TiO_2.

PTES or APTES was reacted with the previously synthesized **Pd-PPh_3/TiO_2** either at r.t overnight in a mixture of 95% EtOH, 5% H_2O, or at 120 ºC during 4 h using EtOH as solvent. At the end of the reaction, the samples were centrifugated, washed with milli-Q H_2O and EtOH and dried overnight in an oven at 105 ºC.

In Table 7, the synthesis conditions and codes to identify these new systems are summarized. The reactions were first analyzed by TEM. The corresponding micrographs are displayed in Figure 22 and the data corresponding to characterization by TEM and ICP are summarized in Table 8.

Table 7. Optimization of synthesis conditions for **Pd-PPh$_3$/TiO$_2$** modified with TESs and PAs.[a]

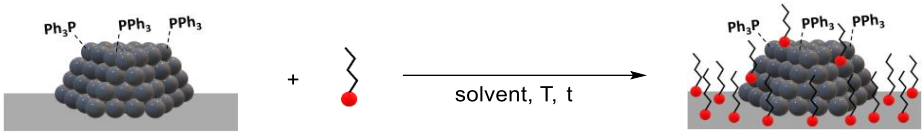

Pd-PPh$_3$/TiO$_2$

TESs@Pd-PPh$_3$/TiO$_2$
PAs@Pd-PPh$_3$/TiO$_2$

Entry	[C], M	mmol/mg TiO$_2$	Code
1	0.13	0.013	**PTES@Pd-PPh$_3$/TiO$_2$-1**
2	0.01	0.003	**APTES@Pd-PPh$_3$/TiO$_2$-2**
3	0.13	0.006	**APTES@Pd-PPh$_3$/TiO$_2$-3**
4	0.13	0.013	**APTES@Pd-PPh$_3$/TiO$_2$-4**
5	1	0.005	**APTES@Pd-PPh$_3$/TiO$_2$-5**
6	4	0.02	**APTES@Pd-PPh$_3$/TiO$_2$-6**
7[b]	4	0.02	**APTES@Pd-PPh$_3$/TiO$_2$-7**
8	0.13	0.013	**IL-Cl@Pd-PPh$_3$/TiO$_2$-8**
9	0.13	0.013	**IL-NTf$_2$@Pd-PPh$_3$/TiO$_2$-9**
10	0.13	0.013	**IL-OAc@Pd-PPh$_3$/TiO$_2$-10**
11[c][e]	0.01	0.003	**PA@Pd-PPh$_3$/TiO$_2$-11**
12[d][e]	0.01	0.003	**APA@Pd-PPh$_3$/TiO$_2$-12**

[a]Synthesis conditions: **Pd-PPh$_3$/TiO$_2$** previously synthesized was added to a solution of TESs (for determined mmol TESs/mg **Pd-PPh$_3$/TiO$_2$** ratio) on mixture EtOH:milli-Q H$_2$O (95:5, v/v) and it was let react at r.t. overnight. [b]Reaction was performed at 120 ºC in autoclave during just 4 h using EtOH as solvent. [c] **Pd-PPh$_3$/TiO$_2$** system was added to a solution of PA on THF and it was let react r.t. overnight. [d]**Pd-PPh$_3$/TiO$_2$** system was added to a solution of APA on milli-Q H$_2$O and it was let react r.t. overnight. [e]With aging.

As described in Chapter 3, the Pd NPs in the **Pd-PPh$_3$/TiO$_2$** catalyst exhibited a mean size of 2.37 ± 0.19 nm. When the catalyst was modified by deposition of PTES (Entry 1), the size of Pd NPs slightly increased to 2.65 ± 0.80 nm and a Pd content of 3.38 wt% was measured by ICP. When APTES was used as modifier, the mean size of the NPs varied from 1.86 (Entry 4) to 2.74 nm (Entry 3), indicating little effect of the treatment on the Pd NPs. However, relevant decreases in Pd content were observed, indicating that the

deposition of modifiers containing an amine group could induce the leaching of Pd from the previously synthesized material. The presence of P (from PPh_3) and Si (from the organosilane) were also confirmed by ICP. When imidazolium groups were present at the end of the alkyl chain, the NPs size was comprised between 1.87 (Entry 10) and 2.44 nm (Entry 9). The distribution for these catalysts was lower than 1.0 nm.

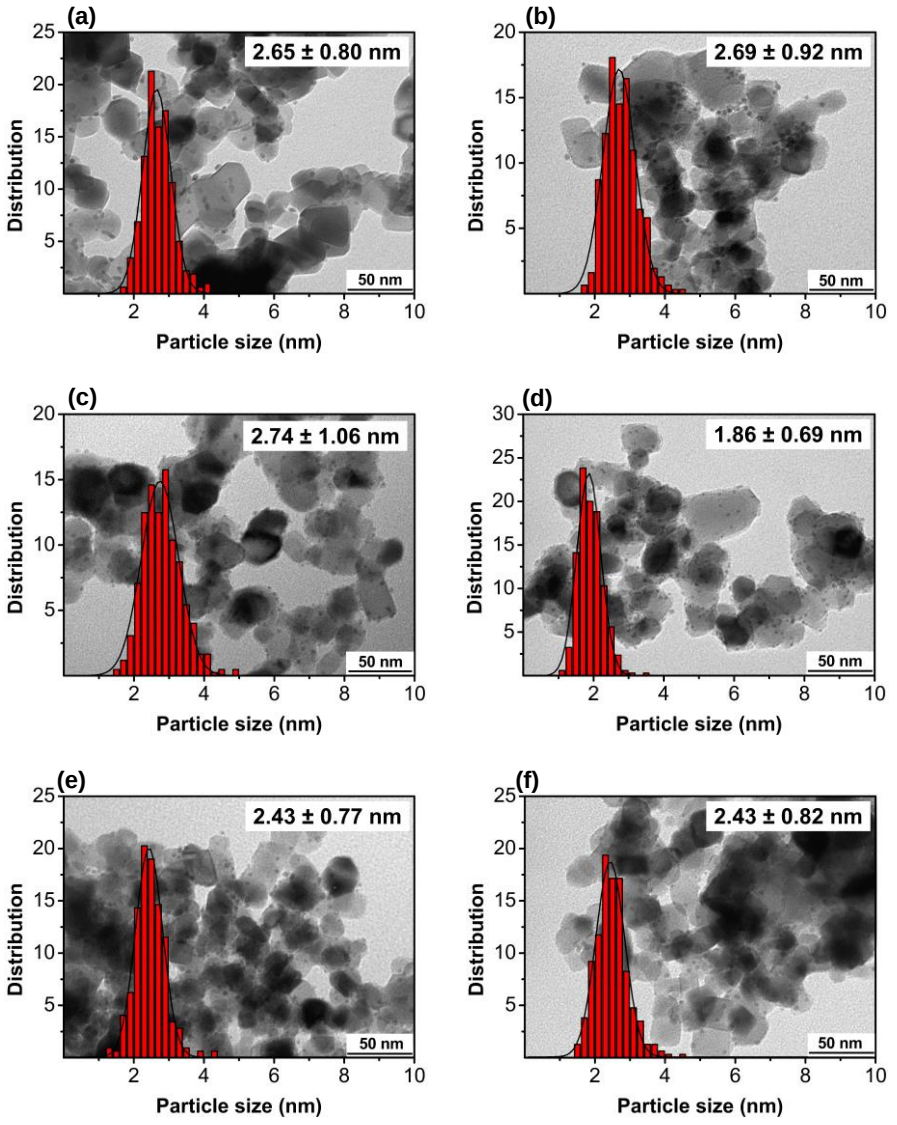

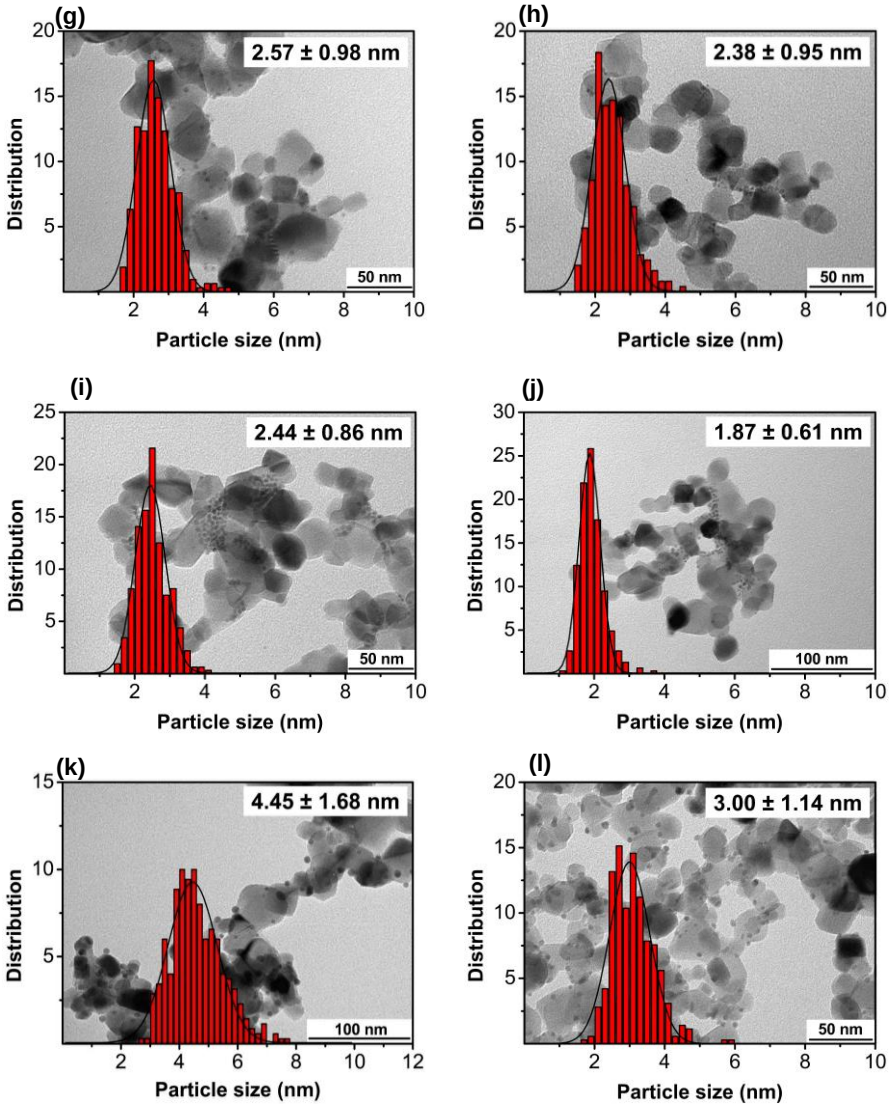

Figure 22. TEM images of **PTES@Pd-PPh$_3$/TiO$_2$-1** (a), **APTES@Pd-PPh$_3$/TiO$_2$-2** (b), **APTES@Pd-PPh$_3$/TiO$_2$-3** (c), **APTES@Pd-PPh$_3$/TiO$_2$-4** (d), **APTES@Pd-PPh$_3$/TiO$_2$-5** (e), **APTES@Pd-PPh$_3$/TiO$_2$-6** (f), **APTES@Pd-PPh$_3$/TiO$_2$-7** (g), **IL-Cl@Pd-PPh$_3$/TiO$_2$-8** (h), **IL-NTf$_2$@Pd-PPh$_3$/TiO$_2$-9** (i), **IL-OAc@Pd-PPh$_3$/TiO$_2$-10** (j), **PA@Pd-PPh$_3$/TiO$_2$-11** (k), **APA@Pd-PPh$_3$/TiO$_2$-12** (l).

However, once more, the Pd content was lower than expected. Surprisingly, when PAs were deposited over **Pd-PPh$_3$/TiO$_2$**, larger NP sizes than for TESs were measured. A size of 4.45 ± 1.68 nm was obtained when PA is used (Entry 11) and 3.00 ± 1.14 nm was observed when APA was employed in the

synthesis (Entry 12). This result therefore indicated that the deposition of PAs over **Pd-PPh$_3$/TiO$_2$** caused a restructuration of the Pd NPs. In contrast, for these catalysts, the Pd content was almost the same than in the original material. These results therefore suggest that the reaction of the previously synthesised material with PAs does not induce Pd leaching but could produce restructuration such as Ostwald's ripening.

Table 8. Characterization data for the deposition of TESs and PAs over previously synthesized **Pd-PPh$_3$/TiO$_2$** system.[a]

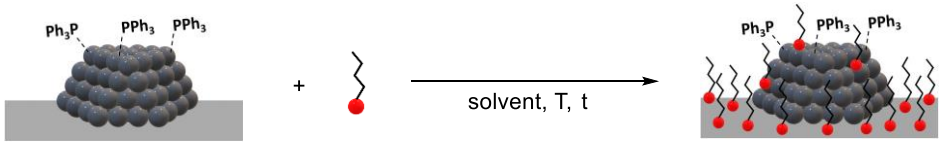

Pd-PPh$_3$/TiO$_2$

TESs@Pd-PPh$_3$/TiO$_2$
PAs@Pd-PPh$_3$/TiO$_2$

Entry	System	Size (nm)[b]	Pd wt%[c]	P wt%[c]
1	**PTES@Pd-PPh$_3$/TiO$_2$-1**	2.65 ± 0.80	3.38	-
2	**APTES@Pd-PPh$_3$/TiO$_2$-2**	2.69 ± 0.92	3.04	0.21
3	**APTES@Pd-PPh$_3$/TiO$_2$-3**	2.74 ± 1.06	2.98	0.15
4	**APTES@Pd-PPh$_3$/TiO$_2$-4**	1.86 ± 0.69	2.57	-
5	**APTES@Pd-PPh$_3$/TiO$_2$-5**	2.43 ± 0.77	2.05	0.09
6	**APTES@Pd-PPh$_3$/TiO$_2$-6**	2.43 ± 0.82	1.60	0.07
7[d]	**APTES@Pd-PPh$_3$/TiO$_2$-7**	2.57 ± 0.98	1.88	0.09
8	**IL-Cl@Pd-PPh$_3$/TiO$_2$-8**	2.38 ± 0.95	1.81	-
9	**IL-NTf$_2$@Pd-PPh$_3$/TiO$_2$-9**	2.44 ± 0.86	2.51	0.21
10	**IL-OAc@Pd-PPh$_3$/TiO$_2$-10**	1.87 ± 0.61	2.98	-
11[e][g]	**PA@Pd-PPh$_3$/TiO$_2$-11**	4.45 ± 1.68	3.10	0.82
12[f][g]	**APA@Pd-PPh$_3$/TiO$_2$-12**	3.00 ± 1.14	3.15	-

[a]Synthesis conditions: **Pd-PPh$_3$/TiO$_2$** previously synthesized was added to a solution of TESs (for determined mmol TESs/mg **Pd-PPh$_3$/TiO$_2$** ratio) on mixture EtOH:milli-Q H_2O (95:5, v/v) and it was let react at r.t. overnight. [b]Determined by TEM. [c]Determined by ICP. [d]Reaction was performed at 120 ºC in autoclave during just 4 h using EtOH as solvent. [e] **Pd-PPh$_3$/TiO$_2$** system was added to a solution of PA on THF and it was let react r.t. overnight. [f]**Pd-PPh$_3$/TiO$_2$**

system was added to a solution of APA on milli-Q H_2O and it was let react r.t. overnight. [g]With aging.

Comparing the NP sizes obtained *via* the two approaches described in this work, modification over the pre-synthesised **Pd-PPh$_3$/TiO$_2$** NPs (Table 8) yielded smaller Pd NPs and narrower distributions than when the TiO_2 support was modified in the first step (Table 5). However, lower Pd contents were obtained.

Comparing the results obtained by deposition of various concentrations of APTES, several differences were observed. Indeed, a decrease in Pd content when the concentration of APTES was increased. For **APTES@Pd-PPh$_3$/TiO$_2$-6** and **APTES@Pd-PPh$_3$/TiO$_2$-7** (Table 8, Entry 6 and Entry 7), these values were as low as 1.60 and 1.88 wt%, respectively. This was attributed to the leaching of part of the Pd NPs from of the support in agreement with the observation of a yellow-brown color of the supernatant when catalysts were washed during their synthesis. This was confirmed by the detection of colloidal Pd NPs when TEM analysis of these materials was performed (Figure 23).

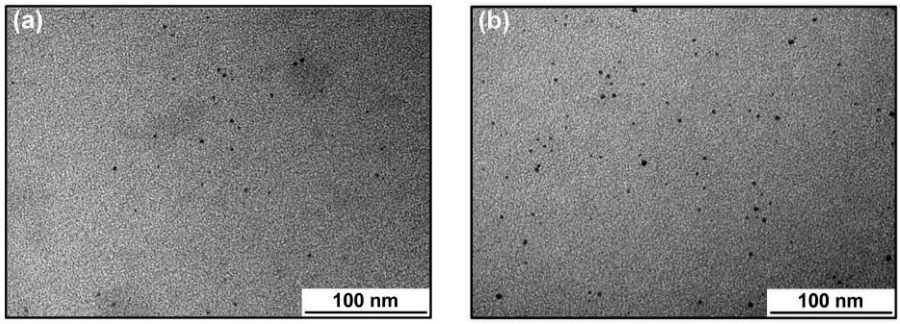

Figure 23. Nanoparticles out of the support in **APTES@Pd-PPh$_3$/TiO$_2$-5** (a) **APTES@Pd-PPh$_3$/TiO$_2$-7** (b).

Moreover, for the samples in which high concentration of APTES was used such as **APTES@Pd-PPh$_3$/TiO$_2$-7**, detailed TEM analysis revealed the presence of a new layer at the surface of the material (Figure 24). This type of layer will also be described for **APTES@Pd-PPh$_3$/TiO$_2$-4** by mapping using the HR-TEM technique.

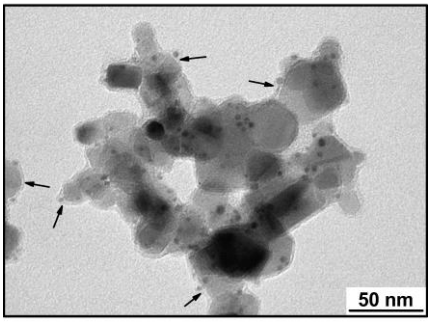

Figure 24. TEM image of **APTES@Pd-PPh$_3$/TiO$_2$-7**.

FT-IR and TGA analyses were also performed on **APTES@Pd-PPh$_3$/TiO$_2$-4** (Figure 25). Comparing the FT-IR spectra of this sample with that of **APTES@TiO$_2$-3** (Figure 25 (a)) (same concentrations and condition), the same signals were detected.

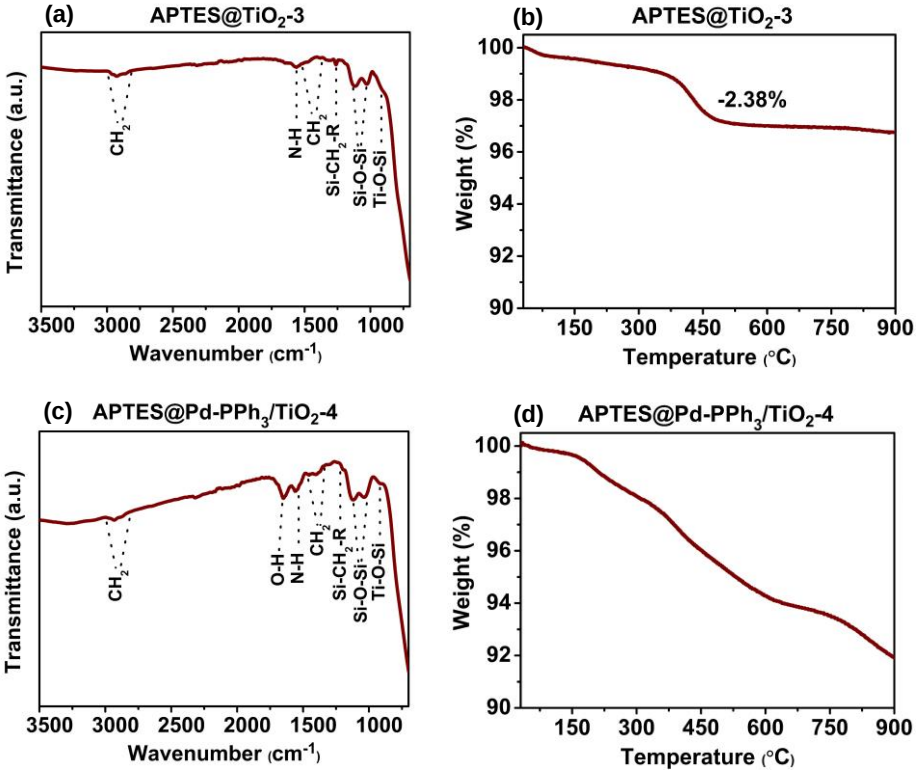

Figure 25. FT-IR spectra and TGA of **APTES/TiO$_2$-3** (a), (b) and FT-IR spectra and TGA of **APTES@Pd-PPh$_3$/TiO$_2$-4** (c), (d).

However, the intensity of the band at ≈ 1558 cm^{-1} corresponding to N-H bending was higher. Analysis by TGA curve revealed a total weight loss of *ca*. 9%, which is a much higher value than that observed for **APTES@TiO_2-3** (Figure 25 (b)). This indicated that a much greater amount of organic material is present at the surface of this material. Moreover, the profile of the curve was also different.

FT-IR and TGA techniques were also used to compare **APTES@Pd-PPh_3/TiO_2-7** with the support modified in the same conditions (**APTES@TiO_2-7**). Similarly to the previous sample, the FT-IR spectra (Figure 26 (a) and (c)) displayed the same bands although the intensity for the band attributed to N-H also increase intensity (≈ 1541 cm^{-1}).

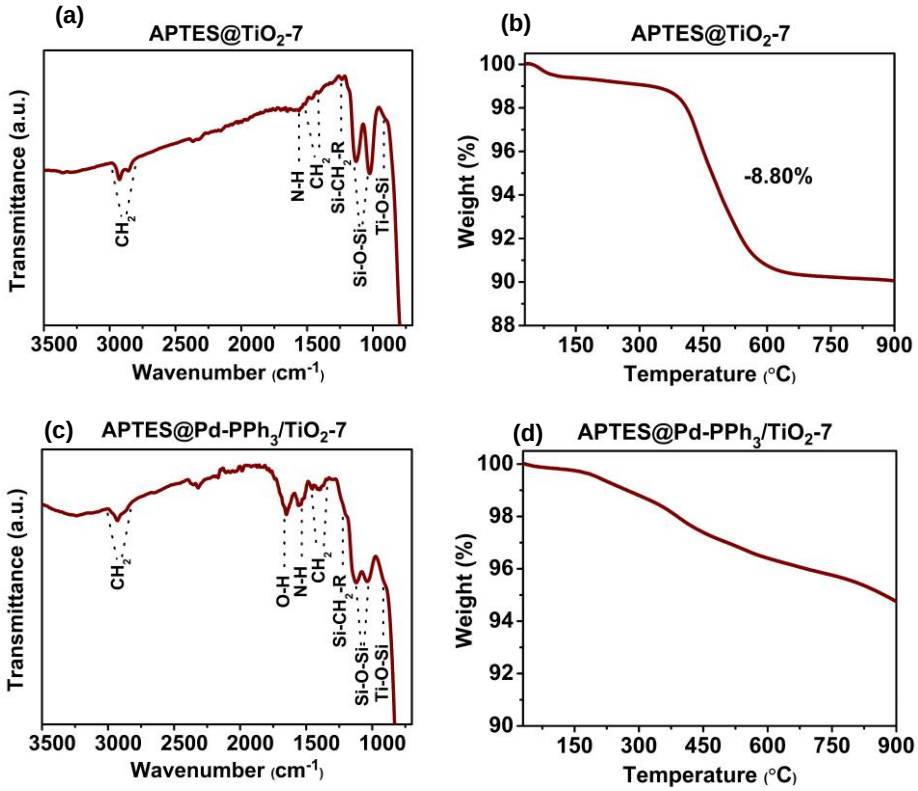

Figure 26. FT-IR spectra and TGA of **APTES@TiO_2-7** (a), (b) and FT-IR spectra and TGA of **APTES@Pd-PPh_3/TiO_2-7** (c), (d).

However, in this case, TGA analysis of **APTES@Pd-PPh_3/TiO_2-7** curve (Figure 26 (d)) revealed a weight loss of approximately 6%, which is lower than for **APTES@TiO_2-7** (Figure 26 (b)).

APA@Pd-PPh$_3$/TiO$_2$-12 was analyzed by TGA (Figure 27 (b)). A weight loss of *ca*. 3.5 wt% was observed, which was larger than that obtained for deposition of NH_2-PA over TiO_2 (**APA@TiO2-3**) (Figure 27 (a)). This indicated that a greater amount of organic material was deposited using this approach.

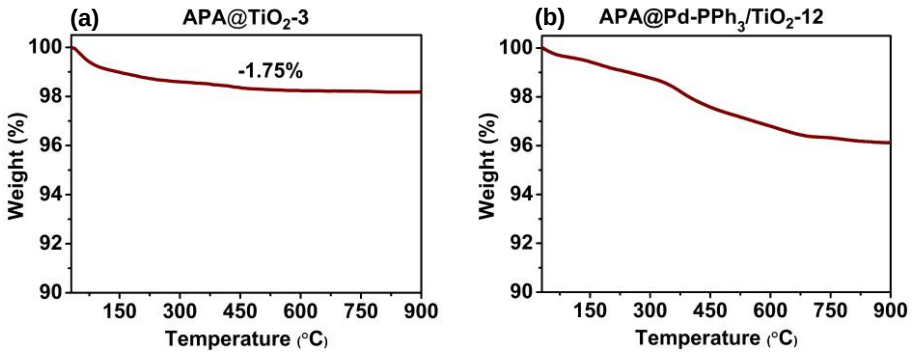

Figure 27. TGA of **APA@TiO$_2$-3** (a) and **APA@Pd-PPh$_3$/TiO$_2$-12** (b).

Some of these catalysts were also characterized by HR-TEM. For **APTES@Pd-PPh$_3$/TiO$_2$-4** (Figure 28 (a)), as previously detected by TEM, the presence of a thin layer at the surface of the material was observed. Similar observation was reported by Liu et al. using APTES as modifier.[23] This layer was *ca*. 2 nm thick and wrapped both support and Pd particles. By EDS mapping (Figure 28 (c)), the Si-based nature of this layer was confirmed at the surface of TiO_2 and Pd NPs. Therefore, this evidenced a structural difference for the materials obtained by this approach when compared with those synthesized by reverse deposition.

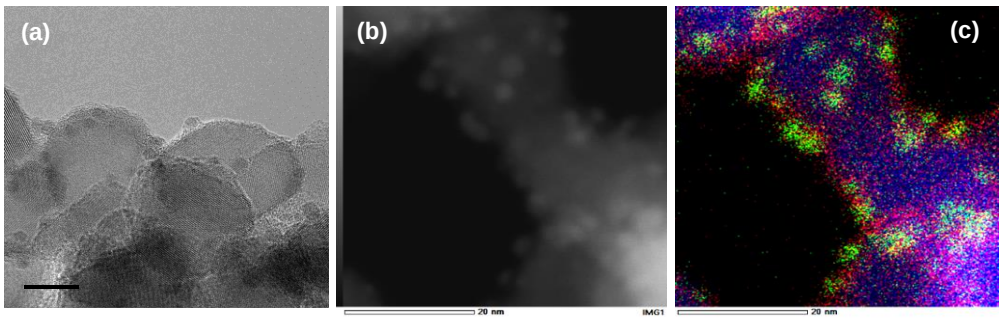

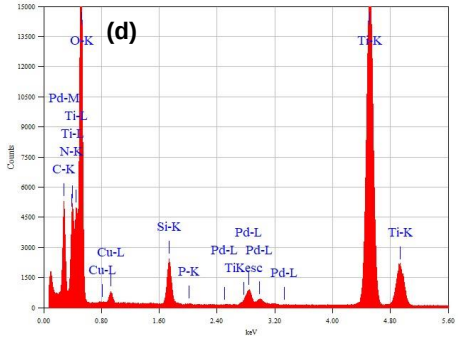

Figure 28. (a) HR-TEM image, (b) HR-HAADF STEM, (c) EDS mapping overlay (green, Pd; red, Si; blue, Ti), (d) spectrum of **APTES@Pd-PPh$_3$/TiO$_2$-4**.

The **IL-Cl@Pd-PPh$_3$/TiO$_2$-8** catalyst was also characterized by HR-TEM (Figure 29). Agglomerations were detected in some regions of the support (Figure 29 (a) and (b)). EDS mapping revealed the presence of a thin layer of IL-Cl at the surface of TiO$_2$, but it was unclear whether the Pd NPs were also covered. Microanalysis confirmed the presence of P from the PPh$_3$ ligands.

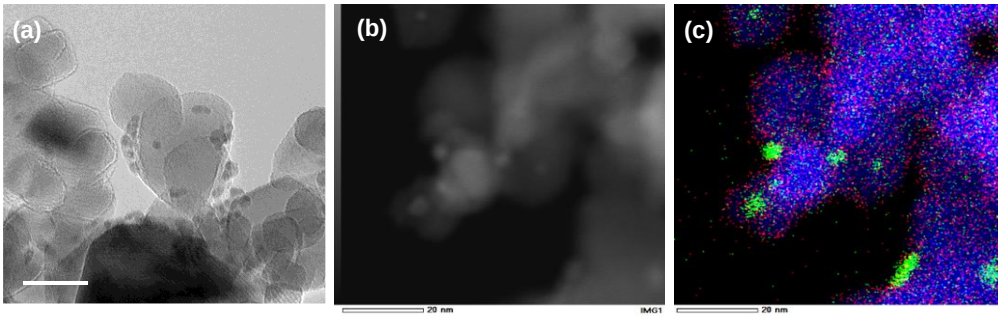

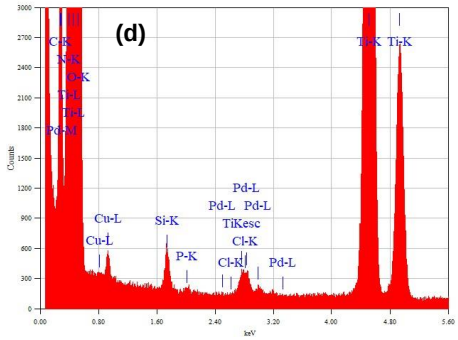

Figure 29. (a) HR-TEM image, (b) HR-HAADF STEM, (c) EDS mapping overlay (green, Pd; red, Si; blue, Ti), (d) spectrum of **IL-Cl@Pd-PPh$_3$/TiO$_2$-8**.

PA@Pd-PPh$_3$/TiO$_2$-11 was also analyzed by HR-TEM and EDS mapping (Figure 30). Highly crystalline Pd NPs were observed (Figure 30 (a)). P was located at the surface of the support, but it was unclear whether P was also present at the Pd NPs surface (Figure 30 (c)).

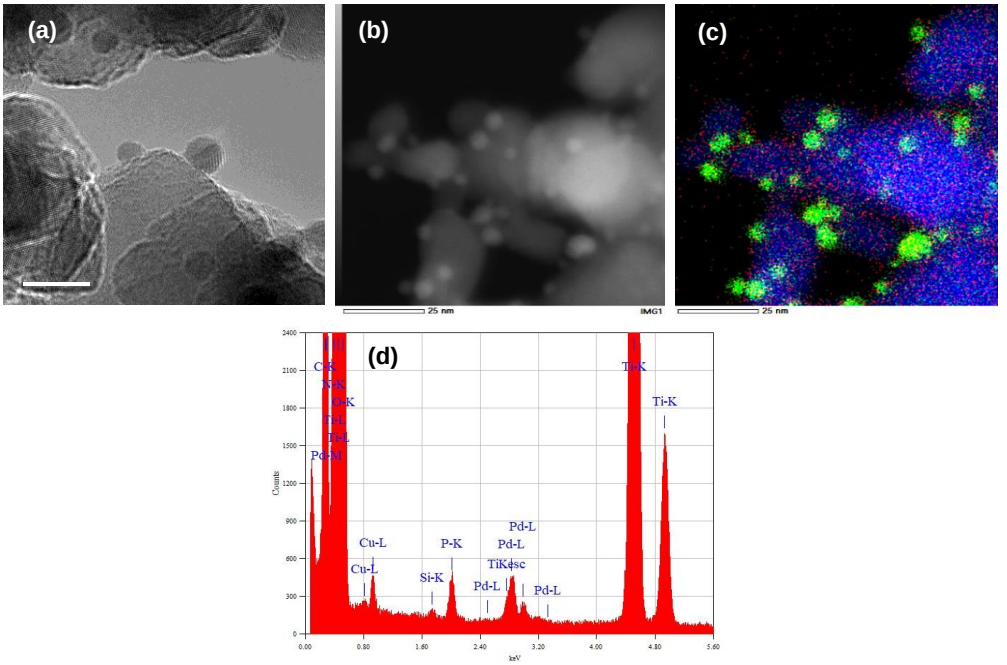

Figure 30. (a) HR-TEM image, (b) HR-HAADF STEM, (c) EDS mapping overlay (green, Pd; red, P; blue, Ti), (d) spectrum of **PA@Pd-PPh$_3$/TiO$_2$-11**.

When **APA@Pd-PPh$_3$/TiO$_2$-12** was analyzed by HR-TEM and mapping (Figure 31), the presence of P could again be located at the surface of the support but it was unclear whether P was also present over the surface of the Pd NPs (Figure 31 (c)).

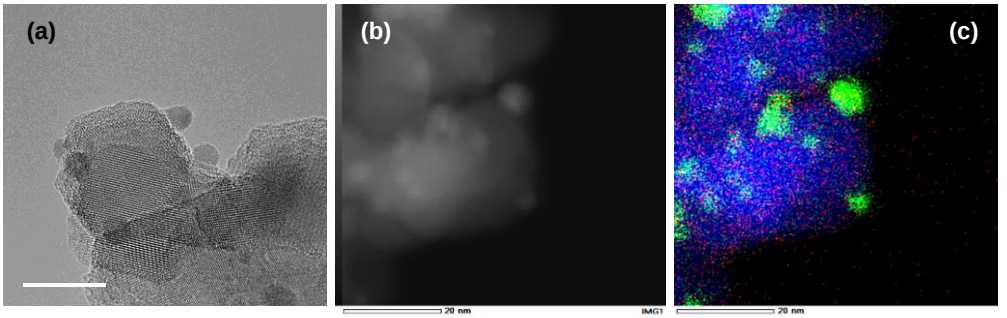

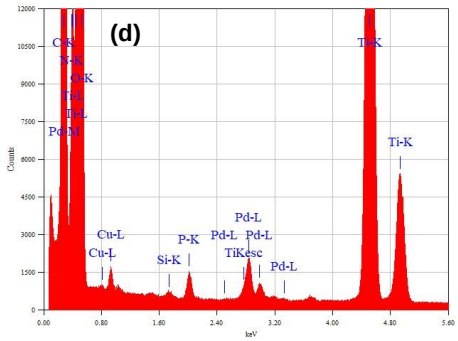

Figure 31. (a) HR-TEM image, (b) HR-HAADF STEM, (c) EDS mapping overlay (green, Pd; red, P; blue, Ti), (d) spectrum of **APA@Pd-PPh$_3$/TiO$_2$-12**.

XPS was also employed for the analysis of some of these catalysts (Figure 32). The data obtained were compared with those of the unmodified **Pd-PPh$_3$/TiO$_2$** catalyst. All the spectra were referenced using the C1s signal and set at 285.0 eV. Presence of Si2p, N1s and P2p for **APTES@Pd-PPh$_3$/TiO$_2$-4** catalyst and N1s and P2p for **APA@Pd-PPh$_3$/TiO$_2$-12** were detected. Pd spectra was studied with more detail (Figure 32 (b)). When P based modifier was used (**APA@Pd-PPh$_3$/TiO$_2$-12**), no significant differences with the unmodified catalyst were observed. However, for sample containing the Si based modifiers, the BEs observed was higher. For **APTES@Pd-PPh$_3$/TiO$_2$-4**, a difference of 1 eV was observed (336.0 eV) with the reference catalyst, which could be due to the interaction with the amine functional group from APTES, as previously reported by Kim et al.[58]

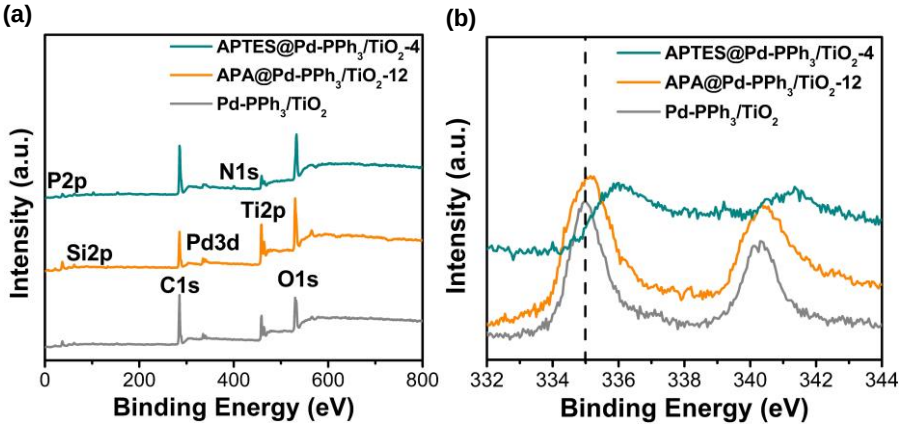

Figure 32. Stacked XPS image of overview (a) and Pd3d high resolution spectra (b) for the newly synthesized catalysts.

They also observed an increase of BE for Pd when APTES is used on the synthesis of Pd NPs over CNTs and attributed this difference due to the interaction of Pd with amine functional groups and also to the particle size (1.85 nm). **APTES@Pd-PPh$_3$/TiO$_2$-4** also exhibited a very small size (1.86 nm). But, as was previously observed for **Pd-PPh$_3$/IL-Cl@TiO$_2$-8,** which also has a size in this range (1.89 nm), BE was *ca*. 335 eV. So, a combination of interaction of amine and small size could produce the BE observed for **APTES@Pd-PPh$_3$/TiO$_2$-4**. Mori et al. also reported high BEs for Pd catalysts on support modified with amines, although the shifts were less prononced.[25]

Table 9. XPS results for different **mod@Pd-PPh$_3$/TiO$_2$-x** catalyst and **Pd-PPh$_3$/TiO$_2$**.

Entry	System	Pd$^{\delta+}$ (%)
1	**Pd-PPh$_3$/TiO$_2$**	12.5
2	**APTES@Pd-PPh$_3$/TiO$_2$-4**	63.8
3[a]	**APA@Pd-PPh$_3$/TiO$_2$-12**	21.9

[a]With aging step.

The relative amount of Pd$^{\delta+}$ also revealed different for samples (Table 9). In unmodified **Pd-PPh$_3$/TiO$_2$**, a value of 12.5% was measured (Entry 1), which was attributed to the manipulation of the sample during analysis. When the aminophosphonic acid was used in the synthesis of **APA@Pd-PPh$_3$/TiO$_2$-12**, the proportion of Pd$^{\delta+}$ was 21.9% (Entry 3). These values remained similar to that of the reference **Pd-PPh$_3$/TiO$_2$** catalyst. However, a value as high as 64% was obtained **APTES@Pd-PPh$_3$/TiO$_2$-4** (Entry 2). Additionally, for the same catalyst, the BE for Si 2p was detected at 103 eV instead of at 102 eV which is the value reported in literature[58] and no P was detected. This could be explained by the displacement of the ligand from the surface of NP during the deposition of APTES over the Pd NPs. For the material containing NH$_2$-PA, namely **APA@Pd-PPh$_3$/TiO$_2$-12**, the presence of P (peak at 133 eV) and N (peak at 400 eV attributed to C–NH$_2$) was confirmed.[58]

The results from the synthesis and characterization of a series of different catalyst obtained by deposition of organosilane and organophosphonic acid modifiers over previously synthesized Pd NPs supported on TiO$_2$ can be summarized as follow:

- Several families of modifiers were used and variables such as the presence of a functional group on the modifiers, the concentration of modifier, the temperature of synthesis, etc. were evaluated.
- These materials were analised by TEM. When organosilanes were employed on the synthesis of catalysts, smaller Pd NPs were obtained compared with those modified by organophosphonic acids.
- In terms of composition, no significant differences in Pd content were measured by ICP when organosilanes or organophosphonic acids were used. However, comparing the results obtained when the modification were performed using APTES at different concentrations, it was observed that at higher amount of APTES employed, lower Pd content was obtained. This was attributed to Pd leaching during the synthesis.
- When HR-TEM was employed in the analysis of representative catalyst, a fine layer of modifier was observed over the NPs.

5.2.4. Hydrogenation of CO_2 into formates using modified catalysts

In this section, the catalytic experiments carried out using the modified catalysts prepared in Sections 5.2.2. and 5.2.3. are described. The results obtained using the **Pd-PPh$_3$/modifier@TiO$_2$-x** and **modifier@Pd-PPh$_3$/@TiO$_2$-x** catalysts are summarized in Tables 10−15 and in Tables 16−19, respectively. First, a screening was performed to evaluate the effect of the different modifications carried out on catalysts. The catalytic reactions were evaluated *via* NMR analysis. In all cases, the only product formed was the expected formate.

5.2.4.1. Hydrogenation of CO_2 into formates using catalysts formed by deposition of Pd NPs over modified TiO_2 supports

These tests were performed at 80 ºC using 36 bar of CO_2/H_2 (1:1) pressure during 15 h in the presence of $KHCO_3$ as a base and using water as solvent (Scheme 8).

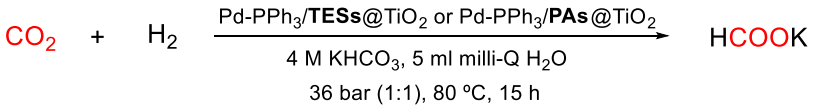

Scheme 8. Hydrogenation CO_2 to formate employing **Pd-PPh$_3$/modifier@TiO$_2$-x** systems as catalyst.

- **Effect of anchoring group**

Both TESs and PAs modified systems were tested in catalysis using the same concentration, mmol modifier/mg TiO_2 ratio and same substituent on the anchor atom (APTES and APA). In Table 10, the results obtained with these systems are displayed and compared with those provided by the unmodified **Pd-PPh$_3$/TiO$_2$** catalyst.

As previously described in Chapter 3, the **Pd-PPh$_3$/TiO$_2$** systems reached a TON of 881 (Entry 1) under these conditions. When **Pd-PPh$_3$/APTES@TiO$_2$-2** was used as catalyst, an increase was observed and a TON of 1057 was reached (Entry 2). In contrast, using the organophosphonic acid based modified material **Pd-PPh$_3$/APA@TiO$_2$-3** (Entry 3), a decrease in activity was observed and the lowest TON value of the series was measured (694). These results therefore indicated that when the catalyst is formed by deposition of the Pd NPs over the modified support, the nature of the modifier affects the catalyst activity. A positive effect is observed when APTES was used whereas a negative effect was evidenced using APA.

Table 10. Catalytic activity of **Pd-PPh$_3$/modifier@TiO$_2$-x** with different anchor atoms for CO_2 hydrogenation to formate.[a]

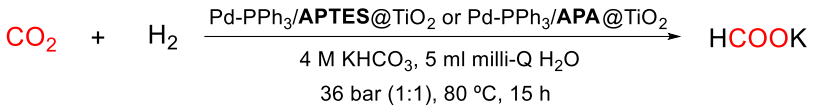

Entry	Catalyst	Anchor atom	TON[b]
1	**Pd-PPh$_3$/TiO$_2$**	-	881
2	**Pd-PPh$_3$/APTES@TiO$_2$-2**	Si	1057
3[c]	**Pd-PPh$_3$/APA@TiO$_2$-3**	P	694

[a]Reaction conditions: 20 mg of **Pd-PPh$_3$/modified@TiO$_2$-x** NPs, 4 M $KHCO_3$, 5 ml milli-Q H_2O, 80 ºC, pTotal= 36 bar, p(CO_2) = p(H_2), 15 h. [b]TON= mmol formate/mmol total of Pd, calculated by NMR using 1,4-dioxane as internal standard. [c]With aging.

- **Effects of reaction conditions for the support modification using APTES**

Next, the effect of the reaction conditions used for the support modification using APTES was investigated. The results are summarized in Table 11.

Table 11. Catalytic activity of **Pd-PPh$_3$/APTES@TiO$_2$-x** with different supports modified with APTES for CO_2 hydrogenation to formate.[a]

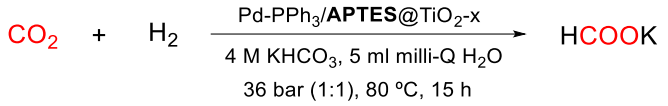

Entry	Catalyst	TON[b]
1	**Pd-PPh$_3$/TiO$_2$**	881
2	**Pd-PPh$_3$/APTES@TiO$_2$-2**	1057
3	**Pd-PPh$_3$/APTES@TiO$_2$-3**	868
4	**Pd-PPh$_3$/APTES@TiO$_2$-4**	853
5	**Pd-PPh$_3$/APTES@TiO$_2$-5**	858
6	**Pd-PPh$_3$/APTES@TiO$_2$-6**	623
7	**Pd-PPh$_3$/APTES@TiO$_2$-7**	615

[a]Reaction conditions: 20 mg of **Pd-PPh$_3$/APTES@TiO$_2$-x**, 4 M $KHCO_3$, 5 ml milli-Q H_2O, 80 ºC, pTotal= 36 bar, p(CO_2) = p(H_2), 15 h. [a]TON= mmol formate/mmol total of Pd, calculated by NMR using 1,4-dioxane as internal standard.

The results obtained show 3 distinct effects compared with the unmodified catalyst (Entry 1). As described in the previous section, when low concentration of APTES (0.01 M, 0.003 mmol/mg TiO_2) was used to modify the support, a positive effect on the activity of the resulting **Pd-PPh$_3$/APTES@TiO$_2$-2** catalyst was observed (Entry 2). When the concentration of APTES was increased up to 1 M (up to 0.013 mmol/mg TiO_2) (Catalysts **Pd-PPh$_3$/APTES@TiO$_2$-3-5,** Entries 3-5), the TONs obtained were similar to that obtained with the unmodified catalyst (range 860-870), suggesting that the excess of APTES “cancelled out” the positive effect observed at lower concentrations. It is noteworthy that the temperature used for the modification of the support, despite affecting the amount of organic material at the support surface, did not affect the catalyst activity under these

conditions. This trend was confirmed using the catalysts **Pd-PPh$_3$/APTES@TiO$_2$-6** and **Pd-PPh$_3$/APTES@TiO$_2$-7** (Entries 6 and 7), containing supports modified using even higher concentrations of APTES (4 M, 0.02 mmol/mg TiO_2). Indeed, these catalysts provided the lowest TONs of the series: 623 and 615, respectively. The similarity of these results once again indicated that the temperature used for the support synthesis did not affect the activity in catalysis.

These results are in contrast with those reported by Mori et al.[25] using a phenylamine containing organosilane to modify SiO_2, since they observed an increase in catalytic activity when the amount of phenylamine was increased.

- **Effect of the aging step on APA@TiO$_2$-x**

Table 12 displays the results obtained using the catalysts obtained by deposition of Pd NPs over TiO_2 modified by APA with and without aging step. When the fresh **Pd-PPh$_3$/APA@TiO$_2$-2** catalyst was used, a TON of 458 was obtained while the activity of the catalyst **Pd-PPh$_3$/APA@TiO$_2$-3** increased with a TON of 694 (Entry 2). This clearly showed the positive effect of the aging step on this catalyst.

Table 12. Catalytic activity of **Pd-PPh$_3$/APA@TiO$_2$-x** which has suffered or not an aging step for CO_2 hydrogenation to formate.[a]

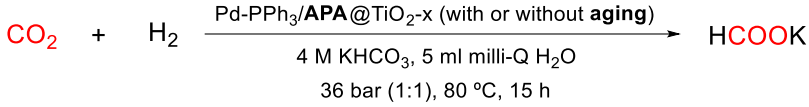

Entry	Catalyst	TON[b]
1[c]	**Pd-PPh$_3$/APA@TiO$_2$-2**	458
2[d]	**Pd-PPh$_3$/APA@TiO$_2$-3**	694

[a]Reaction conditions: 20 mg of **Pd-PPh$_3$/APA@TiO$_2$-x**, 4 M $KHCO_3$, 5 ml milli-Q H_2O, 80 ºC, pTotal= 36 bar, p(CO_2) = p(H_2), 15 h. [b]TON= mmol formate/mmol total of Pd, calculated by NMR using 1,4-dioxane as internal standard. [c]Without aging. [d]With aging.

- **Effect of functional group in the modifier structure**

Another parameter which could give effect in catalysis is the presence of a functional group at the end of the alkyl chain of the modifier (Table 13). To evaluate this effect, the results obtained with the catalysts containing TiO_2 support modified by Si-based modifiers containing an alkylic chain (PTES),

an amine group (APTES) and an ionic liquid (IL-Cl) under the same conditions were compared (Entries 1 to 3).

Table 13. Catalytic activity of **Pd-PPh$_3$@modifier/TiO$_2$-x** with different groups at the end of the alkyl chain for CO_2 hydrogenation to formate.[a]

Entry	Catalyst	Group	TON[b]
1	**Pd-PPh$_3$/PTES@TiO$_2$-1**	-	588
2	**Pd-PPh$_3$/APTES@TiO$_2$-3**	NH_2	868
3	**Pd-PPh$_3$/IL-Cl@TiO$_2$-9**	Imidazolium	820
4[c]	**Pd-PPh$_3$/PA@TiO$_2$-3**	-	635
5[c]	**Pd-PPh$_3$/APA@TiO$_2$-1**	NH_2	694

[a]Reaction conditions: 20 mg of **Pd-PPh$_3$/modified@TiO$_2$-x** NPs, 4 M $KHCO_3$, 5 ml milli-Q H_2O, 80 ºC, pTotal= 36 bar, p(CO_2) = p(H_2), 15 h. [b]TON= mmol formate/mmol total of Pd, calculated by NMR using 1,4-dioxane as internal standard. [c]With aging.

The results obtained using the corresponding catalysts where PAs with alkylic chain or with amine group were also compared (Entries 4-5).

For the catalysts formed by modifications with organosilanes, the presence of a functional group (either NH_2 or imidazolium group) was clearly beneficial to the catalyst activity since an increase in TON was observed from 588 (for PTES, Entry 1) to *ca.* 850 for APTES and IL-Cl- modified catalysts (Entries 2 and 3).

Similar effect was observed for PAs-modified catalysts (Entry 4 *vs*. 5), although a less pronounced increase was measured (635 *vs*. 694).

- **Effect of anion and synthesis conditions in Ionic Liquid containing TESs modifiers**

The effect of the anion reaction conditions on catalysts synthesized by deposition of Pd NPs over TiO_2 previously modified by organosilanes containing an IL functionality was looked at by comparison of the catalytic results using catalysts **Pd-PPh$_3$/IL-X@TiO$_2$-x** (Table 14). The results obtained with the catalysts **Pd-PPh$_3$/IL-Cl@TiO$_2$-8, 9** that differ from the

conditions used during the support modification, clearly indicate that low concentration (0.022 M) and temperature (80 ºC) during the synthesis improves the catalyst performance when compared with harsher conditions (0.12 M, 110 ºC) (Entry 2 *vs*. Entry 3) as the TONs obtained were 1043 and 820, respectively.

Table 14. Catalytic activity of **Pd-PPh$_3$/IL-X@TiO$_2$-x** with different anions for CO_2 hydrogenation to formate.[a]

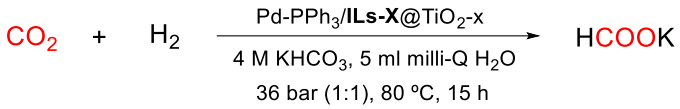

Entry	System	Anion	TON[b]
1	**Pd-PPh$_3$/TiO$_2$**	-	881
2	**Pd-PPh$_3$/IL-Cl@TiO$_2$-8**	Cl^-	1043
3	**Pd-PPh$_3$/IL-Cl@TiO$_2$-9**	Cl^-	820
4	**Pd-PPh$_3$/IL-NTf$_2$@TiO$_2$-10**	NTf_2^-	681
5	**Pd-PPh$_3$/IL-OAc@TiO$_2$-11**	OAc^-	1030
6	**Pd-PPh$_3$/IL-OAc@TiO$_2$-12**	OAc^-	776

[a]Reaction conditions: 20 mg of **Pd-PPh$_3$/IL-X@TiO$_2$** NPs, 4 M $KHCO_3$, 5 ml milli-Q H_2O, 80 ºC, pTotal= 36 bar, p (CO_2) = p(H_2), 15 h. [b]TON= mmol formate/mmol total of Pd, calculated by NMR using 1,4-dioxane as internal standard.

Based on previous results using organosilane modifiers (Table 11), the concentration is expected to be the parameter responsible of this difference. This was confirmed by the results obtained with the catalysts **Pd-PPh$_3$/IL-OAc@TiO$_2$-11** and **Pd-PPh$_3$/IL-OAc@TiO$_2$-12** which only differ by the concentrations used during their support synthesis (Entry 5 *vs*. Entry 6). Indeed, the catalyst **Pd-PPh$_3$/IL-OAc@TiO$_2$-11** containing the support modified at the lower concentration provided a TON of 1030 while when **Pd-PPh$_3$/IL-OAc@TiO$_2$-12** was used, a TON of 776 was obtained. These results were therefore in agreement with the trend previously observed in this work. When the catalyst containing a support modified with an organosilane containing an hydrophobic IL (Entry 4) was used, the lowest TON value of the series was obtained (681). This thus indicated that the hydrophilic character of the IL functionality in the modifier was beneficial to this catalytic reaction.

- **Effect of the presence of ligand (PPh_3) during in the NP synthesis**

The presence of PPh_3 as ligand during the synthesis of the Pd NPs over supports modfied with APTES and IL-OAc was evaluated (Table 15).

Table 15. Catalytic activity of **Pd-PPh_3/modifier@TiO_2-x** and **Pd@modifier/TiO_2-x** for CO_2 hydrogenation to formate.[a]

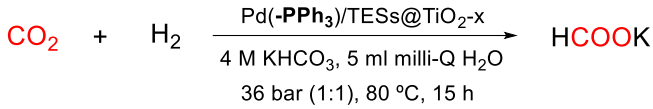

Entry	Catalyst	Ligand	TON[b]
1	**Pd-PPh_3/TiO_2**	PPh_3	881
2	**Pd-PPh_3/APTES@TiO_2-3**	PPh_3	868
3[c]	**Pd/APTES@TiO_2-3**	-	917
4	**Pd-PPh_3/IL-OAc@TiO_2-12**	PPh_3	776
5[c]	**Pd/IL-OAc@TiO_2-12**	-	826

[a]Reaction conditions: 20 mg of catalyst, 4 M $KHCO_3$, 5 ml milli-Q H_2O, 80 ºC, pTotal= 36 bar, $p(CO_2) = p(H_2)$, 15 h. [b]TON= mmol formate/mmol total of Pd, calculated by NMR using 1,4-dioxane as internal standard. [c]In absence of PPh_3.

Entry 1 describes the unmodified catalyst, in which PPh_3 is present with a TON of 881. In both cases, slightly higher TON values were obtained in the absence of PPh_3 (Entry 1 *vs.* Entry 2 and Entry 3 *vs.* Entry 4). When **Pd-PPh_3/APTES@TiO_2-3** was used, a TON of 868 was obtained (Entry 2), while the system without PPh_3, **Pd/APTES@TiO_2-3** provided a TON of 917 (Entry 3). **IL-OAc, Pd-PPh_3/IL-OAc@TiO_2-12**, which was synthesised in the presence of PPh_3, reached a TON of 776 (Entry 4) while its analogue without PPh_3 **Pd/IL-OAc@TiO_2-12** yielded a TON of 826 (Entry 5).

The catalytic results described in this section using the catalyst formed by deposition of Pd NPs over previously modified TiO_2 supports can be summarized as follow:

- The modification of the TiO_2 support by oganosilanes provided a beneficial effect in catalysis compared with the catalyst containing unmodified TiO_2 or TiO_2 modified by organophosphonic acids.
- The concentration is a key parameter during the support modification and lower values provide catalysts with higher activities. In contrast,

the temperature used during the modification, despite affecting the amount of organics at the surface of the support, does not influence the activity of the catalysts.

- The presence of a functional group (either NH_2 or imidazolium) in the modifiers improve the activity of the catalysts compared with those containing a simple alkyl chain.
- When using organophosphonic acids as modifiers, an aging step is beneficial to the activity of the resulting catalyst.
- The presence of PPh_3 as ligand during the deposition of the NPs over the support does not relevantly affect the catalyst activity. A slight detrimental effect was even evidenced.

5.2.4.2. Hydrogenation of CO_2 into formates using catalysts formed by modifications of pre-synthesized Pd-PPh_3/TiO_2

The catalysts synthesized by the deposition of the modifier over **Pd-PPh_3/TiO_2** previously synthesized were evaluated in the CO_2 hydrogenation into formate (Scheme 9). The effects of the nature of the anchoring atom, the conditions for the deposition of the organosilanes, the presence of amine and IL functionality and the effect of the anion in the ionic liquid were evaluated and will be described separately (Tables 16−19).

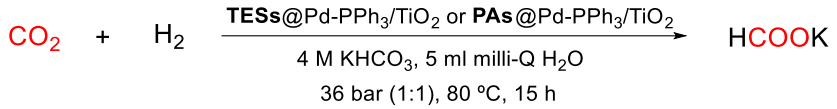

Scheme 9. Hydrogenation CO_2 to formate employing **modifier@Pd-PPh_3/TiO_2-x** systems as catalyst.

- **Effect of the modifier's anchoring atom**

Table 16 summarizes the results obtained by deposition of organosilane and organophosphonic acid under the same conditions (same concentration, mmol modifier/mg TiO_2 ratio and amine substituent on the organosilane and organophosphonic acid). Note that the catalyst modified by deposition of PA was submitted to an aging process prior to catalysis.[11] The results were compared with the results obtained with the unmodified catalyst (Entry 1). The system containing a Si as anchoring atom, **APTES@Pd-PPh_3/TiO_2-2**,

provided a TON of 581 (Entry 2). When APA was used as modifier, the **APA@Pd-PPh$_3$/TiO$_2$-12** catalyst reached a a TON of 844 (Entry 3).

Table 16. Catalytic activity of **modifier@Pd-PPh$_3$/TiO$_2$-x** with different anchor atoms for CO_2 hydrogenation to formate.[a]

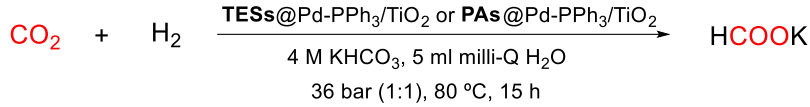

Entry	System	Anchor atom	TON[b]
1	**Pd-PPh$_3$/TiO$_2$**	-	881
2	**APTES@Pd-PPh$_3$/TiO$_2$-2**	Si	581
3[c]	**APA@Pd-PPh$_3$/TiO$_2$-12**	P	844

[a]Reaction conditions: 20 mg of **modifier@Pd-PPh$_3$/TiO$_2$-x**, 4 M $KHCO_3$, 5 ml milli-Q H_2O, 80 ºC, pTotal= 36 bar, p(CO_2) = p(H_2), 15 h. [b]TON= mmol formate/mmol total of Pd, calculated by NMR using 1,4-dioxane as internal standard. [c]With aging.

As the unmodified catalyst provided a TON of 881, it can be concluded that the deposition of the organosilane over the presynthesised catalyst had a detrimental effect on the CO_2 hydrogenation while the deposition of PA has no significant effect. These results are in contrast with those obtained using the catalyst where Pd NPs were deposited over the modified support since in this case, the use of the organosilane was the most beneficial to the catalytic activity, even enhancing the TON value compared to that of the unmodified catalyst. This evidences the importance of the synthetic strategy when such catalysts are modified with organic molecules.

- **Variation of reaction conditions for the deposition of APTES over Pd-PPh$_3$/TiO$_2$**

Table 17 are summarized the results obtained for hydrogenation of CO_2 to formate using catalysts formed by deposition of APTES at different concentrations. When the system obtained at low concentration of APTES, the TON obtained was 581, as previously mentioned in the previous section (Entry 2). When higher concentration (0.13 M) was used, the resulting catalysts, **APTES@Pd-PPh$_3$/TiO$_2$-3** and **APTES@Pd-PPh$_3$/TiO$_2$-4** provided much higher activity with TONs of 940 and 992, respectively (Entries 3 and 4). This value is higher than that obtained with the unmodified catalyst.

Table 17. Catalytic activity of **APTES@Pd-PPh$_3$/TiO$_2$-x** with different anchor atoms for CO_2 hydrogenation to formate.[a]

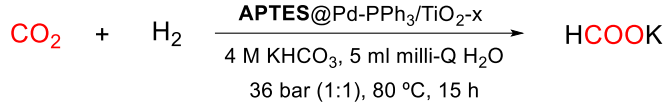

Entry	System	TON[b]
1	**Pd-PPh$_3$/TiO$_2$**	881
2	**APTES@Pd-PPh$_3$/TiO$_2$-2**	581
3	**APTES@Pd-PPh$_3$/TiO$_2$-3**	940
4	**APTES@Pd-PPh$_3$/TiO$_2$-4**	992
5	**APTES@Pd-PPh$_3$/TiO$_2$-5**	581
6	**APTES@Pd-PPh$_3$/TiO$_2$-6**	570
7	**APTES@Pd-PPh$_3$/TiO$_2$-7**	589

[a]Reaction conditions: 20 mg of **APTES@Pd-PPh$_3$/TiO$_2$-x**, 4 M $KHCO_3$, 5 ml milli-Q H_2O, 80 ºC, pTotal= 36 bar, p(CO_2) = p(H_2), 15 h. [b]TON= mmol formate/mmol total of Pd, calculated by NMR using 1,4-dioxane as internal standard.

In contrast, when the **APTES@Pd-PPh$_3$/TiO$_2$-5** system was used, which was formed using 1 M of APTES, a decrease in activity was observed with a TON of 581 (Entry 5). Similar results were obtained using the catalysts formed using 4 M of APTES **APTES@Pd-PPh$_3$/TiO$_2$-6** and **APTES@Pd-PPh$_3$/TiO$_2$-7** with TON of 570 and 589, respectively (Entry 6 and Entry 7). These results indicated that when the catalysts are synthesized by deposition of the APTES modifier over the presynthesised **Pd-PPh$_3$/TiO$_2$** catalyst, the APTES concentration used for the modification is critical as low and high values are detrimental to the catalytic activity while an intermediate value enhances (slightly) the catalytic performance in this reaction. The negative effect at high APTES concentration could be explained by the blocking of Pd active sites by the modifier. The result observed using the catalyst formed at low APTES concentration is more difficult to rationalize.

- **Effect of the functional group in the modifier structure**

Table 18 summarizes the catalytic results obtained using catalysts modified by organosilanes containing a propyl, a propylamine or a propyl-imidalozium

groups and those modified by PAs containing a butyl and a propylamine substituent.

Interestingly, all these catalysts exhibited activities similar to that of the unmodified catalyst, except that modified by an organosilane containing an imidazolium function. It is noteworthy that, as described in the previous section, the **APTES@Pd-PPh$_3$/TiO$_2$-4** catalyst showed a slight positive effect compared to the reference catalyst.

Table 18. Catalytic activity of **modifier@Pd-PPh$_3$/TiO$_2$-x** with different groups at the end of the alkyl chain for CO_2 hydrogenation to formate.[a]

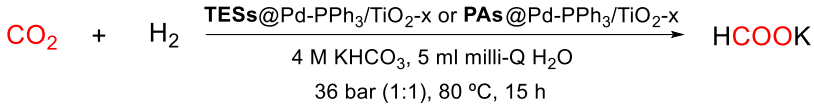

Entry	System	Group	TON[b]
1	**Pd-PPh$_3$/TiO$_2$**	-	881
2	**PTES@Pd-PPh$_3$/TiO$_2$-1**	-	862
3	**APTES@Pd-PPh$_3$/TiO$_2$-4**	NH_2	992
4	**IL-Cl@Pd-PPh$_3$/TiO$_2$-8**	Imidazolium	388
5[c]	**PA@Pd-PPh$_3$/TiO$_2$-11**	-	912
6[c]	**APA@Pd-PPh$_3$/TiO$_2$-12**	NH_2	844

[a]Reaction conditions: 20 mg of **modifier@Pd-PPh$_3$/TiO$_2$-x**, 4 M $KHCO_3$, 5 ml milli-Q H_2O, 80 ºC, pTotal= 36 bar, p(CO_2) = p(H_2), 15 h. [b]TON= mmol formate/mmol total of Pd, calculated by NMR using 1,4-dioxane as internal standard. [c]With aging.

The results described here are in clear contrast with those obtained when the support was first modified prior to the deposition of Pd NPs, for which the presence of a functional group (either amine or imidazolium) in the modifier clearly improved the performance of the resulting catalysts. This might be due to the beneficial effect of this group in the anchoring of the NPs when present at the support surface prior to the NP deposition while such a group does not influence the catalytic activity when deposited after NP formation. This thus suggests that the presence of this group does not influence the catalysis but only the preparation of the catalyst.

- **Effect of the nature of the anion on catalysts modified by Ionic Liquid-containing APTES**

The catalytic performance of catalysts modified by ionic liquid-containing modifiers with distinct anions in the hydrogenation of CO_2 to formate are summarized Table 19. The 3 catalysts tested, namely **IL-Cl@Pd-PPh$_3$/TiO$_2$-8** (Entry 2), **IL-NTf$_2$@Pd-PPh$_3$/TiO$_2$-9** (Entry 3), and **IL-OAc@Pd-PPh$_3$/TiO$_2$-10** (Entry 4), provided lower TONs (388, 281 and 551, respectively) than the unmodified catalyst, indicating that the deposition of IL-containing organosilanes over the Pd NPs was detrimental to the catalytic performance of the **Pd-PPh$_3$/TiO$_2$** material.

Table 19. Catalytic activity of **IL-X@Pd-PPh$_3$/TiO$_2$-x** for CO_2 hydrogenation to formate.[a]

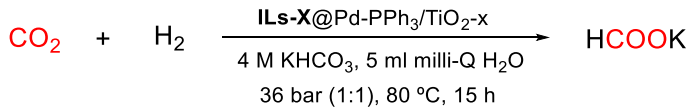

Entry	System	Anion	TON[b]
1	**Pd-PPh$_3$/TiO$_2$**	-	881
2	**IL-Cl@Pd-PPh$_3$/TiO$_2$-8**	Cl^-	388
3	**IL-NTf$_2$@Pd-PPh$_3$/TiO$_2$-9**	NTf_2^-	281
4	**IL-OAc@Pd-PPh$_3$/TiO$_2$-10**	OAc^-	551

[a]Reaction conditions: 20 mg of **IL-X@Pd-PPh$_3$/TiO$_2$-x**, 4 M $KHCO_3$, 5 ml milli-Q H_2O, 80 ºC, pTotal= 36 bar, p(CO_2) = p(H_2), 15 h. [b]TON= mmol formate/mmol total of Pd, calculated by NMR using 1,4-dioxane as internal standard.

Within the series, the catalyst modified with an hydrophobic IL yielded the lowest activity, as previously observed when the support was modified prior to Pd NPs deposition. The highest TON was obtained using **IL-OAc@Pd-PPh$_3$/TiO$_2$-10**, which could be attributed to the beneficial role of imidazolium based-OAc ILs in catalysis.[38,59]

The catalytic results described in this section, using the catalysts formed by deposition of organosilane and organophosphonic acid modifiers over previously synthesized Pd NPs supported on TiO_2 in the CO_2 hydrogenation into formates, can be summarized as follow:

- The deposition of organosilane and organophosphonic acid modifiers over previously synthesized Pd NPs supported on TiO_2 was not beneficial, in most cases, to the activity of the catalyst.
- The deposition of organophosphonic acid modifiers had very little effect on the catalytic activity of the resulting materials.
- The deposition of organosilanes containing an IL substituent had a detrimental effect on the catalytic activity of the resulting materials.
- The presence of a functional group (either NH_2 or imidazolium) in the modifiers did not improve the activity of the catalysts compared with those containing a simple alkyl chain.

5.2.5. Reusability tests

After evaluating the activity of the newly synthesized catalysts, recyclability tests were performed with some of the most active systems. During these experiments, the catalysts were recovered by filtration over a Nylon membrane after each cycle, washed several times with milli-Q H_2O and dry under vacuum for several hours.

First, a series of experiments using **Pd/APTES@TiO_2-3**, **Pd-PPh_3/APTES@TiO_2-2** and **PA@Pd-PPh_3/TiO_2-11** as catalysts were carried out at 60 and 80 ºC to evaluate the effect of temperature on these catalysts's stability (Scheme 10). Fresh and used catalysts were analyzed by ICP and TEM to determine if changes in composition and/or structure had taken place during the reactions.

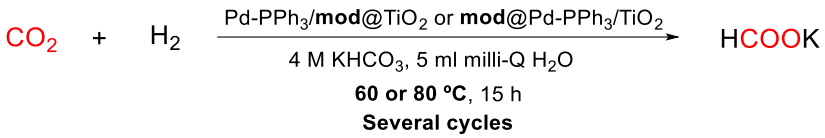

Scheme 10. Recycling experiments in the hydrogenation of CO_2 into formate employing several catalysts at different temperatures.

The results of the reactions performed at 60 ºC are summarized in Figure 33. **Pd-PPh_3/APTES@TiO_2-2** was the most active system with an initial TON of 1118 followed for **Pd/APTES@TiO_2-3** with a TON of 963 and **PA@Pd-PPh_3/TiO_2-11** with a TON of 915. However, during the following cycles, all three systems suffered a decrease in activity, with **Pd-PPh_3/APTES@TiO_2-2**

providing a TON of 380 during the 2nd cycle. The strongest decrease was observed for **PA@Pd-PPh$_3$/TiO$_2$-11**.

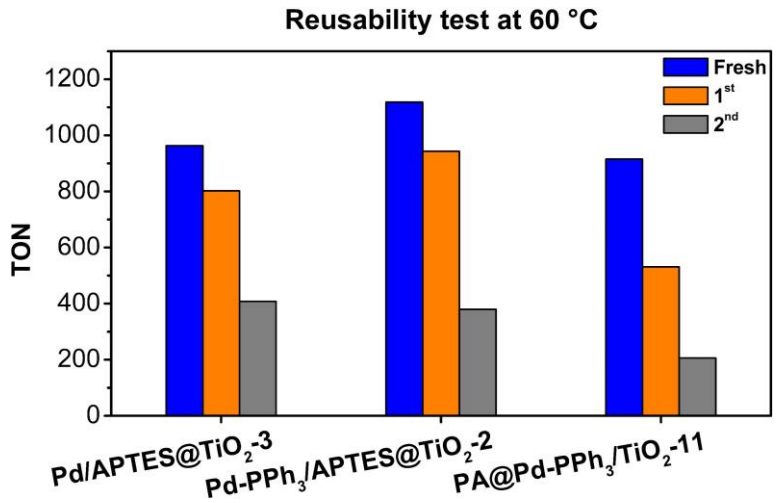

Figure 33. Recycling experiments with different systems at 60 ºC for CO_2 hydrogenation to formate. Conditions: 20 mg of catalyst, 4 M $KHCO_3$, 5 ml milli-Q H_2O, pTotal= 36 bar, p(CO_2) = p(H_2), 60 ºC, 15 h. TON= mmol formate/mmol total of Pd, calculated by NMR using 1,4-dioxane as internal standard.

The same trend was observed when the catalytic experiments were performed at 80 ºC (Figure 34).

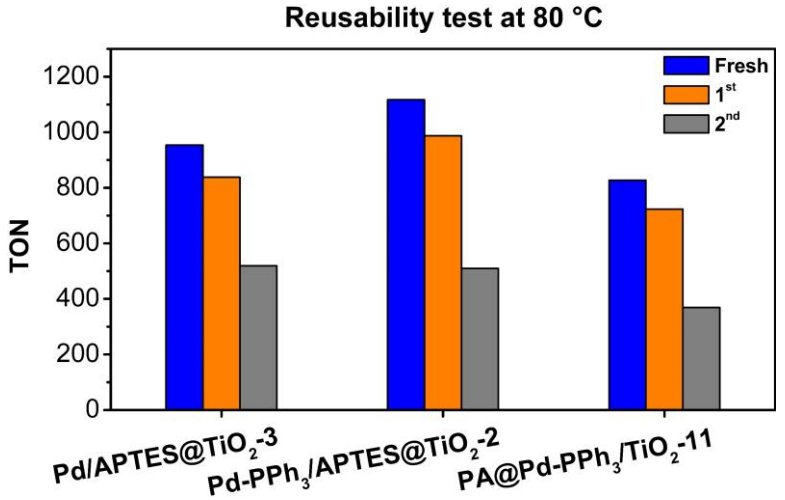

Figure 34. Recycling experiments with different systems at 80 ºC for CO_2 hydrogenation to formate. Conditions: 20 mg of catalyst, 4 M $KHCO_3$, 5 ml milli-Q

H_2O, pTotal= 36 bar, $p(CO_2) = p(H_2)$, 80 ºC, 15 h. TON= mmol formate/mmol total of Pd, calculated by NMR using 1,4-dioxane as internal standard.

The most active system was **Pd-PPh$_3$/APTES@TiO$_2$-2** with an initial TON of 1117, followed for **Pd/APTES@TiO$_2$-3** with a TON of 954 and **PA@Pd-PPh$_3$/TiO$_2$-11** with a TON of 827. When the catalysts were recovered and reused in the hydrogenation of CO_2, strong declines in activity were observed for all catalysts.

However, it is noteworthy that slight improvements were observed at 80 ºC, especially in the case of **PA@Pd-PPh$_3$/TiO$_2$-11** whose activity didn't decrease as strongly as at 60 ºC.

No significant decrease in Pd content was observed by ICP for any of the catalysts, indicating that leaching was not responsible for the losses of activity observed.

When TEM analysis was performed on these systems after the 2nd cycle, (Table 20), a small increase in size was detected after reactions at 60 ºC and 80 ºC for **Pd/APTES@TiO$_2$-3** and **Pd-PPh$_3$/APTES@TiO$_2$-2**.

Table 20. Particle size of different systems before and after recycling experiments for CO_2 hydrogenation to formate.[a][b]

Entry	Catalyst	Size (nm)[c]	Size (nm)[d]	Size (nm)[e]
1[f]	**Pd/APTES@TiO$_2$-3**	2.52 ± 0.95	3.26 ± 0.97	3.48 ± 1.39
2	**Pd-PPh$_3$/APTES@TiO$_2$-2**	2.23 ± 0.78	3.26 ± 0.90	3.43 ± 1.20
3[g]	**PA@Pd-PPh$_3$/TiO$_2$-11**	4.45 ± 1.68	3.87 ± 1.23	3.59 ± 1.49

[a]Reaction conditions: 20 mg of catalyst, 4 M $KHCO_3$, 5 ml milli-Q H_2O, pTotal= 36 bar, $p(CO_2) = p(H_2)$, 15 h. [b]Particle size was obtained by TEM. [c]Before catalysis. [d]After 2nd cycle at 60 ºC. [e]After 2nd cycle at 80 ºC. [f]In absence of PPh_3. [g]With aging.

Moreover, a broadening of the size distributions was observed for reactions at 80 ºC. In contrast, for **PA@Pd-PPh$_3$/TiO$_2$-11**, a decrease in mean size was observed. However, large agglomerations were also detected (Figure 35).

These results indicated that the deactivation of these catalysts during recycling is due to agglomerations of Pd-NPs as previously described for **Pd-PPh$_3$/TiO$_2$** in Chapter 3.

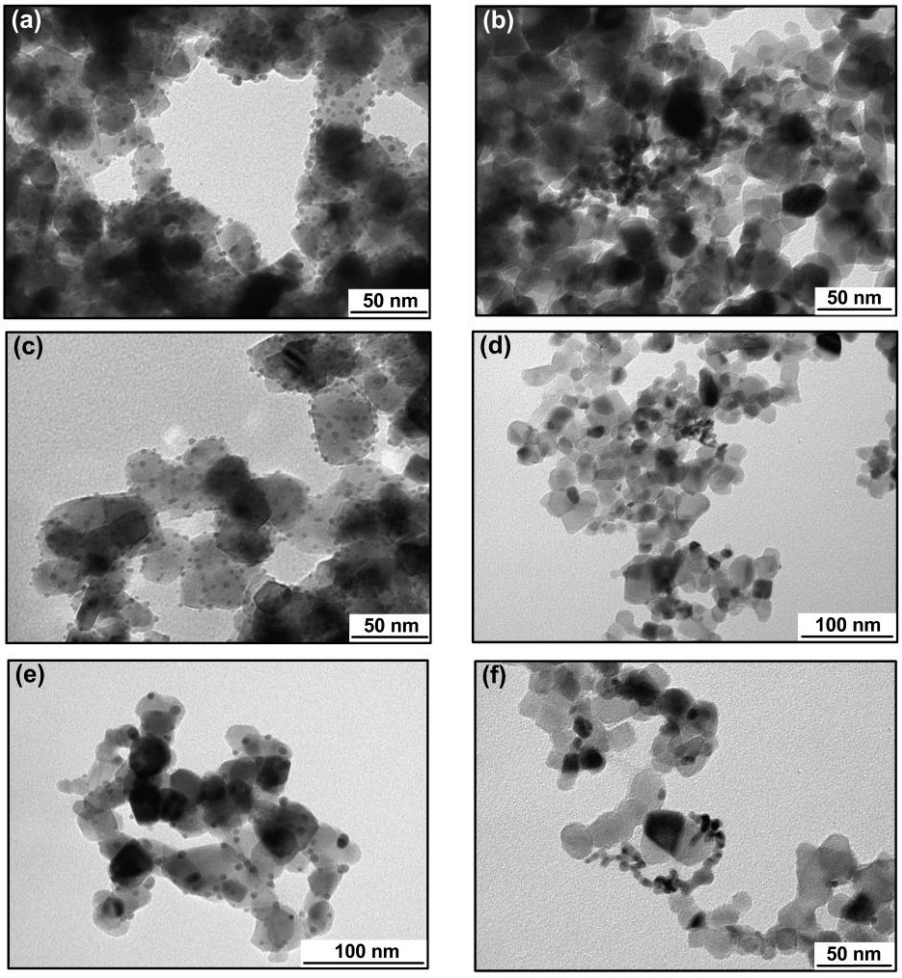

Figure 35. TEM images before and after two recovery experiments carried out at 80 ºC of **Pd/APTES@TiO_2-3** (a), (b); **Pd-PPh_3/APTES@TiO_2-2** (c), (d) and **PA@Pd-PPh_3/TiO_2-11** (e), (f).

In view of the little effect of reaction temperature on the stability of these catalysts, the following recycling tests were performed at 80 ºC. Initially, the series of catalysts **Pd-PPh_3/modifier@TiO_2-x** were employed to evaluate the effects of the modifiers on the reusability of the materials (Scheme 11).

$$CO_2 + H_2 \xrightarrow[\text{4 M } KHCO_3\text{, 5 ml milli-Q } H_2O]{\text{Pd-PPh}_3\text{/mod@TiO}_2} HCOOK$$

80 ºC, 15 h

Several cycles

Scheme 11. Hydrogenation CO_2 to formate at different temperatures.

The results obtained for two or three cycles employing **Pd/APTES@TiO_2-3**, **Pd-PPh_3/APTES@TiO_2-2**, **Pd-PPh_3/APA@TiO_2-3** and **Pd-PPh_3/IL-Cl@TiO_2-8** are summarized in Figure 36. In all cases, a strong decrease in activity was observed after 2 cycles. However, the catalysts containing the support previously modified by APTES suffered a minimal loss of activity during the first cycle and a large decrease during the 2nd cycle. In contrast, the catalysts where the support was modified by NH_2-PA and an organosilane containing a IL group suffered a large loss of activity during the 1st recycling but maintained their activity during the 2nd recycling. To check whether the activity could be maintained during a 3rd recycling, an extra run was carried out. However, the activity of both catalysts decreased during this last experiment. Once again, when TEM analysis of these catalysts was performed after the recycling experiments, large agglomerations were detected in all samples while no dramatic changes in mean size were measured on non-agglomerated Pd NPs.

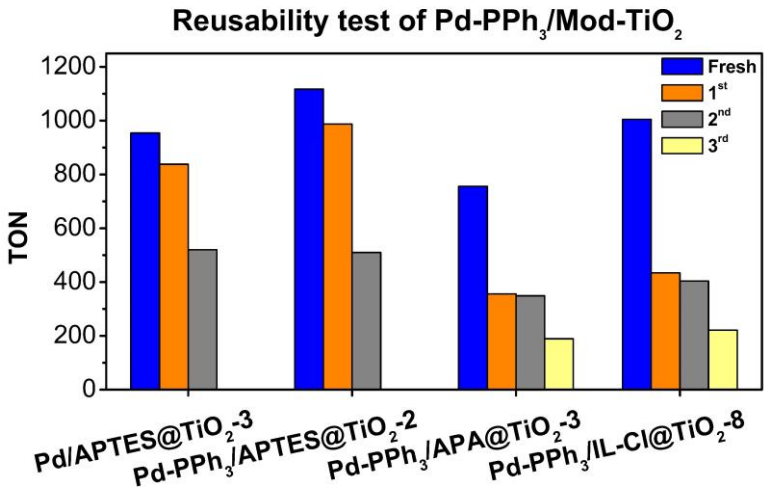

Figure 36. Recycling experiments with **Pd-PPh_3@modifier/TiO_2-x** for CO_2 hydrogenation to formate. Conditions: 20 mg of catalyst, 4 M $KHCO_3$, 5 ml milli-Q H_2O, pTotal= 36 bar, $p(CO_2) = p(H_2)$, 80 ºC, 15 h. TON= mmol formate/mmol total of Pd, calculated by NMR using 1,4-dioxane as internal standard.

The same conditions were employed for the recyclability experiments using **mod@Pd-PPh_3/TiO_2** catalysts (Scheme 12). The results obtained were summarized in Figure 37.

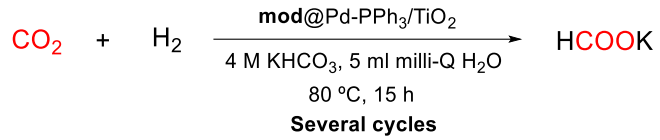

Scheme 12. Hydrogenation CO_2 to formate employing several catalysts at different temperatures.

For these catalysts, the initial activities were lower than when with those for which the Pd NPs were deposited over the modified supports. However, despite a general drop in activity at each run, several catalysts showed a much more gradual decrease. Indeed, **APTES@Pd-PPh$_3$/TiO$_2$-4** was the most active system of this series with an initial TON of 904. When recycled, this catalyst provided a TON of 724 after the 1st recycling, 662 after the 2nd recycling and 524 after the 3rd recycling.

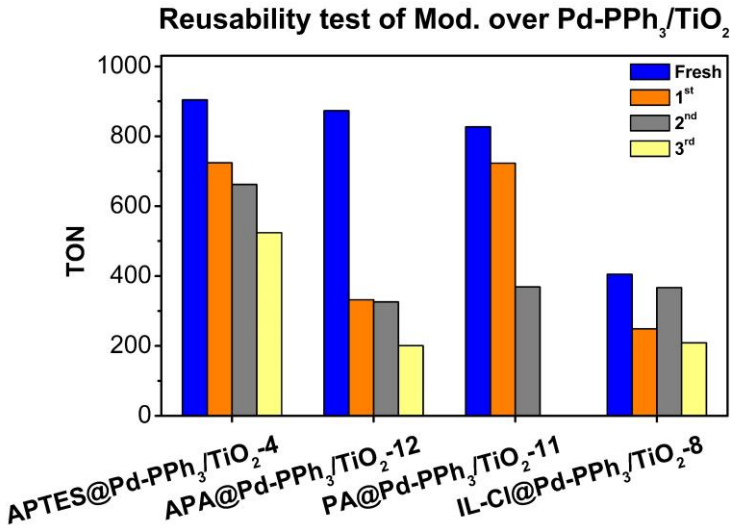

Figure 37. Recycling experiments with **modifier@Pd-PPh$_3$/TiO$_2$-x** for CO_2 hydrogenation to formate. Conditions: 20 mg of catalyst, 4 M $KHCO_3$, 5 ml milli-Q H_2O, pTotal= 36 bar, p(CO_2) = p(H_2), 80 ºC, 15 h. TON= mmol formate/mmol total of Pd, calculated by NMR using 1,4-dioxane as internal standard.

For the catalysts in which deposition of an organophosphonic acid was performed over the previously synthesized **Pd-PPh$_3$/TiO$_2$**, distinct behaviors were observed depending on the functional groups contained in the modifiers. For **APA@Pd-PPh$_3$/TiO$_2$-12**, containing an PA with an amine function, a drastic decrease in activity was observed during the first recycling, with a drop

of TON value from 873 to 332. No relevant decrease in activity was observed during the 2nd recycling while a drop to a TON of 201 was measured for the 3rd recycling. In contrast, when the catalyst contained a PA modifier with a butyl chain, the activity loss during the first recycling was much smaller (from a TON of 827 to 723) while a sudden drop to 369 was observed during the 2nd recycling.

For the catalysts modified by an organosilane containing a IL group, much lower activities were measured (TONs in the range 405 initially to 209 after 3 recyclings). Interestingly, although the catalyst activity suffered a severe decrease during the 1st recycling, an increase in TON from 249 to 367 was observed during the 2nd recycling prior to a decrease to 209. TEM analysis of the spent catalysts after 2 recyclings (Figure 38) revealed that the mean sizes of the Pd NPs in these materials was in all cases in the range 3.5-4 nm (Table 21). For **APTES@Pd-PPh$_3$/TiO$_2$-4**, which initially containing Pd NPs of *ca.* 2 nm, a significant increase in size was therefore evident.

Table 21. Particle size of different systems before and after two recovery experiments for CO_2 hydrogenation to formate. [a][b]

Entry	System	Size (nm)[c]	Size (nm)[d]
1	**APTES@Pd-PPh$_3$/TiO$_2$-4**	1.86 ± 0.69	3.55 ± 1.25
2[e]	**APA@Pd-PPh$_3$/TiO$_2$-12**	3.00 ± 1.14	3.58 ± 1.61
3[e]	**PA@Pd-PPh$_3$/TiO$_2$-11**	4.45 ± 1.68	3.59 ± 1.49
4	**IL-Cl@Pd-PPh$_3$/TiO$_2$-8**	2.38 ± 0.95	3.88 ± 1.78

[a]Reaction conditions: 20 mg of **modifier@Pd-PPh$_3$/TiO$_2$-x**, 4 M $KHCO_3$, 5 ml milli-Q H_2O, 80 ºC, pTotal= 36 bar, p(CO_2) = p(H_2), 15 h. [b]Particle size was obtained by TEM. [c]Before catalysis. [d]After 2nd cycle. [e]With aging.

Similar observation was made for **IL-Cl@Pd-PPh$_3$/TiO$_2$-8** for which the Pd NPs mean size increased from 2.4 nm to *ca*. 4 nm, although for this catalyst, the presence of agglomerations was more pronounced. For the catalysts modified with PAs, no large variation in size was observed but large agglomerations were detected. ICP analyses of the spent catalysts were also performed.

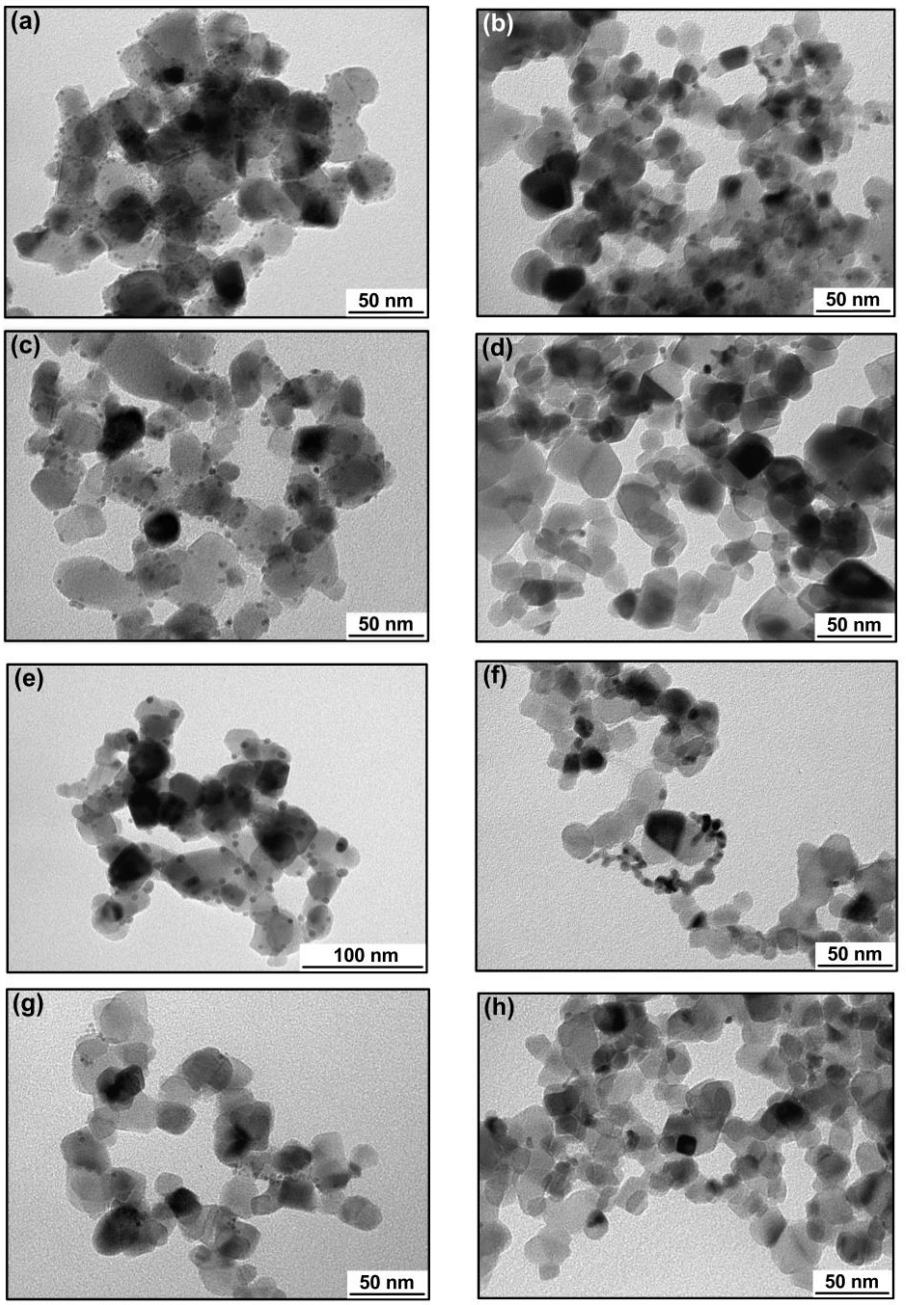

Figure 38. TEM images before and after two recovery experiments carried out at 80 ºC of **APTES@Pd-PPh$_3$/TiO$_2$-4** (a), (b); **APA@Pd-PPh$_3$/TiO$_2$-12** (c), (d); **PA@Pd-PPh$_3$/TiO$_2$-11** (e), (f) and **IL-Cl@Pd-PPh$_3$/TiO$_2$-8** (g), (h).

However, due to the small amount of materials recovered, the results were not conclusive as in all samples, larger Pd content were measured in the spent catalysts than in the fresh materials. These measurements will be repeated in the near future.

The catalyst **APTES@Pd-PPh$_3$/TiO$_2$-4** was also analyzed by TGA after the 3rd cycle (Figure 39), showing that the presence of organics remained at a value of *ca*. 5%.

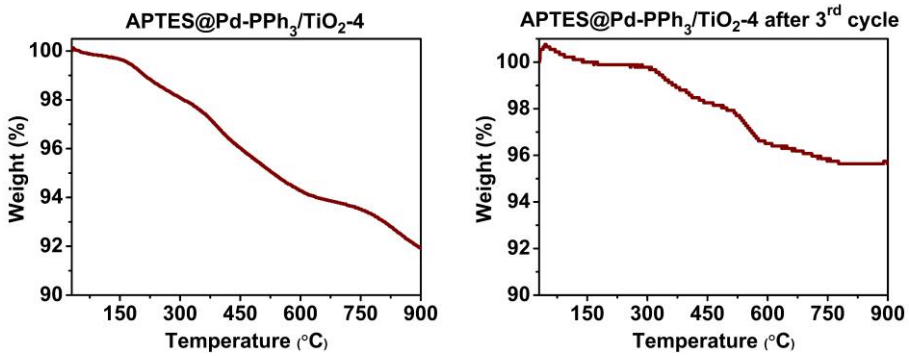

Figure 39. TGA before catalysis (a) and after three cycles (b) of **APTES@Pd-PPh$_3$/TiO$_2$-4**.

The recycling experiments described in this section therefore show that the synthetic procedure used for the modification of the **Pd-Ph$_3$/TiO$_2$** catalyst affects the reusability of these materials in the CO_2 hydrogenation into formate.

The catalysts formed by modification of the support prior to Pd NP deposition suffer a rapid decrease in activity during their recycling and reuse in spite of the initial beneficial effect. In contrast, some of the materials where the modifiers were deposited over the previously anchored Pd NPs onto TiO_2 show a much more gradual decrease in activity and reached a TON > 500 after the 3rd recycling.

To evidence the improvement in reusability obtained by catalyst modification in this chapter, the TON values obtained with the unmodified catalyst **Pd-PPh$_3$/TiO$_2$** during the recycling experiments are compared with those of **APTES@Pd-PPh$_3$/TiO$_2$-4** in Figure 40. Note that the experiments using **APTES@Pd-PPh$_3$/TiO$_2$-4** were performed at 80 ºC, while those using **Pd-PPh$_3$/TiO$_2$** were carried out at 60 ºC. Despite a superior initial activity of the unmodified catalyst, both materials exhibited similar TON values after the 1st

recycling and in the 2nd and 3rd recyclings, the modified catalyst clearly showed a better performance.

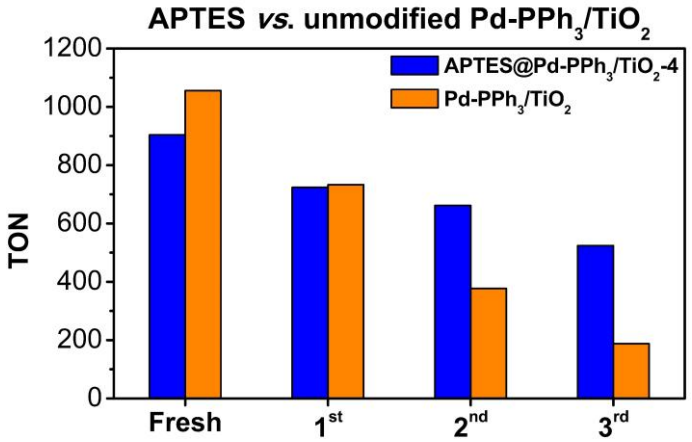

Figure 40. Comparation of recycling experiments with **APTES@Pd-PPh$_3$/TiO$_2$-4** and **Pd-PPh$_3$/TiO$_2$** for CO_2 hydrogenation to formate. Conditions: 20 mg of catalysts, 4 M $KHCO_3$, 5 ml milli-Q H_2O, pTotal= 36 bar, p(CO_2) = p(H_2), 15 h. Temperatures employed for **APTES@Pd-PPh$_3$/TiO$_2$-4** and **Pd-PPh$_3$/TiO$_2$** were 80 and 60 ºC, respectively. TON= mmol formate/mmol total of Pd, calculated by NMR using 1,4-dioxane as internal standard.

Important differences were observed by TEM analyses of the spent catalysts since for **APTES@Pd-PPh$_3$/TiO$_2$-4**, an increasing of size from 1.86 ± 0.69 nm to 3.55 ± 1.25 nm was measured after two cycles, but no agglomerations were observed. In contrast, the Pd NPs in **Pd-PPh$_3$/TiO$_2$** were largely agglomerated after the recyclings and exhibited a mean size of *ca.* 5 nm. These results thus suggest that the presence of APTES provided additional stabilization and as such limited the degree of agglomerations of the Pd NPs. This is in agreement with the results reported by Liu et al. who described that the coverage of Au NPs with APTES improved their recovery.[23]

5.3. Conclusions

In this chapter, a series of supported Pd-NPs based materials were successfully synthesized using modifiers of different nature (APTES, ILs and PAs) following two distinct approaches. The so-called reverse deposition approach requires in the first place to modify the TiO_2 support prior to Pd NPs deposition while the 2nd approach was the modification of a pre-synthesized

Pd-PPh$_3$/TiO$_2$, described in Chapter 3, by deposition of the modifier over its surface. For the first method employed, the most important remarks can be summarized as follow:

- Modifications with organosilanes provide smallest particle size compared to organophosphonic acids. The concentration of APTES and the nature of the anion in ILs have an effect on the NP size. When no -NH$_2$ group is present in organosilanes and organophosphonic acids, larger NPs, formation of unsupported NPs and agglomerations were observed.
- No significant differences in composition between samples were measured by ICP.

When modification of a pre-synthesized **Pd-PPh$_3$/TiO$_2$**, by deposition of the modifier over its surface was carried out, it is possible to conclude:

- Modifications with organosilanes provide smaller Pd NPs compared with systems obtained with the use of organophosphonic acids.
- No significant differences were detected in terms of content for the catalysts modified with organosilanes or organophosphonic acids. However, comparing the materials modified with APTES at different concentrations, it was observed that at higher amount of APTES employed, lower Pd content was obtained. This was attributed to leaching during the synthesis.
- The newly prepared materials, including the modifed TiO$_2$ supports, were characterized by techniques such as TEM, HRTEM, EDS, FT-IR, TGA, ICP etc. By HR-TEM a fine layer of modifier was revealed over the NPs.

All these catalysts were used in the hydrogenation of CO$_2$ to formate, and their performance compared with those of the unmodified catalyst **Pd-PPh$_3$/TiO$_2$**.

In view of the results obtained, the following conclusions can be drawn:

- The modification of the TiO$_2$ support by oganosilanes provided a beneficial effect in catalysis compared with the catalyst containing unmodified TiO$_2$ or TiO$_2$ modified by organophosphonic acids.
- The concentration is a key parameter during the support modification and lower values provide catalysts with higher activities. In contrast,

the temperature used during the modification, despite affecting the amount of organics at the surface of the support, does not influence the activity of the catalysts.

- The presence of a functional group (either NH_2 or imidazolium) in the modifiers improved the activity of the catalysts compared with those containing a simple alkyl chain.
- When using organophosphonic acids as modifiers, an aging step is beneficial to the activity of the resulting catalyst.
- The deposition of organosilane and organophosphonic acid modifiers over previously synthesized Pd NPs supported on TiO_2 was not beneficial, in most cases, to the activity of the catalyst.
- The deposition of organosilanes containing an IL substituent had a detrimental effect on the catalytic activity of the resulting materials.
- The presence of a functional group (either NH_2 or imidazolium) in the modifiers did not improve the activity of the catalysts compared with those containing a simple alkyl chain.

In terms of recyclability, the experiments performed showed that the synthetic procedure used for the modification of the **Pd-Ph_3/TiO_2** catalyst affect the reusability of these materials in the CO_2 hydrogenation into formate.

- The catalysts formed by modification of the support prior to Pd NP deposition suffer a rapid decrease in activity during their recycling and reuse in spite of the initial beneficial effect.
- Some of the materials where the modifiers were deposited over the previously anchored Pd NPs onto TiO_2 show a much more gradual decrease in activity and reached a TON > 500 after the 3rd recycling.

5.4. Experimental section

Materials and Methods

$Pd(dba)_2$, PPh_3, TiO_2 (Titanium (IV) oxide nanopowder, 21 nm primary particle size (TEM), ≥ 99.5% trace metals basis, rutile-anatase mixture, specific surface area 35-65 m^2/g) and the rest of compounds employed for modification were purchased from Sigma-Aldrich and used without any further purification. All solvents were dried from a solvent purification system (SPS) and deoxygenated. Tetrahydrofuran was further dried by refluxing in

the presence of sodium/acetophenone. Milli-Q water was employed in catalytic experiments. Any other solvent or reagent employed was reagent grade. Hydrogen (5.0) was purchased from Carburos Metálicos and CO_2 (5.3) was purchased from Abelló Linde. All the synthesis were performed using Schlenk techniques under Argon and glovebox using nitrogen as inert gas. The synthesis of nanoparticles were carried in Fischer-Porter bottles and catalytic tests were performed in a stainless steel high-pressure reactor Hel CAT-7 (7 x 10 ml).

Characterization techniques

Transmission Electron Microscopy (TEM)

Measurements were performed at the "Unitat de Microscopia dels Serveis de Recursos Cientifics I Tècnics de la Universitat Rovira i Virgili" in Tarragona with JEOL 1011 electron microscope operated at 100 kV with resolution of 3 Å. The samples were prepared by deposition of several drops of the reaction crude onto a copper grid. The particles size distributions were determined by a manual analysis. At least 300 particles on a given grid were measured to obtain a statistical size distribution and mean diameter.

Environmental Scanning Electron Microscope (ESEM)

The equipment used was FEI ESEM Quanta 600 from "Unitat de Microscopia dels Serveis de Recursos Cientifics I Tècnics de la Universitat Rovira i Virgili" in Tarragona. This microscope has an integrated analysis system OXFORD INSTRUMENTS. Energy-dispersive X-ray spectroscopy (EDX) analysis was carried out using this technique (BSED detector and HV (20 kV)).

Field Emission Scanning Electron Microscope (FESEM)

The microscope used for FESEM analysis was Themo Scientific Scios2. from "Unitat de Microscopia dels Serveis de Recursos Cientifics I Tècnics de la Universitat Rovira i Virgili" in Tarragona.

Inductively Coupled Plasma-Optical Emission Spectrometry (ICP-OES)

The inductively coupled plasma-optical emission spectrometer ICP-OES ARCOS FHS16 employed is in "Servei de Recursos Cientifics I Tècnics de la Universitat Rovira i Virgili" in Tarragona. The digestion of samples were made employing aqua regia in Milestone Ethos Easy Advanced microwave

digestion system. Quantification of metals is performed by comparison with the respective calibration curve constructed in the range of 0-20 ppm.

Nuclear Magnetic Resonance (NMR)

The equipment used were Bruker Avance Neo 400 with probe Smart (PI HR-400-S1-BBF/H/D-5.0-Z SP N) and sample case of 24 positions VARIAN Varian NMRSYS 400 (reverse probe 5mm Auto-X 1H/31P-15N, probe 5mm autoswitchable PFG and 5mm probe One Probe). Measurements were performed in "Servei de Recursos Cientifics I Tècnics de la Universitat Rovira i Virgili" in Tarragona. Dry and deoxygenated 1,4-dioxane was used as internal standard for catalytic experiments.

Thermogravimetric Analysis (TGA)

Thermogravimetric analysis experiments were carried out with a Mettler Toledo TGA2 thermo-balance equipped with a gas flow system. For a typical TGA experiment, a small amount of sample (5-30 mg) was placed in an alumina crucible and heated at a rate of 10 °C/min in N_2 atmosphere (50 ml/min) within a temperature range of 30-900 °C.

High Resolution Transmission Electron Microscopy (HR-TEM)

The morphology, crystallographic information and chemical analysis of the Pd nanoparticles were studied by Transmission electron microscopy in "Unitat de Microscopia dels Serveis de Recursos Cientifics I Tècnics de la Universitat Rovira i Virgili" in Tarragona.

TEM specimens were prepared by placing a drop of a Tetrahydrofuran (THF) solution containing the NPs onto a holey carbon coated copper micro-grid.

A JEOL F200 TEM ColdFEG operated at 200 kV was used for the Transmission Electron Microscopy characterization. TEM images were acquired with a Gatan OneView camera, a CMOS-based and optical fibre-coupled detector of 4096 by 4096 pixels. Gatan Digital Micrograph program was used to process the TEM images. STEM images (1024 x 1024 pixels) were recorded from the JEOL bright-field (BF) and High-Angle Annular Dark-Field (HAADF) detectors with a camera length of 400 mm. Samples were inserted in a JEOL beryllium double-tilt holder for energy dispersive X-Ray Spectroscopy (EDS). STEM-EDS mapping was recorded from an EDS

Centurio detector (silicon drift) with an effective area of 100 mm^2 and 133 eV of energy resolution. STEM-EDS maps (512 x 512 pixels) were processed with the JEOL Analysis software.

X-ray Photoelectron Spectroscopy (XPS)

XPS measurements were performed at room temperature with a SPECS PHOIBOS 150 hemispherical analyzer (SPECS GmbH, Berlin, Germany)) in a base pressure of 5 x 10-10 mbar using monochromatic Al K alpha radiation (1486.74 eV) as excitation source operated at 300 W. The energy resolution as measured by the FWHM of the Ag3d5/2 peak for a sputtered silver foil was 0.62 eV. The spectra were calibrated with respect to the C1s at 285.0 eV. Measurements were carried out in the Fundació Institut Català de Nanociència i Nanotecnologia (ICN2). The XPS data were curve-resolved using the CASAXPS software after Shirley background subtraction. The spectra were fitted with the minimum number of peaks needed to reproduce the spectral features.

Analyses were carried out with CasaXPS software and calibrating with C1s at 285 eV in the overview spectra.

Synthesis of catalytic materials

Modification of TiO_2 with *n*-propyltriethoxysilane (PTES) and (3-aminopropyl)triethoxysilane (APTES)

In a general synthesis of (A)PTES@TiO_2-x, a solution (mixture EtOH:milli-Q H_2O 95:5 v/v), of the accorded concentration of PTES or APTES were prepared into a Schlenk (under Ar). Then, the corresponding amount of TiO_2 (mmol (A)PTES/mg TiO_2) was added to the solution under vigorous stirring. Reaction was stirred at room temperature overnight. Then, the mixture was centrifuged. Supernatant was removed and the solid was washed several times with milli-Q H_2O and EtOH and was dried at 80 ºC under vacuum for several hours. Other supports were synthesized with variations in conditions. It is specified when it is the case. For synthesis performed at 120 ºC, 2 g of TiO_2, accorded amount of (A)PTES and 10 ml of EtOH were introduced in an autoclave. The mixture was heated 4 h at 120 ºC. After synthesis, modified-TiO_2 was centrifuged and washed several times with milli-Q H_2O and EtOH and it was dried at 105 ºC into an oven overnight.

Synthesis of Ionic Liquids (ILs)

1. *Synthesis of 1-n-butylimidazole*

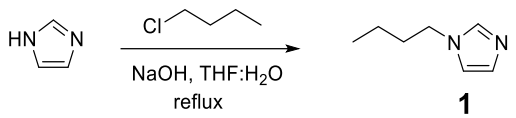

1

1: 1-*n*-butylimidazole was synthesized according to literature procedures[60] with some variations. In a round-bottom flask, imidazole (6.81 g, 0.1 mol) and NaOH (4 g, 0.1 mol) were added to a round-bottom flask with H_2O (4 ml) and stirred until the complete dissolution of imidazole. Then, 1-chlorobutane (11 ml, 0.105 mol) was diluted with THF (12.1 ml) and was added to the reaction flask. Reaction was left under reflux for 12 h. After this time, the crude was cooled to r.t. and was rotaevaporated to remove THF. Water was added (20 ml) and the product was extracted with DCM (3 x 40 ml). Organic phases were combined and washed with 10% NaOH solution (2 x 8 ml) and H_2O (3 x 8 ml) and dried over sodium sulfate. Filtration and evaporation of the volatiles provided the desired product as a yellow oil (9.04 g, 73%). NMR is in agreement with reported spectra.[61] ^{1}H-NMR (400 MHz, DMSO-d_6): δ 7.60 (s, 1 H), 7.15 (s, 1 H), 6.87 (s, 1 H), 3.94 (t, J= 7 Hz, 2 H), 1.71−1.62 (m, 2 H), 1.26−1.16 (m, 2 H), 0.87 (t, J= 7.4 Hz, 3 H).

2. *Synthesis of 1-Butyl-3-[3-(triethoxysilyl)propyl]imidazolium Chloride*

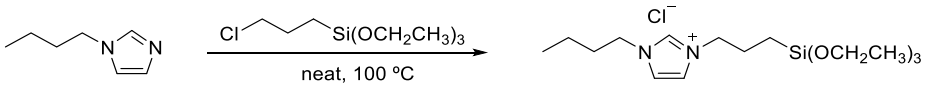

1 **2**

The product **2** was synthesized according to literature procedures[62] with some variations. In a 100 ml Schlenk, the product **1** (5.1 ml, 38.8 mmol) and (3-chloropropyl)triethoxysilane (9.35 ml, 38.8 mmol) were introduced. Then, the mixture was heated at 100 ºC for 48 h and cooled to room temperature. The product was washed several times with Et_2O and dried under vacuum at 60 ºC to obtain a yellow/orange oil (13.01 g, 92%). NMR is in agreement with reported spectra.[63] ^{1}H-NMR (400 MHz, DMSO-d_6): δ 9.44 (s, 1 H), 7.85 (s, 2 H), 4.23-4.13 (m, J= 7.0 Hz, 4 H), 3.73 (q, J= 7.0 Hz, 6 H), 1.87-1.73 (m, 4 H), 1.23 (m, 2 H), 1.13 (t, J= 6.9 Hz, 9 H), 0.88 (t, J= 7.44 Hz, 3 H), 0.51-0.46 (m, 2 H).

3. *Synthesis of 1-Butyl-3-[11-(triethoxysilyl)undecyl]imidazolium Bis(trifluoromethane)sulfonimide*

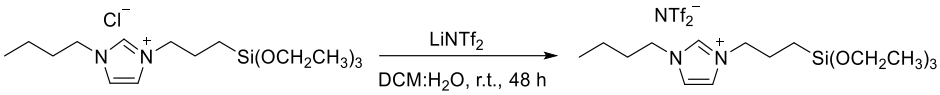

2 **3**

The product **3** was synthesized according to literature procedures but including some variations.[41c,64] In a 100 ml Schlenk, the product **2** (500 mg, 1.37 mmol) and $LiNTf_2$ (413 mg, 1.44 mmol) were introduced and 2.3 ml of H_2O and 2.5 ml of DCM were added. Then, the mixture was stirred at r.t. for 48 h and the product was extracted with DCM several times and the organic phase was washed with H_2O. $MgSO_4$ was added and after filtration and drying at 60 ºC, a brown oil was obtained. (649.0 mg, 91%) NMR is in agreement with reported spectra.[41c,44] ^{1}H-NMR (400 MHz, DMSO-d_6): δ 9.17 (s, 1 H), 7.79 (d, 2 H), 4.19-4.10 (m, 4 H), 3.74 (q, J= 6.97 Hz, 6 H), 1.87-1.73 (m, 4 H), 1.29-1.21 (m, J= 7.44 Hz, 2 H), 1.14 (t, J= 7.23 Hz, 9 H), 0.90 (t, J= 7.31 Hz, 3 H), 0.51-0.47 (m, 2 H).

4. *Synthesis of 1-Butyl-3-[3-(triethoxysilyl)propyl]imidazolium Acetate*

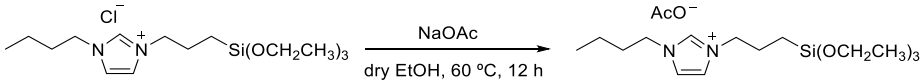

2 **4**

The product **4** was synthesized according to literature procedures but including some variations.[44,65] In a 25 ml Schlenk, the product **2** (3 g, 8.2 mmol and NaOAc (783.8 mg, 9.55 mmol) were introduced. Dry EtOH was added (11 ml) and the mixture stirred at 60 ºC for 12 h. At this point, the mixture was cooled to r.t. and the product was washed several times with EtOH and dried under vacuum at 60 ºC to give an orange oil as product (2.95 g, 93% yield). ^{1}H-NMR (500 MHz, DMSO-d_6): δ 9.51 (s, 1 H), 7.82 (d, 2 H), 4.22-4.11 (m, 4 H), 3.74 (q, J= 6.98 Hz, 6 H), 1.87-1.73 (m, 4 H), 1.53 (s, 3 H), 1.28-1.20 (m, 2 H), 1.14 (t, J= 7.08 Hz, 9 H), 0.89 (t, J= 7.32 Hz, 3 H), 0.51-0.45 (m, 2 H).

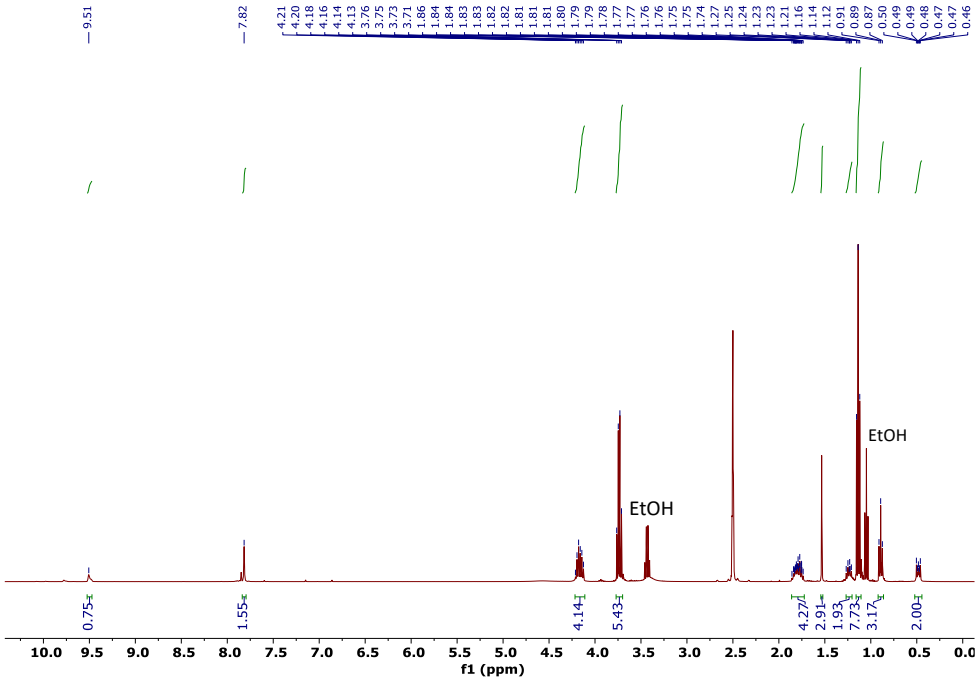

Figure S1. ^{1}H-NMR of compound **4** in DMSO-d_6.

Modification of TiO_2 with Ionic Liquids (ILs)

The synthesis of IL-Cl/TiO_2-8 was performed according to reported procedures.[62] A suspension of 2 g of TiO_2 in 80 ml of milli-Q H_2O was added to a previously prepared solution of 659.08 mg (1.8 mmol) of IL-Cl in 2 ml of milli-Q H_2O. Mixture was stirred at 80 ºC for 12 h. After reaction, the mixture was centrifuged and washed twice with milli-Q and once with EtOH. After that, it was dried under vacuum at 60 ºC.

For other ILs (Cl^-, NTf_2^- and OAc^-, 0.12 and 0.13 M): the solution of IL-Cl was diluted in dry toluene to get the desired concentration and TiO_2 was added (500 mg). The mixture was stirred at reflux overnight. Then, it was cooled and then centrifuged (after this, a yellow layer was observed over the solid). Then, it was washed several times with acetone. It was dry under vacuum at 60 ºC. For NTf_2^-, the same procedure was followed. For OAc^-, TiO_2 was added to a solution of IL-OAc (mixture EtOH:milli-Q H_2O 95:5 v/v) and the mixture was heated at 80 ºC overnight. The product was washed with EtOH several times and dried under vacuum at 60 ºC.

Modification of TiO_2 with Phosphonic acids (PAs)

The modification of TiO_2 with PAs was performed according to literature procedures with some variations.[47,52,66] Solutions contained 83.35 µmol of modifier per each square meter of TiO_2 nanopowder which corresponded approximately to a 10-fold excess in respect to build a monolayer in the surface of support.

Solution 10 mM of 3-aminopropylphosphonic acid (APA), (1.46 mmol, 202.84 mg) in 146 ml of milli-Q H_2O was prepared. Then, 0.5 g of TiO_2 was added and the mixture was stirred at r.t. overnight. After this time, the suspension was centrifuged, washed with abundant milli-Q water, EtOH and acetone. The solid was dried at 120 ºC in an oven. One of prepared samples was not subject to an annealing treatment. But it is necessary to produce condensation reactions to give strong bonds between PAs and metal oxide.[11] So, in this case, after the reaction, the solid was separated by centrifugation, the solvent was removed and solid was placed into an oven at 100 ºC overnight. After that, the solid was aged into a Quartz furnace at 120 ºC under air flow during 6 h. Then, it was washed with abundant milli-Q water and centrifuged every time (5 times). The solid was dried overnight at 100 ºC. When butylphosphonic acid was employed (PA), the synthesis was performed under the same conditions. The only difference was that THF was used as reaction media and for washing and centrifugation.

Synthesis of Pd NPs with PPh_3 as ligand over different modified TiO_2 supports through Organometallic approach

The catalysts were prepared to obtain a 4 wt% theorical content of Pd over TiO_2. In a common experiment, metal precursor ($Pd(dba)_2$), 0.2 eq. of stabilizer (PPh_3) and modified TiO_2 were weighted in the glove box and charged in a Fischer-Porter bottle. Then, solvent (THF) was added, the Fischer-Porter was closed, purged with hydrogen several times and then charged with 3 bar of H_2. The mixture was then heated at 60 ºC and stirred at 700 rpm overnight. After the reaction, the mixture was cooled to room temperature and degassed. Samples for TEM analysis were prepared by deposition of several drops of the reaction crude onto a copper grid. The rest of the reaction crude was concentrated and washed several times with

abundant hexane. The catalyst was dried under vacuum during several hours.

Deposition of modifier over previously synthesized Pd-PPh$_3$/TiO$_2$ systems

PTES and APTES: Specified concentration of PTES or APTES (and determined mmol (A)PTES/mg **Pd-PPh$_3$/TiO$_2$** ratio) and **Pd-PPh$_3$/TiO$_2$** previously synthesized were mixed. At r.t., the synthesis was carried out overnight in Schlenk using a mixture of 95% EtOH, 5% milli-Q H_2O, while reactions at 120 ºC reaction were performed in an autoclave during 4 h using EtOH as solvent. In both cases, samples were dried overnight in an oven at 105 ºC and stored inside the glove box.

ILs: Mixture of a specified concentration of IL-Anion and previously synthesized **Pd-PPh$_3$/TiO$_2$** system was prepared at r.t. using a mixture of 95% EtOH, 5% milli-Q H_2O, overnight.

PAs: Mixture of a specified concentration of PAs and previously synthesized **Pd-PPh$_3$/TiO$_2$** system were mixed at r.t. using milli-Q H_2O as solvent (for synthesis with APA) or THF (for synthesis with PA), overnight.

X-ray photoelectron spectroscopy (XPS)

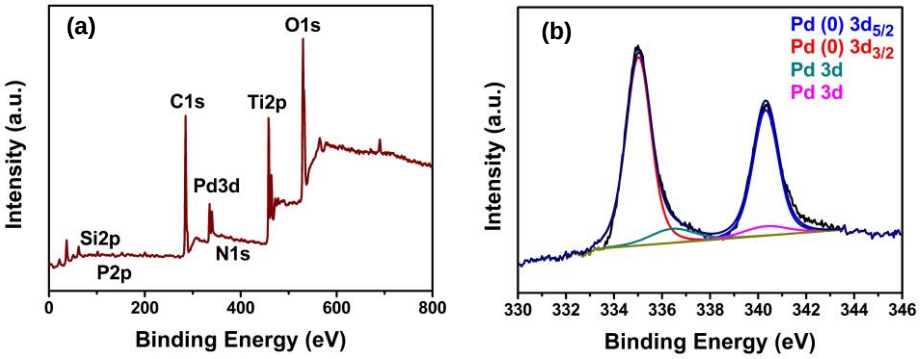

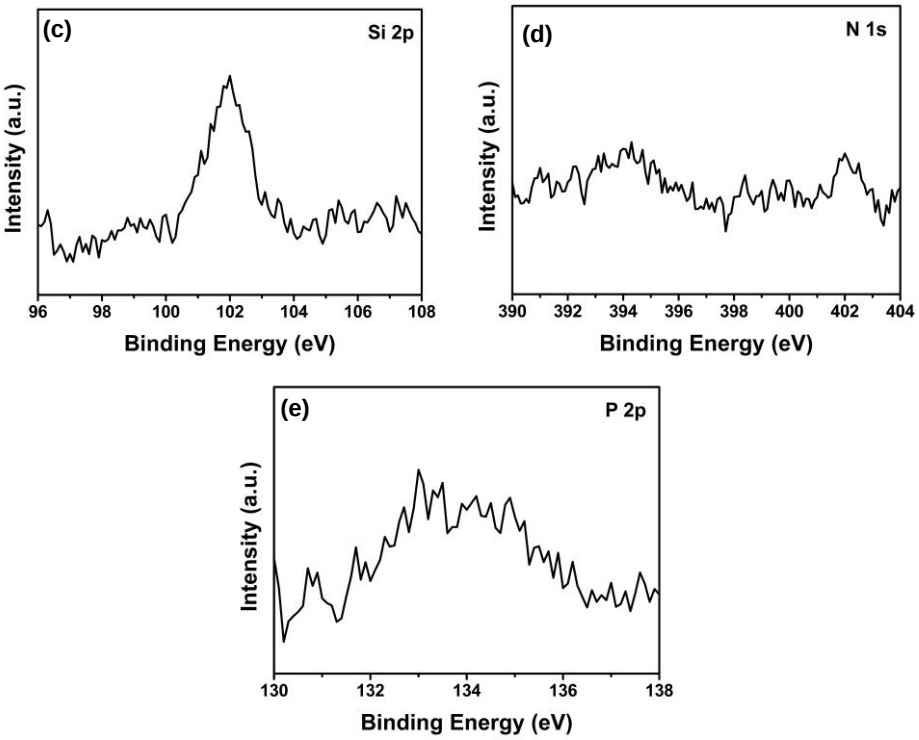

Figure S2. XPS images of **Pd-PPh$_3$/IL-Cl@TiO$_2$-8**: overview (a), Pd3d (b), Si2p (c), N1s (d), P2p (e).

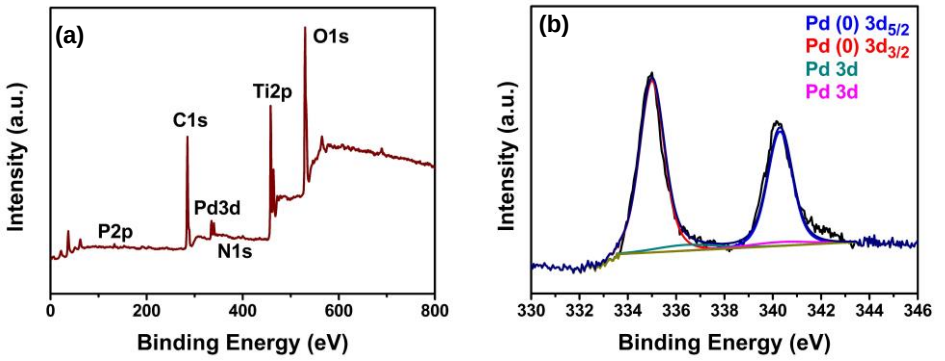

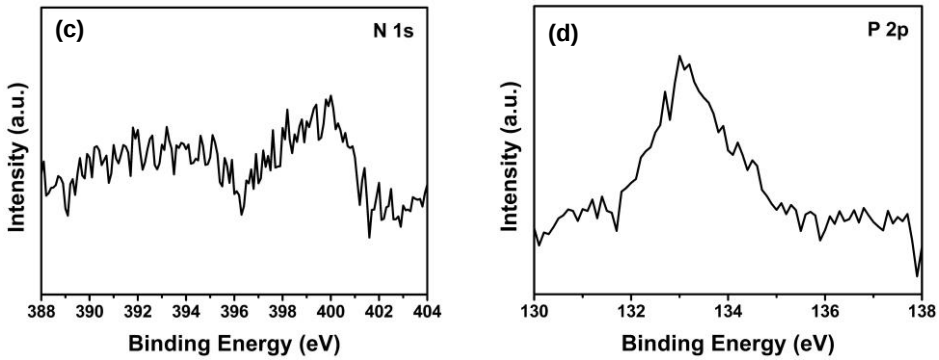

Figure S3. XPS images of **Pd-PPh$_3$/APA@TiO$_2$-3**: overview (a), Pd3d (b), N1s (c), P2p (d).

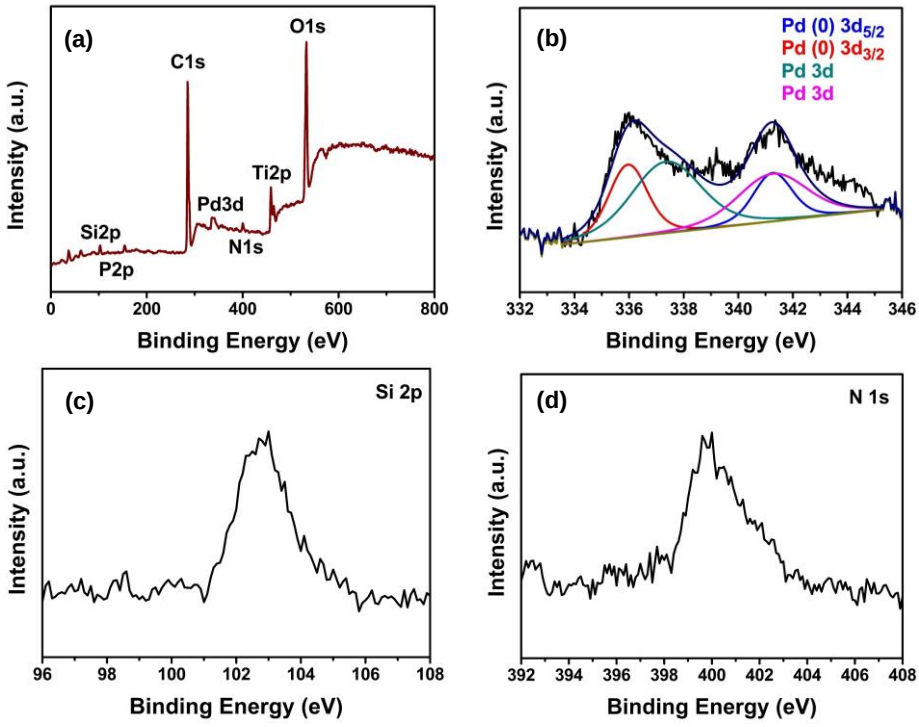

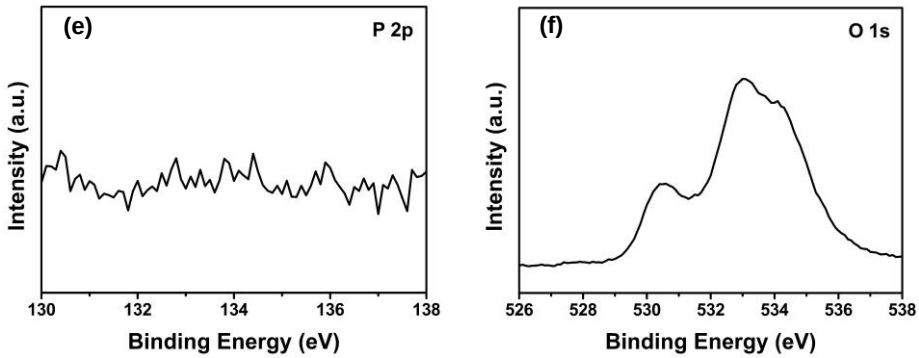

Figure S4. XPS images of **APTES@Pd-PPh$_3$/TiO$_2$-4**: overview (a), Pd3d (b), Si2p (c), N1s (d), P2p (e) and O1s (f).

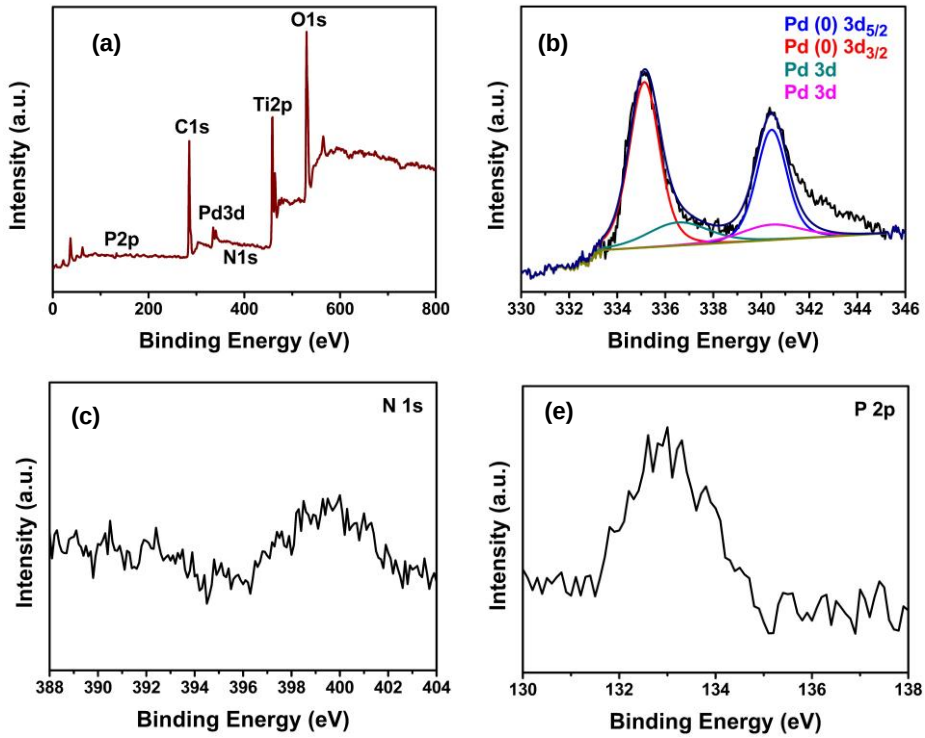

Figure S5. XPS images of **APA@Pd-PPh$_3$/TiO$_2$-12**: overview (a), Pd3d (b), N1s (c), P2p (d).

Catalytic experiments for CO_2 reduction to formate

Stainless steel high-pressure reactor HEL CAT-7 (7 x 10 ml) was charged with TiO_2 supported palladium nanoparticles (20 mg), 20 mg of 1,4-dioxane

and 5 ml of a 4 M base solution employing milli-Q water. The reactor was first flushed with 3 cycles of hydrogen to remove the air. Then, the reactor was charged with 10 bar of H_2 and heated at 40 ºC under stirring for twenty minutes. At this point, the reactor was depressurized, purged several times with CO_2 and charged with 18 bar of CO_2 and let under stirring for 20 minutes. Then, the reactor was charged with 18 bar of H_2 (1:1, CO_2:H_2) and heated to reach the temperature under 600 rpm of stirring. The experiment was left 15 h and after this time, the reactor was allowed to cool in an ice bath. When the reactor was cooled, it was depressurized and opened. A small amount of the sample was centrifuged and 100 µl of supernatant were analysed by NMR using D_2O as deuterated solvent.

- **Characterization data of spent catalysts after one catalysis**

Table S1. Loadings for Pd, P and Si of different systems before and after one catalytic experiment for CO_2 hydrogenation to formate.[a][b]

Entry	System	Pd wt%[c]	P wt%[c]	Si wt%[c]	Pd wt%[d]	P wt%[d]
1	**Pd-PPh_3/PTES @TiO_2-1**	3.46	0.18	0.85	3.30	0.06
2	**Pd-PPh_3/APTES @TiO_2-2**	2.75	0.19	0.57	2.55	0.03
3[e]	**Pd/APTES@ TiO_2-3**	3.36	-	0.81	3.40	0.01
4	**Pd-PPh_3/IL-Cl@TiO_2-8**	3.25	-	-	3.37	0.05
5	**Pd-PPh_3/IL-OAc@TiO_2-11**	3.17	0.24	0.89	3.35	0.03
6[f]	**Pd-PPh_3/PA@TiO_2-1**	2.68	0.82	-	3.23	0.04

[a]Reaction conditions: 20 mg of **modifier@Pd-PPh_3/TiO_2-x**, 4 M $KHCO_3$, 5 ml milli-Q H_2O, 80 ºC, pTotal= 36 bar, p(CO_2) = p(H_2), 15 h. [b]Pd, P and Si contents were obtained by ICP. [c]Before catalysis. [d]After catalysis. [e]In absence of PPh_3. [f]With aging.

Table S2. Particle size of different systems before and after one catalytic experiment for CO_2 hydrogenation to formate.[a][b]

Entry	System	Particle size (nm)[c]	Particle size (nm)[d]
1	**Pd-PPh$_3$/PTES@TiO$_2$-1**	5.75 ± 1.79	6.86 ± 0.65
2	**Pd-PPh$_3$/APTES@TiO$_2$-2**	2.23 ± 0.78	4.13 ± 1.58
3[e]	**Pd/APTES@TiO$_2$-3**	2.52 ± 0.95	4.09 ± 0.93
4	**Pd-PPh$_3$/IL-Cl@TiO$_2$-8**	1.89 ± 0.82	4.61 ± 2.07
5	**Pd-PPh$_3$/IL-OAc@TiO$_2$-11**	2.48 ± 0.97	4.35 ± 1.89
6[f]	**Pd-PPh$_3$/PA@TiO$_2$-1**	Out of support and agglom.	3.73 ± 2.15

[a]Reaction conditions: 20 mg of **modifier@Pd-PPh$_3$/TiO$_2$-x**, 4 M $KHCO_3$, 5 ml milli-Q H_2O, 80 ºC, pTotal= 36 bar, p(CO_2) = p(H_2), 15 h. [b]Particle size was obtained by TEM. [c]Before catalysis. [d]After catalysis. [e]In absence of PPh_3. [f]With aging.

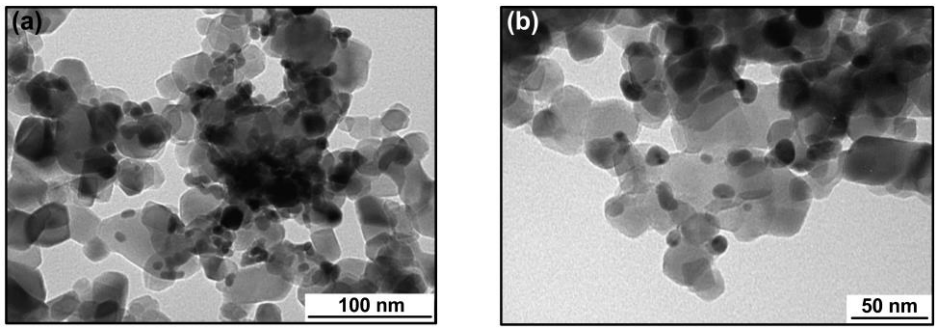

Figure S6. TEM images from **Pd-PPh$_3$/PTES@TiO$_2$-1** before (a) and after (b) catalysis at 80 ºC.

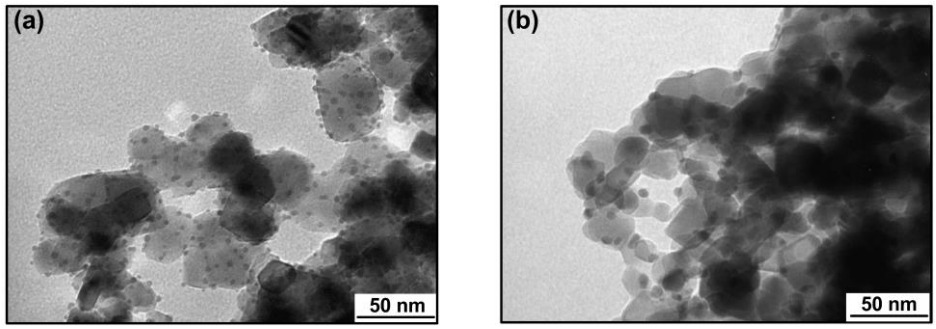

Figure S7. TEM images from **Pd-PPh$_3$/APTES@TiO$_2$-2** before (a) and after (b) one catalysis at 80 ºC.

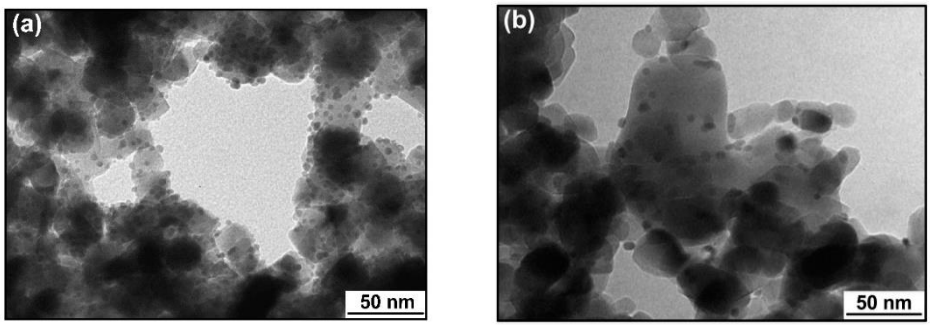

Figure S8. TEM images from **Pd/APTES@TiO_2-3** before (a) and after (b) catalysis at 80 ºC.

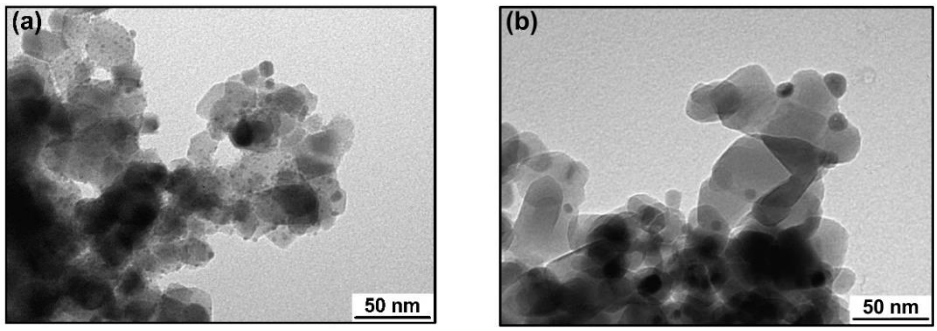

Figure S9. TEM images from **Pd-PPh_3/IL-Cl@TiO_2-8** before (a) and after (b) catalysis at 80 ºC.

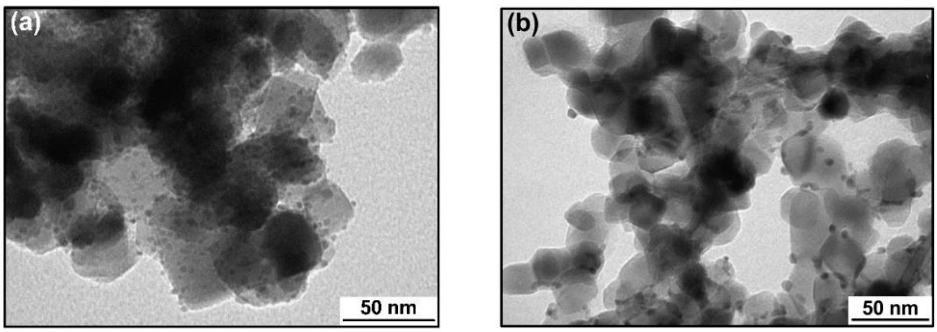

Figure S10. TEM images from **Pd-PPh_3/IL-OAc@TiO_2-11** before (a) and after (b) one catalysis at 80 ºC.

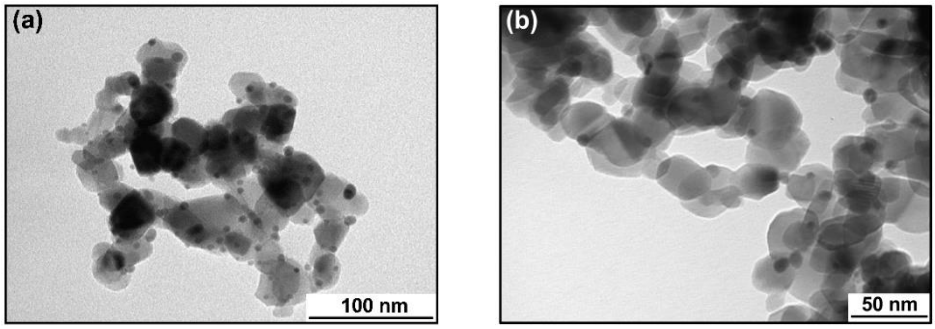

Figure S11. TEM images from **Pd-PPh$_3$/PA@TiO$_2$-1** before (a) and after (b) catalysis at 80 ºC.

- **Effect of time**

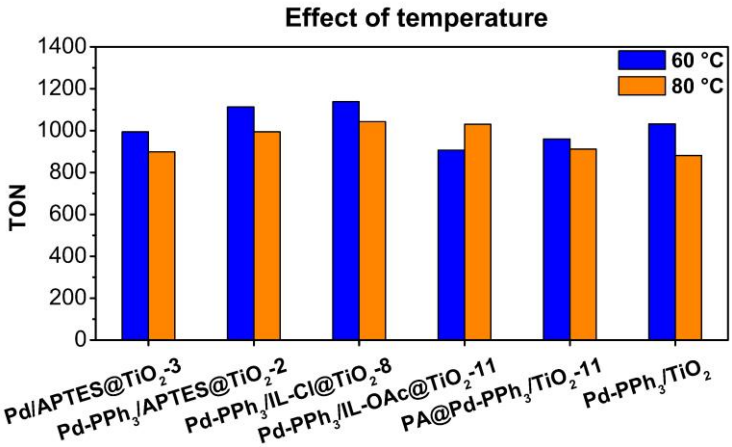

Figure S12. Effect of time in catalytic activity of different catalyst for CO_2 hydrogenation to formate. Conditions: 20 mg of **Pd-PPh$_3$/modifier@TiO$_2$-x** or **modifier@Pd-PPh$_3$/TiO$_2$-x**, 4 M $KHCO_3$, 5 ml milli-Q H_2O, 80 ºC, pTotal= 36 bar, $p(CO_2) = p(H_2)$. TON= mmol formate/mmol total of Pd, calculated by NMR using 1,4-dioxane as internal standard.

Table S3. Effect of time in catalytic activity of different catalyst for CO_2 hydrogenation to formate.[a]

Entry	System	Time (h)	TON[b]
1[c]	**Pd/APTES@TiO$_2$-3**	15	917
2[c]	**Pd/APTES@TiO$_2$-3**	30	1065
3	**Pd-PPh$_3$/APTES@TiO$_2$-2**	15	994
4	**Pd-PPh$_3$/APTES@TiO$_2$-2**	30	1240

5	**Pd-PPh$_3$/IL-Cl@TiO$_2$-8**	15	1043
6	**Pd-PPh$_3$/IL-Cl@TiO$_2$-8**	30	929
7	**Pd-PPh$_3$/IL-OAc@TiO$_2$-11**	15	1030
8	**Pd-PPh$_3$/IL-OAc@TiO$_2$-11**	30	1103
9[d]	**PA@Pd-PPh$_3$/TiO$_2$-11**	15	912
10[d]	**PA@Pd-PPh$_3$/TiO$_2$-11**	30	920
11	**Pd-PPh$_3$/TiO$_2$**	15	881
12	**Pd-PPh$_3$/TiO$_2$**	30	876

[a]Reaction conditions: 20 mg of **Pd-PPh$_3$/modifier@TiO$_2$-x** or **modifier@Pd-PPh$_3$/TiO$_2$-x**, 4 M $KHCO_3$, 5 ml milli-Q H_2O, 80 ºC, pTotal= 36 bar, p(CO_2) = p(H_2). [b]TON= mmol formate/mmol total of Pd, calculated by NMR using 1,4-dioxane as internal standard. [c]In absence of PPh_3. [d]With aging.

- **Effect of temperature**

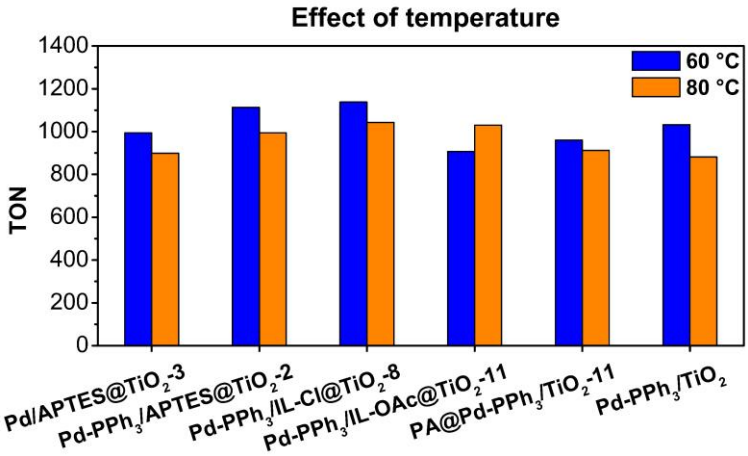

Figure S13. Effect of temperature in catalytic activity of different catalyst for CO_2 hydrogenation to formate. Conditions: 20 mg of **Pd-PPh$_3$/modifier@TiO$_2$-x** or **modifier@Pd-PPh$_3$/TiO$_2$**, 4 M $KHCO_3$, 5 ml milli-Q H_2O, pTotal= 36 bar, p(CO_2) = p(H_2), 15 h. TON= mmol formate/mmol total of Pd, calculated by NMR using 1,4-dioxane as internal standard.

Table S4. Effect of temperature in catalytic activity of different catalyst for CO_2 hydrogenation to formate.[a]

Entry	System	Temperature (ºC)	TON[b]
1[c]	**Pd/APTES@TiO_2-3**	60	994
2[c]	**Pd/APTES@TiO_2-3**	80	899
3	**Pd-PPh_3/APTES@TiO_2-2**	60	1113
4	**Pd-PPh_3/APTES@TiO_2-2**	80	994
5	**Pd-PPh_3/IL-Cl@TiO_2-8**	60	1138
6	**Pd-PPh_3/IL-Cl@TiO_2-8**	80	1043
7	**Pd-PPh_3/IL-OAc@TiO_2-11**	60	907
8	**Pd-PPh_3/IL-OAc@TiO_2-11**	80	1030
9[d]	**PA@Pd-PPh_3/TiO_2-11**	60	960
10[d]	**PA@Pd-PPh_3/TiO_2-11**	80	912
11	**Pd-PPh_3/TiO_2**	60	1056
12	**Pd-PPh_3/TiO_2**	80	881

[a]Reaction conditions: 20 mg of **Pd-PPh_3/modifier@TiO_2-x** or **modifier@Pd-PPh_3/TiO_2**, 4 M $KHCO_3$, 5 ml milli-Q H_2O, pTotal= 36 bar, $p(CO_2) = p(H_2)$, 15 h. [b]TON= mmol formate/mmol total of Pd, calculated by NMR using 1,4-dioxane as internal standard. [c]In absence of PPh_3. [d]With aging.

Recycling experiments

After every catalytic experiment, the content of a catalysis vial was filtered through a Nylon membrane. The solid was washed several times with abundant milli-Q H_2O and dried under vacuum for several hours. Then, a new catalysis was carried out.

- **Reusability tests at different temperatures**

Table S5. Recycling experiments with different systems at 60 ºC for CO_2 hydrogenation to formate.[a]

Entry	System	Fresh[b]	1st[b]	2nd[b]
1[c]	**Pd/APTES@TiO_2-3**	963	802	408
2	**Pd-PPh_3/APTES@TiO_2-2**	1118	943	380

3[d]	**PA@Pd-PPh$_3$/TiO$_2$-11**	915	531	206

[a]Reaction conditions: 20 mg of catalyst, 4 M $KHCO_3$, 5 ml milli-Q H_2O, 60 ºC, pTotal= 36 bar, $p(CO_2) = p(H_2)$, 15 h. [b]TON= mmol formate/mmol total of Pd, calculated by NMR using 1,4-dioxane as internal standard. [c]In absence of PPh_3. [d]With aging.

Table S6. Particle size of different systems before and after recycling experiments for CO_2 hydrogenation to formate.[a][b]

Entry	System	Pd wt%[c]	P wt%[c]	Si wt%[c]	Pd wt%[d]
1[e]	**Pd/APTES@TiO$_2$-3**	3.36	-	0.81	3.57
2	**Pd-PPh$_3$/APTES@TiO$_2$-2**	2.75	0.19	0.57	2.43
3[f]	**PA@Pd-PPh$_3$/TiO$_2$-11**	3.10	0.82	-	3.25

[a]Reaction conditions: 20 mg of catalyst, 4 M $KHCO_3$, 5 ml milli-Q H_2O, 60 ºC, pTotal= 36 bar, $p(CO_2) = p(H_2)$, 15 h. [b]Particle size was obtained by TEM. [c]Before catalysis. [d]After 2nd cycle. [e]In absence of PPh_3. [f]With aging.

Table S7. Particle size of different systems before and after recycling experiments for CO_2 hydrogenation to formate.[a][b]

Entry	System	Size (nm)[c]	Size (nm)[d]
1[e]	**Pd/APTES@TiO$_2$-3**	2.52 ± 0.95	3.26 ± 0.97
2	**Pd-PPh$_3$/APTES@TiO$_2$-2**	2.23 ± 0.78	3.26 ± 0.90
3[f]	**PA@Pd-PPh$_3$/TiO$_2$-11**	4.45 ± 1.68	3.87 ± 1.23

[a]Reaction conditions: 20 mg of catalyst, 4 M $KHCO_3$, 5 ml milli-Q H_2O, 60 ºC, pTotal= 36 bar, $p(CO_2) = p(H_2)$, 15 h. [b]Particle size was obtained by TEM. [c]Before catalysis. [d]After 2nd cycle. [e]In absence of PPh_3. [f]With aging.

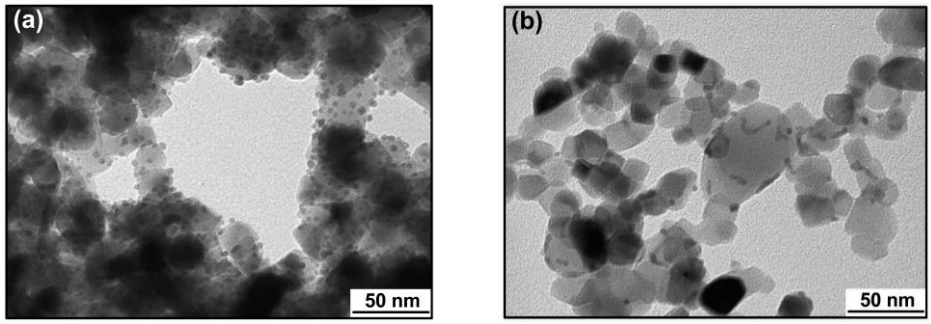

Figure S14. TEM images of **Pd/APTES@TiO$_2$-3** before (a) and after (b) two recovery experiments carried out at 60 ºC.

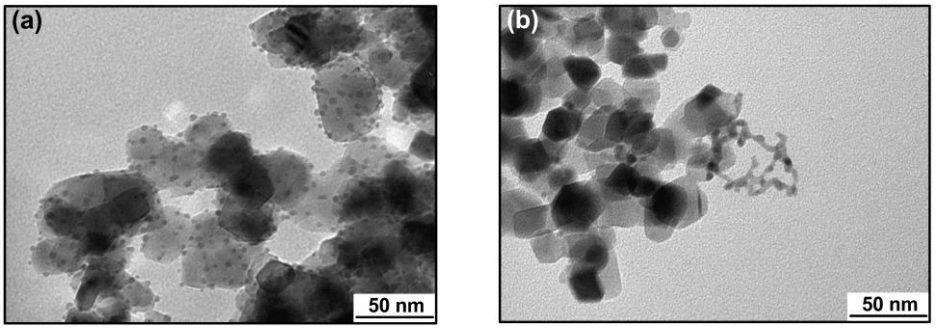

Figure S15. TEM images of **Pd-PPh$_3$/APTES@TiO$_2$-2** before (a) and after (b) two recovery experiments carried out at 60 ºC.

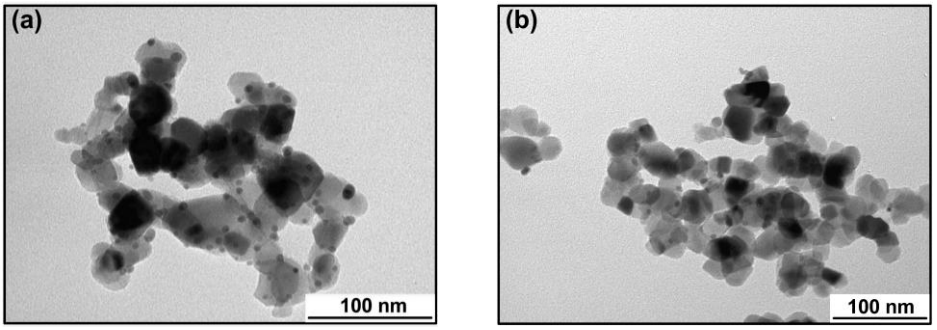

Figure S16. TEM images of **PA@Pd-PPh$_3$/TiO$_2$-11** before (a) and after (b) two recovery experiments carried out at 60 ºC.

Table S8. Recycling experiments with different systems at 80 ºC for CO_2 hydrogenation to formate.[a]

Entry	System	Fresh[b]	1st[b]	2nd[b]
1[c]	**Pd/APTES@TiO$_2$-3**	954	838	516
2	**Pd-PPh$_3$/APTES@TiO$_2$-2**	1117	987	510
3[d]	**PA@Pd-PPh$_3$/TiO$_2$-11**	827	723	369

[a]Reaction conditions: 20 mg of catalyst, 4 M $KHCO_3$, 5 ml milli-Q H_2O, 80 ºC, pTotal= 36 bar, p(CO_2) = p(H_2), 15 h. [b]TON= mmol formate/mmol total of Pd, calculated by NMR using 1,4-dioxane as internal standard. [c]In absence of PPh_3. [d]With aging.

Table S9. Particle size of different systems before and after recycling experiments for CO_2 hydrogenation to formate.[a][b]

Entry	System	Pd wt%[c]	P wt%[c]	Si wt%[c]	Pd wt%[d]
1[e]	**Pd/APTES@TiO$_2$-3**	3.36	-	0.81	4.56

2	**Pd-PPh$_3$/APTES@TiO$_2$-2**	2.75	0.19	0.57	6.09
3[f]	**PA@Pd-PPh$_3$/TiO$_2$-11**	3.10	0.82	-	3.58

[a]Reaction conditions: 20 mg of catalyst, 4 M $KHCO_3$, 5 ml milli-Q H_2O, 80 ºC, pTotal= 36 bar, $p(CO_2) = p(H_2)$, 15 h. [b]Particle size was obtained by TEM. [c]Before catalysis. [d]After 2nd cycle. [e]In absence of PPh_3. [f]With aging.

Table S10. Particle size of different systems before and after recycling experiment for CO_2 hydrogenation to formate.[a][b]

Entry	System	Size (nm)[c]	Size (nm)[d]
1[e]	**Pd/APTES@TiO$_2$-3**	2.52 ± 0.95	3.48 ± 1.39
2	**Pd-PPh$_3$/APTES@TiO$_2$-2**	2.23 ± 0.78	3.43 ± 1.20
3[f]	**PA@Pd-PPh$_3$/TiO$_2$-11**	4.45 ± 1.68	3.59 ± 1.49

[a]Reaction conditions: 20 mg of catalyst, 4 M $KHCO_3$, 5 ml milli-Q H_2O, 80 ºC, pTotal= 36 bar, $p(CO_2) = p(H_2)$, 15 h. [b]Particle size was obtained by TEM. [c]Before catalysis. [d]After 2nd cycle. [e]In absence of PPh_3. [f]With aging.

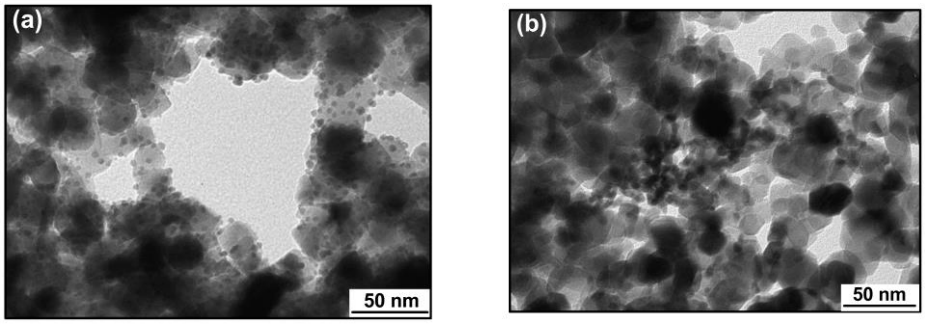

Figure S17. TEM images of **Pd/APTES@TiO$_2$-3** before (a) and after (b) two recovery experiments carried out at 80 ºC.

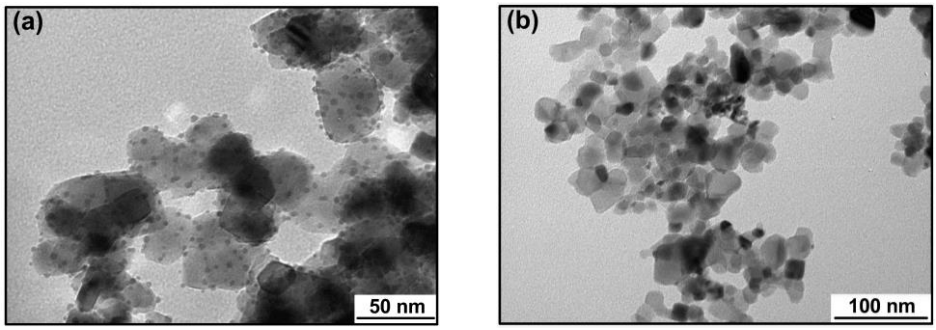

Figure S18. TEM images of **Pd-PPh$_3$/APTES@TiO$_2$-2** before (a) and after (b) two recovery experiments carried out at 80 ºC.

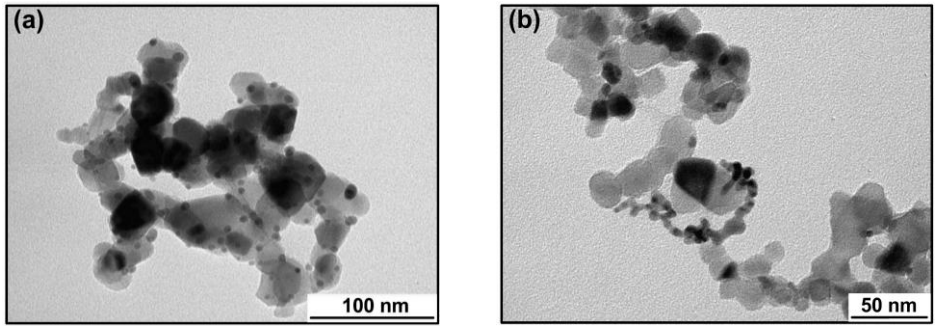

Figure S19. TEM images of **PA@Pd-PPh$_3$/TiO$_2$-11** before (a) and after (b) two recovery experiments carried out at 80 ºC.

- **Recycling experiments with different types of modifiers include on the catalyst**

Table S11. Recycling experiments with **Pd-PPh$_3$@modifier/TiO$_2$-x** for CO_2 hydrogenation to formate.[a]

Entry	System	Fresh[b]	1st[b]	2nd[b]	3rd[b]
1[c]	**Pd/APTES@TiO$_2$-3**	954	838	519	-
2	**Pd-PPh$_3$/APTES@TiO$_2$-2**	1117	987	510	-
3[d]	**Pd-PPh$_3$/APA@TiO$_2$-3**	756	356	349	189
4	**Pd-PPh$_3$/IL-Cl@TiO$_2$-8**	1005	434	404	221
5[e]	**Pd-PPh$_3$/IL-Cl@TiO$_2$-8**	946	542	447	-

[a]Reaction conditions: 20 mg of **modifier@Pd-PPh$_3$/TiO$_2$-x**, 4 M $KHCO_3$, 5 ml milli-Q H_2O, 80 ºC, pTotal= 36 bar, p(CO_2) = p(H_2), 15 h. [b]TON= mmol formate/mmol total of Pd, calculated by NMR using 1,4-dioxane as internal standard. [c]With aging.

Table S12. Recycling experiments with **modifier@Pd-PPh$_3$/TiO$_2$-x** for CO_2 hydrogenation to formate.[a]

Entry	System	Fresh[b]	1st[b]	2nd[b]	3rd[b]
1	**APTES@Pd-PPh$_3$/TiO$_2$-4**	904	724	662	524
2[c]	**APA@Pd-PPh$_3$/TiO$_2$-12**	873	332	326	201
3[c]	**PA@Pd-PPh$_3$/TiO$_2$-11**	827	723	369	-
4	**IL-Cl@Pd-PPh$_3$/TiO$_2$-8**	405	249	367	209

[a]Reaction conditions: 20 mg of **modifier@Pd-PPh$_3$/TiO$_2$-x**, 4 M $KHCO_3$, 5 ml milli-Q H_2O, 80 ºC, pTotal= 36 bar, p(CO_2) = p(H_2), 15 h. [b]TON= mmol formate/mmol total of Pd, calculated by NMR using 1,4-dioxane as internal standard. [c]With aging.

Table S13. Comparation of recycling experiments with **APTES@Pd-PPh$_3$/TiO$_2$-4**[a] and **Pd-PPh$_3$/TiO$_2$**[b] for CO_2 hydrogenation to formate.

Entry	System	Fresh[c]	1st[c]	2nd[c]	3rd[c]
1	**APTES@Pd-PPh$_3$/TiO$_2$-4**	904	724	662	524
2	**Pd-PPh$_3$/TiO$_2$**	1056	733	377	188

[a]Reaction conditions: 20 mg of **APTES@Pd-PPh$_3$/TiO$_2$-4**, 4 M $KHCO_3$, 5 ml milli-Q H_2O, 80 ºC, pTotal= 36 bar, p(CO_2) = p(H_2), 15 h. [b]Reaction conditions: 20 mg of **Pd-PPh$_3$/TiO$_2$**, 4 M $KHCO_3$, 5 ml milli-Q H_2O, 60 ºC, pTotal= 36 bar, p(CO_2) = p(H_2), 15 h. [c]TON= mmol formate/mmol total of Pd, calculated by NMR using 1,4-dioxane as internal standard.

5.5. References

[1] (a) K. T. Wan, M. E. Davis, *Nature* **1994**, *370*, 6489, 449−450; (b) N. Shibasaki-Kitakawa, H. Honda, H. Kuribayashi, T. Toda, T. Fukumura, T. Yonemoto, *Bioresour. Technol.* **2007**, *98*, 2, 416−421; (c) R. Liu, R. Jin, J. An, Q. Zhao, T. Cheng, G. Liu, *Chem. Asian J.* **2014**, *9*, 5, 1388−1394; (d) Y. Leng, J. Liu, P. Jiang, J. Wang, *J. Chem. Eng.* **2014**, *239*, 1−7; (e) P. Cong, R. D. Doolen, Q. Fan, D. M. Giaquinta, S. Guan, E. W. McFarland, D. M. Poojary, K. Self, H. W. Turner, W. H. Weinberg, *Angew. Chem. Int. Ed.* **1999**, *38*, 4, 484−488; (f) B. Uysal, B. S. Oksal, *Res. Chem. Intermed.* **2015**, *41*, 3893−3911.

[2] K. Yamaguchi, C. Yoshida, S. Uchida, N. Mizuno, *J. Am. Chem. Soc.* **2005**, *127*, 2, 530−531.

[3] (a) J. M. Planeix, N. Coustel, B. Coq, V. Brotons, P. S. Kumbhar, R. Dutartre, P. Geneste, P. Bernier, P. M. Ajayan, *J. Am. Chem. Soc.* **1994**, *116*, 17, 7935−7936; (b) P. D. Kent, J. E. Mondloch, R. G. Finke, *J. Am. Chem. Soc.* **2014**, *136*, 5, 1930−1941; (c) A. Dobrzeniecka, P. J. Kulesza, *ECS J. Solid State Sci. Technol.* **2013**, *2*, 12, M61−M66; (d) D. Astruc, F. Lu, J. R. Aranzaes, *Angew. Chem. Int. Ed.* **2005**, *44*, 48, 7852−7872.

[4] C. M. Crudden, M. Sateesh, R. Lewis, *J. Am. Chem. Soc.* **2005**, *127*, 28, 10045−10050.

[5] Y. Lou, J. Xu, Y. Zhang, C. Pan, Y. Dong, Y. Zhu, *Mater. Today Nano* **2020**, *12*, 100093.

[6] (a) T. W. van Deelen, C. Hernández Mejía, K. P. de Jong, *Nat. Catal*. **2019**, *2*, 955−970; (b) L. Liu, A. Corma, *Chem. Rev*. **2018**, *118*, 4981−5079. (c) R. Sun, Y. Liao, S.-T. Bai, M. Zheng, C. Zhou, T. Zhang, B. F. Sels, *Energy Environ. Sci*. **2021**, *14*, 1247−1285.

[7] (a) L. Fan, J. Zhang, K. Maa, Y. Zhang, Y.-M. Hu, L. Kong, A.-P. Jia, Z. Zhang, W. Huang, J.-Q. Lu, *J. Catal*. **2021**, *397*, 116–127; (b) Z. Zhang, L. Zhang, M. J. Hülseya, N. Yana, *Mol. Catal*. **2019**, *475*, 110461.

[8] Y. Himeda, *CO_2 Hydrogenation Catalysis*, **2021**, WILEY-VCH GmbH, ISBN: Print ISBN:9783527346639, Online ISBN:9783527824113; K. Mori, H. Yamashita,

Chapter 7. *Design and Architecture of Nanostructured Heterogeneous Catalysts for CO_2 Hydrogenation to Formic Acid/Formate*.
[9] (a) Z. Zhang, L. Zhang, S. Yao, X. Song, W. Huang, M. J. Hülsey, N. Yan, *J. Catal*. **2019**, *376*, 57−67; (b) J. Zhang, W. Liao, H. Zheng, Y. Zhang, L. Xia, B.-T. Teng, J.-Q. Lu, W. Huang, Z. Zhang, *J. Catal*. **2022**, *405*, 152−163.
[10] C. A. Schoenbaum, D. K. Schwartz, J. W. Medlin, *Acc. Chem. Res*. **2014**, *47*, 1438−1445.
[11] A. H. Jenkins, J. W. Medlin, *Acc. Chem. Res*. **2021**, *54*, 21, 4080−4090.
[12] (a) L. Xu, T. Cui, J. Zhu, X. Wang, M. Ji, *New J. Chem*. **2021**, *45*, 6293−6300; (b) B. Chen, M. Dong, S. Liu, Z. Xie, J. Yang, S. Li, Y. Wang, J. Du, H. Liu, B. Han, *ACS Catal.* **2020**, *10*, 8557−8566; (c) S. Masuda, K. Mori, Y. Futamura, H. Yamashita *ACS Catal*. **2018**, *8*, 2277−2285.
[13] P. Hao, D. K. Schwartz, J. W. Medlin, *ACS Catal*. **2018**, *8*, 11165−11173.
[14] (a) Q. Sun, X. Fu, R. Si, C.-H. Wang, N. Yan, *ChemCatChem* **2019**, *11*, 5093−5097; (b) T. Umegaki, Y. Satomi, Y. Kojima, *J. Jpn. Inst. Energ*. **2019**, *96*, 487−492.
[15] (a) Y. Kuwahara, Y. Fujie, T. Mihogi, H. Yamashita *ACS Catal.* **2020**, *10*, 6356−6366; (b) G. Yang, Y. Kuwahara, K. Mori, C. Louis, H. Yamashita, *Appl. Catal. B: Environ* **2011**, *283*, 119628.
[16] Q. Chen, N. L. Yakovlev, *Appl. Surf. Sci*. **2010**, *257*, 1395−1400.
[17] D. Meroni, L. Lo Presti, G. Di Liberto, M. Ceotto, R. G. Acres, K. C. Prince, R. Bellani, G. Soliveri, S. Ardizzone, *J. Phys. Chem. C* **2017**, *121*, 430−440.
[18] C. Schmitt. Thesis: *Surface modification of oxide nanoparticles using phosphonic acids: characterization, surface dynamics, and dispersion in sols and nanocomposites*. Material chemistry. Université Montpellier, **2015**.
[19] A. Glaser, J. Foisner, H. Hoffmann, G. Friedbacher, *Langmuir* **2004**, *20*, 13, 5599−5604.
[20] (a) R. Klaysri, T. Tubchareon, P. Praserthdam, *J. Ind. Eng. Chem.* **2017**, *45*, 229−236; (b) F. Cheng, S. M. Sajedin, S. M. Kelly, A. F. Lee, A. Kornherr, *Carbohydr. Polym*. **2014**, *114*, 246−252.
[21] (a) R. K. Sharma, M. Yadav, R. Gaur, R. Gupta, A. Adholeya, M. B. Gawande, *ChemPlusChem* **2016**, *81*, 1312−1319; (b) M. Demirelli, E. Karaoğlu, A. Baykal, H. Sözeri, E. Uysal *J. Alloys Compd*. **2014**, *582*, 201−207.
[22] S. A. Didas, S. Choi, W. Chaikittisilp, C. W. Jones*, Acc. Chem. Res.* **2015**, *48*, 2680−2687.
[23] Q. Liu, X. Yang, Y. Huang, S. Xu, X. Su, X. Pan, J. Xu, A. Wang, C. Liang, X. Wang, T. Zhang, *Energy Environ. Sci*. **2015**, *8*, 3204−3207.
[24] Q. Liu, X. Yang, L. Li, S. Miao, Y. Li, Y. Li, X. Wang, Y. Huang, T. Zhang, *Nat. Commun*. **2017**, *8*, 1407.
[25] K. Mori, S. Masuda, H. Tanaka, K. Yoshizawa, M. Chee, H. Yamashita, *Chem. Commun*., **2017**, *53*, 4677−4680.
[26] V. Srivastava, *Catal. Surv. from Asia*. **2021**, *25*, 192−205.

[27] I. M. Gindri, C. P. Frizzo, C. R. Bender, A. Z. Tier, M. A. P. Martins, M. A. Villetti, G. Machado, L. C. Rodriguez, D. C. Rodrigues, *ACS Appl. Mater. Interfaces* **2014**, *6*, 11536−11543.
[28] B. Xina, J. Hao, *Chem. Soc. Rev.* **2014**, *43*, 7171−7187.
[29] M. H. G. Prechtl, Nanocatalysis in Ionic Liquids, **2017**, Wiley-VCH. Print ISBN: 978-3-527-33910-5; P. Migowsky, K. L. Luska, W. Leitner, Chapter 12: Nanoparticles on Supported Ionic Liquid Phases–Opportunities for Application in Catalysis.
[30] J. Lemus, J. Palomar, M. A. Gilarranz, J. J. Rodriguez, *Adsorption*, **2011**, *17*, 561−571.
[31] (a) R. Venkatesan, M. H. G. Prechtl, J. D. Scholten, R. P. Pezzi, G. Machadoc, J. Dupont, *J. Mater. Chem*. **2011**, *21*, 3030; (b) Y. Zhang, Y. Zhao, C. Xia, *J. Mol. Catal. A Chem*. **2009**, *306*, 107−112.
[32] K. S. Yoo, *J. Nanosci. Nanotechnol*. **2016**, *16*, 4302−4309.
[33] (a) U. Nishan, S. U. Haq, A. Rahim, M. Asad, A. Badshah, A.-u.-H. A. Shah, A. Iqbal, N. Muhammad, *ACS Omega* **2021**, *6*, 32754−32762; (b) R. Linhardt, Q. M. Kainz, R. N. Grass, W. J. Stark, O. Reiser, *RSC Adv*. **2014**, *4*, 8541; (c) H. Veisi, M. Pirhayati, A. Kakanejadifard, *Tetrahedron Lett*. **2017**, *58*, 4269−4276.
[34] C. P. Mehnert, R. A. Cook, N. C. Dispenziere, M. Afeworki, *J. Am. Chem. Soc.* **2002**, *124*, 12932−12933.
[35] A. Bordet, W. Leitner, *Acc. Chem. Res*. **2021**, *54*, 2144−2157.
[36] S. Udayakumar, V. Raman, H.-L. Shim, D.-W. Park, *Appl. Catal. A: Gen*, **2009**, *368*, 97−104.
[37] G. Gurau, H. Rodríguez, S. P. Kelley, P. Janiczek, R. S. Kalb, R. D. Rogers, *Angew. Chem. Int. Ed*. **2011**, *50*, 12024−12026.
[38] (a) Y. Wu, Y. Zhao, H. Wang, B. Yu, X. Yu, H. Zhang, Z. Liu, *Ind. Eng. Chem. Res*. **2019**, *58*, 6333−6339; (b) M. I. Qadir, A. Weilhard, J. A. Fernandes, I. de Pedro, B. J. C. Vieira, J. C. Waerenborgh, J. Dupont, *ACS Catal*. **2018**, *8*, 1621−1627.
[39] (a) A. Bordet, G. Moos, C. Welsh, P. Licence, K. L. Luska, W. Leitner, *ACS Catal*. **2020**, *10*, 13904−13912; (b) G. Moos, M. Emondts, A. Bordet, W. Leitner, *Angew. Chem. Int. Ed*. **2020**, *59*, 11977−11983.
[40] S. Rengshausen, C. Van Stappen, N. Levin, S. Tricard, K. L. Luska, S. DeBeer, B. Chaudret, A. Bordet, W. Leitner, *Small* **2021**, *17*, 2006683.
[41] (a) L. Offner-Marko, A. Bordet, G. Moos, S. Tricard, S. Rengshausen, B. Chaudret, K. L. Luska, W. Leitner, *Angew. Chem. Int. Ed*. **2018**, *57*, 12721−12726; (b) K. L. Luska, A. Bordet, S. Tricard, I. Sinev, W. Grünert, B. Chaudret, W. Leitner, *ACS Catal*. **2016**, *6*, 3719−3726; (c) L. Goclik, L. Offner-Marko, A. Bordet, W. Leitner, *Chem. Commun*. **2020**, *56*, 9509−9512.
[42] (a) K. L. Luska, J. Julis, E. Stavitski, D. N. Zakharov, A. Adamsa, W. Leitner, *Chem. Sci*. **2014**, *5*, 4895−4905; (b) S. El Sayed, A. Bordet, C. Weidenthaler, W. Hetaba, K. L. Luska, W. Leitner, *ACS Catal*. **2020**, *10*, 2124−2130; (c) A. Bordet, S. El Sayed, M. Sanger, K. J. Boniface, D. Kalsi, K. L. Luska, P. G. Jessop, W. Leitner, *Nat. Chem*. **2021**, *13*, 916−922.

[43] K. Philippot, B. Chaudret, *C. R. Chim*. **2003**, *6*, 1019−1034.
[44] S. J. Louis Anandaraj, L. Kang, S. DeBeer, A. Bordet, W. Leitner, *Small* **2023**, 2206806.
[45] (a) B. Feng, Z. Zhang, J. Wang, D. Yang, Q. Li, Y. Liu, H. Gai, T. Huang, H. Song, *Fuel* **2022**, *325*, 124853; (b) Q. Li, T. Huang, Z. Zhang, M. Xiao, H. Gai, Y. Zhou, H. Song, *Mol. Catal*. **2021**, *509*, 111644.
[46] C. Queffelec, M. Petit, P. Janvier, D. A. Knight, B. Bujoli, *Chem. Rev.* **2012**, *112*, 7, 3777−3807.
[47] F. Brodard-Severac, G. Guerrero, J. Maquet, P. Florian, C. Gervais, P. H. Mutin, *Chem. Mater*. **2008**, *20*, 5191−5196.
[48] G. Guerrero, P. H. Mutin, A. Vioux, Chem. Mater. **2001**, *13*, 11, 4367−4373.
[49] (a) L. Zeininger, L. Portilla, M. Halik, A. Hirsch, *Chem. Eur. J.* **2016**, *22*, 13506−13512; (b) P. Hao, D. K. Schwartz, J. W. Medlin, *Appl. Catal. A- Gen*. **2018**, *561*, 1−6.
[50] (a) L. D. Ellis, R. M. Trottier, C. B. Musgrave, D. K. Schwartz, J. W. Medlin, *ACS Catal.* **2017**, *7*, 8351−8357; (b) N. Gys, L. Siemons, B. Pawlak, K. Wyns, K. Baert, T. Hauffman, P. Adriaensens, F. Blockhuys, B. Michielsen, S. Mullens, V. Meynen, *Appl. Surf. Sci*. **2021**, *566*, 150625.
[51] J. Zhang, L. D. Ellis, B. Wang, M. J. Dzara, C. Sievers, S. Pylypenko, E. Nikolla, J. W. Medlin, *Nat. Catal*. **2018**, *1*, 148−155.
[52] J. Zhang, S. Deo, M. J. Janik, J. W. Medlin, *J. Am. Chem. Soc*. **2020**, *142*, 5184−5193.
[53] A. Wanag, A. Sienkiewicz, P. Rokicka-Konieczna, E. Kusiak-Nejman, A. W. Morawski, *J. Environ. Chem. Eng.* **2020**, *8*, 103917.
[54] Z. Li, B. Hou, Y. Xu, D. Wu, Y. Sun, W. Hu, F. Deng, *J. Solid. State Chem.* **2005**, *178*, 1395−1405.
[55] (a) W. Zhuang, Y. Zhang, L. He, R. An, B. Li, H. Ying, J. Wu, Y. Chen, J. Zhou, X. Lu, *Micropor. Mesopor. Mater*. **2017**, *239*, 158−166; (b) E. Ukaji, T. Furusawa, M. Sato, M. Suzuki, *Appl. Surf. Sci*. **2007**, *254*, 563569.
[56] T. Rajkumar, G. Ranga Rao, *Mater. Chem. Phys*. **2008**, *112*, 853−857.
[57] D. Geldof, M. Tassi, R. Carleer, P. Adriaensens, A. Roevens, V. Meynen, F. Blockhuys, *Surf. Sci*. **2017**, *655*, 31−38.
[58] Y. Kim, H. Lee, S. Yang, J. Lee, H. Kim, S. Hwang, S. W. Jeon, D. H. Kim, *J. Catal.* **2021**, *404*, 324−333.
[59] (a) A. Weilhard, M. I. Qadir, V. Sans, J. Dupont, *ACS Catal.* **2018**, *8*, 1628−1634; (b) A. Weilhard, S. P. Argent, V. Sans, *Nat. Commun.* **2021**, *12*, 231.
[60] T. L. Price Jr., U. H. Choi, D. V. Schoonover, M. Arunachalam, R. Xie, S. Lyle, R. H. Colby, H. W. Gibson, *Macromolecules* **2019**, *52*, 1371−1388.
[61] Y. Dai, S. Wang, J. Wu, J. Tang, W. Tang, *RSC Advances*, **2012**, *2*, 12652−12656.
[62] Q. Dou, L. Liu, B. Yang, J. Lang, X. Yan, *Nat. Commun*. **2017**, *8*, 2188.
[63] K. R. Roshan, G. Mathai, J. Kim, J. Tharun, G.-A. Park, D.-W. Park, *Green Chem*. **2012**, *14*, 2933.

[64] S. Delacroix, F. Sauvage, M. Reynaud, M. Deschamps, S. Bruyère, M. Becuwe, D. Postel, J.-M. Tarascon, A. Nguyen Van Nhien, *Chem. Mater.* **2015**, *27*, 7926−7933.
[65] J. R. Li, C. Chen, Y. L. Hu, *ChemistrySelect* **2020**, *5*, 14578−14582.
[66] R. Helmy, A. Y. Fadeev, *Langmuir* **2002**, *18*, 8924−8928.

CHAPTER 6

Catalytic reduction reactions with potassium formate using ligand-capped Pd NPs supported over TiO_2

UNIVERSITAT ROVIRA I VIRGILI
EFFICIENT VALORIZATION OF CO2 INTO FORMATE THROUGH NANOCATALYSIS
María Dolores Fernández Martínez

6.1. Introduction

In the previous chapters of this thesis, a series of Pd based catalysts were used in the transformation of CO_2 into formate. The aim of this transformation was to obtain a high-added value product such as formate from which H_2 can be extracted at a later stage. Although formates have less volumetric energy density than formic acid, they present some advantages as they are non-corrosive and no irritant solids, which facilitates their handling and transport.[1] Using formate to generate hydrogen or to hydrogenate molecules of interest is integrated in the concept of circular H_2 storage and release. Therefore, ideally, a catalyst active in the hydrogenation of CO_2 could also be active in the reverse reaction and could use formate to hydrogenate other substrates. In Chapter 1, examples of catalytic systems for the reversible H_2 storage and release were presented for both the reversible transformation of CO_2/formic acid and bicarbonate/formate. Most of them are based on Pd nanocatalysts mainly deposited over carbon-based supports. The ability of such catalysts to liberate H_2 (or equivalent) from formic acid/formates can therefore be used to perform tandem or cascade reactions where the reduction of a substrate of interest can be completed and the product used in subsequent reactions.

In this chapter, a preliminary study on the application of the catalyst **Pd-PPh$_3$/TiO$_2$** in the reduction of nitroaromatics such as nitrophenols and nitrarenes into the corresponding aryl amines is described using potassium formate as reducing agent. The reduction was also performed in the presence of aldehyde in the so-called reductive amination process, where nitro reduction, condensation and imine reduction steps take place.

6.1.1. Reduction of nitroarenes using formic acid/formate

Aryl amines are important intermediates in the synthesis of many compounds with applications in the areas of agrochemicals, polymers or dyes.[2] They also are present in many pharmaceutical products such as Paracetamol,[3] derivate from a *p*-aminophenol, Bicalutamide,[4] Nilutamide[5] and Erlotinib[6] (Figure 1). The reduction of nitroarenes into aniline derivatives was initially performed via the Béchamp reduction with nitronaphthalene and nitrobenzene as substrates using metallic Fe and HCl but generated large amounts of metallic waste.[7] As such, intense efforts have been focused on the development of

new and efficient catalysts for the reduction of nitroaromatics to obtain the aniline products in a more sustainable manner.

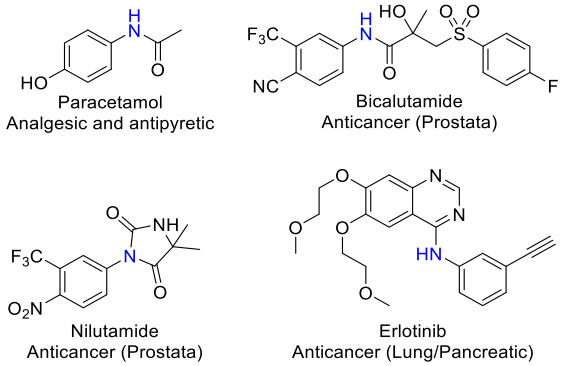

Figure 1. Pharmaceutical products with aril amine core structure.

One important aspect of this reaction is the use of the reductant. Among the conventionally used reductants, H_2, $NaBH_4$, silyl hydrides and hydrazine hydrate were reported.[8]

More recently, the *in situ* generation of H_2 from formic acid and its salts have emerged as a clean alternative for this process (Scheme 1). This hydrogen storage and release is based on the interconversion of CO_2 (or bicarbonate) and FA (or formate).

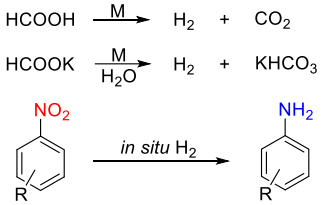

Scheme 1. Reduction of nitroarenes by transfer hydrogenation.

4-Nitrophenol (4-NP) is one of the molecules belonging to this family and is involved in many chemical processes and products such as dyes, pesticides and drugs.[9] However, this molecule is present in soils and waters causing a high environmental impact.[10] Moreover, it is also very toxic, mutagenic, carcinogenic and presents embryotoxic risks, and as such this molecule and its derivates are currently considered one of the top priority pollutants for the United States Environmental Protection Agency (US EPA)[11] The chemical

reduction of these species (Scheme 2) is an alternative to degrade these compounds and minimize its effects.

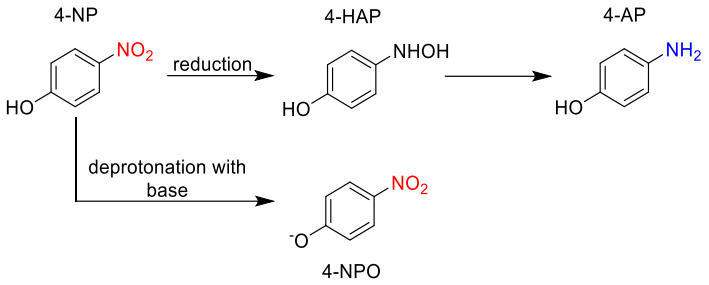

Scheme 2. Synthesis of 4-aminophenol (4-AP) through the reduction of 4-NP to 4-hydroxyaminophenol (4-HAP). In presence of base, 4-NP it is deprotonated to 4-nitrophenoxide (4-NPO).

Moreover, the 4-aminophenol (4-AP) resulting from the reduction of 4-NP is an important fine chemical used in agriculture, medicine and chemical industry, among other fields.[12]

Depending on the pH of the media, this type of compound can be found as ammonium cations, neutral molecules or phenolate ions (Scheme 3).

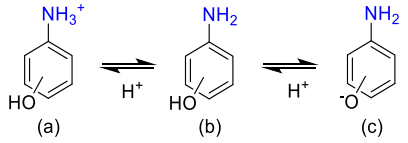

Scheme 3. Ammonium cation (a), neutral molecule (b) or phenolate ion (c) of nitrophenols depending on the pH of the media.

Fe, Pd, Ag, Au, Pt and Ni based catalysts were reported for the reduction of 4-nitrophenol using various types of reductants[13] With these catalysts, the reduction of 4-nitrophenol is usually carried out in the presence of $NaBH_4$. The amount of $NaBH_4$ employed varies from less than 10 equiv. up to more than 100 or even 1000 equiv.[14]

For instance, Chen and coworkers developed a system based on supported Ag nanoparticles over N-doped graphene with the aim of study the mechanism of the 4-NP reduction and the role played by H_2O.[15] They confirmed the presence of six intermediates and that hydrogen atoms present on the amine comes from H_2O rather than $NaBH_4$ based on isotopic labelling. Among the other metals employed in that process, Pd remains the most

active and the most employed. In 2015, Wang and coworkers employed a Pd monometallic and PdAu bimetallic systems over multi-walled carbon nanotubes (MWCNT) for the reduction of 4-NP into 4-AP.[16] The bimetallic system revealed more active than the monometallic catalyst and reached an activity factor up to 205 $s^{-1} \cdot g^{-1}$. Luo and coworkers developed a water-soluble system based on Pd_8 nanoclusters (NCs) with mercaptosuccinic acid (H_2SMA) as the ligand (Figure 2).[17] Conversion of 92% and a TOF of 4 s^{-1} were reached with $NaBH_4$ as reductant. This system also demonstrated good recyclability during four cycles with a decrease in activity during the fifth run (73%). DFT calculations were performed to explain the interactions between 4-NP and Pd_8 clusters under proton-rich conditions.

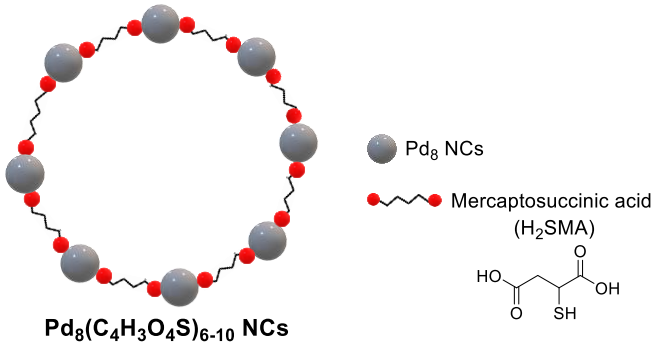

Figure 2. Pd_8 nanoclusters (NCs) with mercaptosuccinic acid (H_2SMA) as the ligand for the reduction of 4-NP into 4-AP.

Ayad et al. reported another system in which ''water-soluble'' Pd nanoparticles were stabilized by a benzyl bisphosphonic acid ligand and sodium ascorbate was used as reductant.[18,19] These nanoparticles exhibited a mean size of 6 nm. The ligand influences the activity due to the mass transfer of the organic substrates towards the NP surface in the aqueous environment.

They performed a very detailed kinetic and thermodynamic study with this system with variations in the initial substrate and $NaBH_4$ concentrations, reaction temperatures, and mass of Pd nanoparticles used for catalytic reduction. They concluded that kinetics are highly dependent on the reactant ratio and assumed that all steps of this reaction proceed only on the surface of Pd nanoparticles.

Gong and coworkers developed a $Pd/Fe_3O_4@C$ system for the reduction of 4-NP with $NaBH_4$ and the hydrodechlorination of chlorophenols using H_2 as reductant and with 1 equiv. of base (Scheme 4).[20] The magnetic character of the Fe_3O_4 core allowed an easy separation of the catalyst from the reaction medium and its re-use in five consecutive hydrodechlorination cycles without loss of activity. This system was highly active in both transformations. The role of the base during the hydrodechlorination is to neutralize the HCl formed to avoid the deactivation of the catalyst. The best results were obtained using NaOH in aqueous solution.

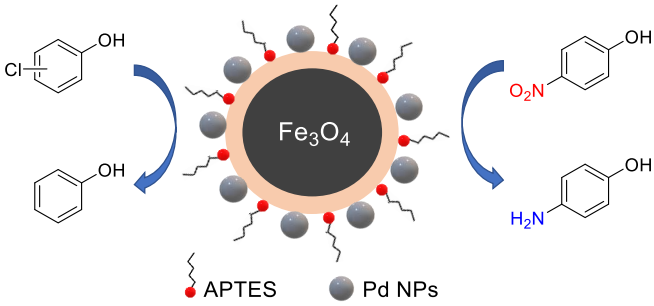

Scheme 4. $Pd/Fe_3O_4@C$ catalyst for the reduction of 4-NP and the hydrodechlorination of chlorophenols.

A related catalytic system was developed by Hemmati and coworkers using a nanocomposite with Fe_3O_4 NPs at core and Pd NPs as outer shell coated by *Fritillaria imperialis* flower extract.[21] This catalyst was active in the reduction of 4-NP and other nitroarenes using hydrazine hydrate as reductant in a mixture ethanol/water (1:2). For both nitrobenzene and 4-NP, the yields obtained were 98% with TOF of 544 x 10^{-3} s^{-1} at 80 ºC in 30 min.

Another catalyst employed for the hydrodechlorination of 4-chloro-2-amino phenol was based on Ni and was developed by Kamble and coworkers.[22] This molecule is an effluent from pharmaceutical and dye industries, as such must be transformed into a greener product that doesn't damage the environment. 98% yield was obtained using $NaBH_4$ as reductant at room temperature.

The influence of the solvent was also analyzed for reduction of 4-NP to 4-AP with $NaBH_4$. Ringe and coworkers study the effect of different solvent media (water, alcohols) in this reaction using catalysts based on Ag and Au NPs.[23]

Polarity, oxygen solubility or viscosity are some of the parameters that influenced the efficiency of the process.

There are also several examples of metal-free systems that are highly active in this transformation.[12c,24] Wang and coworkers developed a N,P-dual-doped multilayer graphene (NPG) system for the reduction of 4-NP with only 1 mg of NPG in aqueous solution of $NaBH_4$ (10 equiv.).[24] The TOF obtained in this work was up to 2.37 x 10^{-2} min^{-1}, which is higher than the values reported for others graphene systems and other catalysts based on noble metals. This catalyst was recycled six times without any loss of activity.

Formic acid was also employed for the reduction of 4-NP to 4-AP. Duprat and coworkers used a system based on Pd@Al_2O_3 in a flow reactor for this process. [25] Authors study the possible pathways and the possible intermediates that are formed during the reaction through the use of on-line HPLC and UV. Further studies by NMR and UV provided more information on this dynamic study. The presence of two of the observed species was confirmed as byproducts and not as intermediate. Other authors reported the use of formic acind and formate for the reduction of 4-NP to 4-AP.[26,27,28]

The reduction of nitroarenes into aniline derivatives is also a reaction of interest and some of the reducing agent used for that reaction are H_2, $NaBH_4$, silyl hydrides, etc.[8] Using H_2 as reductant, several examples described interesting results. Li et al. developed a system based on Pd NPs supported over SiO_2 modified with bicationic imidazolium ionic liquids for the reduction of nitrobenzenes into anilines in neat or aqueous medium.[29] The most active catalyst remained efficient even after 15 recyclings. Baiker and coworkers also employed H_2 as reductant for the selective hydrogenation of 3-nitrostyrene in the presence of ILs. [30] Supports of different nature were employed and depending on the acidic or basic conditions used, the selective reduction of the vinyl group could be achieved using CNTs as support (under basic conditions) or the reduction of the nitro substituent when SiO_2 was used (under acidic conditions) with yields exceeding 90% and TOFs up to 100 h^{-1}. In terms of recyclability, the activity of the catalyst supported over CNTs remained unchanged for 3 runs, but during the 4th and 5th cycles, the yields drastically decreased. Interestingly, upon IL addition during the 6th cycle, the initial yield could be restored.

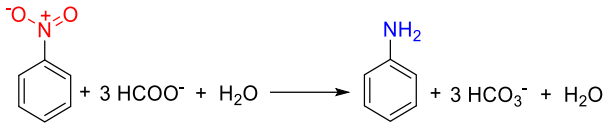

Scheme 5. Reduction of nitrobenzene to aniline using formate in aqueous media.

Formic acid and formates were used in literature for the reduction of other nitroarenes (Scheme 5).[31]

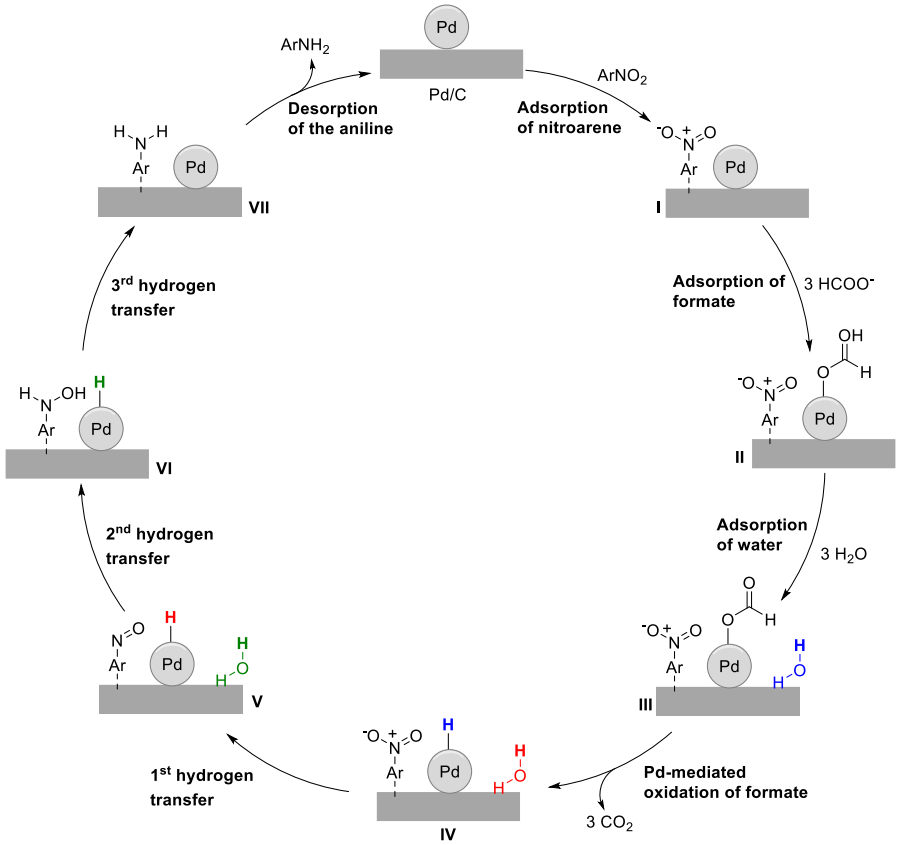

Scheme 6. General mechanism of the transfer hydrogenation using formic acid/formate for hydrogenation of nitroarenes by Pd/C catalyst.

Sasson and coworkers studied the mechanism for this reaction using Pd/C (Scheme 6) and concluded that the dehydrogenation of formic acid/formates is the rate-limiting step.[31,32] First, the nitroarene is adsorbed by the support to form the system I. In consecutive II and III systems, the adsorptions of formate and water also take place. While formate is coordinated over Pd species to

form [PdII(HCOO)], water molecules are adsorbed onto the support. Pd mediates the oxidation of formate to CO_2 and an active [Pd-H] species is formed (system IV). Then, hydrogen transfer occurs to nitroarene to form a nitroso-arene adsorbed intermediate system V. This species suffers two hydrogen transfers to form hydroxylamine and finally, aniline on systems VI and VII. Then, the desorption of the product occurs.[31,32] Isotope effect studies indicated that hydrogen transfer is the rate-determining step.[31]

Hu et al. employed both FA and formates for the reduction of *p*-chloronitrobenzene in EtOH using Au NPs supported over ZrO_2.[33] They compared the results obtained using several formates. The selectivity to the corresponding amine was up to 99.9% when $HCOONH_4$ (4 equiv.) was employed, which was very superior to that obtained with H_2. The activities obtained using various formate derivates followed the order: HCOOH < HCOONa < HCOOK < $HCOONH_4$. During the same year, Portada et al. employed $HCOONH_4$ (1.1 or 3.3 equiv.) as hydrogen source for the mechanochemical catalytic transfer hydrogenation of nitroarenes.[26] These authors employed Pd/C as catalyst (2 mol% Pd) for that purpose and used a mechanochemical process in neat or liquid-assisted grinding mixer mill (with MeOH). They also performed the reduction of 4-NP at 1 g scale and in a second step, synthesized paracetamol. Other pharmaceutical products were also obtained via this methodology. Good yields were obtained when electron donor groups were present on nitroarenes (94-99%). In terms of selectivity, good results were obtained for nitrile, ketones, ester, acids and alkenes. However, lower selectivities were obtained for chlorine and benzyl ether.

Apart from Pd, other metals were employed among which non-noble metals were reported.[31] In general, temperatures in the range of 100-120 ºC are used although some catalysts based on Zn, Co-Zn and Cu were active at room temperature using formates as reducing agents (Scheme 7).[31,34,35] Ranu and coworkers used copper nanoparticles and $HCOONH_4$ in ethylene glycol at 120°C for reduction of aromatic nitrocompounds with yields of 79-90%.[34] They compared the performance of their synthesized Cu NPs and those metallic Cu powder and the use of other hydrogen sources such as hydrazine and H_2 gas. They obtained the best results with $HCOONH_4$.

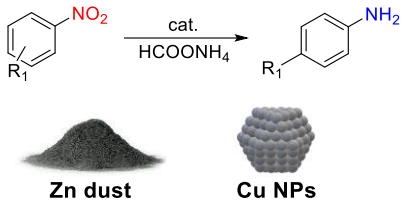

Scheme 7. Examples of Zn and Cu based catalysts for the reduction of nitrocompounds to amines with formate as reductant.

Gouwda et al. employed commercial Zn dust activated with HCl treatment and $HCOONH_4$ in MeOH at r.t. during 2-10 min in good yileds (90-95%).[35] They also obtained good results when HCOOH was employed.

6.1.2. Direct reductive amination of aldehydes using formic acid/formate

Secondary amines are important molecules as intermediates and building blocks for products like agrochemicals, detergents, dyes, herbicides, pharmaceuticals, pigments.[36] Reductive amination (RA) is by far the most preferable methodology to obtain these products, because of the high atom-economy associated to this process.[37] It is necessary to distinguish direct reductive amination (DRA) and indirect or stepwise reductive amination (IRA) (Scheme 8).

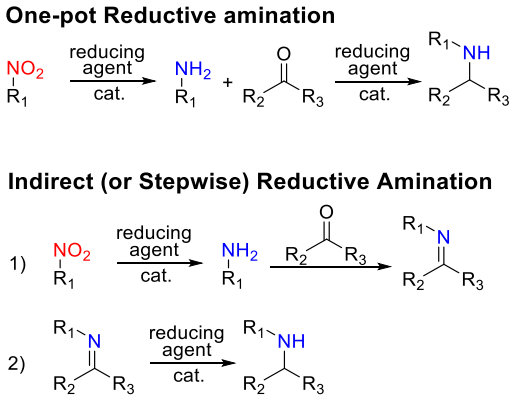

Scheme 8. Direct reductive amination (DRA) and indirect or stepwise reductive amination (IRA).

DRA occurs when the carbonyl compound and the primary amine are mixed in one-pot in the presence of the reductant. However, for the IRA, the

preformation of the intermediate imine first takes place (or iminium salt if the amine is secondary) prior to the reduction to the amine.[37,38] Consequently, the one-pot reductive amination of aldehydes with nitroarenes is a very interesting procedure because it allows one to obtain diverse *N*-alkylated or *N*-benzylated anilines by simple reduction of nitro compounds, followed by condensation with aldehydes and subsequent reduction of the imine intermediates.

The proposed mechanism of DRA reaction is presented in Scheme 9.

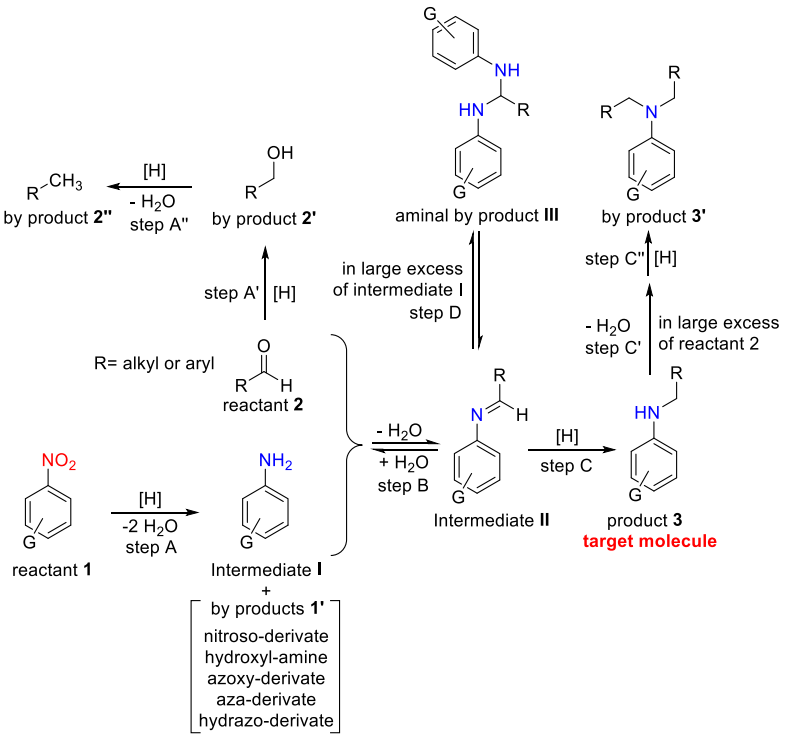

Scheme 9. Mechanism of RA in the synthesis of a secondary aniline from nitroarene and aldehyde.

Starting from reactant 1 (a nitrobenzene), this is reduced to intermediate I (an aniline) in step A. Then, condensation with reactant 2 (aldehyde or ketone, normally) occurs to give an imine (intermediate II), which is also reduced giving the corresponding desired secondary amine (product 3). However, several by-products can appear in the process, lowering the yield and selectivity of the process. By-products from the reduction of the nitro and the

aldehyde to alcohol could be produced. Alcohol could also react on a hydrogenolysis reaction to give the alkane. Strong excess of both amine or aldehyde can also promote the reaction of by-products, such as aminal or more substituted amine. So, apart from the conditions of catalysis that can affect or displace the equilibrium in several steps, the proportions of starting materials can also affect the selectivity of the process.

DRA is usually reported in the presence of H_2 and using Pd-based catalysts.[37] Several examples described the use of 1 atm of H_2 and in alcohols as solvents. The range of Pd loadings reported is broad, going from 0.16 mol% Pd[39] up to 10.5 mol%.[40]

In this process, formic acid and formates salts were also reported as reducing agents.

For instance, Zhou et al. reported the use of Co NPs embedded in mesoporous nitrogen-doped carbon (Co@CN-800) in the presence of formic acid for reductive amination of aromatic and alkylic nitrocompounds and aldehydes and cetones (Scheme 10).[41]

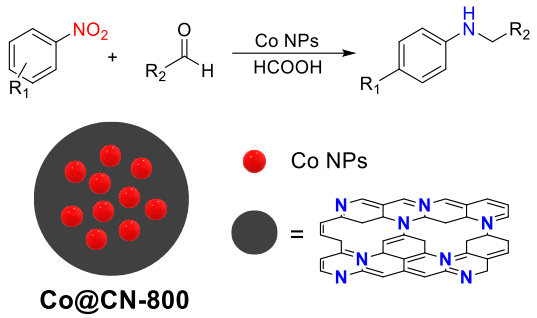

Scheme 10. Example of Cobalt based catalysts for reductive amination with HCOOH as reductant.

The nitrogen atoms present on the support surface lead to the formation of N-H^+ groups and hydridic Co-H^- which were proposed to be the active species. A Co loading of 16 mol% was employed with 4.5 equiv. of FA to reach yields between 88-95%. The catalyst could be recycled eight times without loss of activity. Similar Co based systems were also reported by the same authors using HCOOH as hydrogen surrogate.[42,43]

Jagadeesh and coworkers developed a nitrogen-doped, graphene-activated nanoscale Co_3O_4-based catalysts (Co_3O_4/NGr@C) for DRA under milder

conditions.[44] A Co loading of 4 mol% was used with HCOOH in the presence of NEt_3 for the reductive amination of nitroarenes and aldehydes, obtaining yields between 83 and 95%. This catalyst could also be reused six times without loss of activity.

In 2008 Byun et al. used Pd/C (10 mol%) with $HCOONH_4$ for DRA using a mixture of ^{i}PrOH and H_2O (10:1 v/v) as solvent mixture.[45] From this study, the following reaction mechanism was proposed (Scheme 11).

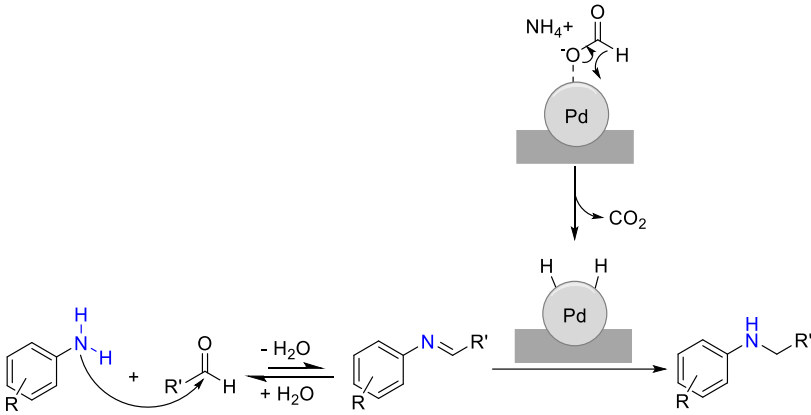

Scheme 11. Mechanism of RA nitroarene and aldehyde using Pd catalyst and in the presence of $HCOONH_4$ as reductant.

A high range of products were obtained by one-pot DRA under mild reaction conditions and very short reaction times (10-60 min in most cases).

Bhanage and coworkers also use formate salts as hydrogen source in the indirect reductive amination using a polymer supported triphenylphosphine-palladium acetate complex PS-TPP-$Pd(OAc)_2$ as catalyst precursor.[46] The highest yields were obtained for 10 mol% of Pd, DMF as solvent, 85 ºC and 6 h of reaction. Anhydrous conditions were used for both steps: the formation of the imine and the hydrogenation yielding the amine. Yields between 56 and 84% were obtained when HCOONa was used (3 equiv.).

HCOONa was also employed by Jiménez and coworkers for DRA using cyclohexanone as reagent instead of an aldehyde.[47] Pd/C was used as catalyst and at 80 ºC, 100% conversion was reached with the imine (85%) as the major product. However, at higher temperatures, a shift in selectivity was observed in favor of the amine.

A bimetallic AgPd system supported over mesoporous graphitic carbon nitride (*mpg*-C_3N_4) also revealed active in the DRA of nitroarenes and aldehydes in the presence of FA.[48] $Ag_{40}Pd_{60}$ NPs were first synthesized in the presence of oleylamine and oleic acid as surfactants, providing particles with diameters of 2.5 ± 0.5 nm, which were subsequently deposited over mpg-C_3N_4 in a second step. Less than 1 mol% of Pd was employed with 4 equiv. of HCOOH in H_2O at 50 ºC for 20 h. In this study, only aromatic aldehydes were used and yields between 65-99% were achieved.

Gold based catalysts were also reported in this process (Scheme 12) and Cao and coworkers developed a system based on Au NPs of 2.2 nm supported over titania with rutile phase (Au/TiO_2-R) for DRA with FA in water.[49]

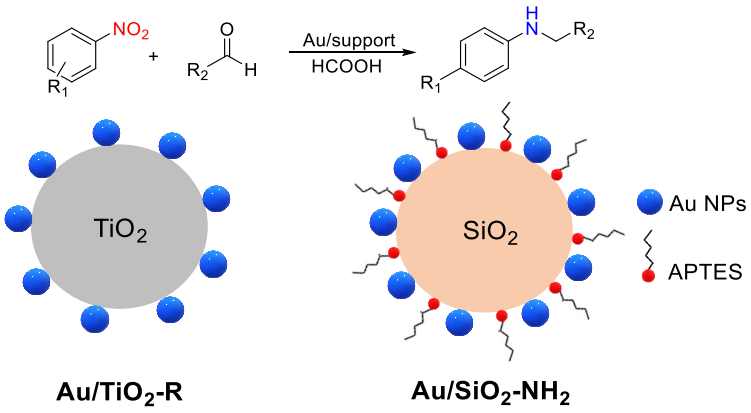

Scheme 12. Gold based catalysts for reductive amination with HCOOH as reductant.

A loading of 1 mol% of Au was employed for this reaction and yields between 83 and 99% were obtained. Moreover, the catalyst could be reused in five cycles without any loss of activity. Interestingly, using 1,2-dinitrobenzene with benzaldehyde, benzimidazole was produced in 87% yield. Another example was developed by Rossi and coworkers, who employed a system based on Au/SiO_2-NH_2. For DRA, a very low metal loading (0.76 mol% of Au) was used in the presence of NEt_3 to activate FA over the Au surface.[50] Yields between 41 and 92% were obtained using this system.

To sum up, the reduction of nitroaromatics is a reaction of interest, especially when performed using environmentally friendly reagents. A few examples

using formic acid or formates as reducing agent were reported for these processes, although the performance of the catalysts must be improved to allow their application in industrial processes.

In this chapter, a preliminary study on the reduction of a series of nitrophenols and nitroarenes using **Pd-PPh$_3$/TiO$_2$** and potassium formate as reducing agent is described. This catalyst was also tested in the DRA reaction of alkylic and aromatic aldehydes with nitrobenzene in the presence of potassium formate.

6.2. Results and discussion

6.2.1. Catalytic reduction of nitrophenols and nitroarenes

First, the reduction of 4-nitrophenol (4-NP) into 4-aminophenol (4-AP) was monitored over time to determine the appropriate reaction time for these reactions. At this point, a quick optimization of the reaction conditions was performed prior to an exploration of the scope of nitrophenols and nitroarenes containing different functional groups that could be transformed with this system.

Initial tests were performed employing 0.5 mmol of 4-NP in the presence of 0.6 mol% of Pd in an aqueous solution 4 M of HCOOK (20 equiv.) at 60 ºC. Initially, the reaction was performed during 1 h and 100% conversion of the substrate was observed by ^{1}H-NMR. Therefore, the monitoring of the reaction over time was performed to determine the appropriate reaction time to be used during the optimization of conditions.

Reactions were carried out at different times and the results analysed by ^{1}H-NMR in DMSO-d_6 using 1,3,5-trimethylbenzene (TMB) as internal standard. Note that when the monitoring of the reaction was performed by taking aliquots, the reaction stopped after taking the first sample. The results displayed in Figure 3 thus correspond to the conversion and selectivity of independent reactions.

After 15 min of reaction, the conversion was 59% with 99% selectivity to 4-AP. After 30 min of reaction the conversion was 79%, but the selectivity to the desired product lowered to 97%. Full conversion of the substrate was observed after 45 min of reaction and a slight decrease in selectivity was

measured at early reaction times (86% after 1 h) although it was maintained at long reaction times (up to 18 h).

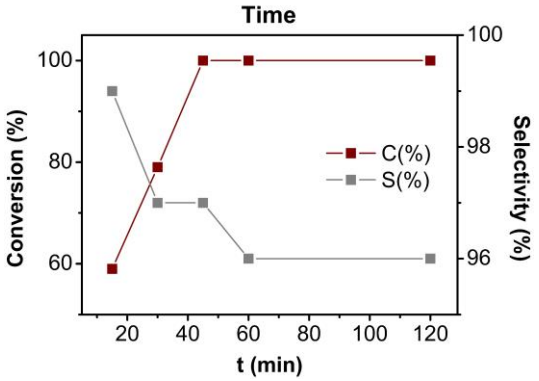

Figure 3. Monitoring of the catalytic reduction of 4-NP with **Pd-PPh$_3$/TiO$_2$** catalyst over time.

Using these data, the initial TOF (at 15 min of reaction) was 408 h^{-1} corresponding to a value of 2.02 x 10^{-3} $mmol_{4\text{-}NP}\cdot mg_{cat}^{-1}\cdot min^{-1}$ (moles of NP converted per mg of catalyst per min). With this activity, **Pd-PPh$_3$/TiO$_2$** is among the most active catalysts for this reaction. In most cases, the reported values for Pd catalysts are in the range 10^{-3}-10^{-6} in $mmol_{4\text{-}NP}\cdot mg_{cat}^{-1}\cdot min^{-1}$.The most active system was developed by Wang and coworkers which reported a value of 2.37 x 10^{-2} $mmol_{4\text{-}NP}\cdot mg_{cat}^{-1}\cdot min^{-1}$ using the metal free N,P-dual doped graphene as catalyst with 10 equiv. of $NaBH_4$ as reductant at room temperature.[24] Other metal-free systems as S, N co-doped carbon nanotubes and N-doped graphene have activities of 2.08-2.15 x 10^{-2} $mmol_{4\text{-}NP}\cdot mg_{cat}^{-1}\cdot min^{-1}$.[51,52] In the presence of metal (Ag and Pd) highest activities were found in the range of 2.62-3.11 x 10^{-3} $mmol_{4\text{-}NP}\cdot mg_{cat}^{-1}\cdot min^{-1}$.[53,54] All of them used $NaBH_4$ as reductant.

The by-products formed were detected by ^{1}H-NMR between 6.58 and and 7.15 ppm. Duprat and coworkers also reported the detection of these signals and proposed that they could correspond to the formation of *N*-(4-hydroxyphenyl)formamide.[25] FA and formate can act as both a hydrogen donor and formylating agent.

Next, several reaction conditions were explored including variations of parameters such as concentration of HCOOK, solvent and temperature. The

results are summarized in Table 1. For these experiments, the reaction time was set at 30 min. As previously indicated, when the reaction was performed in water using 4 M of HCOOK and at 60 ºC, the conversion was 79% (Entry 1). When the HCOOK concentration was lowered to 2 M (Entry 2), the conversion decreased to 47%. Moreover, when the reaction was performed at 30 ºC, the conversion dropped to 30% even when 4 M HCOOK was used (Entry 3). At this temperature, increasing the formate concentration to 8 M increased the conversion to 52% (Entry 4).

However, when a mixture of EtOH:H_2O (4:1 v/v) was used as solvent (Entry 5 and Entry 6), a striking enhancement of the conversion was measured and at 30 ºC, full conversion was observed using 4 M or 2 M of HCOOK with selectivities to 4-AP of 97 and 94%, respectively.

Table 1. Catalytic hydrogenation of 4-nitrophenol with **Pd-PPh$_3$/TiO$_2$** catalyst employing different conditions of reaction.[a]

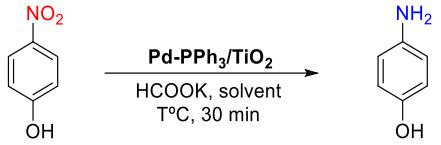

Entry	[HCOOK] (M)	Solvent	T (ºC)	C (%)[b]	S (%)[b]
1	4	H_2O	60	79	97
2	2	H_2O	60	47	98
3	4	H_2O	30	30	98
4	8	H_2O	30	52	94
5	4	EtOH:H_2O[c]	30	99	97
6	2	EtOH:H_2O[c]	30	99	94

[a]Reaction conditions: 0.5 mmol 4-NP, 10 mg of **Pd-PPh$_3$/TiO$_2$** NPs (0.6 mol% Pd), 2.5 ml of solvent, 30 min. [b]Measured by ^{1}H-NMR using TMB as internal standard. [c]EtOH:milli-Q H_2O (4:1 v/v).

These results suggest that the increase of activity observed could be due to a faster H-transfer from EtOH than from water. Solubility difference can be discarded because both starting material and the products are soluble in the two solvent systems used.

Next, a series of nitrophenol and nitroarenes were tested as substrates in this reaction using the optimized conditions (2 M HCOOK (10 equiv.), 30 ºC using EtOH:H_2O (4:1 v/v) as solvent system) during 45 min. the results are summarized in Table 2.

When 4-NP was reacted under these conditions, total conversion with 95% selectivity were obtained (Entry 1). Using nitrophenol substrates containing a methyl group in different positions of the aromatic rings were tested (Entries 2 and 3), full conversions with excellent selectivities (>95%) were also achieved.

When substrate **3** was used, containing a chloride substituent in the nitrophenol (Entry 4), full conversion was again achieved but the selectivity was shifted in favor of the dechlorinated product 4-AP, indicating that both nitro reduction and hydrochlorination reactions had taken place.[20,22]

When nitroarenes were employed as substrates in this reaction, the results revealed highly dependent on the substituents present at the aromatic ring. Using nitrobenzene, full conversion with total selectivity to aniline was observed (Entry 5). The same behavior was observed when 4-nitroacetophenone was tested as substrate (Entry 7). In contrast, when substrates containing a vinyl group (Entry 5) or an ethynyl substituent (Entry 9) were tested, no conversion was observed. This suggests that decomposition of the formate does not yield H_2 in the reaction mixture as Pd NPs are excellent alkyne hydrogenation catalysts and if H_2 would be released, hydrogenation of the vinyl or ethynyl group would be expected. When the substrate included a formyl group, only 14% conversion was obtained with 90% selectivity. Reduction of the formyl substituent was also detected. When 1,2-dinitrobenzene was used as substrate (Entry 8), 30% conversion to the diamine product was obtained. This might be due to the potential bidentate character of the substrate/product that slows down its desorption from the NP surface. Finally, the results using 4-phenylisocianate as substrate are displayed in Entry 11. Full conversion was obtained, but total selectivity to ethyl (4-aminophenyl)carbamate was observed. This result can be explained by the presence of the highly activated carbon in the isocyanate group that underwent nucleophilic attack from EtOH.

Table 2. Catalytic hydrogenation of different nitrocompounds with **Pd-PPh$_3$/TiO$_2$** catalyst using optimal conditions.[a]

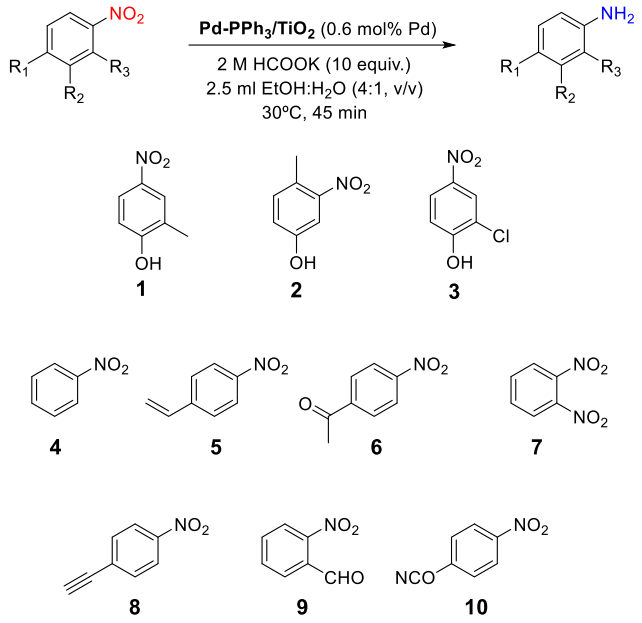

Entry	Substrate	C (%)[b]	$S_{product}$ (%)[b]	$S_{byproduct}$ (%)[b]
1	4-NP	>99	95	-
2	1	>99	96	-
3	2	>99	99	-
4	3	>99	-	95
5[c]	4	>99	>99	0
6[c]	5	<1	0	-
7[c]	6	>99	>99	0
8[c]	7	30	>99	0
9[c]	8	0	0	-
10[c]	9	14	90	10
11[c]	10	>99	0	>99

[a]Reaction conditions: 0.5 mmol substrate, 10 mg of **Pd-PPh$_3$/TiO$_2$** NPs (0.6 mol% Pd), 2 M HCOOK (10 equiv.), 2.5 ml EtOH:milli-Q H_2O (4:1 v/v), 30 ºC, 45 min. [b]Measured by ^{1}H-NMR using TMB as internal standard. [c]Measured by ^{1}H-NMR and GC-MS.

The preliminary results described in this section therefore demonstrate that the **Pd-PPh$_3$/TiO$_2$** is active in the dehydrogenation of formate and that in the presence of reducible substrates such as nitrophenols, the reduction of the nitro group was highly efficient. When the substrates were nitroarenes, a high dependence on the substituents at the aromatic ring was observed. Experiments to confirm the mechanism involved in these reactions and the exact role that potassium formate plays (in transfer hydrogenation or in the decomposition to H_2 and CO_2) are planned.

6.2.2. Preliminary results into the reductive amination of nitrobenzene in the presence of aldehydes using formate

In this section, the preliminary results obtained in the reductive amination of nitrobenzene with butyraldehyde or benzaldehyde will be described using **Pd-PPh$_3$/TiO$_2$** as catalyst and formate as reducing agent. The corresponding experiments were performed in water, in the presence of different concentrations of HCOOK, temperature and times.

The results obtained for the reductive amination using nitrobenzene and butyraldehyde in the presence of **Pd-PPh$_3$/TiO$_2$** and formate were summarized on Table 3.

Table 3. Direct reductive amination of nitrobenzene and butyraldehyde with **Pd-PPh$_3$/TiO$_2$** catalyst employing different conditions of reaction.[a]

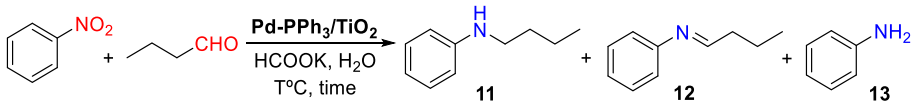

Entry	T (ºC)	t (h)	C (%)[b]	S_{11} (%)[b]	S_{12} (%)[b]	S_{13} (%)[b]
1	r.t.	1	89	17	16	66
2	r.t.	3	100	89	1	9
3	60	10 min	100	58	15	27
4	60	1	100	88	3	9
5	60	3	100	94	3	3

[a]Reaction conditions: 1 mmol nitrobenzene and 1.3 mmol butyraldehyde, 20 mg of **Pd-PPh$_3$/TiO$_2$** (0.6 mol% Pd), 4 M HCOOK (20 equiv.), 5 ml of milli-Q H_2O. [b]Conversion and selectivity were measured by GC-MS.

This reaction consists in 3 steps: reduction of the nitrobenzene into aniline, condensation of the aniline with the aldehyde substrate, and hydrogenation of the imine formed into the desired amine product. When the reaction was performed at room temperature (Entry 1 and Entry 2) 17% of the desired amine were obtained after 1 h of reaction and 89% after 3 h, at which time the conversion reached 100% but with a selectivity to amine of 90%. At 60 ºC, the reaction was very fast and only after 10 minutes of reaction (Entry 3), 100% of conversion was obtained with 58% of selectivity to the amine. After 1 h (Entry 4), the selectivity reached 88% to amine and 94% after 3 h (Entry 5).

Therefore, an increase in temperature from room temperature to 60 ºC increased the initial rate of the reaction although after 3 h similar results were obtained.

Next, benzaldehyde was used as aldehyde substrate and parameters such as mol% of Pd, concentration of HCOOK and temperature were earied. For these experiments, nitrobenzene was first added to the reaction and was reacted during one hour prior to the addition of the aldehyde. These results are presented in Table 4.

Table 4. Direct reductive amination of nitrobenzene and benzaldehyde with **Pd-PPh$_3$/TiO$_2$** catalyst employing different conditions of reaction.

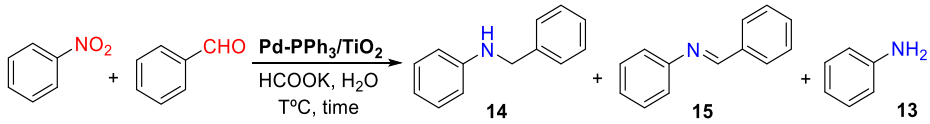

Entry	mol% Pd	[HCOOK] (M)	T (ºC)	C (%)[c]	S_{14} (%)[c]	S_{15} (%)[c]	S_{13} (%)[c]
1[a]	0.4	4	r.t.	100	1	98	1
2[a]	0.8	4	r.t.	100	8	92	0
3[a]	0.4	8	r.t.	93	22	57	0
4[a]	0.4	8	80	100	48	39	13
5[b]	0.6	8	50	100	91	1	8

[a]Conditions: 0.3 mmol nitrobenzene and 0.45 mmol benzaldehyde, 1 ml of milli-Q H_2O, 15 h.
[b]Conditions: 1 mmol nitrobenzene and 1.5 mmol benzaldehyde, 5 ml of milli-Q H_2O, 15 h.
[c]Conversion and selectivity were measured by GC-MS.

When the reaction was performed at room temperature using 0.4 mol% of Pd at 4 M of HCOOK (13 equiv.), full conversion was obtained after 15 h (Entry 1) but very low selectivity to the desired imine. The imine intermediate was the major product with a selectivity of 98%. When the reaction was repeated using 0.8 mol% Pd (Entry 2), very similar results were obtained and only 8% selectivity to the final amine product was reached. Using 0.4 mol% Pd and 8 M of formate, the selectivity increased to 22%. However, surprisingly, the nitrobenzene conversion slightly decreased. When the temperature was increased to 80 ºC, using 0.4 mol% of Pd and 8 M of HCOOK (26 equiv.) (Entry 4), 100% of conversion was obtained but only 48% selectivity to the amine was achieved. Increasing the catalyst loading to 0.6 mol% of Pd, and using 8 M of HCOOK (40 equiv.), 100% conversion was observed with good selectivity (91%) to the desired amine.

These results therefore showed that the catalyst **Pd-PPh$_3$/TiO$_2$** was active in the reductive amination of nitrobenzene using an aromatic aldehyde as substrate, and that the selectivity towards either the imine or amine products could be tuned by variations of the reaction conditions.

6.3. Conclusions

In this chapter, the **Pd-PPh$_3$/TiO$_2$** catalyst previously used in the hydrogenation of CO_2 to formate was here employed for the reduction of nitrophenols and nitroarenes in water using potassium formate as reducing agent. The following conclusions can be drawn:

- These preliminary results demonstrate that the **Pd-PPh$_3$/TiO$_2$** is active in the dehydrogenation of formate and that in the presence of reducible substrates such as nitroaromatics, the reduction of the nitro group was highly efficient. When the substrates were nitroarenes, a high dependence on the substituents at the aromatic ring was observed.
- Using 4-nitrophenol as substrate, an initial TOF (at 15 min of reaction) of 408 h^{-1} was obtained, which is among the best activities reported for this reaction, including when conventional reductants such as $NaBH_4$ are used. When chloronitrophenol was employed as substrate, reduction and dechlorination reactions took place.

- Preliminary results on the reductive amination using nitrobenzene and butyraldehyde/benzaldehyde in water were also presented. For butyraldehyde, 100% of conversion and 91% of selectivity to the desired amine were obtained at r.t. in 3 h of reaction, (0.6 mol% Pd, 4 M HCOOK (20 equiv.)). However, when the reaction was carried out using benzaldehyde as substrate, full selectivity to the imine product (mainly using r.t.) or to the amine (0.6 mol% Pd, 8 M HCOOK (40 equiv.) and 50 ºC) could be achieved.

6.4. Experimental section

Materials and methods

All substrates employed for the catalytic experiments were purchased from Aldrich, BDLpharm and Acros Organics and used as received without further purification. Milli-Q water was employed in catalytic experiments. Any other solvent or reagent employed was reagent grade. Reactions were carried out under aerobic conditions, employing tubes or flasks with septum taps. All products of catalysis were analysed by ^{1}H-NMR or GC-MS and they were found reported on literature: 4-AP and aniline, [55] 3-vinylaniline, [56] 4′-aminoacetophenone, [57] 2-nitroaniline, [58] 4-ethynylaniline, [59] 2-aminobenzaldehyde [60] and ethyl (4-aminophenyl)carbamate, [61] *N*-benzylaniline[49] and *N*-butylaniline.[62]

The details concerning the synthesis and characterization of **Pd-PPh$_3$/TiO$_2$** NPs were described in the Experimental Section of Chapter 3.

Characterization techniques

Nuclear Magnetic Resonance (NMR)

The equipment used were Bruker Advance Neo 400 with probe Smart (PI HR-400-S1-BBF/H/D-5.0-Z SP N) and sample case of 24 positions VARIAN Varian NMRSYS 400 (reverse probe 5 mm Auto-X 1H/31P-15N, probe 5 mm autoswitchable PFG and 5 mm probe One Probe). Measurements were performed in “Servei de Recursos Cientifics I Tècnics de la Universitat Rovira i Virgili” in Tarragona. 1,3,5-Trimethoxybenzene (TMB) was used as internal standard for catalytic experiments.

GC-MS

Column employed is Agilent 19091S-433UI HP-5ms Ultra Inert (dimensions: 30 m x 250 µm x 0.25 µm). The method employed have an initial setpoint of 60 ºC with a rate of 30 ºC/min until 280 ºC. This is hold during 5 min. an increase with a rate of 40 ºC/min until 320 ºC to hold during 2 min. A post run at 310 ºC was performed. 1 µl of sample was injected and the mode employed was split.

Catalytic reduction of nitrophenol using potassium formate at different times

Table S1. Catalytic hydrogenation of 4-nitrophenol with **Pd-PPh$_3$/TiO$_2$** catalyst at different times.[a]

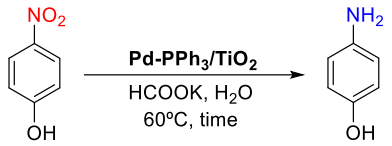

Entry	t (min)	C (%)[b]	S (%)[b]
1	15	59	99
2	30	79	97
3	45	>99	97
4	60	>99	96
5	120	>99	96
6	1080	>99	96

[a]Reaction conditions: 0.5 mmol 4-NP, 10 mg of **Pd-PPh$_3$/TiO$_2$** NPs (0.6 mol% Pd), 2.5 ml of milli-Q H_2O, 4 M HCOOK, 60 ºC. [b]Measured by ^{1}H-NMR using TMB as internal standard.

In a general experiment, 4 M of HCOOK (20 equiv.) was added to a tube, 2.5 ml of milli-Q H_2O were added and the tube was introduced into a preheated oil bath preheated at 60 ºC under stirring at 1200 rpm. Then, 10 mg of **Pd-PPh$_3$/TiO$_2$** (0.6 mol% of Pd) were introduced into the tube and, finally, 69.56 mg (0.5 mmol) of 4-NP was added. The tube was closed with a septum tap and let react the required time. After this time, the tube was removed from the oil bath and let get room temperature. 100 µl of the crude were taken to analysed by ^{1}H-NMR. TMB (1,3,5-trimethylbenzene) was used as internal standards and 600 µl of DMSO-d6 were added to the NMR tube.

Catalytic reduction of nitrophenols and nitroarenes using potassium formate

The same procedure which was previously described for the reduction of nitrophenol was employed using 0.5 mmol of substrate, 0.6 mol% of Pd, 2 M of HCOOK (10 equiv.), 2.5 ml of EtOH:milli-Q H_2O (4:1 v/v), 30 ºC and 45 min. Products were analysed by ^{1}H-NMR using TMB as internal standard, taking 100 µl of the crude.

For nitroarenes, the setup of the reactions was the same, but the work up was different. After reaction, the tubes were removed from the bath at 30 ºC. Then, TMB was added and the content of the tubes was filtered through celite and washed with distilled H_2O and DCM. Organic phases were extracted several times with DCM. Organic phases were put together and $MgSO_4$ were added. The mixture was filtered and evaporated under reduced pressure. Products were analysed by ^{1}H-NMR and GC-MS.

Reductive amination with nitrobenzene and butyraldehyde

Reactions were performed in 100 ml round bottom flasks. First, HCOOK, milli-Q H_2O and catalyst were added and stirred in a preheated bath at the required temperature. Then, nitrobenzene was added, followed by the aldehyde. The flask was closed with a septum tap and the mixture reacted during the specified time. Then, the reaction mixture was cooled to r.t., the content of the flasks was filtered through celite and washed with distilled H_2O and DCM. Organic phases were extracted several times with DCM. Organic phases were put together and $MgSO_4$ were added. The mixture was filtered and evaporated under reduced pressure. Products were analysed by GC-MS.

Reductive amination with nitrobenzene and benzaldehyde

Reactions were performed into 100 ml round bottom flasks. First, HCOOK, milli-Q H_2O and the catalyst were added and stirred in a preheated bath at the required temperature. Then, nitrobenzene was added and reacted during 1 h. Then, aldehyde was added, the flask was closed with a septum tap and the reaction left during the specified time. After that, reaction mixture was cooled to r.t., the content of the flasks was filtered through celite, and washed with distilled H_2O and DCM. Organic phases were extracted several times with DCM. Organic phases were put together and $MgSO_4$ were added.

Mixture was filtered and it was evaporated under reduced pressure. Products were analysed by GC-MS.

6.5. References

[1] A. Bahuguna, Y. Sasson, *ChemSusChem* **2021**, *14*, 1258−1283.
[2] (a) V. Pandarus, R. Ciriminna, F. Béland and M. Pagliaro, *Adv. Synth. Catal*. **2011**, *353*, 1306; (b) Y. Mikami, A. Noujima, T. Mitsudome, T. Mizugaki, K. Jitsukawa, K. Kaneda, *Chem. Lett*. **2010**, *39*, 223; (c) F. Cárdenas-Lizana, S. Gómez-Quero, M. A. Keane, *Catal. Commun*. **2008**, *9*, 475.
[3] (a) F. Ellis, *Paracetamol: a curriculum resource*, Royal Society of Chemistry, Cambridge **2002**; (b) A. S. Travis, *Manufacture and uses of the anilines: a vast array of processes and products*, The chemistry of Anilines Part 1, Wiley, **2009**, p. 764.
[4] (a) P. F. Schellhammer, *Expert Opin. Pharmacother*. **2002**, *3*, 1313; (b) Y. Fradet, N. James, J. Maher, *Expert Rev. Anticancer Ther*. **2004**, *4*, 37; (c) W. A. See, C. J. Tyrrell, *J. Cancer Res. Clin. Oncol*. **2006**, 132; (d) I. I. Müderris, F. Bayram, B. Ozçelik, M. Güven, *Gynecol. Endocrinol*. **2002**, *16*, 63.
[5] (a) W. Kassouf, S. Tanguay, A. G. Aprikian, *J. Urol*. **2003**, *169*, 1742; (b) M. Moguilewsky, C. Bertagna, M. Hucher, *J. Steroid Biochem.* **1987**, 871; (c) A. C. Hsieh, C. J. Ryan, *Cancer J*. **2008**, *14*, 11.
[6] (a) Z. Li, M. Xu, S. Xing, W. Ho, T. Ishii, Q. Li, X. Fu, Z. Zhao, *J. Biol. Chem.* **2007**, *282*, 3428; (b) A. Dudek, K. Kmak, J. Koopmeiners, M. Keshtgarpour, *Lung Cancer* **2006**, *51*, 89.
[7] A. Béchamp, *Ann. Chim. Phys*. **1854**, *42*, 186.
[8] H. K. Kadam, S. G. Tilve, *RSC Adv*. **2015**, *5*, 83391.
[9] A. Serrà, R. Artal, M. Pozo, J. Garcia-Amorós, E. Gómez, *Catalysts* **2020**, *10*, 458.
[10] A. Serrà, E. Gómez, L. Philippe, *Catalysts* **2019**, *9*, 974.
[11] (a) WWAP (UNESCOWorldWater Assessment Programme). The United Nations World Water Development Report **2019**: *Leaving No One Behind*, UNESCO: Paris, France, **2019**; (b) United States Environmental Protection Agency. *Health and Environmental Effect Profiles*, United States Environmental Protection Agency: Washington, DC, USA, **1980**; (c) United States Environmental Protection Agency. *Health Effects Assessment for Nitrophenols*, United States Environmental Protection Agency: Washington, DC, USA, **1987**; (d) L. H. Keith, W. A. Telliard, *Environ. Sci. Technol*. **1979**, *13*, 416−423.
[12] (a) T. Komatsu, T. Hirose, *Appl. Catal. A Gen*. **2004**, *276*, 95−102; (b) C. V. Rode, M. J. Vaidya, R. Jaganathan, R. V. Chaudhari, *Chem. Eng. Sci*. **2001**, *56*, 299−1304; (c) X. Ren, L. Tang, J. Wang, E. Almatrafi, H. Feng, X. Tang, J. Yu, Y. Yang, X. Li, C. Zhou, Z. Zeng, G. Zeng, *Water Res*. **2021**, *201*, 117360.
[13] (a) C. K. Chua, M. Pumera, L. Rulíšek, *J. Phys. Chem. C* **2012**, *116*, 4243−4251; (b) J. Lee, J. C. Park, H. Song, *Adv. Mater*. **2008**, *20*, 1523−1528; (c) Y. Z. Li, Y. L. Cao, J. Xie, D. Z. Jia, H. Y. Qin, Z. T. Liang, *Catal. Commun*. **2015**, *58*, 21−25; (d) M. Polášek, F. Tureček, *J. Am. Chem. Soc*. **2000**, *122*, 9511−9524; (e) M. J. Vaidya, S.

M. Kulkarni, R. V. Chaudhari, *Org. Process Res. Dev*. **2003**, *7*, 202−208; (f) M. L. Wang, T. T. Jiang, Y. Lu, H. J. Liu, Y. Chen, *J. Mater. Chem. A* **2013**, *1*, 5923−5933; (g) D. H. Zhang, L. Chen, G. L. Ge, *Catal. Commun*. **2015**, *66*, 95−99.

[14] (a) T. Sun, Z. Zhang, J. Xiao, C. Chen, F. Xiao, S. Wang, Y. Liu, *Sci. Rep*. **2013**, *3*, 1, 2527; (b) H. Li, L. Han, J. Cooper-White, I. Kim, *Green Chem.* **2012**, *14*, 3, 586; (c) X. Duan, M. Xiao, S. Liang, Z. Zhang, Y. Zeng, J. Xi, S. Wang, *Carbon* **2017**, *119*, 326–331; (d) F. Yang, S. Dong, C. Wang, Y. Li, *RSC Adv*. **2016**, *6*, 58, 52620−52626; (e) C. Wang, F. Yang, W. Yang, L. Ren, Y. Zhang, X. Jia, L. Zhang, Y. Li, *RSC Adv*. **2015**, *5*, 35, 27526−27532; (f) X. Gu, W. Qi, X. Xu, Z. Sun, L. Zhang, W. Liu, X. Pan, D. Su, *Nanoscale* **2014**, *6*, 12, 6609−6616.

[15] X. Kong, H. Zhu, C. Chen, G. Huang, Q. Chen, *Chem. Phys. Lett*. **2017**, *684*, 148−152.

[16] C.-H. Liu, J. Liu, Y.-Y. Zhou, X.-L. Cai, Y. Lu, X. Gao, S.-D. Wang, *Carbon* **2015**, *94*, 295−300.

[17] P. An, R. Anumula, C. Cui, Y. Liu, F. Zhan, Y. Tao, Z. Luo, *Nano Res.* **2019**, *12*, 2589−2596.

[18] A. I. Ayad, D. Luart, A. O. Dris, E. Guénin, *Nanomaterials* **2020**, *10*, 1169.

[19] A. I. Ayad, C. B. Marín, E. Colaco, C. Lefevre, C. Méthivier, A. O. Driss, J. Landoulsi, E. Guénin, *Green Chem*. **2019**, *21*, 6646−6657.

[20] F. Li, Y. Liu, T. Ma, D. Xu, X. Lia, G. Gong, *New J. Chem*. **2017**, *41*, 4014−4021.

[21] H. Veisi, B. Karmakar, T. Tamoradi, R. Tayebee, S. Sajjadifar, S. Lotfi, B. Maleki, S. Hemmati, *Sci. Reports* **2021**, *11*, 4515.

[22] R. R. Shetty, S. S. Raut, P. S. Kulkarni, S. P. Kamble, *Ind. Eng. Chem. Res*. **2022**, *61*, 14433−14445.

[23] V. Lomonosov, J. Asselin, E. Ringe, *React. Chem. Eng*. **2022**, *7*, 1728−1741.

[24] J. Xi, Q. Wang, J. Liu, L. Huan, Z. He, Y. Qiu, J. Zhang, C. Tang, J. Xiao, S. Wang, *J. Catal.* **2018**, *359*, 233−241.

[25] X. Zhan, S. Michaud-Chevallier, D. Hérault, F. Duprat, *Org. Process Res. Dev*. **2020**, *24*, 686−694.

[26] T. Portada, D. Margetić, V. Štrukil, *Molecules* **2018**, *23*, 3163.

[27] B. Zeynizadeh, F. M. Aminzadeh, H. Mousavi, *Res. Chem. Intermed*. **2021**, *47*, 3289−3312.

[28] D. O. Bokov, M. Z. Mahmoud, G. Widjaja, W. Suksatan, S. Chupradit, U. S. Altimari, H. A. Hussein, Y. F. Mustafa, M. kazemnejadi, *RSC Adv.* **2022**, *12*, 10933.

[29] J. Li, X.-Y. Shi, Y.-Y. Bi, J.-F. Wei, Z.-G. Chen, *ACS Catal*. **2011**, *1*, 657−664.

[30] M. J. Beier, J.-M. Andanson, A. Baiker, *ACS Catal*. **2012**, *2*, 2587−2595.

[31] A. H. Romero, *ChemistrySelect* **2020**, *5*, 13054−13075 and references *therein*.

[32] H. Wiener, J. Blum, Y. Sasson, *J. Org. Chem*. **1991**, *56*, 4481.

[33] Z. Hu, S. Tan, R. Mi, X. Li, J. Bai, X. Guo, G. Hu, P. Hang, J. Li, D. Li, Y. Yang, X. Yan, *ChemistrySelect* **2018**, *3*, 2850−2853.

[34] A. Saha, B. Ranu, *J. Org. Chem.* **2008**, *73*, 6867−6870.

[35] D. Gowda, B. Mahesh, G. Shankare, *Ind. J. Chem. Sect. B* **2001**, *40*, 75−77.

[36] (a) S. A. Lawrence, *Amines: Synthesis Properties and Applications*; Cambridge University Press: Cambridge, UK, **2004**; (b) A. Ricci, (Ed.) Amino Group Chemistry: From Synthesis to the Life Sciences; Wiley-VCH: Weinheim, Germany, **2008**.
[37] G. Romanazzi, V. Petrelli, A. M. Fiore, P. Mastrorilli, M. M. Dell'Anna, *Molecules* **2021**, *26*, 1120.
[38] A. F. Abdel-Magid, K. G. Carson, B. D. Harris, C. A. Maryanoff, R. D. Shah, *J. Org. Chem.* **1996**, *61*, 3849−3862.
[39] L. Li, Z. Niu, S. Cai, Y. Zhi, H. Li, H. Rong, L. Liu, L. Liu, W. He, Y. Li, *Chem. Commun*. **2013**, *49*, 6843−6845.
[40] (a) M. O. Sydnes, M. Kuse, M. Isobe, *Tetrahedron* **2008**, *64*, 6406−6414; (b) D. Kudo, Y. Masui, M. Onaka, *Chem. Lett*. **2007**, *36*, 918−919.
[41] P. Zhou, Z. Zhang, L. Jiang, C. Yu, K. Lv, J. Sun, S. Wang, *Appl. Catal. B Environ*. **2017**, *210*, 522−532.
[42] L. Jiang, P. Zhou, Z. Zhang, S. Jin, Q. Chi, *Ind. Eng. Chem. Res*. **2017**, *56*, 12556−12565.
[43] P. Zhou, L. Jiang, F. Wang, K. Deng, K. Lv, Z. Zhang, *Sci. Adv*. **2017**, *3*, e1601945.
[44] T. Senthamarai, K. Murugesan, K. Natte, N. V. Kalevaru, H. Neumann, P. C. J. Kamer, R. V. Jagadeesh, *ChemCatChem* **2018**, *10*, 1235−1240.
[45] E. Byun, B. Hong, K. A. De Castro, M. Lim, H. Rhee, *J. Org. Chem*. **2007**, *72*, 9815−9817.
[46] S. S. Ekbote, S. T. Gadge, B. M. Bhanage, *Catalysts* **2014**, *4*, 289−298.
[47] L. E. Arteaga-Pérez, R. Manrique, F. Castillo-Puchi, M. Ortega, C. Bertiola, A. Pérez, R. Jiménez, *Chem. Eng. J.* **2021**, *417*, 129236.
[48] S. Ergen, B. Nişanci, Ö. Metin, *New J. Chem*. **2018**, *42*, 10000−10006.
[49] Q. Zhang, S.-S. Li, M.-M. Zhu, Y.-M. Liu, H.-Y. He, Y. Cao, *Green Chem*. **2015**, *18*, 2507−2513.
[50] J. L. Fiorio, T. P. Araújo, E. C. Barbosa, J. Quiroz, P. H. Camargo, M. Rudolph, A. S. K. Hashmi, L. M. Rossi, *Appl. Catal. B Environ*. **2020**, *267*, 118728.
[51] F. Wang, S. Y. Song, K. Li, J. Q. Li, J. Pan, S. Yao, X. Ge, J. Feng, X. Wang, H. J. Zhang, *Adv. Mater*. **2016**, *28*, 10679.
[52] F. Yang, C. Chi, C.X. Wang, Y. Wang, Y. F. Li, *Green Chem*. **2016**, *18*, 4254.
[53] G. J. Cui, Z. B. Sun, H. Z. Li, X. N. Liu, Y. Liu, Y. X. Tian, S. Q. Yan, *J. Mater. Chem. A* **2016**, *4*, 1771.
[54] X. D. Le, Z. P. Dong, Y. S. Liu, Z. C. Jin, T. D. Huy, M. D. Leb, J. T. Ma, *J. Mater. Chem. A* **2014**, *2*, 19696.
[55] S. Giri, R. Das, C. van der Westhuyzen, A. Maity, *Appl. Catal. B: Environ*. **2017**, *209*, 669−678.
[56] C. Yu, B. Liu, L. Hu, *J. Org. Chem*. **2001**, *66*, 919.
[57] A. Yasuhara, A. Kasano, T. Sakamoto, *J. Org. Chem*. **1999**, *64*, 2301−2303.
[58] L. Jiang, X. Lu, H. Zhang, Y. Jiang, D. Ma, *J. Org. Chem*. **2009**, *74*, 4546.
[59] P. R. Serwinski, P. M. Lahti, *Org. Lett*. **2003**, *5*, 2099−2102.

[60] M. Castaing, S. L. Wason, B. Estepa, J. F. Hooper, M. C. Willis, *Angew. Chem. Int. Ed*. **2013**, *52*, 13280−13283.
[61] A. Garofalo, L. Goossens, A. Lemoine, A. Farce, Y. Arlot, P. Depreux, *J. Enzyme Inhib. Med. Chem*. **2010**, *25*, 2, 158−171.
[62] M. Beller, F. Rataboul, *Chem. Eur. J.* **2004**, *10*, 2983.

CHAPTER 7

Conclusions

UNIVERSITAT ROVIRA I VIRGILI
EFFICIENT VALORIZATION OF CO2 INTO FORMATE THROUGH NANOCATALYSIS
María Dolores Fernández Martínez

Considering the general objectives described in Chapter 2 and according to the results described in Chapter 3-6, the following conclusions can be drawn:

- General conclusions Chapter 3:

A series of Pd based nanocatalysts were prepared using the organometallic approach and characterized. The effect of the nature of the capping ligands and of the solid support on the size of the resulting Pd NPs was evaluated. The results indicated that:

  - The ligand employed influences the size of the resulting Pd NPs. Water-soluble ligands provided smaller sizes while the use of NHC ligand led to larger NPs. When no ligand was employed, the highest particle size (*ca*. 5 nm) was obtained.
  - A strong effect of the support on the size of the Pd NPs was also observed, probably due to the strength of the corresponding metal-support interactions.

The prepared materials were tested in the hydrogenation of CO_2 into formates in water as solvent. The results indicated that:

  - The size of the nanoparticles could not be directly correlated with their catalytic performance and the interactions between the nanoparticles and the support appeared to be critical to the catalyst activity.
  - The **Pd-PPh$_3$/TiO$_2$** catalytic system reached a TON of 1032 (TOF of 69 h^{-1}, [HCOOK]= 1.1 mol/l) at 60 ºC under 36 bar (pCO_2:pH_2= 1).
  - Recycling study revealed unsuccessful and a rapid decrease in activity was observed after each run.

- General conclusions Chapter 4:

PPh_3- and PTA-decorated Pd NPs were studied by means of DFT calculations exploring different phosphine adsorption modes, ligand coverage and interactions of carbonate and bicarbonate species. This study aimed at getting insights into the hydrogenation reactions described in Chapter 3. The most remarkable conclusions obtained were:

  - The most stable adsorption of PPh_3 at the **Pd$_{55}$** surface takes place through the P atom and additional interactions of the carbon atoms from the aromatic rings in η^6 or η^2 fashions were also detected.
  - For PTA, adsorption through the P atom is preferred to the interaction *via* the nitrogen atom.

- Lower energies of adsorption were obtained for PPh_3 than for PTA, which translates into a higher stabilization of the system when this ligand is used.
- Higher degree of coverage of the NP was observed for PTA than for PPh_3. This makes the surface less available for interactions with the substrates in catalysis.
- Bicarbonate adsorption at the NP surface is lower in energy than that of carbonate, which translates in a more favorable interaction.

- General conclusions Chapter 5:

A series of supported Pd-NPs based materials were successfully synthesized using modifiers of different nature (APTES, ILs and PAs) following two distinct approaches. The so-called reverse deposition approach requires in the first place to modify the TiO_2 support prior to Pd NPs deposition while the 2nd approach was the modification of the pre-synthesized **Pd-PPh_3/TiO_2**, by deposition of the modifier over its surface.

All these catalysts were used in the hydrogenation of CO_2 to formate, and their performance compared with those of the unmodified catalyst **Pd-PPh_3/TiO_2**. In view of the results obtained, the following conclusions can be drawn:

- The modification of the TiO_2 support by oganosilanes provided a beneficial effect in catalysis compared with the catalyst containing unmodified TiO_2 or TiO_2 modified by organophosphonic acids.
- The concentration is a key parameter during the support modification and lower values provide catalysts with higher activities. In contrast, the temperature used during the modification, despite affecting the amount of organics at the surface of the support, does not influence the activity of the catalysts.
- When the support was first modified, the presence of a functional group (either NH_2 or imidazolium) in the modifiers improves the activity of the catalysts compared with those containing a simple alkyl chain.
- When using organophosphonic acids as support modifiers, an aging step is beneficial to the activity of the resulting catalyst.

- The deposition of organosilane and organophosphonic acid modifiers over previously synthesized Pd NPs supported on TiO_2 was not beneficial, in most cases, to the activity of the catalyst.
- The deposition of organosilanes containing an IL substituent over previously synthesized Pd NPs supported on TiO_2 had a detrimental effect on the catalytic activity of the resulting materials.

In terms of recyclability, the experiments performed showed that the synthetic procedure used for the modification of the **Pd-Ph$_3$/TiO$_2$** catalyst affect the reusability of these materials in the CO_2 hydrogenation into formate.

- The catalysts formed by modification of the support prior to Pd NP deposition suffer a rapid decrease in activity during their recycling and reuse in spite of the initial beneficial effect.
- Some of the materials where the modifiers were deposited over the previously anchored Pd NPs onto TiO_2 show a much more gradual decrease in activity and reached a TON > 500 after the 3rd recycling.

- General conclusions Chapter 6:

In this chapter, the **Pd-PPh$_3$/TiO$_2$** catalyst previously used in the hydrogenation of CO_2 to formate was here employed for the reduction of nitrophenols and nitroarenes in water using potassium formate as reducing agent.

- **Pd-PPh$_3$/TiO$_2$** revealed active in the dehydrogenation of formate and in the presence of reducible substrates such as nitroaromatics, the reduction of the nitro group was highly efficient. When the substrates were nitroarenes, a high dependence on the substituents at the aromatic ring was observed.
- Using 4-nitrophenol as substrate, an initial TOF (at 15 min of reaction) of 408 h^{-1} was obtained, which is among the best activities reported for this reaction, including when conventional reductants such as $NaBH_4$ are used. When chloronitrophenol was employed as substrate, reduction and dechlorination reactions took place.
- Preliminary results on the reductive amination using nitrobenzene and butyraldehyde/benzaldehyde in water were also presented. For butyraldehyde, 100% of conversion and 91% of selectivity to the desired amine were obtained at r.t. in 3 h of reaction, (0.6 mol% Pd,

4 M HCOOK (20 equiv.)). However, when the reaction was carried out using benzaldehyde as substrate, full selectivity to the imine product (mainly using r.t.) or to the amine (0.6 mol% Pd, 8 M HCOOK (40 equiv.) and 50 ºC) could be achieved.

Appendix

UNIVERSITAT ROVIRA I VIRGILI
EFFICIENT VALORIZATION OF CO2 INTO FORMATE THROUGH NANOCATALYSIS
María Dolores Fernández Martínez

Publications

- D. Sánchez-Resa, J. A. Delgado, M. D. Fernández-Martínez, C. Didelot, A. De Mallmann, K. C. Szeto, M. Taoufik, C. Claver, C. Godard: ‘’Pd, Cu and Bimetallic PdCu NPs Supported on CNTs and Phosphine-Functionalized Silica: One-Pot Preparation, Characterization and Testing in the Semi-Hydrogenation of Alkynes.‘’ *Eur. J. Inorg. Chem*. **2021**, 4970–4978; doi.org/10.1002/ejic.202100806.
- M. D. Fernández-Martínez, C. Godard: ‘’Hydrogenation of CO_2 into Formates by Ligand-Capped Palladium Heterogeneous Catalysts.‘’ *ChemCatChem* **2023**, e202201408; doi.org/10.1002/cctc.202201408.
- M. D. Fernández-Martínez, C. Godard: ‘’Modifications of TiO_2 supported PPh_3-Capped Palladium Nanocatalysts in the CO_2 Hydrogenation into Formates.‘’ *Manuscript in preparation*

Congress and scientific meetings

- 3rd Hetero-elements and Coordination Chemistry: ‘’from Concepts to Applications Meeting’’ (3rd GDRI-HC3A Meeting). 16-17th January 2020, Toulouse (France).
- On-line 18th International Conference on Carbon Dioxide Utilization (ICCDU 2021). 18-22nd July 2021.
  Poster contribution: ‘’Hydrogenation of CO_2 into formate by phosphine-stabilized Pd/TiO_2 catalysts.‘’
- On-line 24th Conference on Organometallic Chemistry (EuCOMC XXIV Virtual Conference). 1-3rd September 2021.
  Poster contribution: ‘’Hydrogenation of CO_2 into high-added value products by supported Palladium heterogeneous catalyst.‘’
- XVII Simposio de Investigadores Jóvenes RSEQ. 23-26th November 2021, Alcalá de Henares (Spain).
  Flash contribution: ‘’Hydrogenation of CO_2 into formate by phosphine-stabilized Palladium heterogeneous catalysts.‘’
- 4th Hetero-elements and Coordination Chemistry: from Concepts to Applications Meeting (4th GDRI-HC3A Meeting). 20-21st January 2022, Barcelona (Spain).

Poster contribution: ‘’Supported Palladium catalyst for the hydrogenation of CO_2 into high-added value products.‘’

- XXXVIII Reunión Bienal de la Sociedad Española de Química. 27-30th June 2022, Granada (Spain).
  Poster contribution: ‘’Phosphine-stabilized Palladium Heterogeneous catalysts for the hydrogenation of CO_2 into high-added value products.‘’
- XXII International Symposium on Homogeneous Catalysis (XXII ISHC). 24-29th July 2022, Lisbon (Portugal).
  Flash presentation and poster contribution: ‘’New heterogeneous systems for CO_2 hydrogenation to formate.‘’
- 1ª Reunión de Química Inorgánica y Organometálica de la Sociedad Catalana de Química (1RQIO-SCQ). 2-3rd February 2023, Barcelona (Spain).
  Poster contribution: ‘’New supported phosphine-stabilized Palladium nanocatalysts for the hydrogenation of CO_2 into formate.‘’

Stage

PhD visiting stay at Leibniz-Institute for Catalysis (LIKAT) in Rostock (Germany) from 1st September to 30th November 2022 under the supervision of Prof. Matthias Beller and Dr. Ralf Jackstell. Work developed on that center was based on the synthesis of new ligands and its use of homogeneous catalysts for hydroformylation.

UNIVERSITAT ROVIRA I VIRGILI
EFFICIENT VALORIZATION OF CO2 INTO FORMATE THROUGH NANOCATALYSIS
María Dolores Fernández Martínez

UNIVERSITAT ROVIRA I VIRGILI
EFFICIENT VALORIZATION OF CO2 INTO FORMATE THROUGH NANOCATALYSIS
María Dolores Fernández Martínez

UNIVERSITAT ROVIRA I VIRGILI
EFFICIENT VALORIZATION OF CO2 INTO FORMATE THROUGH NANOCATALYSIS
María Dolores Fernández Martínez

UNIVERSITAT
ROVIRA i VIRGILI